

# **N-substituted and N-unsubstituted Porphyrinoids: Synthesis, Structure, Spectroscopic Characterization and Applications**

*By*

**SAJAL KUMAR PATRA**

**CHEM11201604008**

**National Institute of Science Education and Research  
(NISER), Bhubaneswar**

*A thesis submitted to the  
Board of Studies in Chemical Sciences  
In partial fulfillment of requirements  
for the Degree of*

**DOCTOR OF PHILOSOPHY**

*of*

**HOMI BHABHA NATIONAL INSTITUTE**


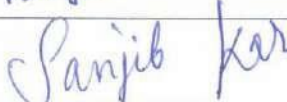
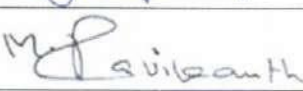
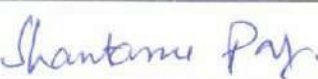

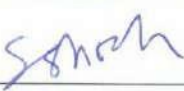
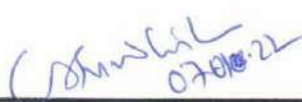


**June- 2021**

# Homi Bhabha National Institute<sup>1</sup>

## Recommendations of the Viva Voce Committee

As members of the Viva Voce Committee, we certify that we have read the dissertation prepared by **SAJAL KUMAR PATRA** entitled **"N-Substituted and N-unsubstituted porphyrinoids: Synthesis, Structure, Spectroscopic Characterization and Applications."** and recommend that it may be accepted as fulfilling the thesis requirement for the award of Degree of Doctor of Philosophy.

Chairman – Dr. Moloy Sarkar		Date: 07-01-2022
Guide / Convener – Dr. Sanjib Kar		Date: 07-01-2022
Examiner–Prof. M. Ravikanth		Date: 7-01-2022
Member 1- Dr. Shantanu Pal		Date: 07-01-2022
Member 2- Dr. Manjusha Dixit		Date: 07-01-2022
Member 3- Dr. S. Ghosh		Date: 07-01-2022
Member 4- Dr. C. S. Purohit		Date: 07-01-2022

Final approval and acceptance of this thesis is contingent upon the candidate's submission of the final copies of the thesis to HBNI.

I/We hereby certify that I/we have read this thesis prepared under my/our direction and recommend that it may be accepted as fulfilling the thesis requirement.

Date: 07-01-2022

Place: NISER, Bhubaneswar

  
(Dr. Sanjib Kar)

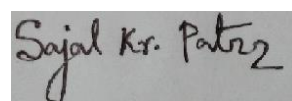
Guide

<sup>1</sup> This page is to be included only for final submission after successful completion of viva voce.

## **STATEMENT BY AUTHOR**

This dissertation has been submitted in partial fulfillment of requirements for an advanced degree at Homi Bhabha National Institute (HBNI) and is deposited in the Library to be made available to borrowers under rules of the HBNI.

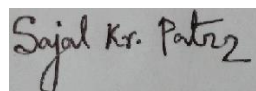
Brief quotations from this dissertation are allowable without special permission, provided that accurate acknowledgement of source is made. Requests for permission for extended quotation from or reproduction of this manuscript in whole or in part may be granted by the Competent Authority of HBNI when in his or her judgment the proposed use of the material is in the interests of scholarship. In all other instances, however, permission must be obtained from the author.

A handwritten signature in black ink on a light gray background. The signature reads "Sajal Kr. Patra" with a stylized flourish at the end.

**SAJAL KUMAR PATRA**

## **DECLARATION**

I, hereby declare that the investigation presented in the thesis has been carried out by me. The work is original and has not been submitted earlier as a whole or in part for a degree / diploma at this or any other Institution / University.

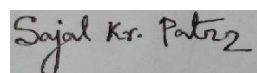
A rectangular box containing a handwritten signature in black ink. The signature is written in a cursive style and reads "Sajal Kr. Patra".

**SAJAL KUMAR PATRA**

# List of Publications

## Journals:

1. <sup>#</sup>“Synthesis of urea derivatives via reductive carbon dioxide fixation into contracted porphyrin analogues”, **S. K. Patra**, K. Sahu, B. Patra, D. K. Sahoo, S. Mondal, P. Mukherjee, H. S. Biswal, S. Kar, *Green Chem.*, **2017**, *19*, 5772–5776.
2. <sup>#</sup>“An N, N'-Bridged Corrole: First Example of a  $N^{21}$ ,  $N^{22}$ -Methylene Bridged Corrole Derivative”, **S. K. Patra**, K. Sahu, B. Patra, S. Mondal, S. Kar, *Eur. J. Org. Chem.* **2018**, 6764–6767.
3. “Grignard reagents mediated demetallation of silver corrole complexes”, B. Patra, **S. K. Patra**, P. Mukherjee, Y. K. Maurya, W. Sinha, S. Kar, *Eur. J. Inorg. Chem.* **2017**, 2363–2368.
4. “Regioselective thiocyanation of corroles and the synthesis of gold nanoparticle–corrole assemblies”, K. Sahu, S. Mondal, B. Patra, T. Pain, **S. K. Patra**, C. Dosche \* and S. Kar \* *Nanoscale Adv.*, **2020**, *2*, 166.
5. <sup>#</sup>“Synthesis, structure, photophysics, and singlet oxygen sensitization by a platinum(II) porphyrin complex, A. Garai, M. Villa, M. Marchini, **S.K. Patra**, T. Pain, S. Mondal, P. Ceroni\* and S. Kar\* *Eur. J. Inorg. Chem.* **2021**, 4089–4095.



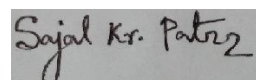
<sup>#</sup> pertaining to this thesis

**SAJAL KUMAR PATRA**

## Conferences:

1. Synthesis of urea derivatives via reductive carbon dioxide fixation into contracted porphyrin analogues. Sajal Kumar Patra, Bratati Patra, Sanjib Kar\*. ACS on Campus held at NISER Bhubaneswar on July 23, 2018. (**Poster Presentation**)
2. Grignard reagents mediated demetallation of silver corrole complexes. Bratati Patra, Sajal Kumar Patra, Sanjib Kar\* ACS on Campus held at NISER Bhubaneswar on July 23, 2018. (**Poster Presentation**)
3. “Synthesis of urea derivatives via reductive carbon dioxide fixation into contracted porphyrin analogues” Sajal Kumar Patra, Bratati Patra and Sanjib Kar\* International Symposium on Recent Advances in Chemistry and Material Sciences (2019) and the Celebration of the International Year of the Periodic Table organized by Indian Chemical Society on 2<sup>nd</sup> and 3rd Aug 2019 at Saha Institute of Nuclear Physics, Kolkata. (**Poster Presentation**)
4. “N, N’ -Bridged corrole: First example of a  $N^{21}$ ,  $N^{22}$ -Methylene-Bridged Corrole Derivative.” Sajal Kumar Patra and Sanjib Kar\* National conference on “Chemistry for sustainable development” two days conference 26-27th Nov 2019 at Department of Chemistry, Sidho-Kanho-Birsha University, Purulia. (**Poster Presentation**)

5. “Synthesis of urea derivatives via reductive carbon dioxide fixation into contracted porphyrin analogues” **Sajal Kumar Patra**, and Sanjib Kar\*  
International conference on materials for the Millennium –MATCON 2021,  
organized online by the Department of Applied Chemistry at the Cochin  
University of Science and Technology during March 15-19th, 2021. (**Oral  
presentation**)



**SAJAL KUMAR PATRA**

## DEDICATIONS

TO MY FAMILY

## ACKNOWLEDGEMENTS

*First of all, I am extremely grateful to **Almighty** for blessing my life and giving me power to overcome all the difficulty that I encountered.*

*I would like to express sincere gratitude to my research supervisor **Dr. Sanjib Kar**, Associate Prof, NISER, for his valuable guidance, encouragement and continuous support throughout the course of my research work. I consider myself blessed for it would have been impossible to achieve this goal without his proper guidance, close monitoring, valuable time and kind care throughout my research tenure. No words of appreciation are enough to express his contributions in the entire period of my research work. I am grateful to **Prof. Sudhakar Panda**, Director of NISER, for the research infrastructure and want to acknowledge **NISER** for providing fellowship.*

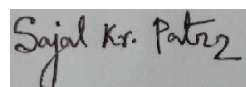
*I sincerely thank my Doctoral committee members, **Dr. Moloy Sarkar (chairman)**, **Dr. C. S. Purohit**, **Dr. Subhadeep Ghosh** and **Dr. Manjusha Dixit** for their valuable suggestions and support during my Ph.D work.*

*I am very much thankful for the technical assistance provided by the staff of NISER. In this context, **Mr. Prakash**, **Mr. Deepak**, **Mr. Sanjaya**, **Mr. Amit** and **Dr. Mriganka** deserved special mention.*

*I thank my friends, seniors and juniors of SCS, NISER for their help. I am grateful to my labmates **Payel**, **Sruti**, **Kasturi**, **Tanmoy**, **Manisha**, **Panisha**, **Bratati**, **Antara di** and **Woormileela di** for their day to day help. My special words of appreciation to my friends **Somnath**, **Jiban** and **Arnab** for boosting my confidence in times of need.*

*Special thank goes to my wife **Payel**, for her selfless support, care and encouragement throughout my entire Ph.D years; without her mental and motivational support it was impossible for me to achieve this position. The completion of work brought more happiness and excitement to her.*

*Last but not the least I wish to thank my parents for their unconditional love, support, sacrifices from the very beginning of my life and also want to thank all my family members, especially my grandfather, late **Gangadhar Patra**, whose contribution in my career is immense to reach this level.*



**SAJAL KUMAR PATRA**

# CONTENTS

	Page No.
<b>SYNOPSIS</b>	<b>11</b>
<b>LIST OF FIGURES</b>	<b>21</b>
<b>LIST OF TABLES</b>	<b>27</b>
<b>LIST OF SCHEMES</b>	<b>28</b>
<b>CHAPTER 1</b>	<b>32</b>
<b>CHAPTER 2</b>	<b>82</b>
<b>CHAPTER 3</b>	<b>134</b>
<b>CHAPTER 4</b>	<b>156</b>

# Synopsis

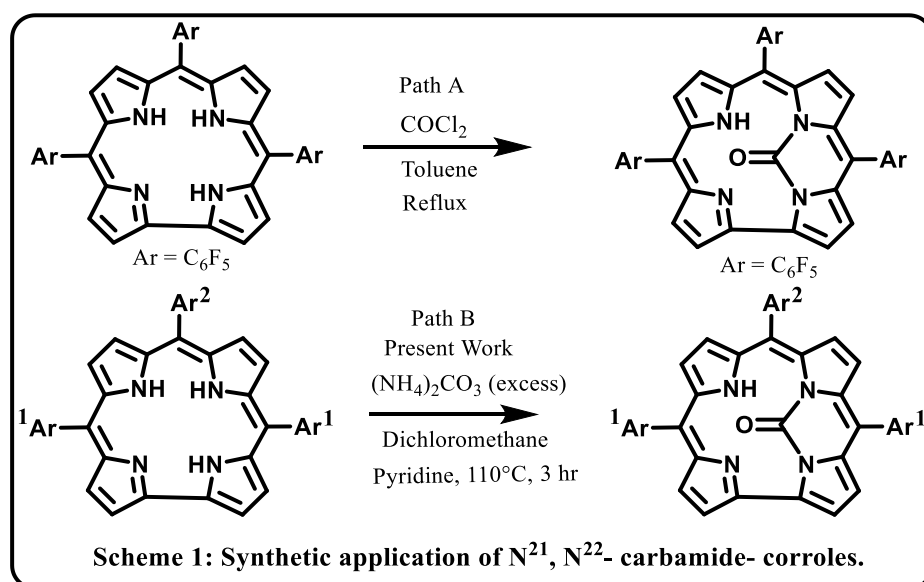
Porphyrin or its different analogues constitute the core skeleton of numerous naturally occurring biological molecules such as hemoglobin, cytochrome c etc. They regulate vital biological processes like oxygen transport, electron transfer, and photosynthesis in plants<sup>1,2</sup>. Due to their enormous biological significance and versatile applications, porphyrins and their modified derivatives are hot topics of research. Different research groups are actively engaged to develop a facile synthetic methodology for its expanded and contracted analogue. One of the most promising contracted porphyrinoids is corrole. Corrole was first reported in 1965.<sup>3</sup> However, it remained nearly unexplored till the development of the facile synthetic protocol in 1999<sup>4,5</sup>. Structurally corrole is in between porphyrin and corrin. It shares a similar skeletal structure of corrin containing direct pyrrole pyrrole ring with  $18\pi$  electron aromatic system like porphyrin<sup>2,6</sup>. Corrole can stabilize the very high oxidation state of metal ions, which makes it an unexceptionally interesting system. Nowadays, corrole and metallocorroles have diverse applications over a multidisciplinary field such as catalysis, sensor, solar cell, medicinal field<sup>7</sup> and so on.

## **Scope of the Present Thesis:**

The present thesis describes different synthetic protocols for modifications and functionalization of corroles. All novel corrole systems are thoroughly characterized by different spectroscopic studies. The mechanistic pathways and importance of these derivatives have been explained. The present thesis composed of four chapters, and the main contents are outlined as follows

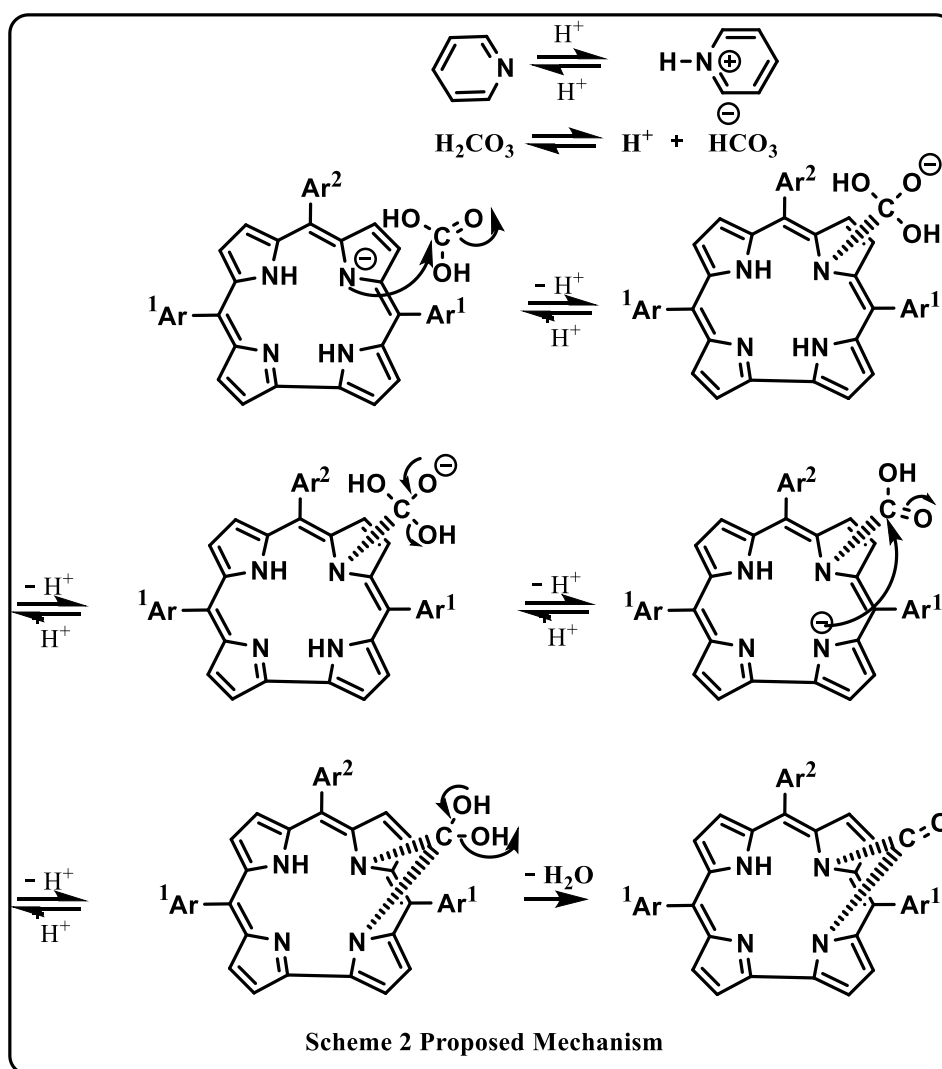
**Chapter 1: Introduction:** This chapter outlines modification of porphyrinoids systems such as contraction, expansion, core modification or isomerization <sup>1,2</sup>. Among these modified systems, contracted analogue, corrole has discussed elaborately. Different synthetic route and functionalization have discoursed here. The superiority of corroles over porphyrin in many cases and its ability to stabilize high oxidation states of metals is explained<sup>6</sup>. Different coordination modes of metallocorroles, versatile applications including catalysis, sensing, dye-sensitized solar cell, and medicinal field, especially cancer research, are also discussed<sup>7</sup>.

**Chapter 2: Synthesis of urea derivatives via reductive carbon dioxide fixation into contracted porphyrin analogue:**



Urea, the wonder molecule, acts as a bridge amid chemistry and biology. Although differently substituted ureas are very common for various applications, but a single synthetic protocol is available for N<sup>21</sup>, N<sup>22</sup>-carbamide-corrole derivatives.<sup>8</sup> However, they used extremely toxic, poisonous and corrosive gas phosgene as a carbonylation agent. To overcome this difficulty entirely novel synthetic protocol has been developed

to synthesize  $N^{21}$ ,  $N^{22}$ -carbamide-corroles. The key feature of this efficient, mild, high-yielding and single-step methodology does not involve any toxic chemicals like phosgene, CO, or isocyanate<sup>9</sup>. Carbon dioxide from ammonium carbonate is confined by the two adjacent inner NH groups ( $N^{21}$  and  $N^{22}$ ) in free base corrole and forms the  $N^{21}$ ,  $N^{22}$ -carbamide-corrole derivatives. In order to simplify the newly designed reaction protocol, series of differently substituted corrole ligand functionalities bearing both electrons releasing and electron-withdrawing functional groups at the corrole periphery has been explored. The reaction withstood most of the reactive functional groups, including cyanide, nitro, halogen substituents, etc.



Here large excess ammonium carbonate salt has been heated to a temperature of  $\sim 110\text{ }^{\circ}\text{C}$ ; which induces a facile release of carbon dioxide. Hence, it is believed that  $\text{HCO}_3^-/\text{H}_2\text{CO}_3$  (a soluble version of  $\text{CO}_2$  gas) drives the desired conversions. Pyridine served dual purposes as a solvent (boiling point:  $116\text{ }^{\circ}\text{C}$ ) and as a weak base for the desired reactions to occur. Based on all these observations, we have also proposed a mechanism for this newly designed reaction (Scheme 2)

All of these newly synthesized  $N^{21}$ ,  $N^{22}$ -carbamide-corrole compounds have been thoroughly characterized by various spectroscopic techniques, including single-crystal X-ray structural analysis of the representative derivatives. The rich and extensive application of substituted urea derivatives certainly points that the discovery of a new methodology can open up an entirely new avenue with broad applications.

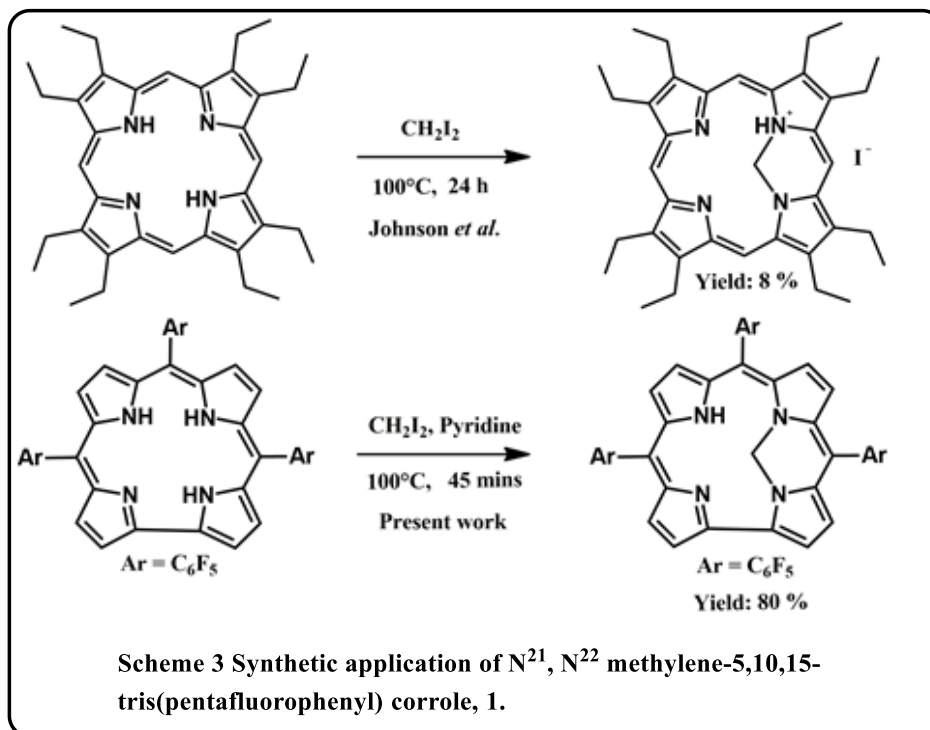
### **Chapter 3: N, N'-Bridged corrole: First example of a $N^{21}$ , $N^{22}$ -Methylene-Bridged Corrole Derivative:**

This chapter deals with the synthesis of a new N, N'-bridged corrole derivative for the first time via the reaction of diiodomethane with 5,10,15-tris(pentafluorophenyl)corrole<sup>10</sup>. Literature survey reveals significantly fewer examples of this type of di-N-substituted corroles. 5,10,15-tris(pentafluorophenyl)corrole backbone is preferred to execute the desired conversion due to its stability as well as extensive application in the synthesis of various metal complexes.<sup>11,12</sup>

Previously Johnson *et al.*<sup>3</sup> reported N, N'- one-carbon bridged porphyrin. Here a similar derivative in the corrole macrocycle has been synthesized successfully by using a modified protocol (Scheme 3).

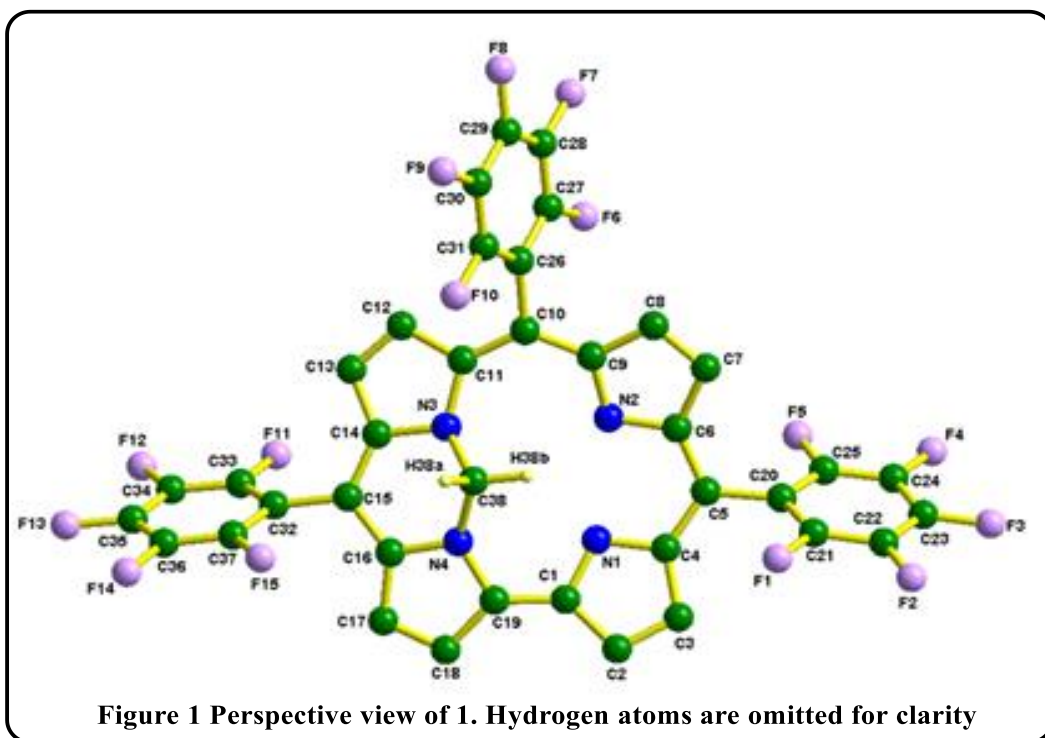
Instead of neat di-iodomethane, a mixture of di-iodomethane and pyridine has been used. Optimization of the  $N^{21}$ ,  $N^{22}$ -methylene bridged corrole formation reaction was

executed. The use of 10 equivalents of  $\text{CH}_2\text{I}_2$  along with pyridine maximized the yield of the desired conversion of the free base corrole to  $N^{21}$ ,  $N^{22}$ -methylene-bridged corrole. The use of pyridine not only drastically increased in yield but also reduction of reaction time and economic viability are observed in this work. Being a mild base, pyridine causes deprotonation of the core NH protons of the corrole ring.

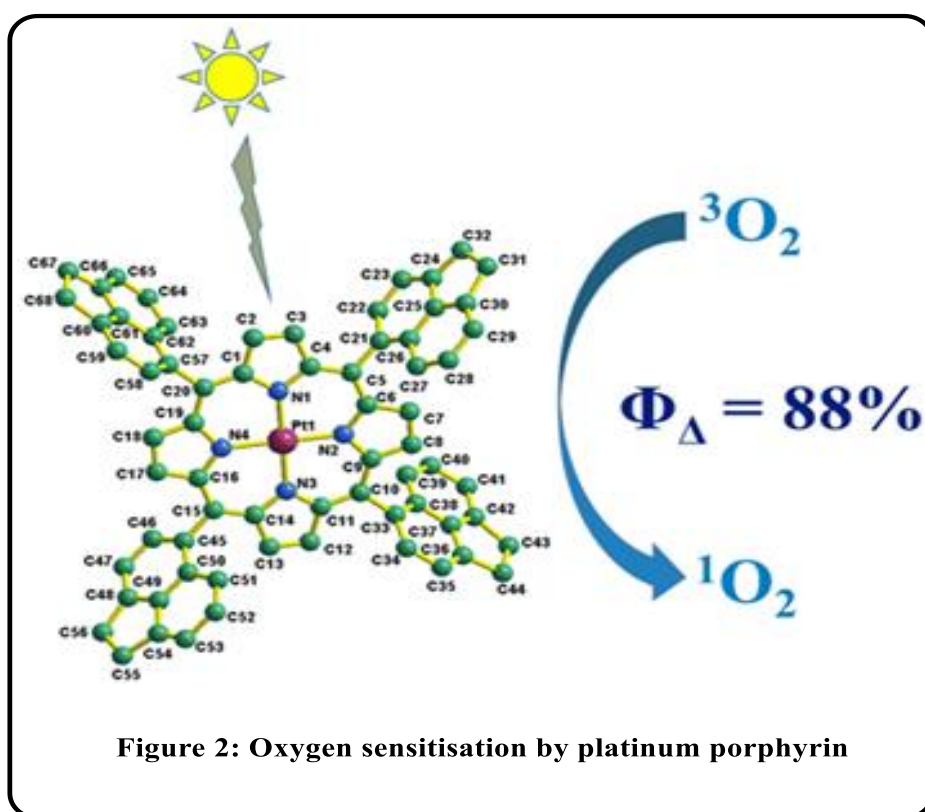


The new macrocycle has been comprehensively characterized by different physicochemical techniques, e.g., NMR ( $^1\text{H}$ ,  $^{19}\text{F}$ ,  $^{13}\text{C}$ ), ESI Mass, and single-crystal X-ray structural analysis (Figure 1).

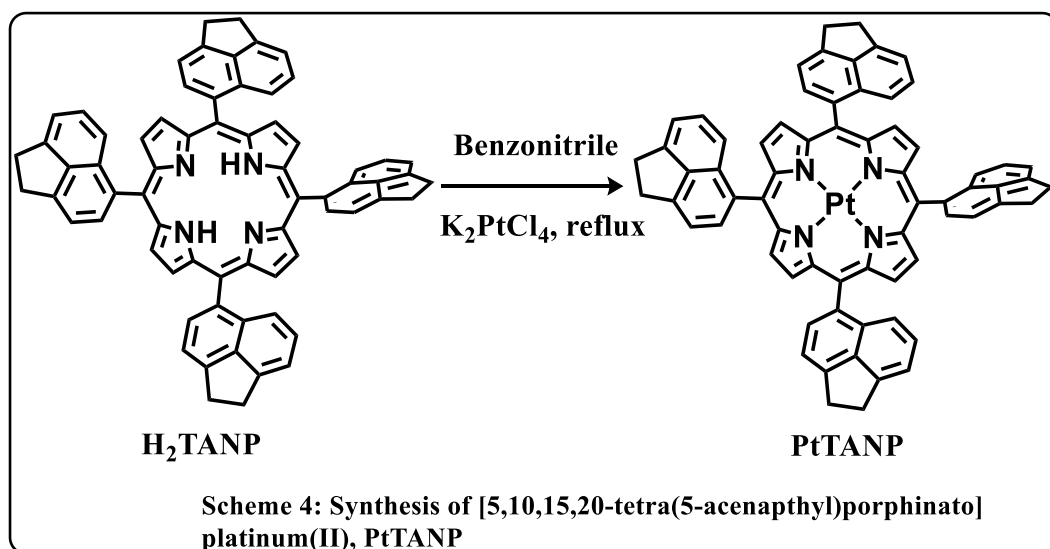
The newly synthesized  $N^{21}$ ,  $N^{22}$ -methylene-corrole derivative, **1** can resemble nicely with the previously reported 21,22-methyleneoctaethylporphyrin. Thus, it is obvious that the novel methylene-corrole derivative and its various metal complexes will be of great interest to study further.



Chapter 4 Synthesis, structure, photophysics, and singlet oxygen sensitization by a platinum(II) porphyrin complex:



Present work describes the synthesis of a novel platinum(II) porphyrin complex [5,10,15,20-tetra(5-acenaphthyl)porphinato]platinum(II), PtTANP with acenaphthyl substitution at the meso position of the porphyrin ring. Free base ligand 5,10,15,20-tetra(5-acenaphthyl) porphyrin, H<sub>2</sub>TANP reacted with platinum precursor complex K<sub>2</sub>PtCl<sub>4</sub> in benzonitrile solution and resulted [5,10,15,20-tetra(5-acenaphthyl)porphinato] platinum(II), PtTANP (Scheme 4).



The purity and identity of the platinum (II) complex, PtTANP is established by its satisfactory elemental analyses, ESI-MS data, NMR, UV-Vis, emission, and single-crystal XRD data. Single-crystal XRD analysis reveals that the geometry around the Pt(II) center is near the perfect square planar geometry. The deviation of Platinum atom from the mean N<sub>4</sub> porphyrin plane is 0.0031 Å, The Pt(II)-N bond distances are in the ranges of 2.005 Å–2.020 Å (Figure 3). The PtTANP derivative exhibited one reversible oxidative couple at +1.10 V and a reversible reductive couple at -1.47 V versus Ag/AgCl (Figure 4).

In deaerated solution, a strong red phosphorescence is observed with emission quantum yield as high as 35% and emission lifetime of 75  $\mu$ s. In air-equilibrated solution PtTANP displays a very weak phosphorescence ( $\Phi_{em} = 0.22\%$ ) with

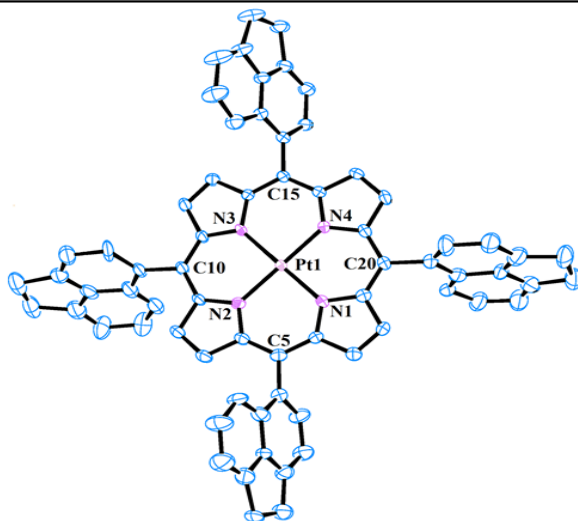


Figure 3: ORTEP diagram of PtTANP. Ellipsoids are drawn at 40% probability

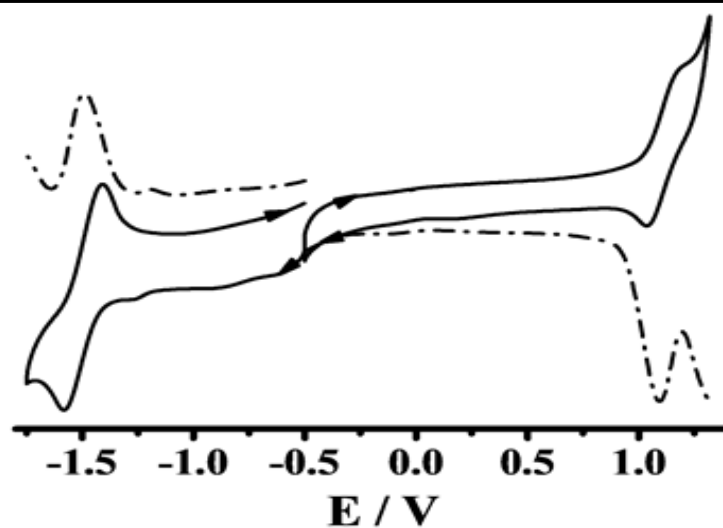
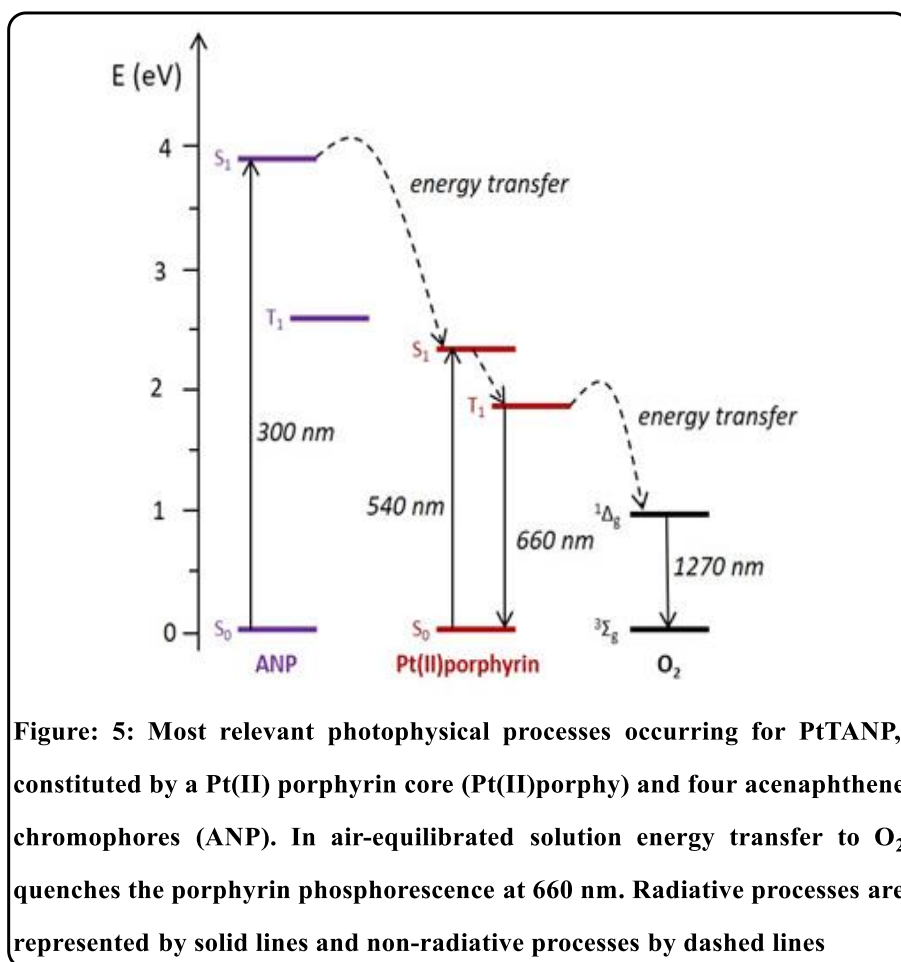


Figure 4: Cyclic voltammogram (black solid line) and differential pulse voltammogram (black dotted line) of PtTANP in dichloromethane under a nitrogen atmosphere. The potentials are vs. Ag/AgCl.

a much shorter lifetime ( $\Phi_{em} = 910$  ns). The PtTANP phosphorescence is strongly quenched by oxygen with a rate constant of  $4.9 \times 10^8 \text{ M}^{-1}\text{s}^{-1}$ . The quenching by oxygen consequences singlet oxygen production with a strong quantum yield of 88%.<sup>13</sup> As a result PtTANP works as a light-harvesting antenna as schematically depicted in Figure 5: upon UV excitation of acenaphthene chromophores, energy transfer to the Pt(II) porphyrin core takes place with unitary efficiency resulting in photosensitized phosphorescence. It was also established that the PtTANP molecule is an excellent photosensitizer with a singlet oxygen production quantum yield of 88% in dichloromethane. These results indicate that the PtTANP molecule will have potential applications in the field of photodynamic therapy as well as oxygen sensors.



### References:

1. A. R. Battersby, C. Fookes, G. Matcham, E. McDonald, *Nature*. **1980**, 285, 17-21
2. K. M. Kadish, K. M. Smith, R. Guilard and Editors, *The Porphyrin Handbook; Volume 2, Heteroporphyrins, Expanded Porphyrins and Related Macrocycles*, Academic Press, **2000**.
3. A. Johnson, I. Kay, *J. Chem. Soc.* **1965**, 1620-1629.
4. Z. Gross, N. Galili, L. Simkhovich, I. Saltsman, M. Botoshansky, D. Blaeser, R. Boese, I. Goldberg, *Org. Lett.* **1999**, 1, 599-602.
5. R. Paolesse, L. Jaquinod, D. J. Nurco, S. Mini, F. Sagone, T. Boschi, K. M. Smith, *Chem. Commun.* **1999**, 1307–1308.
6. J. L. Sessler, S. J. Weghorn, *Expanded, contracted & isomeric porphyrins. Elsevier: 1997; Vol. 15*.
7. I. Aviv-Harel, Z. Gross, *Chem. Eur. J.* **2009**, 15, 8382-8394.
8. I. Saltsman, I. Goldberg, Z. Gross, *Tetrahedron Lett.* **2003**, 44, 5669-5673.
9. S. K. Patra, K. Sahu, B. Patra, D. K. Sahoo, S. Mondal, P. Mukherjee, H. S. Biswal, S. Kar, *Green Chem.*, **2017**, 19, 5772–5776.
10. S. K. Patra, K. Sahu, B. Patra, S. Mondal, S. Kar, *Eur. J. Org. Chem.* **2018**, 6764–6767.
11. A. Ghosh, *Chem. Rev.* **2017**, 117, 3798-3881.
12. R. Orłowski, D. Gryko and D. T. Gryko, *Chem. Rev.* **2017**, 117, 3102–3137.
13. C.M. Che, Y.J. Hou, M.C. Chan, J. Guo, Y. Liu and Y. Wang, *J. Mater. Chem.*, **2003**, 13, 1362-13

## List of Figures

		Page no:
1.	Figure 1.1: Structures of biological significant tetrapyrrolic macrocycle	35
2.	Figure 1.2: Parent structure of porphyrin, porphin	36
3.	Figure 1.3: Core and peripheral modifications of porphyrin	40
4.	Figure 1.4: Various contracted porphyrinoids	41
5.	Figure 1.5: Structural comparison between porphyrin, corrole and corrin	44
6.	Figure 1.6: Different types of meso substituted corrole	48
7.	Figure 1.7: Example of some heterocorrole framework	53
8.	Figure 1.8: Metallocorroles act as oxidation catalysts	65
9.	Figure 1.9: Metallocorroles used as reduction catalysts	66
10.	Figure 1.10: Some examples of iron and rhodium corroles were used as cyclopropanation catalysts.	67
11.	Figure 1.11: example of some Cobalt (III) corrole studied as CO sensing	68
12.	Figure 1.12: First water-soluble corrole reported in vivo medicinal investigation.	70
13.	Figure 1.13: Metal complexes used in dye-sensitized solar cells	71
14.	Figure 2.1: Structures of the FB corroles 1A-4A and the corresponding carbamide- corrole derivatives 1B-4B.	86
15.	Figure 2.2: Structures of the FB corroles 5A-7A and the corresponding carbamide- corrole derivatives 5B-7B	87
16.	Figure 2.3: $^1\text{H}$ NMR spectrum of $\text{N}^{21}, \text{N}^{22}$ -carbamide-5,10,15-triphenylcorrole, 1B in $\text{CDCl}_3$	91

<b>17.</b>	Figure 2.4: $^{13}\text{C}$ NMR spectrum of $\text{N}^{21},\text{N}^{22}$ -carbamide -5,10,15-triphenylcorrole, 1B in $\text{CDCl}_3$	<b>92</b>
<b>18.</b>	Figure 2.5: $^1\text{H}$ NMR spectrum of $\text{N}^{21},\text{N}^{22}$ carbamide- 10-(2,4,5-trimethoxyphenyl)5,15-bis-(4-cyanophenyl)corrole, 2B in $\text{CDCl}_3$	<b>92</b>
<b>19.</b>	Figure 2.6: $^1\text{H}$ NMR spectrum of $\text{N}^{21},\text{N}^{22}$ -carbamide-10-(4,7- dimethoxynaphthalen-1-yl)-5,15-bis(4-cyanophenyl)corrole, 3B in $\text{CDCl}_3$	<b>93</b>
<b>20.</b>	Figure 2.7: $^1\text{H}$ NMR spectrum of $\text{N}^{21},\text{N}^{22}$ -carbamide-5,10,15-tris(4-benzyloxyphenyl)corrole, 4B in $\text{CDCl}_3$	<b>93</b>
<b>21.</b>	Figure 2.8: $^1\text{H}$ NMR spectrum of $\text{N}^{21},\text{N}^{22}$ -carbamide- 5,10,15-tris(4-cyanophenyl)corrole, 5B in $\text{CDCl}_3$	<b>94</b>
<b>22.</b>	Figure 2.9: $^{13}\text{C}$ NMR spectrum of $\text{N}^{21},\text{N}^{22}$ -carbamide- 5,10,15-tris(4-cyanophenyl)corrole, 5B in $\text{CDCl}_3$	<b>94</b>
<b>23.</b>	Figure 2.10: $^1\text{H}$ NMR spectrum of 6B $\text{N}^{21},\text{N}^{22}$ -carbamide- 5,10,15-tris-(2-bromo-5-fluorophenyl)corrole, in $\text{CDCl}_3$	<b>95</b>
<b>24.</b>	Figure 2.11: $^1\text{H}$ NMR spectrum of $\text{N}^{21},\text{N}^{22}$ -carbamide- 5,10,15-tris(4-nitrophenyl)corrole, 7B in $\text{CDCl}_3$	<b>95</b>
<b>25.</b>	Figure 2.12: FT-IR spectrum of 1B (a), 2B (b) and 3B (c) as a KBr pellet.	<b>96</b>
<b>26.</b>	Figure 2.13: FT-IR spectrum of 4B (a), 5B (b) and 6B (c) as a KBr pellet.	<b>97</b>
<b>27.</b>	Figure 2.14: FT-IR spectrum of 7B as a KBr pellet.	<b>98</b>
<b>28.</b>	Figure 2.15: Electronic absorption spectrum of 1B (a), 2B (b) and 3B (c) in toluene.	<b>99</b>
<b>29.</b>	Figure 2.16: Electronic absorption spectrum of 4B (a), 5B (b) and 6B (c) in toluene	<b>100</b>
<b>30.</b>	Figure 2.17: Electronic absorption spectrum	<b>101</b>

	of 7B in dichloromethane	
<b>31.</b>	Figure 2.18: Electronic emission spectrum (excited at the Soret band) of 1B(a), 2B(b) and 3B(c) in toluene	<b>102</b>
<b>32.</b>	Figure 2.19: Electronic emission spectrum (excited at The Soret band) of 4B (a), 5B (b) and 6B (c) in toluene.	<b>103</b>
<b>33.</b>	Figure 2.20: Electronic emission spectrum (excited at the Soret band) of 7B in toluene.	<b>104</b>
<b>34.</b>	Figure 2.21: ESI- MS spectrum of 1B in CH <sub>3</sub> CN shows the measured spectrum with isotopic distribution pattern	<b>104</b>
<b>35.</b>	Figure 2.22: ESI- MS spectrum of 2B in CH <sub>3</sub> CN shows the measured spectrum with isotopic distribution pattern	<b>105</b>
<b>36.</b>	Figure 2.23: ESI- MS spectrum of 3B in CH <sub>3</sub> CN shows the measured spectrum with isotopic distribution pattern.	<b>105</b>
<b>37.</b>	Figure 2.24: ESI- MS spectrum of 4B in CH <sub>3</sub> CN shows the measured spectrum with isotopic distribution pattern	<b>106</b>
<b>38.</b>	Figure 2.25: ESI- MS spectrum of 5B in CH <sub>3</sub> CN shows the measured spectrum with isotopic distribution pattern	<b>107</b>
<b>39.</b>	Figure 2.26: ESI- MS spectrum of 6B in CH <sub>3</sub> CN shows the measured spectrum with isotopic distribution pattern	<b>107</b>
<b>40.</b>	Figure 2.27: ESI- MS spectrum of 7B in CH <sub>3</sub> CN shows the measured spectrum with isotopic distribution pattern.	<b>108</b>
<b>41.</b>	Figure 2.28: Perspective view of 3B. Hydrogen atoms are omitted for clarity.	<b>108</b>
<b>42.</b>	Figure 2.29: Single-crystal X-ray structure of 5B	<b>109</b>

<b>43.</b>	Figure 2.30: Single-crystal X-ray structure of <b>7B</b>	<b>109</b>
<b>44.</b>	Figure 2.31: DFT optimized (B97-d/6-31G*) structure of <b>7B</b>	<b>111</b>
<b>45.</b>	Figure 2.32: (a) IR spectrum of <b>1B</b> : Experimentally recorded FT-IR spectrum (—) and IR spectrum (—) obtained from DFT (B97-D/6-31G*) computation (scaling factor; 0.972, Lorentzian broadening with FWHM ~ 25 cm <sup>-1</sup> ); (b) UV-Vis spectra of <b>1B</b> : Experimental UV-Vis absorption spectrum (—) and TDDFT (TD-B97D/6-31G*)-based absorption spectrum (—) (Lorentzian broadening with FWHM ~ 25 nm); (c) HOMOs and LUMOs responsible for electronic transitions.	<b>121</b>
<b>46.</b>	Figure 3.1: <sup>1</sup> H NMR spectrum of <b>1</b> in C <sub>6</sub> D <sub>6</sub>	<b>139</b>
<b>47.</b>	Figure 3.2: <sup>19</sup> F NMR spectrum of <b>1</b> in C <sub>6</sub> D <sub>6</sub>	<b>140</b>
<b>48.</b>	Figure 3.3: <sup>13</sup> C NMR spectrum of <b>1</b> in C <sub>6</sub> D <sub>6</sub>	<b>140</b>
<b>49.</b>	Figure 3.4: <sup>1</sup> H NMR spectrum of <b>2</b> in C <sub>6</sub> D <sub>6</sub>	<b>141</b>
<b>50.</b>	Figure 3.5: Perspective view of <b>1</b> . Hydrogen atoms are omitted for clarity	<b>142</b>
<b>51.</b>	Figure 3.6: FT-IR spectrum of <b>1</b> as a KBr pellet	<b>144</b>
<b>52.</b>	Figure 3.7: ESI- MS spectrum of <b>1</b> in CH <sub>3</sub> CN shows the measured spectrum with isotopic distribution pattern	<b>144</b>
<b>53.</b>	Figure 3.8: ESI- MS spectrum of <b>2</b> in CH <sub>3</sub> CN shows the measured spectrum with isotopic distribution pattern	<b>145</b>
<b>54.</b>	Figure 3.9: Electronic emission spectrum (excited at the Soret band) of <b>1</b> in toluene	<b>146</b>
<b>55.</b>	Figure 3.10 Electronic absorption (black line) and emission	<b>146</b>

	spectrum (red line) of <b>1</b> in toluene ( $\lambda_{\text{ex}} = 420 \text{ nm}$ )	
<b>56.</b>	Figure 3.11: Fluorescence decay profiles of (a) <b>1A</b> , $\lambda_{\text{em}} = 646 \text{ nm}$ , and (b) <b>1</b> , $\lambda_{\text{em}} = 631 \text{ nm}$ . The black line represents experimental data, whereas the red line represents best fit.	<b>148</b>
<b>57.</b>	Figure 4.1: Structure of the [5,10,15,20-tetra(5-acenaphthyl) porphinato] platinum(II), PtTANP	<b>159</b>
<b>58.</b>	Figure 4.2: $^1\text{H}$ NMR spectrum of PtTANP in $\text{CDCl}_3$	<b>160</b>
<b>59.</b>	Figure 4.3: $^{13}\text{C}$ NMR spectrum of PtTANP in $\text{CDCl}_3$	<b>161</b>
<b>60.</b>	Figure 4.4: ESI- MS spectrum of PtTANP in $\text{CH}_3\text{CN}$ shows the measured spectrum with isotopic distribution pattern.	<b>162</b>
<b>61.</b>	Figure 4.5: Single-crystal X-ray structure of PtTANP. Hydrogen atoms are omitted for clarity	<b>164</b>
<b>62.</b>	Figure 4.6: ORTEP diagram of PtTANP. Ellipsoids are drawn at 40% probability	<b>164</b>
<b>63.</b>	Figure 4.7: Cyclic voltammogram (black solid line) and differential pulse voltammogram (black dotted line) of PtTANP in dichloro- methane under a nitrogen atmosphere. The potentials are vs $\text{Ag}/\text{AgCl}$ .	<b>166</b>
<b>64.</b>	Figure 4.8: Absorption spectra and emission spectra of PtTANP in dichloromethane and toluene air-equilibrated solution.	<b>168</b>
<b>65.</b>	Figure 4.9: Absorption and excitation spectra ( $\lambda_{\text{em}} = 680 \text{ nm}$ ) of PtTANP in air-equilibrated dichloromethane solution	<b>168</b>
<b>66.</b>	Figure 4.10: Absorption spectra in absorption coefficient (black solid line), emission spectra in deaerated (red solid line) dichloro methane solution of PtTANP ( $\lambda_{\text{exc}} = 400 \text{ nm}$ ) at 298K.	<b>169</b>

Emission spectra in a rigid matrix of DCM-MeOH 1:1  
at 77K (dashed blue line)

- 67.** Figure 4.11: Most relevant photophysical processes occurring **170**  
for PtTANP, constituted by a Pt (II) porphyrin core  
(Pt(II)porphy) and four acenaphthene chromophores (ANP).  
In air-equilibrated solution energy transfer to O<sub>2</sub> quenches  
the porphyrin phosphorescence at 660 nm. Radiative  
processes are represented by solid lines and non-radiative  
processes by dashed lines
- 68.** Figure 4.12: Oxygen emission spectra of an air-equilibrated **172**  
dichloromethane solution of perinaphthenone (black line)  
and PtTANP (red line)

## List of Tables

<b>1.</b>	Table 2.1: Isolated yield of product	<b>89</b>
<b>2.</b>	Table 2.2: UV–Vis. Data	<b>101</b>
<b>3.</b>	Table 2.3: Crystallographic Data for 3B, 5B and 7B	<b>110</b>
<b>4.</b>	Table 2.4: Selected X-ray and DFT calculated (B97-D/6-31G*) bond distances (Å) and angles (deg) for 7B	<b>112</b>
<b>5.</b>	Table 2.5: Comparision experimental and computed UV-Vis trasitions of 1B-7B	<b>119</b>
<b>6.</b>	Table 2.6: A comparison of experimental and computed CO stretching frequencies of 1B-7B. A scaling factor of 0.972 is used for the computed vibrational frequencies	<b>120</b>
<b>7.</b>	Table 3.1: Optimization for the formation of $N^{21}$ , $N^{22}$ - Methylene– Bridged Corrole (1A to 1)	<b>138</b>
<b>8.</b>	Table 3.2: Important crystallographic parameters for 1.	<b>142</b>
<b>9.</b>	Table 3.3: Absorption spectral values of Soret and Q bands of 1 in various solvents	<b>147</b>
<b>10.</b>	Table 4.1: Crystallographic data for PtTANP	<b>165</b>
<b>11.</b>	Table 4.2: UV–Vis and electrochemical data	<b>167</b>
<b>12.</b>	Table 4.3: Most relevant photophysical data of PtTANP in air-equilibrated dichloromethane solution. Data in parenthesis refer to deaerated solution	<b>171</b>

## List of Scheme

		Page no:
1.	Scheme 1.1: Synthesis of tetraphenyl porphyrin	37
2.	Scheme 1.2: Synthesis of tetraphenyl porphyrin by Adler-Longo method.	37
3.	Scheme 1.3: Tetraphenyl porphyrin synthesis	38
4.	Scheme 1.4: Synthesis of Subphthalocyanines	41
5.	Scheme 1.5: Synthesis of tribenzosubporphine	42
6.	Scheme 1.6: Synthesis of isocorrole	42
7.	Scheme 1.7: Synthesis of isocorrole	43
8.	Scheme 1.8: Synthetic route for iron norcorrole	43
9.	Scheme 1.9: First synthesis of corrole by Johnson and Kay	46
10.	Scheme 1.10: condensation of Bipyrollic unit by Conlon <i>et al.</i>	47
11.	Scheme 1.11: Synthetic route of 5,10,15-Triphenylcorrole by modified Rothmund reaction	49
12.	Scheme 1.12: Synthesis of 5,10,15-tris(pentafluorophenyl) corrole	50
13.	Scheme 1.13: Meso-substituted A <sub>3</sub> -corrole in water methanol medium by Koszarna and Gryko	51
14.	Scheme 1.14: Synthesis of corrole from DPM and aldehyde by Koszarna and Gryko	51
15.	Scheme 1.15: Synthesis of cis A <sub>2</sub> B corrole by Osuka <i>et al.</i>	52
16.	Scheme 1.16: Synthetic scheme for 10-aza corroles	53
17.	Scheme 1.17: First convenient synthetic route for 21 oxa corrole	54

<b>18.</b>	Scheme 1.18: First reported 22-oxacorrole by Chandrashekar and co-workers	<b>55</b>
<b>19.</b>	Scheme 1.19: Synthetic scheme for meso substituted 21,23 oxa-corrole	<b>55</b>
<b>20.</b>	Scheme 1.20: N-confused and neo-confused corroles synthesis	<b>56</b>
<b>21.</b>	Scheme 1.21: Conversion of free base corrole to metallocorroles	<b>57</b>
<b>22.</b>	Scheme 1.22: N-alkylation of $\beta$ -substituted corroles	<b>60</b>
<b>23.</b>	Scheme 1.23: Preparation of chiral corroles derivative	<b>61</b>
<b>24.</b>	Scheme 1.24: Synthesis of $\beta$ -chlorinated corrole	<b>61</b>
<b>25.</b>	Scheme 1.25: Vilsmeier-Haack formylation of corrole	<b>62</b>
<b>26.</b>	Scheme 1.26: Selective nitration of Ga (III) corrole	<b>62</b>
<b>27.</b>	Scheme 1.27: Synthesis of $\beta$ -carboxy triaryl corroles	<b>63</b>
<b>28.</b>	Scheme 1.28: selective chlorosulphonation of corrole	<b>64</b>
<b>29.</b>	Scheme 1.29: Mechanism for activation of molecular oxygen 92 (A) and decomposition of peroxyxynitrite 85(B)	<b>68</b>
<b>30.</b>	Scheme 2.1: Synthetic application of $N^{21}$ , $N^{22}$ -carbamide- corroles	<b>85</b>
<b>31.</b>	Scheme 2.2: Scope of the synthesis of carbamide-corrole derivatives	<b>88</b>
<b>32.</b>	Scheme 2.3: Proposed mechanism	<b>90</b>
<b>33.</b>	Scheme 3.1: Structures of the $N^{21}$ , $N^{22}$ -methylene-corrole derivatives $N^{21}$ , $N^{22}$ methylene-5,10,15- tris(pentafluorophenyl) corrole, 1, and $N^{21}$ , $N^{22}$ methylene-d2-5,10,15- tris(pentafluorophenyl) corrole, 2	<b>136</b>
<b>34.</b>	Scheme 3.2: Synthetic application of $N^{21}$ , $N^{22}$ methylene-5,10,15- tris(pentafluorophenyl) corrole, 1.	<b>137</b>
<b>35.</b>	Scheme 4.1: Synthesis of [5,10,15,20-tetra(5-acenaphthyl) porphinato] platinum(II), PtTANP	<b>160</b>

## *List of Abbreviations*

<i>Acronyms</i>	<i>Full Name</i>
$^1\text{H}$ NMR	Proton Nuclear Magnetic Resonance
DDQ	2,3-Dichloro-5,6-dicyano-1,4-benzoquinone
$\text{CH}_2\text{Cl}_2$	Dichloromethane
$\text{CHCl}_3$	Chloroform
$^{13}\text{C}$ NMR	Carbon-13 Nuclear Magnetic Resonance
$^{19}\text{F}$ NMR	Fluorine-19 Nuclear Magnetic Resonance
EPR	Electron Paramagnetic Resonance
UV-Vis	Ultraviolet–Visible
NIR	Near-Infrared
DFT	Density Functional Theory
TD-DFT	Time-Dependent Density Functional Theory
HCl	Hydrogen chloride
TFA	Trifluoroacetic acid
$\text{NaNO}_2$	Sodium nitrite
GOF	Goodness of Fit
CCDC	Cambridge Crystallographic Data Centre
TBAP	Tetrabutylammonium perchlorate
$\text{FeCl}_3$	Ferric chloride
Chloranil	tetrachloro-1,4-benzoquinone
HOMO	Highest Occupied Molecular Orbital
HBr	Hydrogen bromide
LUMO	Lowest Unoccupied Molecular Orbital

Anal. Calcd	Analytically Calculated
CH <sub>3</sub> CN	Acetonitrile
FB	Free-Base
TLC	Thin Layer Chromatography
ESI	Electrospray Ionization
CH <sub>3</sub> OH	Methanol
KOH	Potassium hydroxide
CaH <sub>2</sub>	Calcium hydride
KBr	Potassium bromide
expt.	Experimental
Φ	Quantum yield
CO	Carbon Monoxide
Na <sub>2</sub> SO <sub>4</sub>	Sodium sulphate
CD <sub>2</sub> I <sub>2</sub>	Dideuteromethyleneiodide
Cu(OAc) <sub>2</sub> .H <sub>2</sub> O	Copper acetate monohydrate
Co(OAc) <sub>2</sub>	Cobalt acetate
Bu <sub>4</sub> NPF <sub>6</sub>	Tetrabutylammonium hexafluorophosphate
TiO <sub>2</sub>	Titanium dioxide
EtOH	Ethanol
ε	Molar absorption coefficient
NaBH <sub>4</sub>	Sodium borohydride
H <sub>3</sub> TPFC	5,10,15-tris(pentafluorophenyl)corrole
CDCl <sub>3</sub>	Deuterated chloroform

# ***CHAPTER 1***

## ***Emergence and Modifications of corrole***

### **1.1 Introduction**

### **1.2 Nomenclature of porphyrin like system**

### **1.3 Spectroscopic characterization**

### **1.4 Structural Modifications of Porphyrins**

### **1.5 Emergence of corrole**

### **1.6 Various contracted porphyrins and their synthetic protocols**

#### **1.6.1 Subphthalocyanines**

#### **1.6.2 Subporphyrins**

#### **1.6.3 Isocorrole**

#### **1.6.4 Norcorrole**

#### **1.6.5 Corrole**

##### **1.6.5.1 Properties of corrole**

##### **1.6.5.2 Synthesis of corrole**

### **1.7 Core modified corroles and their synthesis**

## **1.8 Metallocorrole and its different coordinations modes**

## **1.9 Functionalization of corrole**

### **1.9.1 Inner core functionalization**

### **1.9.2 Peripheral functionalization of corrole**

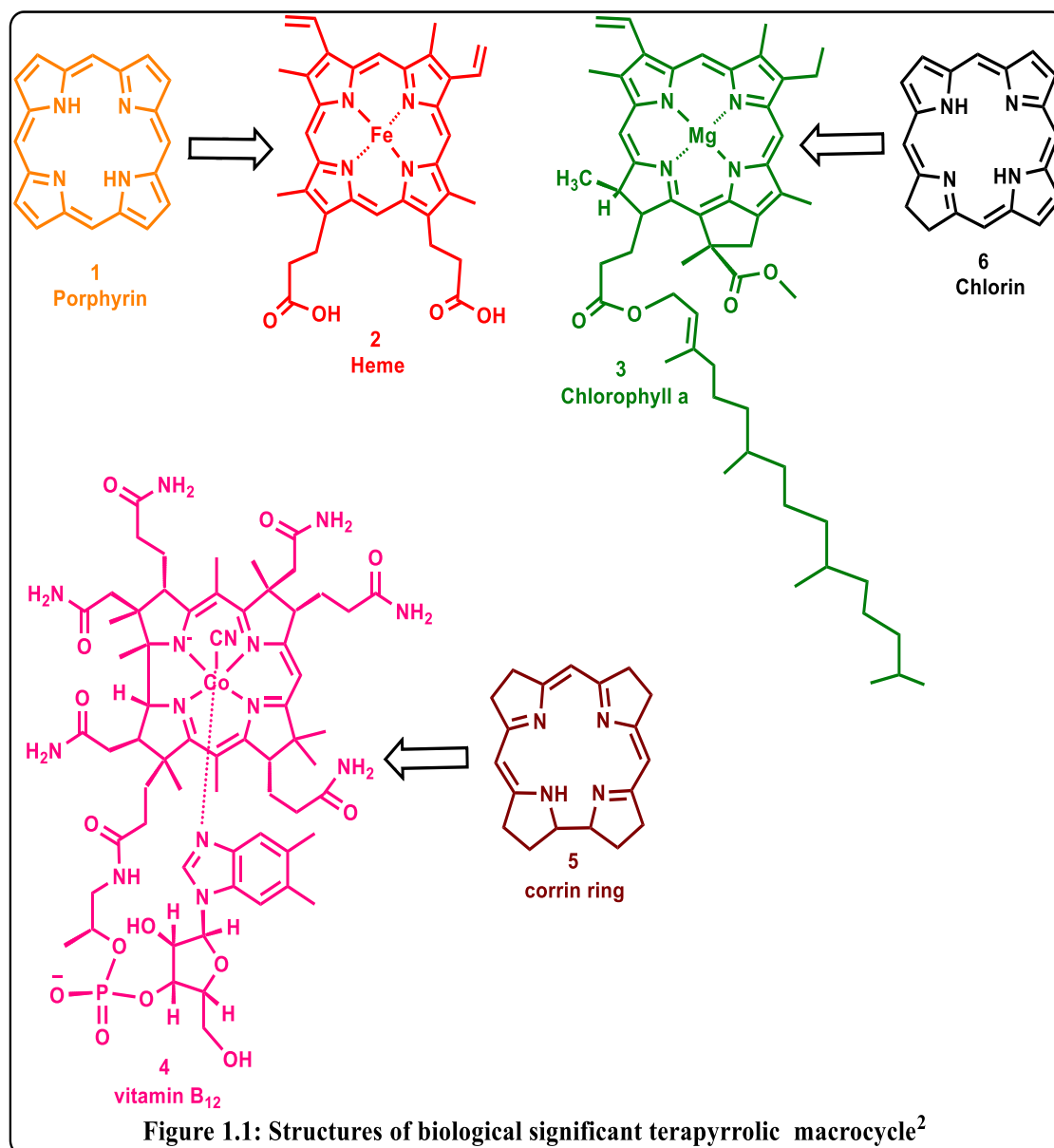
## **1.10 Corrole and Metallocorrole based application**

## **1.10 Objective of my thesis**

## 1.1 Introduction:

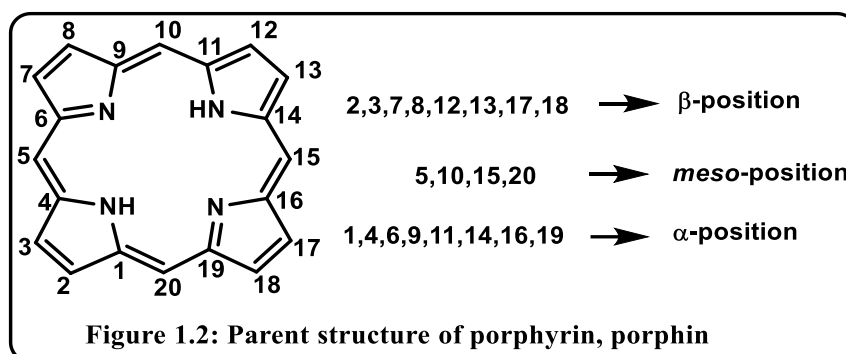
The chemistry of porphyrins or their metal derivative has now become a widely studied area due to their ubiquitous nature and pivotal role in sustaining life on earth. Porphyrin, **1** (Figure 1.1), the naturally occurring tetrapyrrolic macrocycle, take part in innumerable essential biological activities. The important porphyrin derivatives which are responsible for the survival of life on earth are heme, **2** (Figure 1.1) chlorophyll, **3** (Figure 1.1) and vitamin B<sub>12</sub> coenzyme, **4** (Figure 1.1). These are essentially termed as the pigment of life<sup>1</sup>. Various biological functions like oxygen-carrying and storage, electron transfer and photosynthesis<sup>2</sup> in plants are controlled by porphyrin derivative or its analogues. Besides, it is also an efficient sensitizer for photodynamic therapeutic application, shows nonlinear optical properties and also used in catalysis reactions. Therefore, researchers try to synthesize different porphyrin and metalloporphyrin derivative to mimic these complex biological activities. The term porphyrin is obtained from a Greek word 'porphyrus' which means bright and purple. Porphyrin and its derivative are exceptionally coloured and show a powerful absorption band in the visible region. In porphyrins, four pyrrole rings are connected by four sp<sup>2</sup> hybridized carbon atom and are extremely conjugated system. The primary porphyrin nucleus is a C<sub>20</sub> porphin core. Although porphyrins are 22 $\pi$  electron system, only 18 $\pi$  electrons are in the shortest conjugation obeying Huckel's rule of aromaticity. This (4n+2)  $\pi$  electron produces a strong ring current across the macro cyclic core. <sup>1</sup>H NMR spectra of porphyrin are surprising of a very broad range due to large magnetic anisotropy. Inner NH protons resonate at a very high field, whereas peripheral protons (*meso* and  $\beta$ ) comes to resonate at a very low field.

**1.2 Nomenclature of porphyrin like system:** In porphyrin inner core, there are two types of nitrogen atoms, two amino (-NH) and two imino nitrogen<sup>3</sup>. At the time of uncovering, the porphyrinoids were identified by their trivial name based on colour,



size or number of heterocyclic rings followed by the suffixes phyrin or rin. The name Sapphrin is coming from the blue colour of its crystal<sup>5</sup>. A similar trend is maintained for rubirin, which is red coloured. Pentaphyrin and hexaphyrin are termed concerning five and six pyrrole rings, respectively. At first, Franck and Nonn<sup>6</sup> generalized the

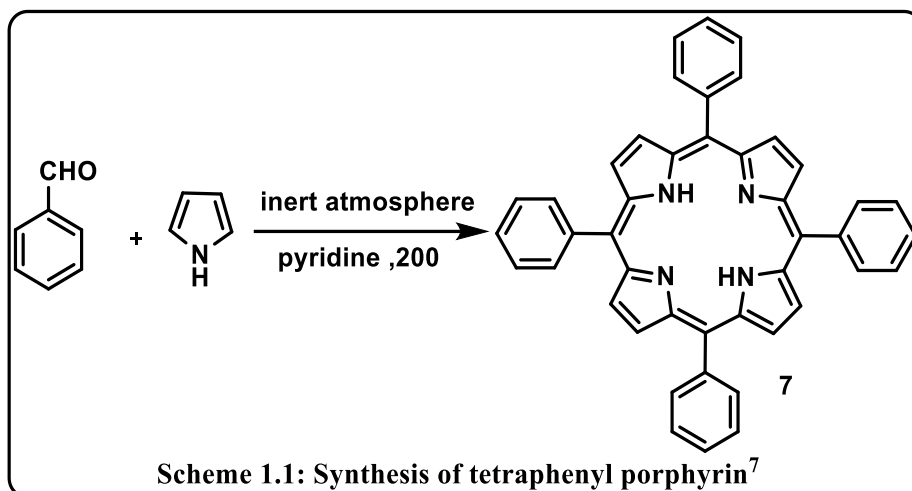
porphyrin nomenclature on the basis of three aspects (a) General name is considered on the basis of a total number of pyrrole rings. (b) Total no of electrons that are in conjugation are designated inside the square bracket. (c) The number of bridging carbon atoms that are connecting the heterocyclic ring also mentioned in the first bracket separated by dot.<sup>3</sup>



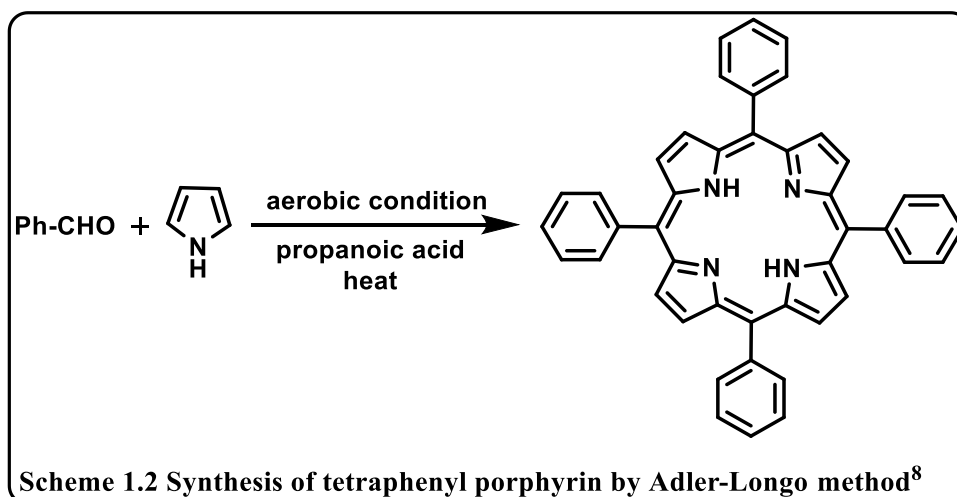
#### The general synthetic protocol of porphyrin:

**Rothemund method:** The first synthesis of porphyrin (Scheme 1.1) by Rothemund<sup>7</sup> in 1935, inspired several researchers around the globe to work on the area of the tetra pyrrolic macrocycles to their peculiar photophysical properties and wide range of applications. This method for synthesis of *meso*-substituted porphyrins is straightforward which involves condensation reaction of pyrrole and aldehyde in the presence of pyridine at high temperature in a sealed bomb without using any oxidant. The main limitation of this method is the low yield of the product as the reaction conditions are too harsh.

**Adler-Longo Method:** Limitations of Rothemund's method were addressed by Adler and Longo<sup>8</sup> in 1967 (Scheme 1.2). Instead of inert condition, they performed the reaction in aerobic condition refluxing pyrrole and aldehyde in propionic acid. This is



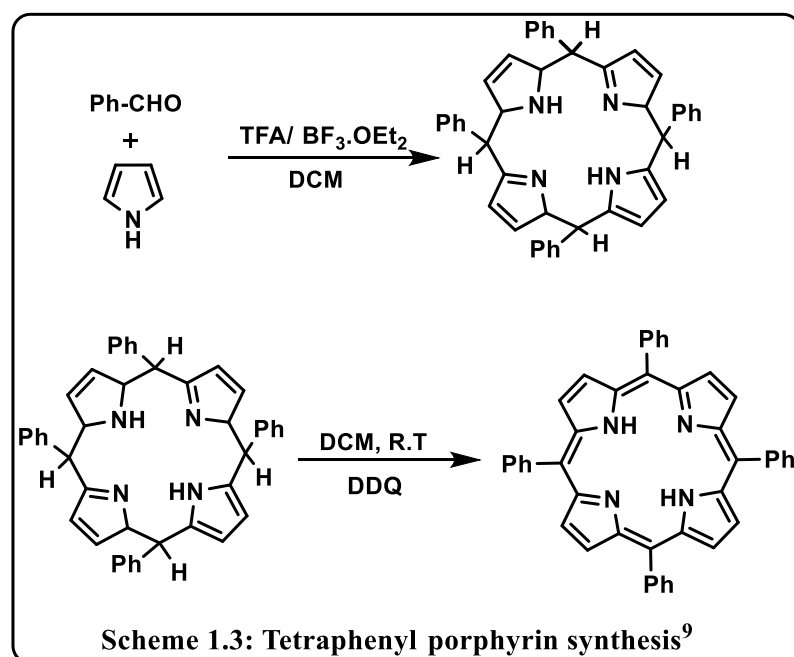
very much malleable procedure for unsymmetrical porphyrin synthesis. But this methodology is inapplicable for porphyrin synthesis for aldehydes containing acid-sensitive group.



**Lindsey Method:** Lindsey<sup>9</sup> developed a modified one-pot two-step methodology (Scheme 1.3) describing the reaction of equimolar pyrrole and benzaldehyde, which was mediated in the presence of trifluoroacetic acid or boron trifluoride in inert condition. In the initial step, porphyrinogen intermediate was formed, and then this intermediate irreversibly converted into tetraphenylporphyrin in the presence of an oxidant such as chloranil or DDQ.

### 1.3 Spectroscopic characterization:

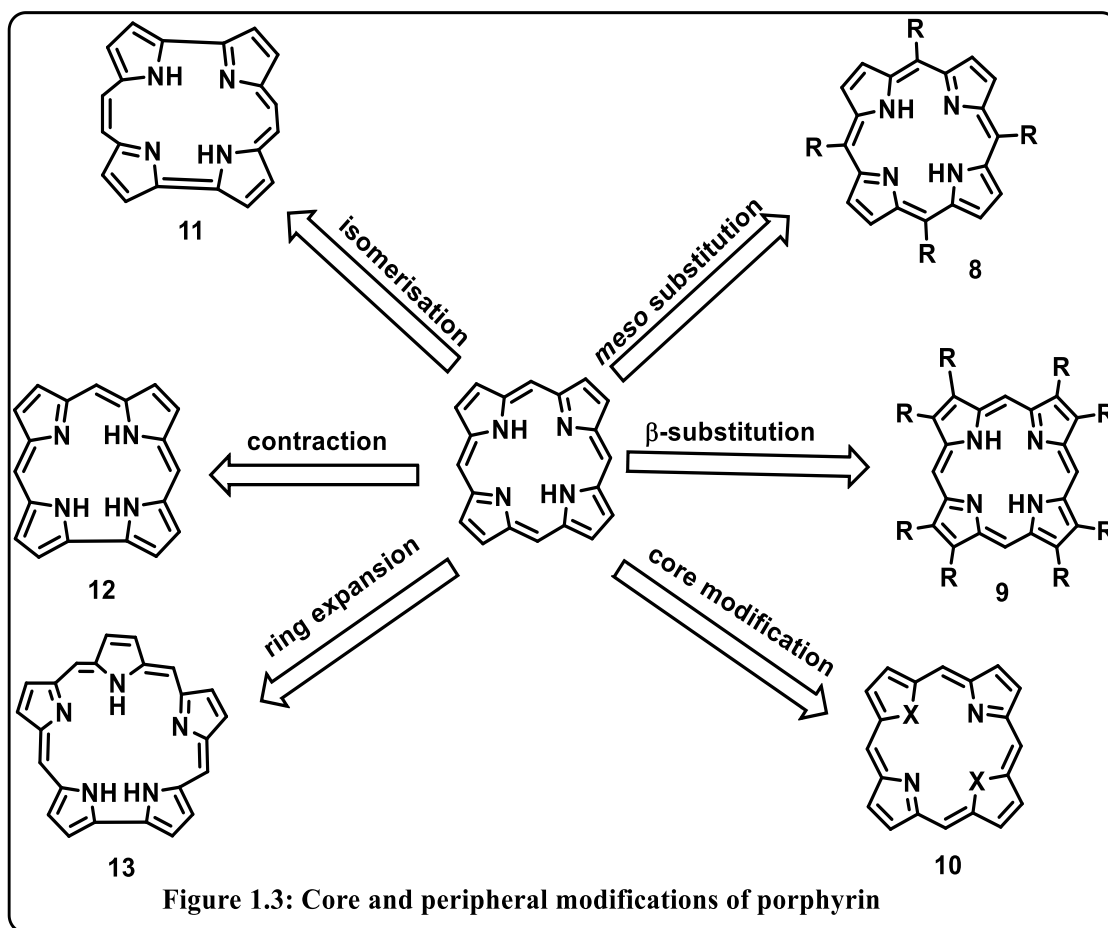
Porphyrin exhibits extreme colour owing to its strong light absorption. The most fascinating property of porphyrins is their characteristic UV-VIS spectra. Its symmetry makes its spectra so interesting. It shows strong absorption with a high value of molar extinction coefficient in the region of 400 nm, which is termed as Soret band and four Q like band<sup>10,11</sup> with lower  $\epsilon$  values in the region of 450 nm to 700 nm.



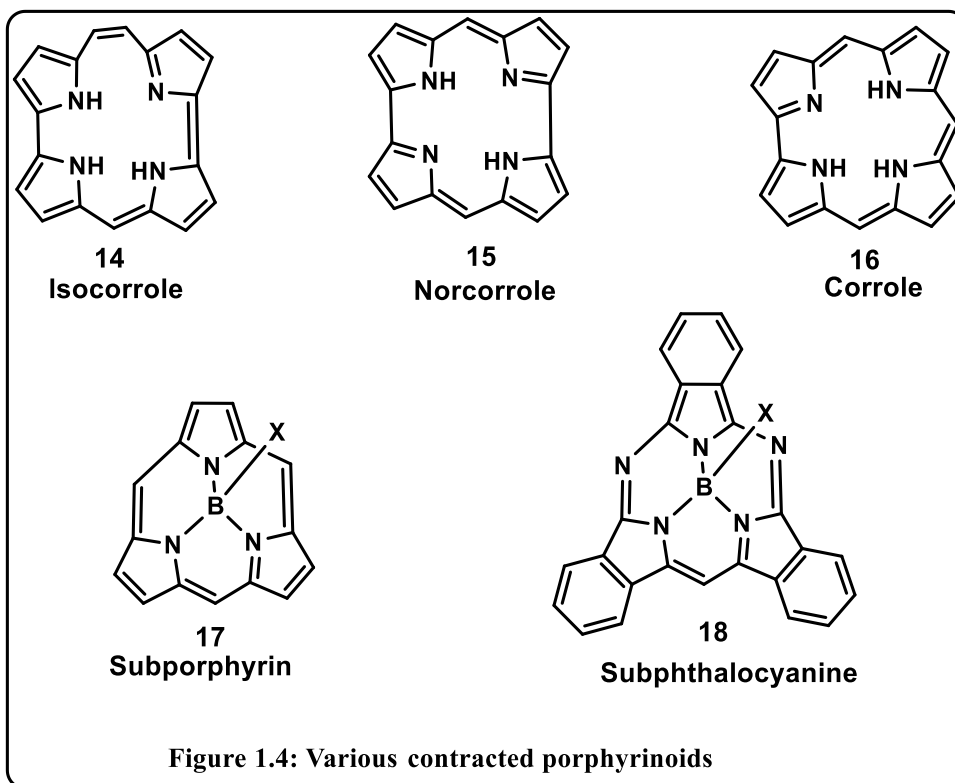
**1.4 Structural Modifications of Porphyrins:** With their unique properties and applicability in various field of science, porphyrins are the hot topic of research. This motivates researchers to flourish the novel porphyrinoids (Figure 1.3) with several well-defined types of modification in the porphyrin nucleus. These structural changes lead to tune the electronic structure resulting in its various functions and applications in different fields. Two primary techniques for the above-mentioned purpose are substitution at meso positions and  $\beta$ - position at the porphyrin ring<sup>3</sup>. Among the two,  $\beta$ -substituted porphyrins **9** (Figure 1.3) are naturally abundant and exist in the different

biological element such as chlorophyll, heme, cytochrome P450 etc. On the other hand, though meso substituted porphyrin **8** (Figure 1.3) has no natural existence but they are used as model compounds for the biological prosthetic groups. In the field of material chemistry<sup>12</sup>, these type of porphyrins is widely used. Besides peripheral change, core modified porphyrins **10** (Figure 1.3) are well known where one of the nitrogen atoms of pyrrole is substituted by heteroatoms like oxygen, sulphur, selenium or carbon atom maintaining the aromaticity of the ring<sup>3</sup>. Different modification of porphyrin ring such as isomerization **11** contraction, **12** expansion, **13** makes porphyrin chemistry so widely spread and enriched. Expanded porphyrins are composed of more than four pyrrole rings that are directly connected or connected through one or more atoms. The inner core moiety is made up of at least 17 atoms<sup>3</sup>. The chemistry of expanded derivatives has been developed intending to incorporate heavier elements in the cavity and stabilize higher coordination number of metal ions, particularly that of lanthanides and actinides<sup>13,14</sup> and also to study the change of its aromatic behaviour and binding affinity towards different anionic and neutral ligands. Isomeric porphyrins are the class of compounds having basic unit  $C_{20}H_{14}N_4$  and produced by staggering of the arrangement of pyrrole rings and meso-carbons. In the case of contracted porphyrins, **12** there are at least three pyrrole rings, or its analogues are in conjugation where one meso carbon or one pyrrole ring is missing compared to parent porphyrin<sup>3,4</sup>.

**1.5 Emergence of corrole:** The emergence of contracted porphyrin is a follow up of the structural discovery of vitamin B<sub>12</sub>, **4** (Figure 1.1). This vitamin is very important in the biological system as lack of this vitamin causes pernicious anaemia, which was considered to be a fatal illness earlier. But after the discovery of this vitamin, this

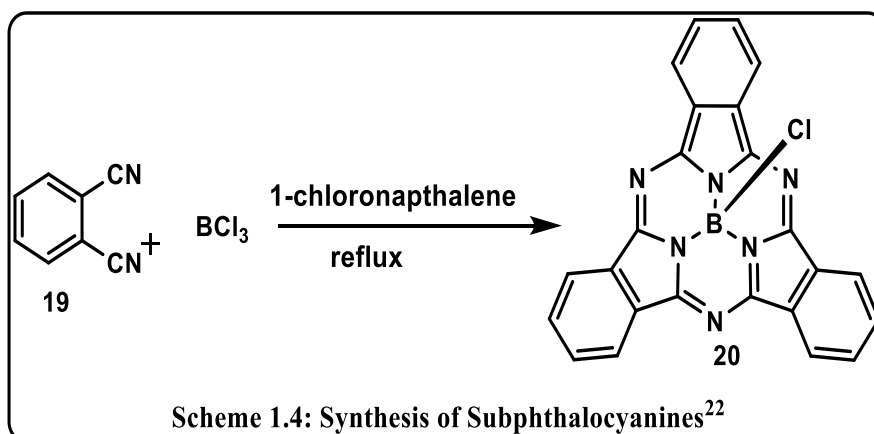


disease became easily curable. The structural elucidation of vitamin B<sub>12</sub> tells that it contains corrin ring, **5** (Figure 1.1) in the core moiety which resembles with porphyrin macrocycle with one carbon atom is missing<sup>15-18</sup>. This is one of the important contracted porphyrin analogues. Later on, scientists are trying to invent a proper synthetic protocol for this vitamin. Johnson and Price planned to synthesize a series of metallic derivatives of pentadehydrocorrin, and from that, they recommended the name corrole<sup>20</sup>. Synthesis of corrole was first reported by Johnson and Kay in the year 1965 and proposed the fact that corroles are tetrahydrocorrins<sup>21</sup> consisting of ten double bonds. Subsequently, several interesting contracted porphyrinoids were enlarged (Figure 1.4).

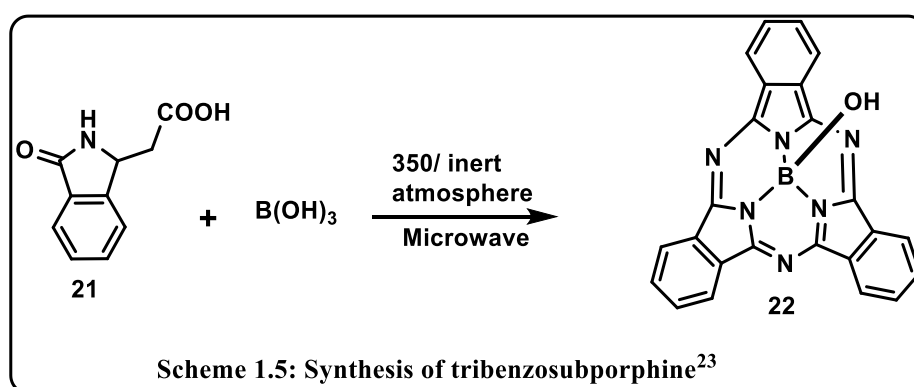


## 1.6 Various contracted porphyrins and their synthetic protocols:

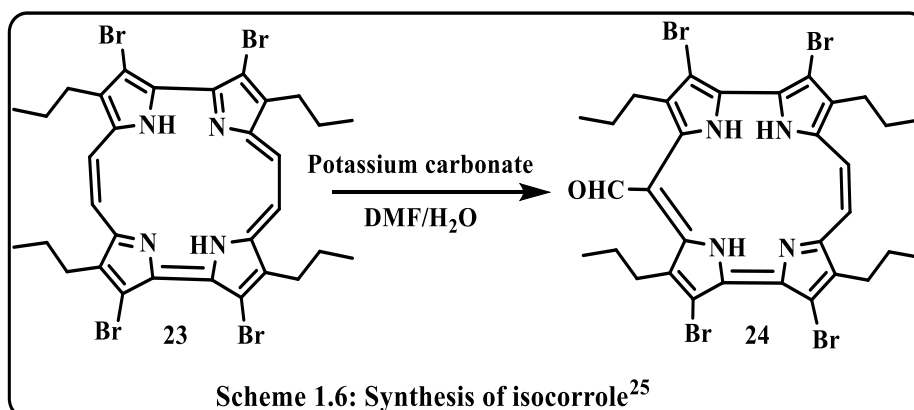
**1.6.1 Subphthalocyanines:** Subphthalocyanines **20** (Scheme 1.4) are aromatic macrocycles with  $14\pi$  electron. These exist as a boron derivative and consist of three N-fused diiminoisoindole units and an axial ligand around the boron atom, which is teracoordinated. Meller and Ossko first synthesized this contracted porphyrin at the time of boron-containing phthalocyanine synthesis<sup>22</sup>.

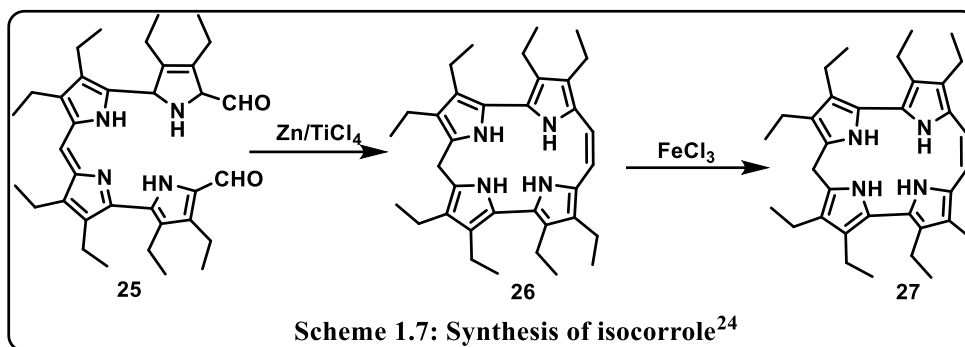


**1.6.2 Subporphyrins:** Subporphyrins **22** (Scheme 1.5) are ring contracted porphyrins containing three pyrrole ring and connected through methine carbon bridge. Osuka and co-worker first reported the synthesis of subporphyrin in the year 2006. The synthesis of tribenzosubporphine involve self-condensation of isoindolinone-3-acetic acid, and the reaction is assisted by boron (III) template. It shows green coloured fluorescent due to aromatic character having  $14\pi$  electrons are in conjugation<sup>23</sup>. The yield of the product of the reaction is very low due to harsh reaction conditions.

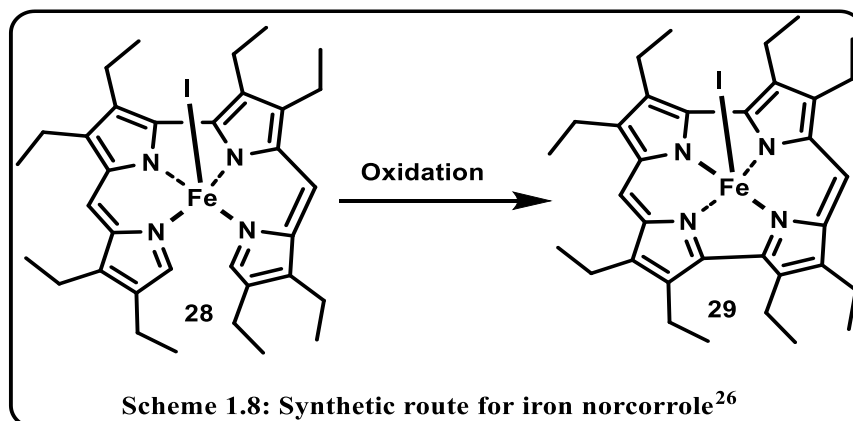


**1.6.3 Isocorrole:** Isocorrole, **24** (Scheme 1.6) an isomeric form of corrole having one less meso carbon atom than porphycene was first reported by Vogel and coworkers in 1990<sup>25</sup>. They have got isocorrole as a side product during the preparation of porphycene through coupling reaction between two diformyl bipyrroles.<sup>24</sup>



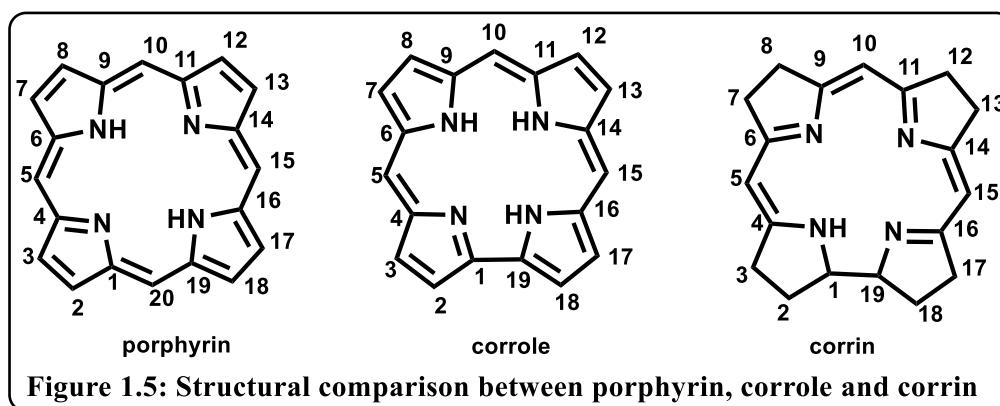


**1.6.4 Norcorrole:** Norcorrole, **29** (Scheme 1.8) is a contracted porphyrin analogue having 16  $\pi$  electrons and was reported by Broring and coworkers<sup>26</sup>. Compared to corrole, it has one less meso carbon atom. Broring and coworkers fruitfully synthesized iron norcorrole from iodido complex of an iron 2, 2'-bidipyrin by an oxidation reaction using  $\text{FeCl}_3$ .



**1.6.5 Corrole:** Over the past decade, the research area of several core-modified porphyrinoids have enlarged. Corroles, **16** (Figure 1.4) are one of the most contributed contracted porphyrinoids. It has attained significant interest due to the close resemblance with the corrin ring in vitamin B<sub>12</sub>. It is structurally in between porphyrin and corrin<sup>3,4</sup>. Due to similarity in some properties with 18 $\pi$  electron aromatic porphyrins, corroles are also closely associated with porphyrins. The absence of meso carbon atom (C-20) in corrole, resulting in direct linkage between two of the pyrrole

rings (Figure 1.5), is the distinct structural feature that differentiates it from porphyrin. The numbering system of corrole is similar to that of porphyrin. Inside the corrole cavity, three amino nitrogens and one imino nitrogen are present. The amino NH undergoes rapid tautomerization in the free base corrole. The absence of one meso carbon atom leads to contraction of the inner  $N_4$  core resulting in enhanced ability to stabilize higher oxidation states of metal ions<sup>3,27</sup>.



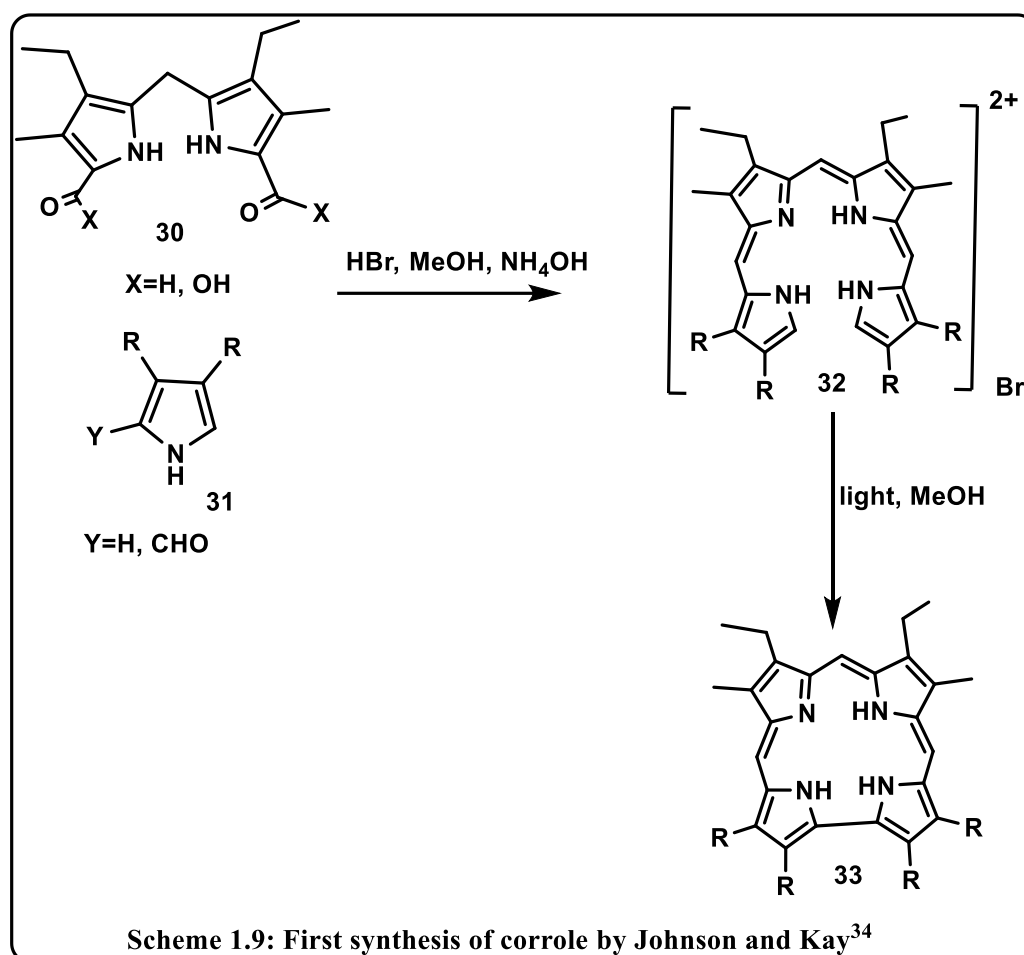
**1.6.5.1 Properties of Corrole:** As the inner core contains three ionizable protons with high NH acidity<sup>3</sup> it behaves as a trianionic ligand, whereas corrin and porphyrin are monoanionic and dianionic, respectively. This characteristic property makes corrole and metallocorrole chemistry so improved. In term of symmetry, it is less symmetrical than porphyrin due to the absence of one meso-carbon atom. The meso-carbon positions are exceptionally sensitive for substitution reactions, particularly towards oxidation. They are extremely coloured compounds. The UV-Vis spectra of corrole reveal an intense band near about 400 nm and less intense bands in the region around 500-600 nm<sup>21,28</sup>. This type of spectra resembles the Q band of porphyrin. The free base corrole are highly fluorescent compounds and exhibit luminescence in the region around 600-700 nm with the fluorescence lifetime in nanosecond scale<sup>25</sup>. <sup>1</sup>H NMR spectra of corrole displays similar characteristic feature as that of porphyrin. The meso and the  $\beta$ - protons

resonate in the deshielding region, and the peaks for meso protons resonate at 8 to 9 ppm, and signals for  $\beta$ - protons appear at ~10 ppm. This type of diatropic ring current indicates the aromatic character of the macrocycle. The inner NH protons give broad singlet in the region -2.00 to -3.00 ppm due to the high acidity of these protons and non-identical tautomers<sup>29</sup>. But at low temperature, three distinct singlet have been observed due to three inner NH protons. In the year of 1971, the first crystal of corrole was characterized by Crowfoot Hodgkin and co-workers<sup>30</sup>. The crystal structure of corrole shows that it is not precisely planar. The deviation from planarity is due to steric crowding inside the core, as C-1 and C-19 are directly linked. But precise structures were provided by X-ray crystallographic study of free base corroles at low temperature in the later years<sup>31</sup>. The molecular structure of 5,10,15-tris(pentafluorophenyl)corrole clearly indicates that only one proton out of three is in the mean corrole plane while the other two, one above and another below the plane resulting in a saddling type structure<sup>32</sup>.

#### **1.6.5.2 General Synthetic Protocols:**

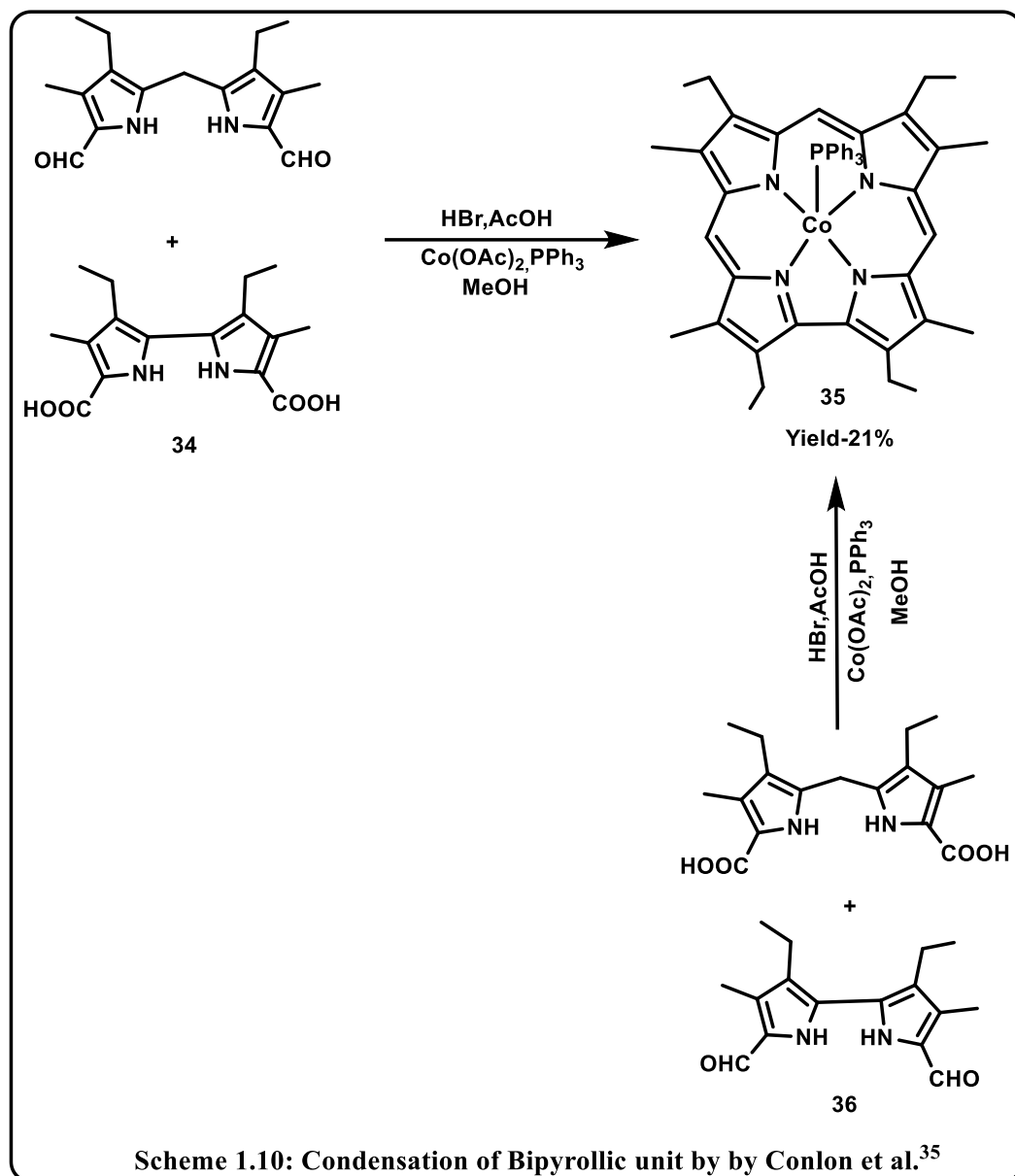
Corrole **33** (Scheme 1.9) was first reported by Johnson and Key in the year 1965. Their strategy was to synthesize corrin ring but accidentally, they synthesized the corrole macrocycle through photochemical cyclization of a, c-biladienes<sup>21</sup> **32**. Following this, several different diverse synthetic strategies have been developed to simplify the synthetic procedure and increase the yield. In this portion, some of the major synthetic approaches have been discussed. The first corrole synthesis involved the photochemical cyclization of a,c-biladienes<sup>18</sup>. In this reaction, methanolic solution of a,c-biladienes were treated with ammonium hydroxide or sodium acetate followed by illuminating the reaction mixture resulting in a green coloured solution. Till now, it is a very much

convenient route for corrole synthesis and the yield of the reaction varies from 20-60% depending on biladienes and the reaction conditions. These a,c-biladienes are stable crystalline dihydrobromide salts **32** and are formed by condensing 2-formylpyrrole and dipyrromethanedicarboxylic acid in 2:1 molar ratio in methanol in the presence of a catalytic amount of acid. In 1994 Vogel *et al.* have reported *p*-chloranil as a versatile oxidant that improves the cyclization step<sup>33</sup>.



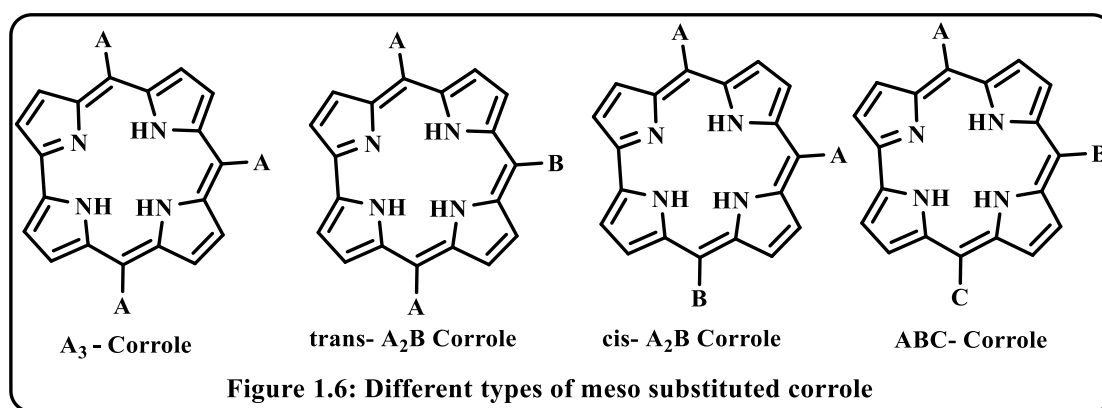
**Bipyrrolic unit through (2+2) condensation reactions:** One of the important procedure for the synthesis of corrole is through the reaction of suitably substituted dipyrane with 2,2'-bipyrrrole **34**. This procedure is reported by Conlon *et al.*<sup>35</sup> In this reaction dipyrane condenses with bipyrrrole under acidic conditions resulting in red precipitation which on heating in the presence of triphenyl phosphine and cobalt(II)

acetate leads to the corresponding cobalt-corrole complex **35** (Scheme 1.10) with moderate yield.<sup>34</sup>



**Direct from substituted pyrrole:** Direct tetramerization of substituted pyrroles leads to the formation of corrole. This synthetic protocol was first reported by Paolesse *et al.*<sup>36</sup> The first  $\beta$ -substituted meso free corrole synthesis involves tetramerization of 3,4-dimethyl-pyrrole-2-carbaldehyde leading to the formation of  $\beta$ -substituted corrole with a yield of 10%.

In another way, corrole can be prepared directly from pyrrole by its reaction with a suitable aldehyde. But this reaction produced porphyrin along with corrole. So for selectively getting corrole, this reaction can be done by suitable substitution on pyrrole or by proper use of templating metal ions.<sup>35</sup> There are four different types of meso substituted corrole depending on the substitution at three meso positions (5, 10, 15) of the corrole periphery.



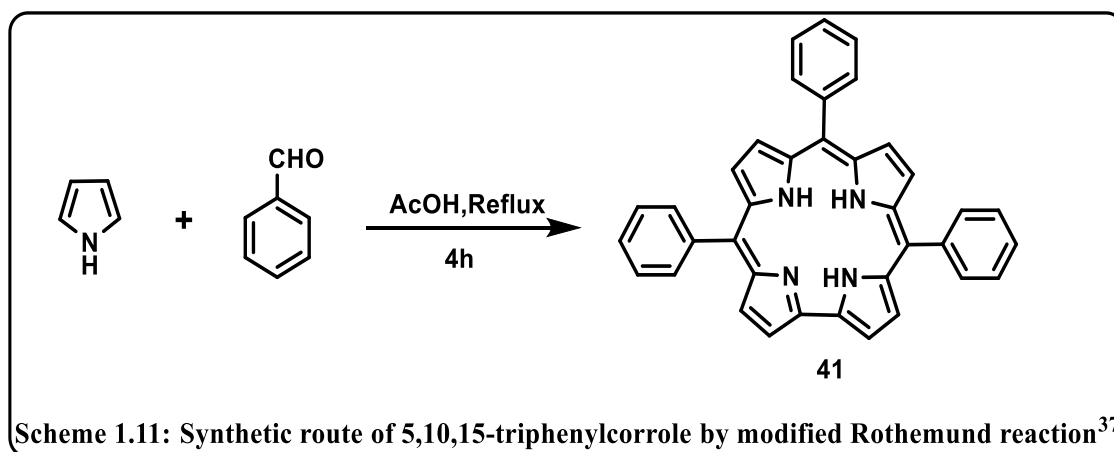
**Synthesis of A<sub>3</sub> corrole:** During the synthesis of porphyrin *meso*-substituted corroles are isolated with low yields. Since the year 1999 only two meso substituted corrole have been reported. Corroles gained significant attention in 1999 when two research groups, Paolesse and Gross independently reported two different synthetic protocols directly from the condensation of aldehyde and pyrrole.

#### One-pot synthesis:

The first reported method for preparation of A<sub>3</sub> corrole is the modified Rothmund reaction which was a widely studied method for preparation of porphyrin earlier. Paolesse *et al.* have reported a procedure which involves the refluxing of a mixture of aldehyde and pyrrole in acetic acid medium for four hours.<sup>37</sup> The yield of the product was highly dependent on the ratio of pyrrole and aldehyde, and the highest yield of triphenylcorrole **41** (Scheme 1.11) was obtained when aldehyde and pyrrole were

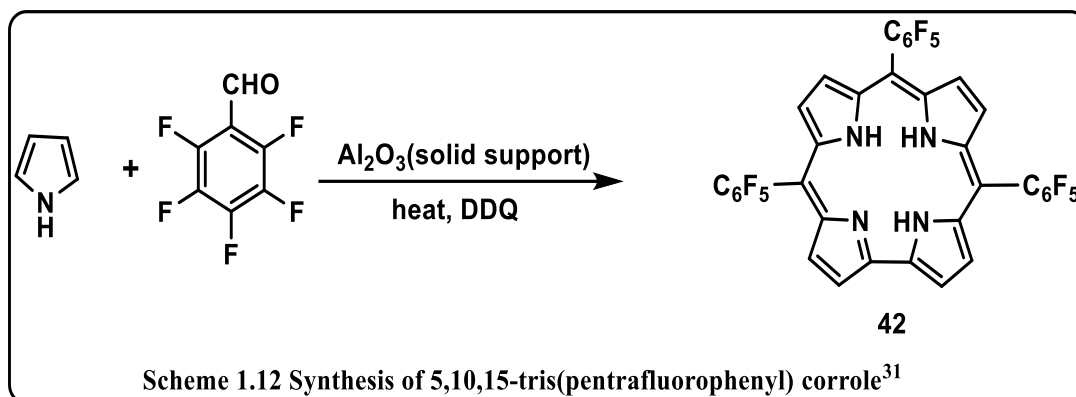
mixed in 1:3 molar ratio. The major limitation of the process was the formation of A<sub>4</sub> porphyrin as a side product.

One of the important solvent free one-pot corrole synthesis was first reported by Gross *et al.* in the year 1999. The reaction involves two steps. In the first step equimolar mixture of pentafluorobenzaldehyde and pyrrole are condensed on a solid support followed by dilution of the mixture with dichloromethane and



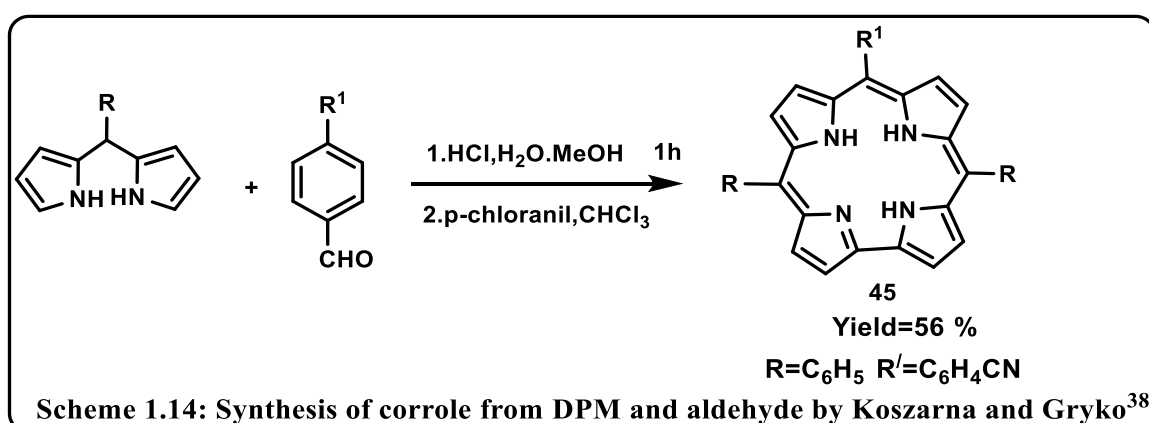
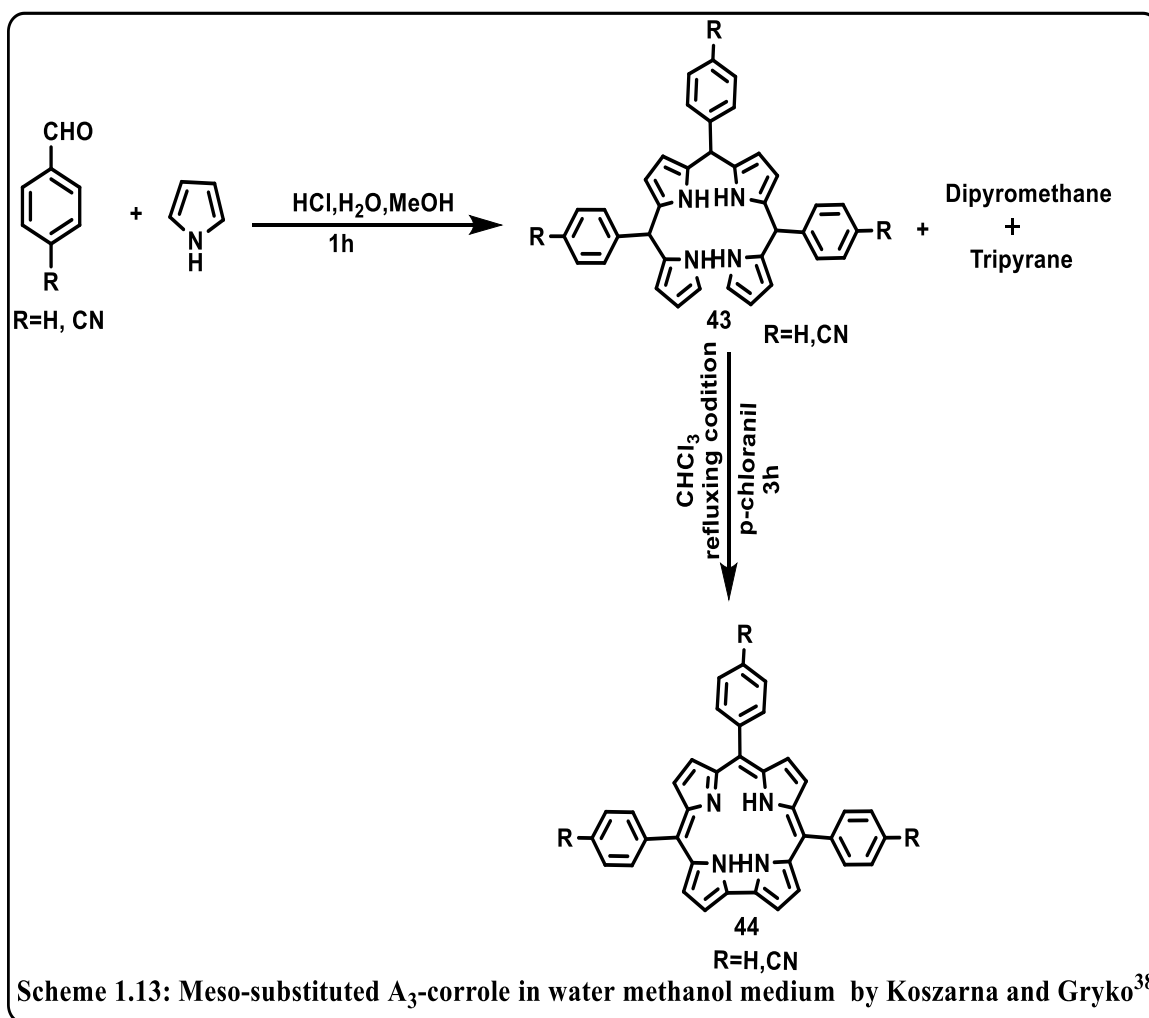
oxidation of the resulting reaction mixture to get the desired corrole **42** (Scheme 1.12). This reaction is highly reactant specific; especially those aldehyde containing electron-withdrawing group works good.<sup>31</sup>

**A modified method for trans-A<sub>2</sub>B and A<sub>3</sub>-corrole synthesis:** Another major advancement for the synthesis of corrole was disclosed in the year 2006 by Koszarna and Gryko group.<sup>38</sup> The motivation behind this synthesis came from a work by Kral and co-workers<sup>39</sup> where bilane was a side product along with the desired dipyrromethane. They maximized the formation of bilane **43** (Scheme 1.13) by tuning the reaction conditions. The novelty of this synthesis was an acid catalyzed condensation of the aldehyde or dipyrromethanes in water methanol mixture. The formation of bilane **43** was highly dependent on the ratio of water and methanol; 1:1 ratio was favoured.



After the formation of bilane, it was precipitated due to its insolubility in the solvent mixture. The reaction mixture thereby obtained was extracted with chloroform without separation of bilane. Then the cyclization of this intermediate to corrole **44** was done by *p*-chloranil. Preparation of A<sub>3</sub>-corroles was done by condensation of pyrrole and aldehyde followed by oxidation, and this method gives up to 30% yield, whereas the yield of A<sub>2</sub>B-corrole **45**, (Scheme 1.14) by condensation of dipyrromethane and aldehyde, produces over 50% product. Although this synthetic procedure gives a new horizon of corrole chemistry, aldehyde with hydrophobic substituents, which leads to insoluble dipyrromethane in this medium, does not allow further condensation. So in these cases, this procedure is inapplicable.

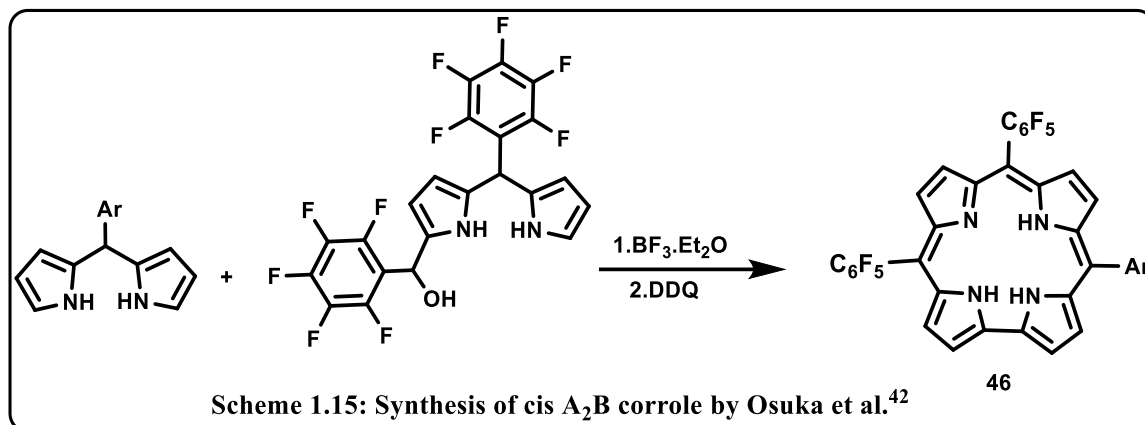
**ABC and cis A<sub>2</sub>B corrole synthesis:** Asymmetrically substituted Porphyrins are formed by a number of a stepwise condensation reaction between dipyrromethanedicarbinol derivatives with pyrrole<sup>40</sup> or reaction with 2,2-bipyrrole.<sup>41</sup> Now-a-days, these methods have no practical importance for the synthesis of A<sub>3</sub> and trans A<sub>2</sub>B-corrole as several suitable synthetic protocols have emerged in the literature. But for the synthesis of ABC and cis-A<sub>2</sub>B corrole, these procedures are still incontrovertible. Gryko and Koszarna synthesized ABC corrole by acid catalyzed condensation reaction between a dipyrromethanedicarbinol precursors with pyrrole



followed by oxidation with DDQ, resulting in the formation of ABC-corrole in a good yield. But this synthetic route is very uncommon as this type of substitution pattern has

less necessity. Besides that, this type of synthesis involves several steps, so these are economically not viable.

A few years ago, Osuka *et al.* synthesized cis-A<sub>2</sub>B corrole **46** (Scheme 1.15) through acid catalyzed (2+2) condensation of 5-(pentafluorophenyl) dipyrromethane-1-carbinol with dipyrromethanes, the 5<sup>th</sup> -position substituted by an aryl group.<sup>42</sup>

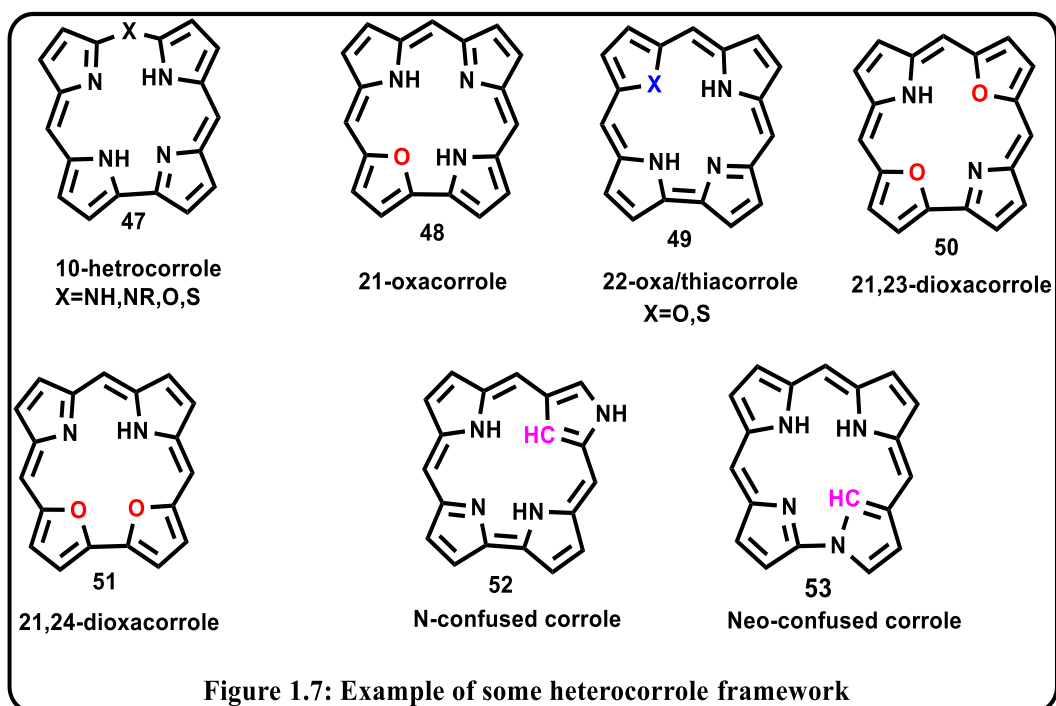


**Core modified corroles and their synthesis:** Introduction of a heteroatom in corrole leads to a class of corrinoids (Figure 1.7). These core modifications involve either replacement of one or two core nitrogen atoms by oxygen, sulphur or carbon atoms or by replacement of one meso-carbon (10-position) by NH, NR or chalcogen atoms leads to the formation of heterocorroles.<sup>43-45</sup>

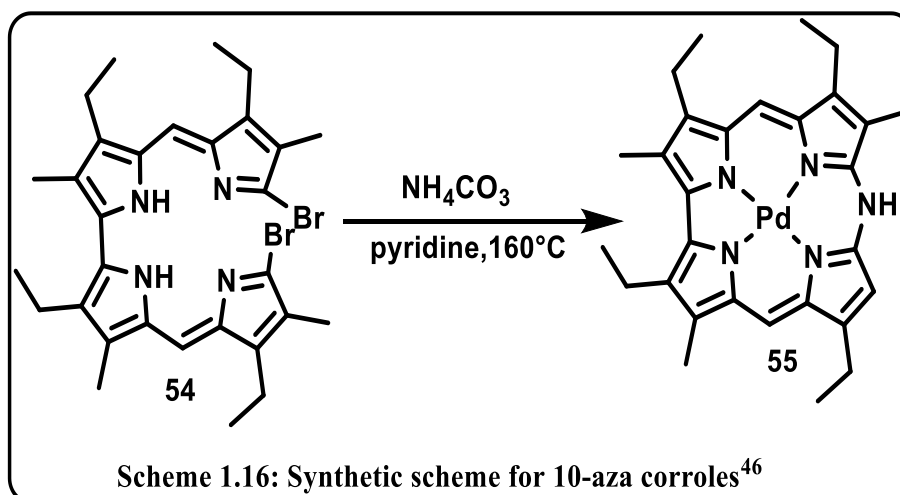
**Following are some example of heterocorrole framework:**

**Synthetic scheme for some of the heterocorrole:**

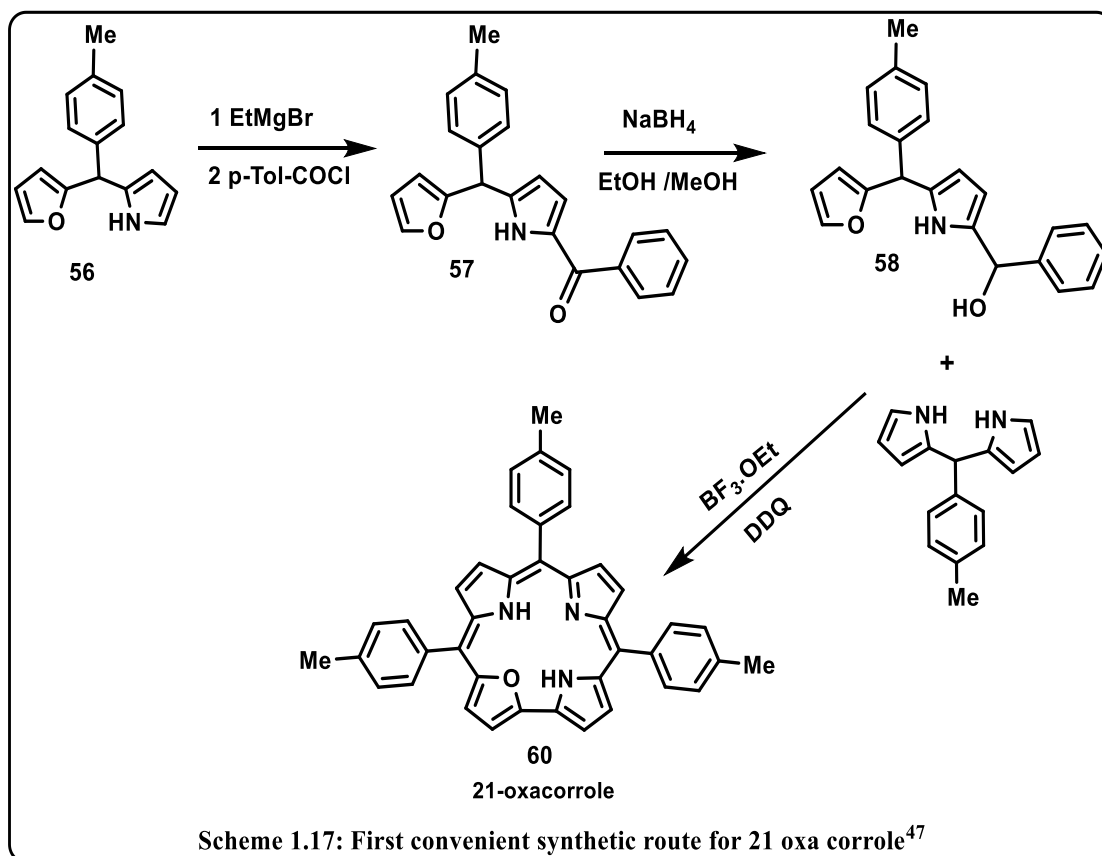
**β substituted 10-aza corrole:** Johnson, Kay and Rodrigo synthesized first β-substituted palladium corroles **55** where one of the meso carbon is substituted by nitrogen atom starting from a metallated dibromo-5,5'-bi(dipyrromethene) **54**. But they cannot isolate the free base corrole by demetallating the metal complex.<sup>46</sup>



**21-Oxacorroles:** The first convenient synthetic protocol of 21-oxacorroles containing a direct bond between furan and pyrrole has developed by Lee and co-worker (Scheme 1.17). The first step of the reaction is an acylation reaction, where p-tolyl-(furan-2-yl)-(pyrrol-2-yl) methane **56** with Grignard reagent ethyl magnesium bromide in THF, and after that addition of p-toluoyl chloride produced the pyrrole acylated **57** with good yield. The reduction of this compound leads to corresponding alcohol **58** excess of

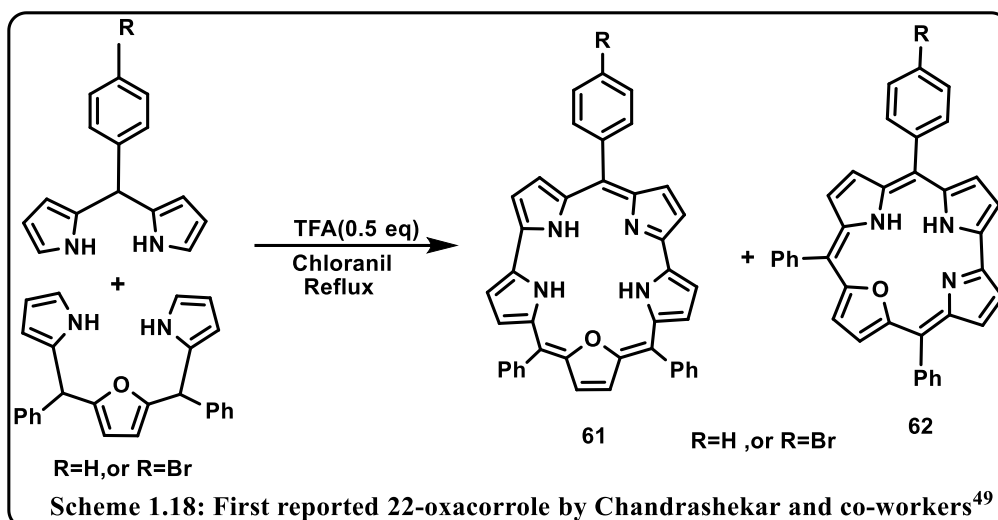


NaBH<sub>4</sub>. After that acid catalyzed (2+2) condensation of this alcohol **58** with meso-aryl dipyromethane results in the formation of the oxacorrole **60** with 9% yield.<sup>47-48</sup>

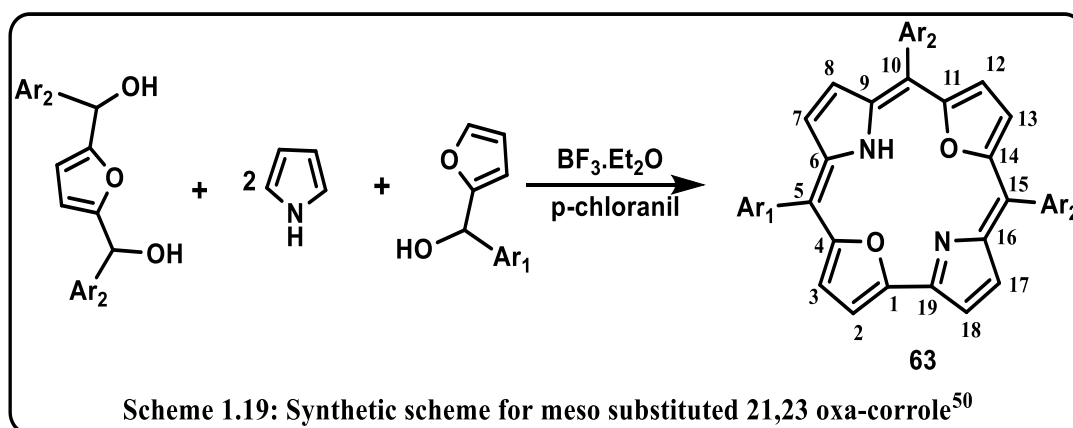


**22-Oxacorrole:** Chandrashekar and co-workers<sup>49</sup> first reported 22-oxacorrole as a side product in the course of their expanded porphyrin synthesis. It is an oxidative coupling reaction between 16-oxatripyrrane and meso aryl dipyromethane in the presence of TFA. Further oxidation by chloranil leads to oxaasmaragdyrin as a major product accompanying with 22 oxacorrole **62** with the yield of 3-4% (Scheme 1.18).

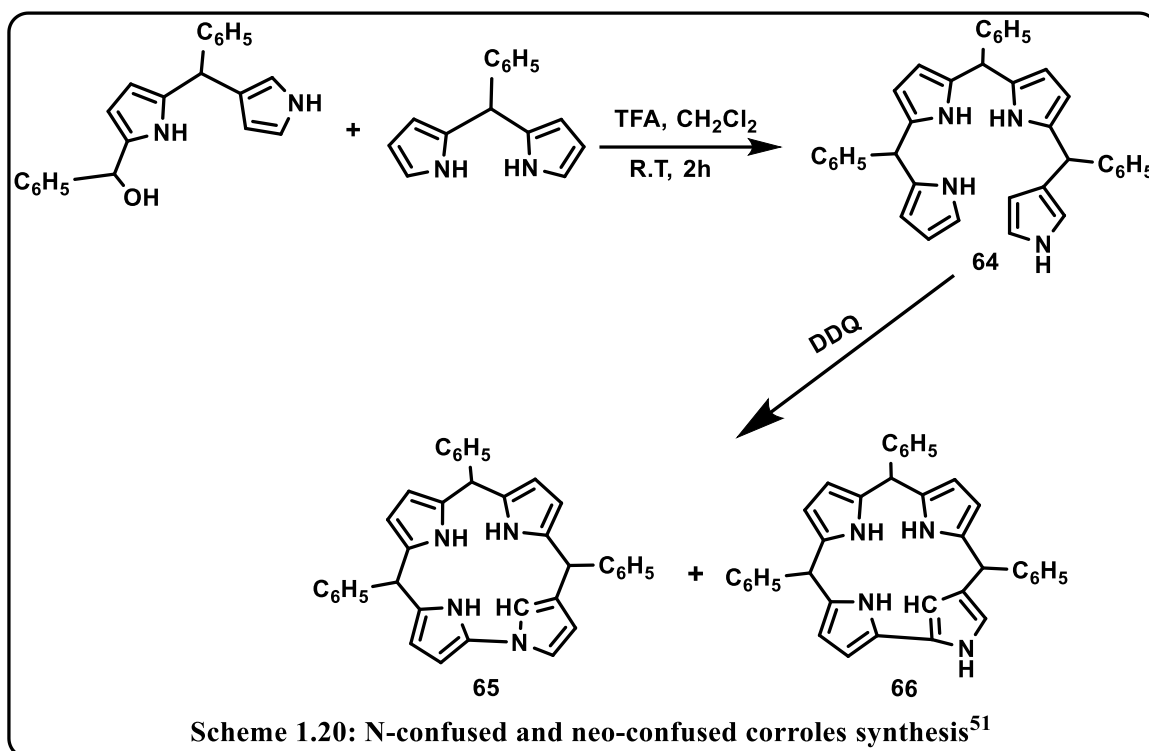
**Meso substituted 21, 23 dioxacorrole:** Latos-Gra'zynski and co-workers<sup>50</sup> first proposed a synthetic route for the preparation of meso substituted 21, 23-dioxacorrole **63**, which involves acid catalyzed condensation of one mole of 2,5-bis(p-tolylhydroxymethyl)furan and phenylhydroxymethylfuran with two moles of pyrrole



in dichloromethane medium followed by oxidation with *p*-chloranil leads to the formation of corresponding dioxacorrole **63** with the yield of 8% (Scheme 1.19).



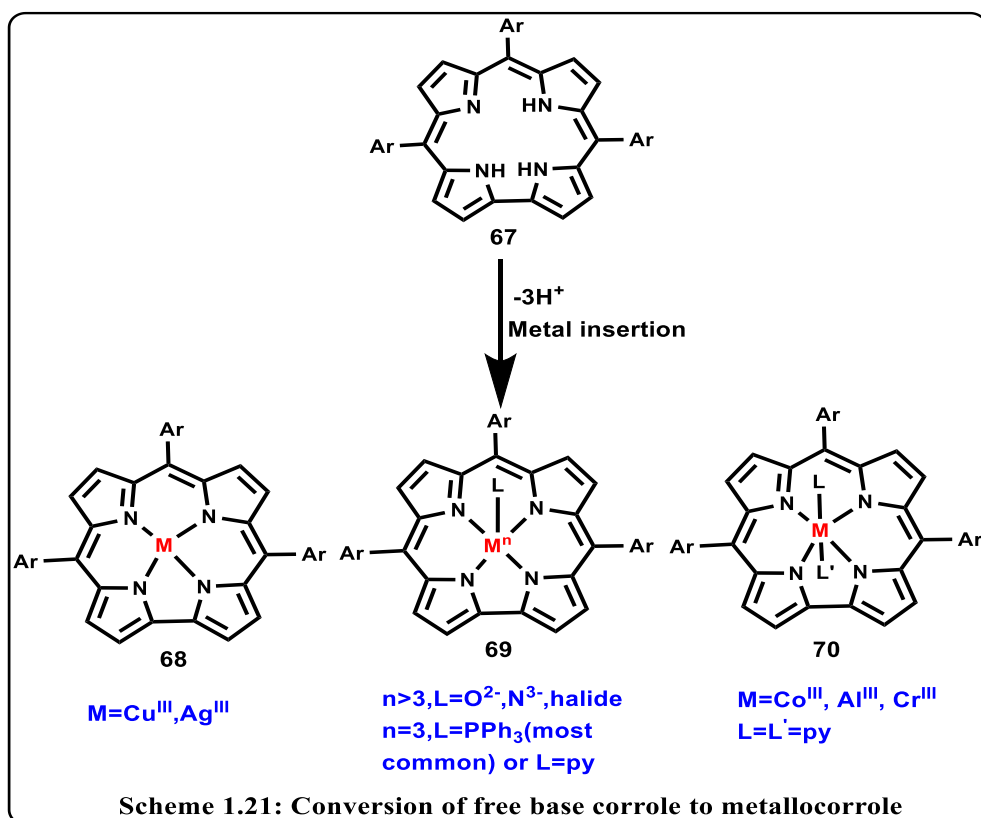
**N-confused and neo-confused corroles:** The N-confused **65** and neo corroles **66** syntheses were reported by Furuta and co-workers<sup>51</sup> (Scheme 1.20) which involve two steps reaction. Initially, condensation of N-confused dipyrromethane monocarbinol with dipyrromethane in the presence of trifluoroacetic acid to give 1-aza-21-carbabilane **64** and then Subsequent oxidation of bilane derivative with DDQ produced NCC<sub>4</sub>-C<sub>6</sub>F<sub>5</sub> in 18% yield along with the formation of NCC<sub>5</sub>-C<sub>6</sub>F<sub>5</sub> in less than 1% yield.



### Metallocorrole and its different coordination mode:

The inner core of corrole contains three NH protons which are sufficiently acidic in nature due to steric reasons. They are very susceptible to deprotonation and easily coordinated to metal ions (Scheme 1.21). The metallocorroles chemistry has explored in the last two decades, although the free base corrole has been invented long back ago. The chemistry of metallocorroles has started to grow up after the invention of a suitable synthetic procedure of corrole. Due to the presence of three NH protons, it behaves as trianionic chelating ligand and also possesses high charge density hence stabilized higher oxidation states of metal ions. Nowadays corroles and metallocorroles are a hot topic of research due to diverse applications in various fields. Metalation of corrole can be classified in two ways i) macrocyclization of tetra pyrrolic unit where metal ion acts as a template and ii) by incorporating a suitable metal into the inner corrole cavity.<sup>3</sup> In

this section, the different methods for insertion of metal into the corrole cavity and their structure with varying modes of coordination will be discussed.



The coordination modes of metallocorroles are not fixed. Its common coordination number varies from four to six. Few transition metals and some main group metals for example  $\text{Cu}(\text{III})$ ,  $\text{Ag}(\text{III})$ ,  $\text{Au}(\text{III})$ ,  $\text{Bi}(\text{III})$ ,  $\text{Sb}(\text{III})$  etc, when are chelated with corroles, gives a square planer geometry **68** with coordination number four.<sup>52-55</sup> This coordination mode also observed for corrole complexes of  $\text{Co}(\text{III})$ ,  $\text{Mn}(\text{III})$  without axial ligand and also  $\text{Ru}(\text{III})$  where it is connected with another  $\text{Ru}$  centre by a triple bond.<sup>21,56-57</sup> Another common coordination modes of metal-binding corrole is Penta-coordinated complex with square pyramidal geometry around the metal ions **69** (Scheme 1.18) and it gives rise to a domed configuration as the central metal ion is axially displaced from  $\text{N}_4$  plane. Such type of structural arrangement is shown for complexes of  $\text{Mn}$ ,  $\text{Fe}$ ,  $\text{Cr}$ ,  $\text{Mo}$ ,  $\text{Rh}$ , or  $\text{P}$  containing neutral, as well as anionic axial

ligands, for example, pyridine, halides, triphenylphosphine, phenyl, methyl and also, exist as oxo, nitride and nitrosyl complexes.<sup>58-60</sup> hexa-coordinated complexes of corroles **70** are also well known such type of geometry is observed for the complexes of Co(III), Al(III), Ga(III) and Rh(III) complexes where the axial position is coordinated by pyridine.<sup>61-64</sup> The corroles generally acts as trianionic and tetradentate ligands in its common metal complexes such as previously discussed cases. But in oxovanadium(IV) and oxotitanium (IV), complexes of corroles show tridentate and dianionic nature.<sup>65</sup> Compare to porphyrin metals coordinate with corroles ring is not so much enriched. The synthesis of new metallocorroles still remains a challenge for researchers. This contracted porphyrin analogue and its metalated derivatives are a field of increasing interest due to their peculiar and unique features. Till 2012, no reports were observed for the corrole complexes with alkali metals, early transition metals, lanthanides and actinide series<sup>66</sup>. Recently several metals among these have been inserted in the corrole cavity, such as Si, Ta, Ce, Tc, Lu<sup>66-67</sup> and the only alkali metal Li.<sup>68</sup>

**Functionalization of corrole:** The corrole core is more sensitive than porphyrin. Especially unusual high acidity of inner hydrogen makes its chemistry so much diverse. The meso positions are also very much reactive and susceptible to oxidation. The functionalization of corrole involves (a)  $\beta$ -pyrrolic positions (b) meso positions (c) N-pyrrolic positions. Both free base corrole and its metal complex undergo functionalization. Sometimes at the time of peripheral functionalization, it is essential to prevent inner core reaction generally by doing metalation<sup>69</sup> which also changes the reactivity of corrole.

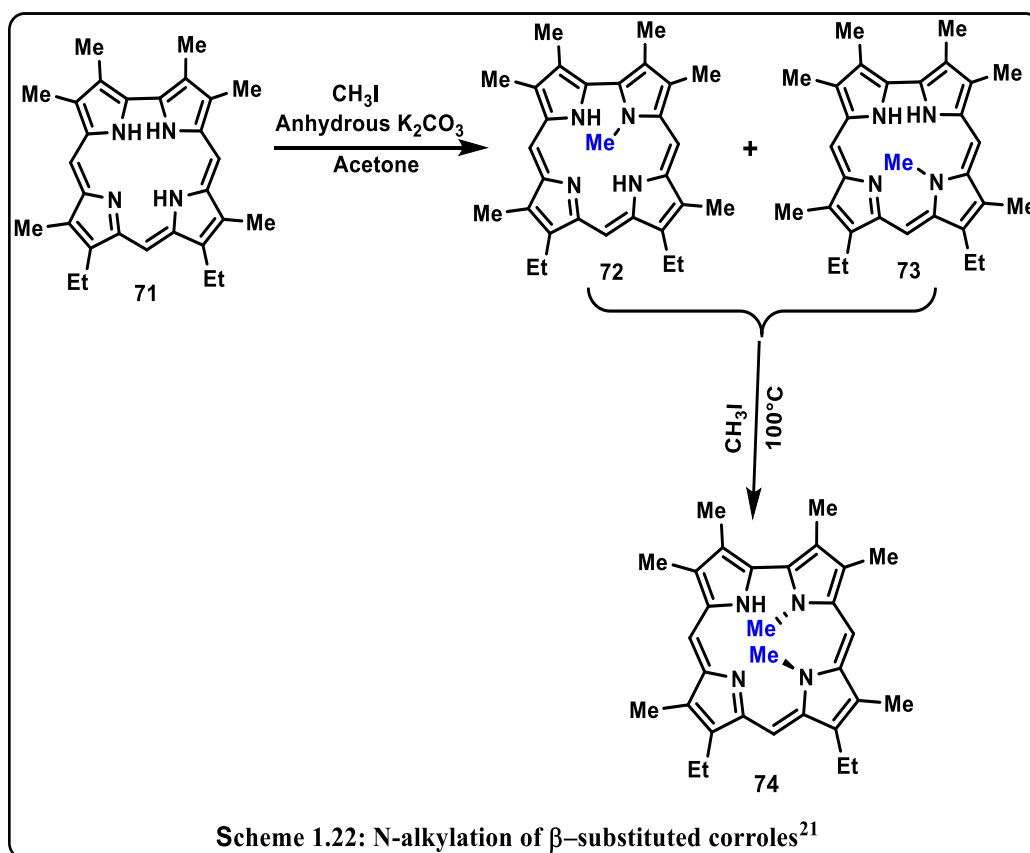
**Inner core functionalization:** The N-alkylation of  $\beta$ -substituted corroles was reported at the time of corrole invention by Johnson and Key.<sup>21</sup> Mixture of two isomeric N-

methyated corroles **72** and **73** (Scheme 1.22) were formed on addition of iodomethane to free base corrole in acetone and the solution was refluxed with anhydrous potassium carbonate. Further reaction of these two methyated corroles that is N-21 and N-22 corrole with iodomethane in a sealed tube and 100 °C temperature produced N-21,N-22 dimethyl isomer **74**. In the case of N-21 derivative, the yield is slightly greater. The same diethyl corrole was also formed under the same reaction conditions with good yield along with starting  $\beta$ -octaalkylcorrole. This synthetic route also extended for an alkylating agent for synthesizing N-substituted corrole derivative.<sup>70-71</sup>

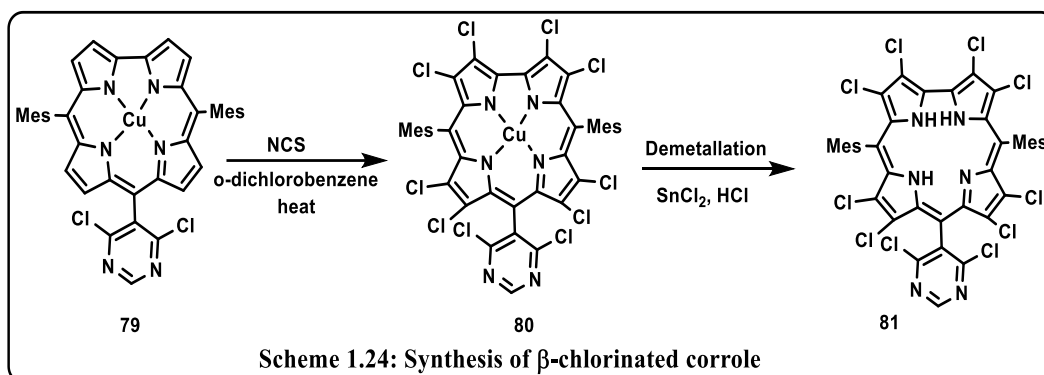
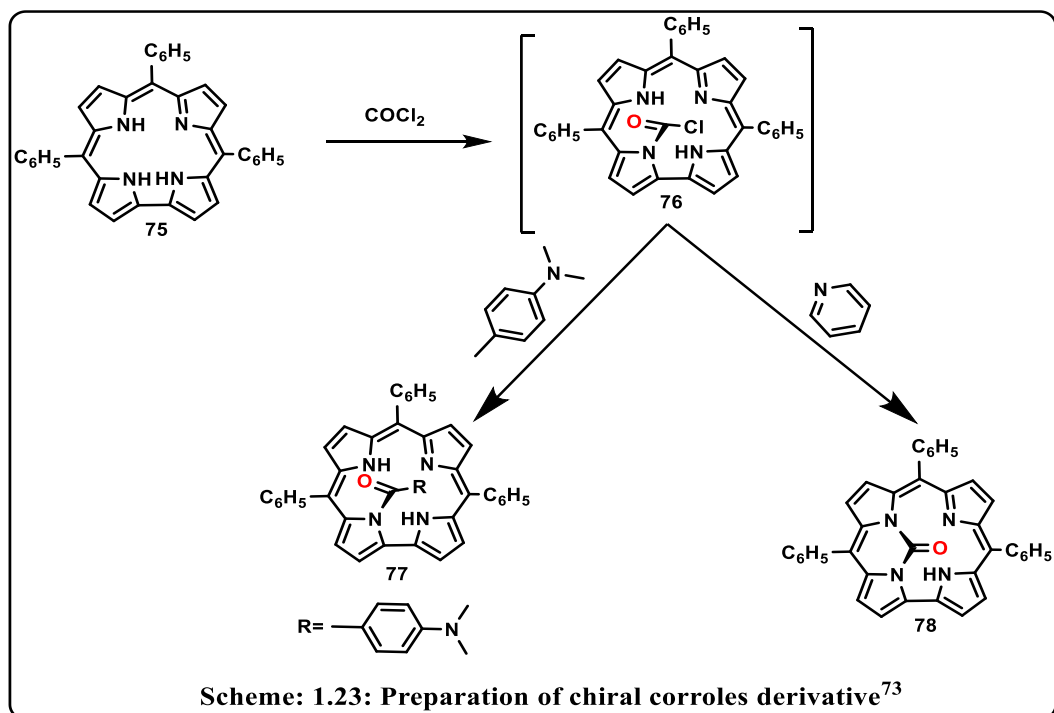
Gross et al. established the chirality of these N-alkylated corroles, although they exist as a racemic mixture during synthesis, which can be easily separated HPLC using a chiral column. They also reported different N-21 and N-22 isomers containing benzyl and picolyl substitutions having good yield, and in all these cases, separation was simple. They have synthesized Zn complex of N-21-picolylcorrole containing axially coordinated pyridine ligand which was reversibly removed after purification leads to formation of a compound where N-picolyl intramolecularly coordinated to the zinc center.<sup>71-72</sup> Besides N-substitution, unusual reactivity of the inner nitrogen atoms also reported during attempting carboxylation using phosgene. Instead of peripheral carboxylation N-acylated product **77** and N-21, N-22 urea derivative **78** (Scheme 1.23) were formed depending on reaction conditions.<sup>72-73</sup>

**Peripheral functionalization:** The peripheral functionalization of corroles mainly involve substitution on  $\beta$ -positions and meso positions. Generally, selective substitution at two or three positions occurs at first. This variation in reactivity of carbon atoms in macrocyclic framework is due to the different electronic environment.

**Halogenation:** Halogenation of corroles mainly involve the  $\beta$ -positions, but *meso* halo corroles are also reported. Different procedure for bromination, chlorination and iodinations is developed, but there is no suitable protocol for fluorination. So, fluoro derivative of corrole cannot be done by fluorination rather, it was synthesized condensations of aldehyde and pyrrole containing a fluorine atom.<sup>74</sup> Maes and coworkers first incorporate chlorine atoms at all  $\beta$ - positions of copper corrole containing *meso*-pyrimidinyl substituent to octachlorinated derivative **80** (Scheme 1.24) where they have used N-chlorosuccinimide as a chlorinating agent.<sup>75-76</sup> Further demetallation of copper complex leads to corresponding corrole derivative **81**.

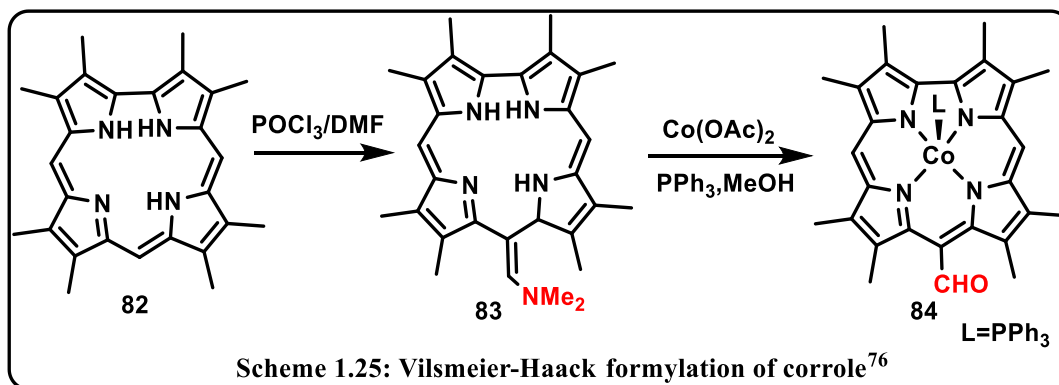


**Formylation:** Paolesse, Smith, and coworkers<sup>76</sup> first reported peripheral functionalization by doing Vilsmeier–Haack formylation of corroles (Scheme 1.25) in the year 1997. They found instead of the introduction of the formyl group at 5 or 15

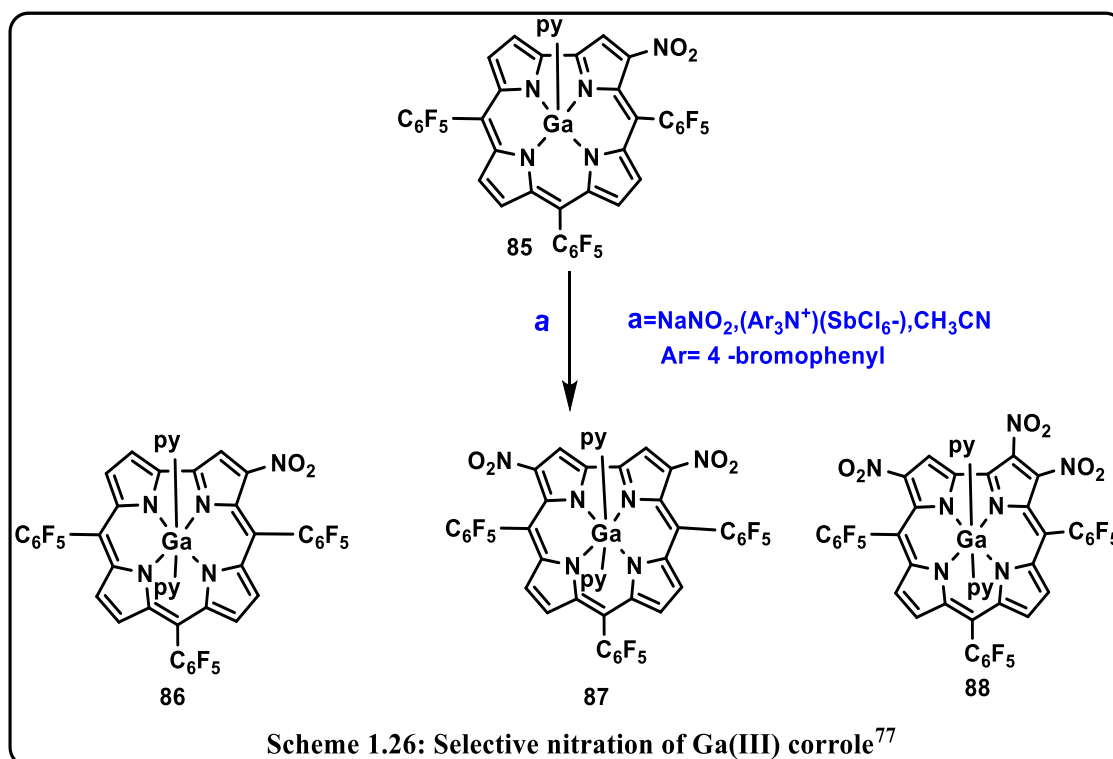


positions, 10-dimethylaminomethene derivative **83** was formed with the addition of Vilsmeier reagent in free base corrole. This derivative was further refluxed with Cobalt acetate and  $\text{PPh}_3$  in methanol medium to produced corresponding *meso* formyl cobalt corrole complexes **84**.

**Nitration:** Various methods were flourished for insertion of nitro groups at  $\beta$ -pyrrolic positions. One of the suitable reagent used for this purpose by Gross and co-worker was  $\text{NaNO}_2$  in the presence of tris(4-bromophenyl)-aminium hexachloroantimonate to Ga(III) corrole (Scheme 1.26) containing nitro group at  $\beta$ -positions.<sup>77</sup>

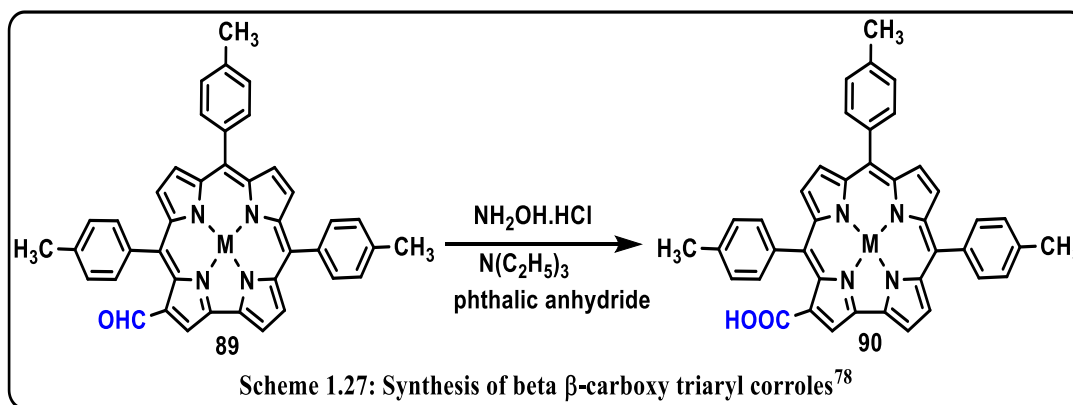


The no. of nitro group inserted depends on the concentration of oxidant. They observed mononitrated corrole **86** with 84% yield and di nitrated product **87** with 9% yield was formed with complete disappearance of starting material when 75 mol% of oxidant and excess of  $\text{NaNO}_2$  were used.



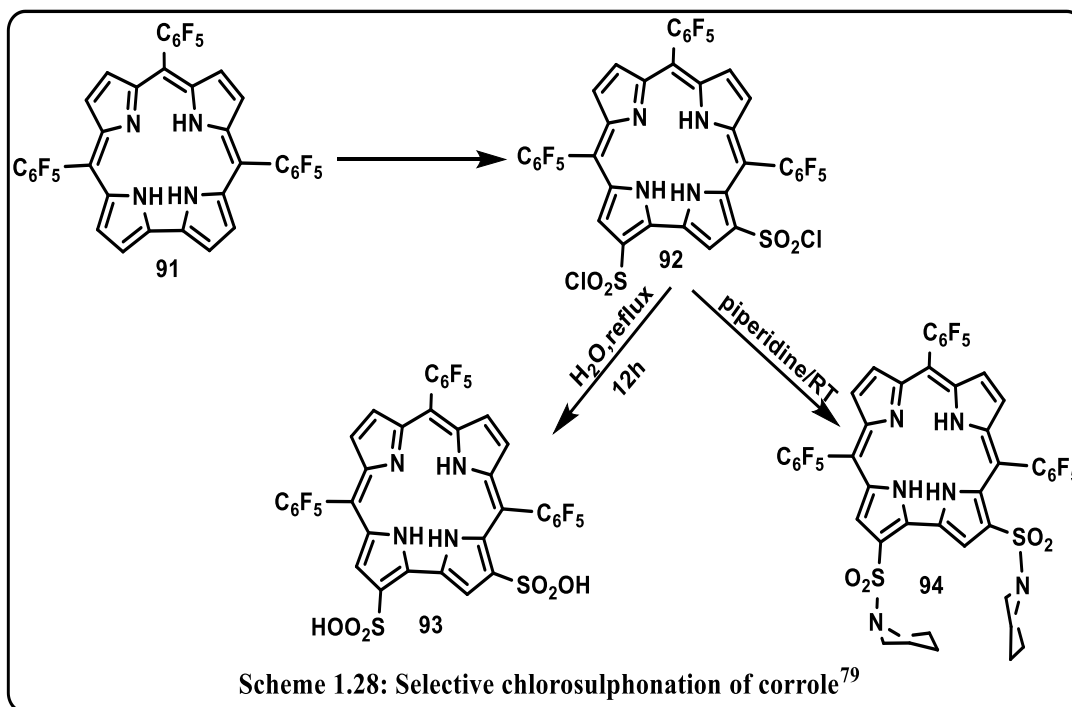
**Carboxylation:** Giribabu and co-workers reported an efficient conversion of formyl group of 3-formyl-5,10,15-triaryl corroles to carboxylic acid **90** (Scheme 1.27) group using hydroxylamine hydrochloride and phthalic anhydride<sup>78</sup>. Later they showed this

protocol is also applicable for porphyrin and various triaryl substituted corroles containing electron releasing group at phenyl ring.



**Sulfonation/Chlorosulfonation:** Gross and co-workers first reported a straightforward and almost quantitative procedure for introduction of the chlorosulfonic acid group to H<sub>3</sub>TPFC using chlorosulfonic acid to form 2,17-bis-chlorosulfonatocorrole **92** (Scheme 1.28).<sup>79-80</sup> The treatment of piperidine to the reaction mixture leading to corresponding bis(sulphonamide) 2,17-bis-sulfonic acid corrole **93** was formed by only water addition to 2, 17-bis-chlorosulfonatocorrole.

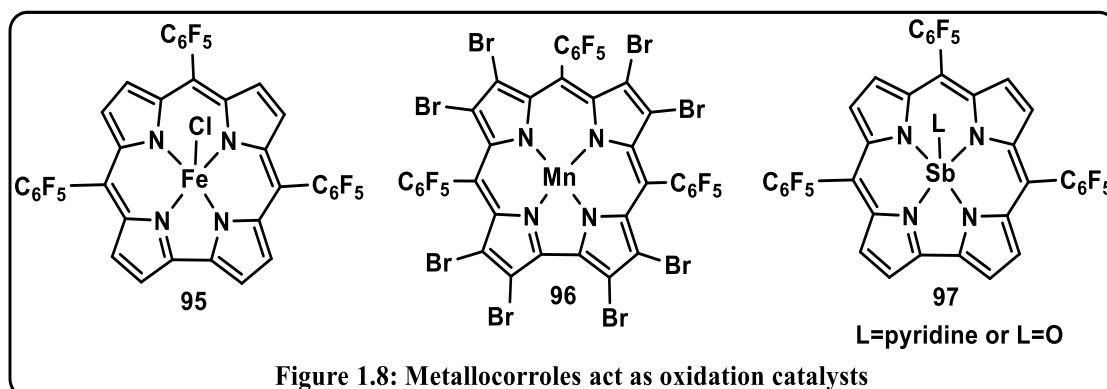
**Corrole and Metallo-corrole based application:** Compare with porphyrin, the corrole chemistry was not so much explored since 1999 due to the lack of suitable synthetic protocols for corroles and their metal derivative. After the discovery of facile synthetic methodology for corrole and its metal complexes different research group has used them for other fields of science such as sensing of gaseous molecules, different catalysis reactions and also in the field of medical science. The unique photophysical properties, the ability for stabilization of higher Oxidation state of metal and high acidity for inner NH makes corrole chemistry so widely applicable. Some of the application have been discussed in this section.<sup>81-82</sup>



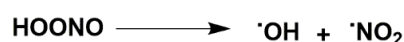
**A catalyst in oxidation reaction:** The hydroxylation reaction of ethylbenzene by iodosylbenzene to produce corresponding alcohol and ketone is catalyzed by iron corrole  $\text{Fe}(\text{tpfc})\text{Cl}$  **95** (Figure 1.8) first reported in the year 1999<sup>83</sup>. But the catalytic activity of the analogous porphyrin  $[\text{Fe}(\text{tpfp})\text{Cl}]$  derivative is much greater and also yield in this reaction. After that, this hydroxylation reaction was further studied using manganese corrole **96** as a catalyst and convert cyclohexene to corresponding products showing its superiority over the former iron complex **95** in terms of yield of product, turnover frequency and also stability after the reaction<sup>84-85</sup>. But the selectivity of the reaction is significantly less. Later, Lubeznova et al. reported antimony corroles **97** exposed as an excellent catalyst to promote aerobic oxidation reaction. This photo-assisted reaction also has high selectivity<sup>86</sup>.

Metalocorroles also exhibit remarkable catalytic properties in the decomposition reaction of reactive oxygen species (ROS), hydrogen peroxide and peroxynitrite<sup>86-88</sup>

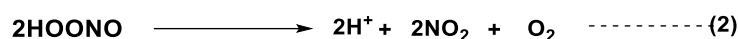
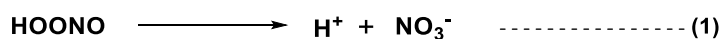
and reactive nitrogen species (RNS). In different biological processes, these species are generated, but a high accumulation of these species leads to oxidation and nitration of biomolecules resulting in nitrooxidative stress.



Now a day these species are identified as a cause of several diseases and disorders related to the cardiovascular and central nervous system, for example, Parkinson's diseases, Alzheimer's diseases Huntington diseases etc. Peroxynitrite being both reactive oxygen and nitrogen species is very much damaged in a biological system. There is no enzyme available in the body system to prevent the decomposition of its protonated form to corresponding radical, which are very dangerous<sup>90-92</sup>.



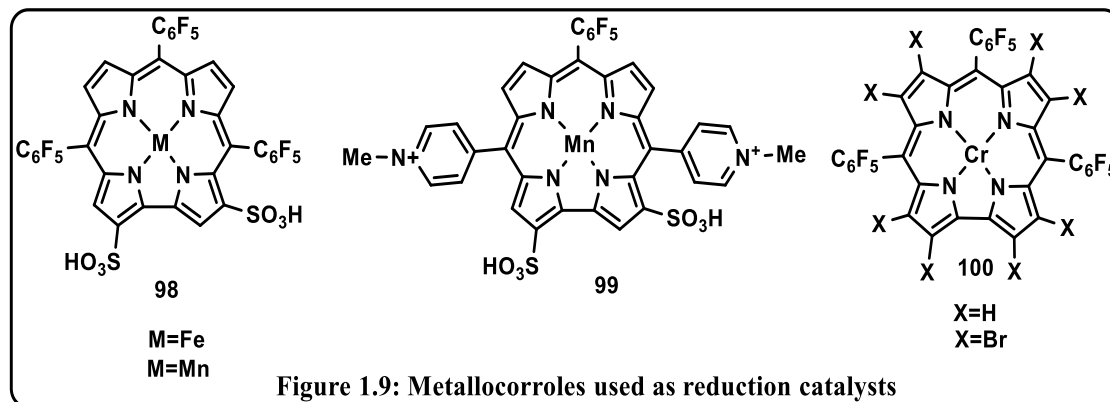
Motivating by earlier outcome regarding the catalytic decomposition of  $\text{H}_2\text{O}_2$  by metallocorroles, later Fe (III) corrole and Mn(III) corrole are also reported as a catalyst for decomposition peroxynitrite, which is both ROS and RNS<sup>88</sup>.



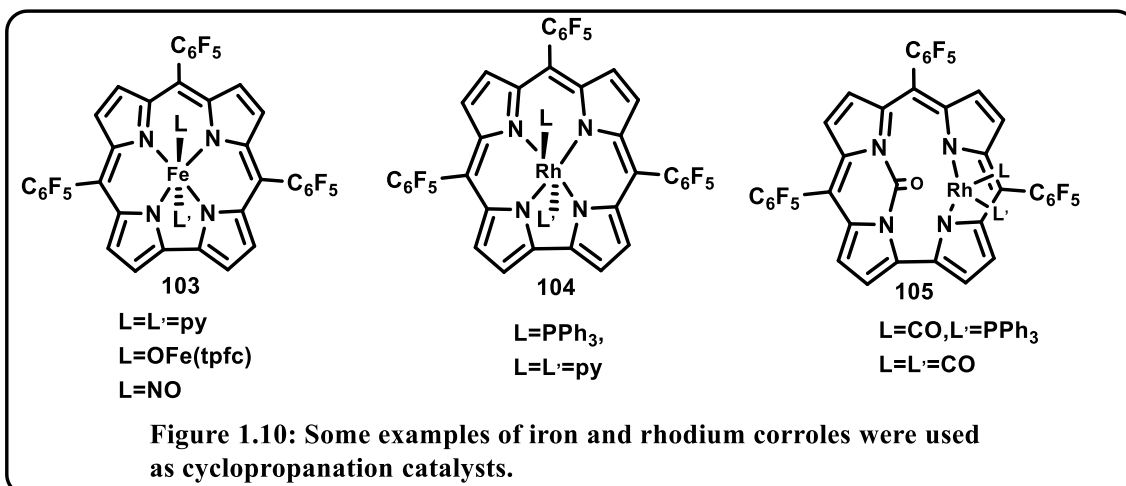
The catalytic activities of both the metallocorroles are remarkable for the detoxification reaction of peroxynitrates. The way they work was found to be different. In the case of

iron(III) corrole catalytic decomposition occurs through isomerization reaction producing nitrate, While the catalytic activity of Mn complex shows novelty and reaction proceeds through disproportionation pathway (Scheme 1.26), which is also confirmed by product quantification ( $\text{NO}_2$  and  $\text{O}_2$ ). Mn (III) corrole **99** (Figure 1.9) with *para*-pyridinium *meso* substitution reveal similar catalytic property with tenfold increase activity for the decomposition of peroxynitrite<sup>93</sup>.

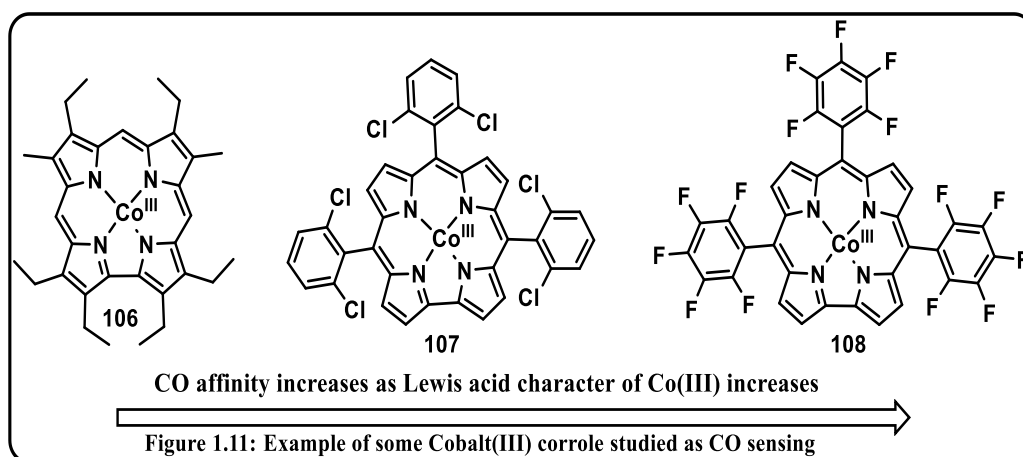
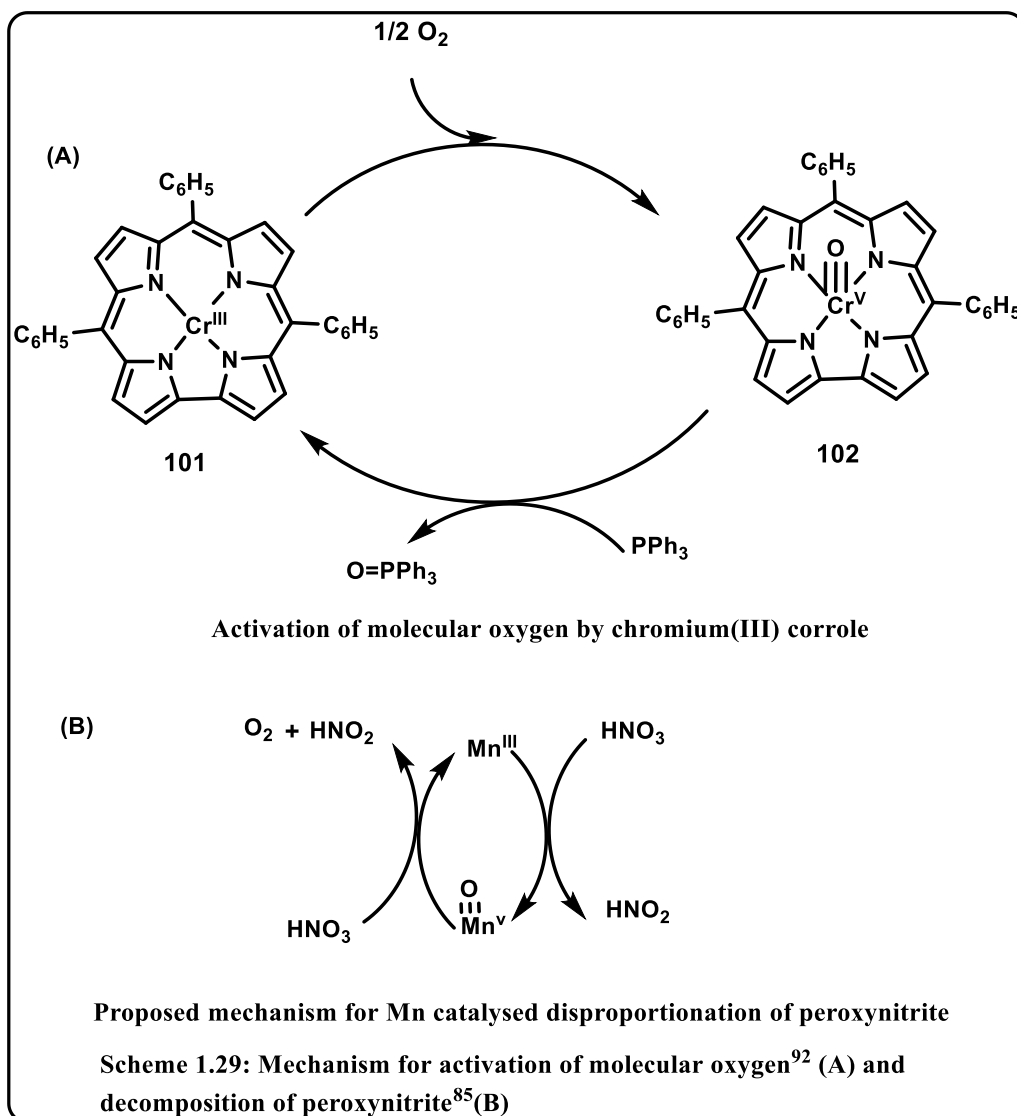
Meier-Callahan *et al.* reported oxidation of Cr (III) complex **100** in the presence of air to corresponding oxo-chromium (V) complex<sup>94</sup>. This aerial dioxygen activation by Cr(III) corrole motivated Mahammed *et al.* to use it as a catalyst for the aerial oxidation reaction of organic molecules. For example (oxo)Cr(V) corrole oxidizes triphenylphosphine to the corresponding oxide, and itself converted to Mn(III) corrole<sup>95</sup>(Scheme 1.29).



**Group Transfer Catalysis:** Cyclopropanation of styrene by ethyl diazoacetate was catalyzed by iron corroles **103** and rhodium corroles **104** and **105** (Figure 1.10). This was the first observation where the corrole metal complex acts as a superior catalyst compare to the corresponding metalloporphyrin analogue<sup>96</sup>.



**Use of corroles and metallocorroles as a sensor:** The peculiar property of corrole to stabilize the higher oxidation state of the metal is responsible for its use in sensing purpose. Co (III) corroles (Figure 1.11) can bind with CO<sup>97-99</sup>, but its porphyrin analogue unable to bind with CO. So corroles complex acts as a sensor for the detection of carbon monoxide. CO detection is very crucial and beneficial for industry and domestic purposes. There are several detectors available commercially for this purpose. Still, there is some limitation of each of them such as electrochemical cell technology has highly CO sensitive detector but it has low life. It was also observed that cobalt (III) corroles exhibiting high selectivity and efficiency to bind with CO versus O<sub>2</sub> and N<sub>2</sub><sup>97</sup>. By studying the absorption property of all cobalt -corrole complex, it was concluded that CO affinity is directly related to Lewis acidity of cobalt complex, and with increasing electron density on cobalt atom it Lewis acidity decreases consequently, affinity towards CO decreases (Figure1.11). Thus cobalt (III) complex containing electron-donating group at  $\beta$ -position **106** are not able to bind with CO, and maximum affinity is observed for those cobalt (III) complex possessing electron-withdrawing group **108** at corrole periphery.<sup>100</sup>



**Application of corrole in the medicinal field:** In the previous section, peroxynitrite decomposition was discussed, which was mediated by metallocorroles to avoid its toxic

effect in the biological system<sup>88</sup>. The excess peroxynitrite leads to atherosclerosis which is a vascular disease caused by an excess of cholesterol in arteries. If it is not treated heart attack may also occur. Lipoprotein in the body system is harmful and responsible for oxidative damage from the earlier finding of decomposition power of iron and manganese corrole researcher concluded that these metallated corroles might be adequate to prevent this type of oxidation reactions<sup>101</sup>.

For the application of corroles and metalocorroles for medicinal purpose, their water solubility and amphiphilic nature play a vital role. For this purpose, C-alkylation by pyridine and N-alkylation of that product brought about the first water-soluble corrole<sup>102</sup> **109** (Figure 1.12). In vivo investigation report reveals that the corrole complex **109** was more effective for preventing endothelial cell proliferation, tumour progression compares to different porphyrin derivative<sup>103</sup>. Introducing sulfonate groups on corrole also makes it highly water-soluble, and presence of polar group on the peripheral position of corrole and metallocorroles were shown to bind strongly to serum albumins which could be either favourable or unfavourable for its medicinal applications. Sulfonated Ga(III) corrole having intense red fluorescent which can congregate with protein in blood cell human serum albumin which can be easily visualize<sup>104-105</sup>. This assembles is efficiently use for therapeutic purpose, has reported. Corrole itself cannot penetrate the cell membranes but in situ protein assemblies can able to introduce easily in cell and accumulated in the cytoplasm specifically bind to the receptor-specific cell and was confirmed by inhibition studies.

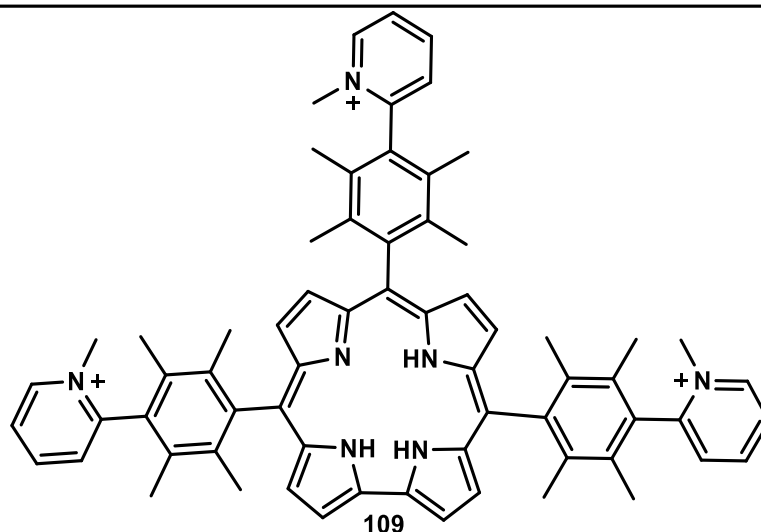
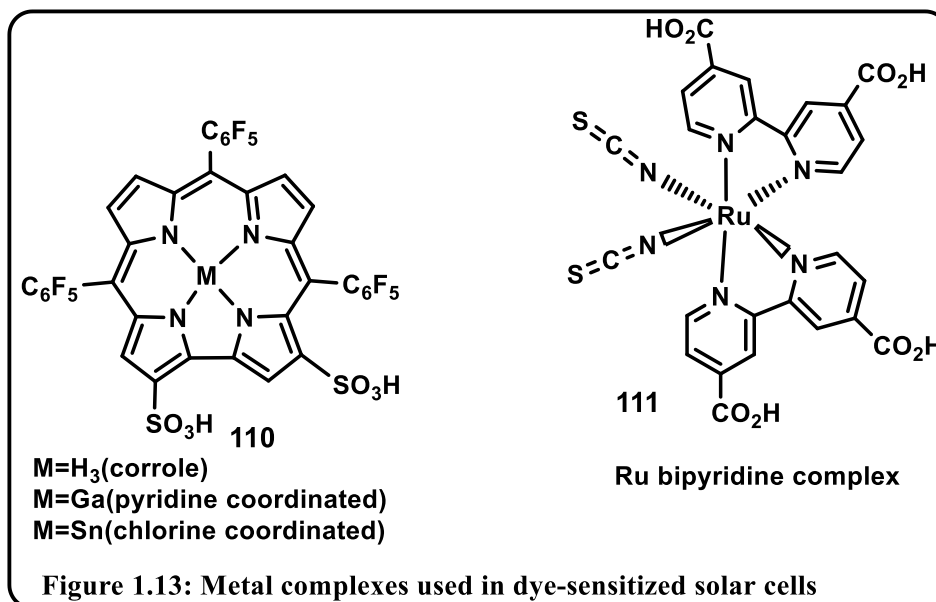


Figure 1.12: First water-soluble corrole reported in vivo medicinal investigation<sup>102</sup>

**Dye sensitized solar cell:** Renewable energies have the prospective to reduced dependence on expensive fossil fuel and increased economic stability which motivate the researchers to the development of renewable energy resources. Dye sensitized solar cells are the most promising, economically friendly alternatives for converting solar energy to electrical energy. Sensitizers play a vital role in the accumulation of solar energy in the cell. Generally, ruthenium bipyridine and different porphyrinoides are used in the above-mentioned purpose<sup>106-107</sup>. Of them, later is more interesting because their photophysical properties can be changed by suitable substituents at *meso* positions or  $\beta$ -positions, even changing central metal atom. As the corrole frontier orbitals have higher energy than the corresponding porphyrin analogue<sup>108</sup> so, they are widely used as a sensitizer in DSSC. Bissulfonated trispentafluorophenyl corrole and its Ga and Sn metal complexes were chosen for this purpose<sup>109</sup>. It was founded that all these complexes were bonded to mesoporous material TiO<sub>2</sub>, but the efficiency of the Sn complex was much less whether free base corrole and its Gallium complex have comparable efficiency. The lower efficiency of the Sn complex is due to the disability

of the excited state to inject electrons into the TiO<sub>2</sub> film. The different measurement showed that suitably substituted corroles were superior as a sensitizer compares with other tetrapyrrolic derivatives. Even cell efficiencies can increase up to half as that of popularly used ruthenium-based sensitizer.



**Objective of present Thesis:** There are many more examples of different functionalized porphyrin derivatives, including peripheral and inner core modifications. Although peripheral substituted corroles are common, N-substituted corroles are very rarely reported. The present thesis describes new synthetic methodologies for the synthesis of such N-substituted corrole derivatives. Further complete characterization of these derivatives is done using different spectroscopic techniques, including single-crystal X-ray diffractions. The present thesis consists of four chapters.

In **chapter 1**, different modifications of porphyrinoids are discussed. Among them, one of the most contributed contracted porphyrin analogue, corrole discovery and other synthetic protocols for corrole preparation and their modifications are described. Later different coordination modes of metallocorroles, corroles and metallocorroles based

applications in the multidisciplinary area has been concisely reviewed. Besides functionalization of corroles are also outlined.

**Chapter 2** deals with the development of an efficient, high yielding, single step and relatively greener methodology for facile synthesis of  $N^{21}$ ,  $N^{22}$  –carbamide corroles derivative. Under the optimized reaction conditions, the free base corroles upon treatment with ammonium carbonate at 110°C in a 3:5 dichloromethane and pyridine mixture and in stirring for 3 hours resulted in the formation of corresponding  $N^{21}$ ,  $N^{22}$ -carbamide- corroles in good yields. The generalisation of new protocol and characterisation of the carbamide derivatives both experimentally and theoretically have been done. Keeping in mind extensive literature on functionalized ureas and their potent pharmaceutical applications, we have chosen this project.

**Chapter 3** describes the synthesis of a new N, N' –bridged corrole derivative by condensing diiodomethane and 5,10,15-tris(pentafluorophenyl)corrole in the presence of pyridine. The characterization of newly synthesized macrocycle has done by different physicochemical techniques, e.g., NMR ( $^1\text{H}$ ,  $^{19}\text{F}$ ,  $^{13}\text{C}$ ), ESI Mass, and single-crystal X-ray structural analysis. The modified protocol gives an overall isolated yield of about 80% where as the previously reported synthetic procedure by Johnson *et al.*, reported 8% yield for the synthesis of 21, 22-methyleneoctaethylporphyrin. Not only drastic increased in yield but also reduction of reaction time and economic viability are observed in this work.

**Chapter 4** deals with the synthesis of a new platinum(II) porphyrin and its characterization. X-ray study reveals a characteristic C-H...Pt interactions with neighbouring PtTANP molecule leading to dimeric structure in solid-state. Cyclic voltammetric and differential pulse voltammetric measurement shows one reversible

oxidation couple at +1.10 V ( $\Delta E_p = 80$  mV) and one reversible reduction couple at -1.47 V ( $\Delta E_p = 80$  mV) versus Ag/AgCl. We have demonstrated that **PtTANP** behaves as a light-harvesting antenna due to the presence of acenaphthene chromophores in the Pt (II) porphyrin. In deaerated solution at 298 K, a strong phosphorescence is observed with a maximum at 660 nm, emission quantum yield of 35% and a lifetime of 75  $\mu$ s but a very weak phosphorescence ( $\Phi_{em} = 0.22\%$ ) with a much shorter lifetime ( $\tau = 910$  ns) is observed in air-equilibrated solution. The quenching by oxygen results in singlet oxygen production with a very high quantum yield of 88%, indicating its potential applications in the field of photodynamic therapy as well as oxygen sensors.

## ***References:***

1. A. R. Battersby, C. Fookes, G. Matcham, E. McDonald, *Nature*. **1980**, 285, 17-21
2. J. M. Berg, S. Lippard, *Principles of bioinorganic chemistry*. Mill Valley, 411s.ed.; *University Science Books*: **1994**.
3. K. M. Kadish, Smith, K. M.; Guillard, R.; Editors, *The Porphyrin Handbook; Volume 2, Heteroporphyrins, Expanded Porphyrins and Related Macrocycles*. *Academic Press*: **2000**.
4. J. L. Sessler, S. J. Weghorn, *Expanded, contracted & isomeric porphyrins*. *Elsevier*: **1997**; Vol. 15.
5. V. J. Bauer, L. J. C. Derrick, D. Dolphin, J. B. Paine, F. L. Harris, M. M. King, J. Loder, S. W. C. Wang, R. B. Woodward, *J. Am. Chem. Soc.* **1983**, 105, 6429-6436.
6. B. Franck, A. Nonn, *Angew. Chem. Int. Ed. Engl.* **1995**, 34, 1795-1811
7. P. Rothmund, *J. Am. Chem. Soc.*, **1935**, 57, 2010-2011
8. A. D. Adler, F. R. Longo, J. D. Finarelli, J. Goldmacher, J. Assour, L. Korsakoff, *J. Org. Chem.*, **1967**, 32, 476-476.
9. J. S. Lindsey, I. C. Schreiman, H. C. Hsu, P. C. Kearney, A. M. Marguerettaz, *J. Org. Chem.*, **1987**, 52, 827-836
10. C. Weiss, *J. Mol. Spectrosc.* **1972**, 44, 37-80.
11. J.-L. Soret, *Compt. Rend.* **1883**, 97, 1269-1273.
12. K. M. Kadish, K. M. Smith, R. Guillard, Editors, *The Porphyrin Handbook; Volume 1, Synthesis and Organic Chemistry*. *Academic Press*: **2000**.
13. J. L. Sessler, D. Seidel, A. E. Vivian, V. Lynch, B. L. Scott, and D. W. Keogh, *Angew. Chem. Int. Ed.* **2001**, 40, No. 3.

14. J. L. Sessler, T. Murai, G. Hemmi, *Inorganic Chemistry*. Vol. 28, No. 17, **1989** 3391.
15. D. C. Hodgkin, J. Kamper, J. Lindsey, M. MacKay, J. Pickworth, J. Robertson, C. B. Shoemaker, J. White, R. Prosen, K. Trueblood, *Proc. R. Soc. Lond. A* **1957**, 242, 228-263.
16. A. Johnson, A. Todd, *Vitam. Horm.* **1957**, 15, 1.
17. R. Bonnett, *Chem. Rev.* **1963**, 63, 573-605
18. A. R. Battersby, *J. Nat. Prod.* **1988**, 51, 629-642.
19. B. Kräutler, B. T. Golding, D. A. J. Wiley & Sons, *Science*. **2008**, 559.
20. A. Johnson, R. Price, *J. Chem. Soc.* **1960**, 1649-1653.
21. A. Johnson, I. Kay, *J. Chem. Soc.* **1965**, 1620-1629.
22. A. Meller, A. Ossko, *Monatsh. Chem.* **1972**, 103, 150-155.
23. Y. Inokuma, A. Osuka *Dalton Trans.* **2008**, 2517–2526.
24. E. Vogel, B Binsack, Y. Hellwig, C. Erben, A. Heger, J. Lex, Y. D. Wu, *Angew. Chem., Int. Ed. Engl.* **1997**, 36, 2612-2615.
25. S. Will, A. Rahbar, H. Schmickler, J. Lex, E. Vogel, *Angew. Chem. Int. Ed. Engl.* **1990**, 29, 1390-1393.
26. M. Bröring, S. Khler, C. Kleeberg, *Angew. Chem. Int. Ed.* **2008**, 47, 5658 –5660.
27. A. Ghosh, K. Jynge, *Chem. Eur. J.* **1997**, 3, 823-8
28. R. Paolesse, F. Sagone, A. Macagnano, T. Boschi, L. Prodi, M. Montalti, N. Zaccheroni, F. Bolletta, K. M. Smith, *J. Porphyrins Phthalocyanines*. **1999**, 3, 364-370.
29. Y. S. Balazs, I. Saltsman, A. Mahammed, E. Tkachenko, G. Golubkov, J. Levine, Z. Gross, *Magn. Reson. Chem.* **2004**, 42, 624–635.

30. H. R. Harrison, J. R. Hodder, D. C. Hodgkin, *J. Chem. SOC. (B)*, **1971**.
31. Z. Gross, N. Galili, L. Simkhovich, I. Saltsman, M. Botoshansky, D. Blaeser, R. Boese, I. Goldberg, *Org. Lett.* **1999**, *1*, 599-602.
32. I. A. Harel, Z. Gross, *Chem. Eur. J.* **2009**, *15*, 8382 – 8394.
33. E. Vogel, S. Will, A. S. Tilling, L. Neumann, J. Lex, E. Bill, A. X. Trautwein, K. Wieghardt, *Angew. Chem., Int. Ed. Engl.* **1994**, *33*, 731–735.
34. R. Orłowski, D. Gryko, D. T. Gryko, *Chem. Rev.* **2017**, *117*, 3102–3137.
35. M. Conlon, A. W. Johnson, W. R. Overend, D. Rajapaksa, C. M. Elson, *J. Chem. Soc. Perkin Trans. 1.* **1973**, 2281–2288.
36. R. Paolesse, E. Tassoni, S. Licoccia, M. Paci, T. Boschi, *Inorganica Chimica Acta* **241** (**1996**) 55-60.
37. R. Paolesse, L. Jaquinod, D. J. Nurco, S. Mini, F. Sagone, T. Boschi, K. M. Smith, *Chem. Commun.* **1999**, 1307–1308.
38. B. Koszarna, D. T. Gryko, *J. Org. Chem.* **2006**, *71*, 3707-17.
39. V. Král, P. Vašek, B. Dolensky, *Collect. Czech. Chem. Commun.* **2004**, *69*, 1126-1136.
40. R. Guillard, D. T. Gryko, G. Canard, J. Barbe, B. Koszarna, S. Brandès and M. Tasior, *Org. Lett.* **2002**, *4*, 4491–4494.
41. D. A. Richard and C. P. James, *Tetrahedron Lett.* **200**, *44*, 3323–3327.
42. S. Ooi, T. Tanaka, and A. Osuka, *Eur. J. Org. Chem.* **2015**, 2015: 130–134.
43. R. Orłowski, D. Gryko and D. T. Gryko, *Chem. Rev.* **2017**, *117*, 3102–3137, and references cited therein.
44. T. Chatterjee, V. S. Shetti, R. Sharma and M. Ravikanth, *Chem. Rev.* **2017**, *117*, 3254–3328, and references cited therein.

45. D. T. Gryko, J. P. Fox and D. P. Goldberg, *J. Porphyrins Phthalocyanines*, **2004**, 08, 1091–1105, and references cited therein.
46. A. W. Johnson, I. T. Kay and R. Rodrigo, *J. Chem. Soc.*, **1963**, 2336–2342.
47. C.-H. C. Lee, W.-S. Cho, J.-W. Ka, H.-J. Kim and P. H. Lee, *Bull. Korean Chem. Soc.*, **2000**, 21, 429–433.
48. W.-S. Cho and C.-H. Lee, *Tetrahedron Lett.*, **2000**, 41, 697– 701.
49. J. Narayanan, B. Sridevi, T. K. Chandrashekar, U. Englisch and K. Ruhlandt-Senge, *Org. Lett.*, **1999**, 1, 587–590. 47. S.
50. M. Pawlicki, L. Latos-Gra'zynski and L. Szterenber, ' *J. Org. Chem.*, **2002**, 67, 5644–5653.
51. K. Fujino, Y. Hirata, Y. Kawabe, T. Morimoto, A. Srinivasan, M. Toganoh, Y. Miseki, A. Kudo and H. Furuta, *Angew. Chem., Int. Ed.*, **2011**, 50, 6855–6859.
52. S. Will, J. Lex, E. Vogel, H. Schmickler, J.-P. Gisselbrecht, C. Haubtmann, M. Bernard, M. Gorss, *Angew. Chem. Int. Ed. Engl.* **1997**, 36, 357-361.
53. K. M. Kadish, C. Erben, Z. Ou, V. A. Adamian, S. Will, E. Vogel, *Inorg. Chem.* **2000**, 39, 3312-3319.
54. K. E. Thomas, A. B. Alemayehu, J. Conradie, C. Beavers, A. Ghosh, *Inorg. Chem.* **2011**, 50, 12844-12851.
55. C. Brückner, R. P. Briñas, J. A. Krause Bauer, *Inorg. Chem.* **2003**, 42, 4495-4497.
56. Z. Ou, C. Erben, M. Autret, S. Will, D. Rosen, J. Lex, E. Vogel, K. M. Kadish, *J. Porphyrins Phthalocyanines* **2005**, 09, 398-412.
57. F. Jérôme, B. Billier, J. M. Barbe, E. Espinosa, S. Dahaoui, C. Lecomte, R. Guillard, *Angew. Chem. Int. Ed.* **2000**, 39, 4051-4053.
58. Z. Gross, *J. Biol. Inorg. Chem.* **2001**, 6, 733-738.

59. L. Simkhovich, A. Mahammed, I. Goldberg, Z. Gross, *Chem. Eur. J.* **2001**, *7*, 1041-55.
60. W. Sinha, N. Deibel, H. Agarwala, A. Garai, D. Schweinfurth, C. S. Purohit, G. K. Lahiri, B. Sarkar, S. Kar, *Inorg. Chem.* **2014**, *53*, 1417-1429.
61. J. H. Palmer, M. W. Day, A. D. Wilson, L. M. Henling, Z. Gross, H. B. Gray, *J. Am. Chem. Soc.* **2008**, *130*, 7786-7787.
62. A. Mahammed, I. Giladi, I. Goldberg, Z. Gross, *Chem. Eur. J.* **2001**, *7*, 4259-65.
63. J. Bendix, I. J. Dmochowski, H. B. Gray, A. Mahammed, L. Simkhovich, Z. Gross, *Angew. Chem. Int. Ed.* **2000**, *39*, 4048-4051.
64. A. Mahammed, Z. Gross, *J. Inorg. Biochem.* **2002**, *88*, 305-309.
65. S. Licoccia, R. Paolesse, E. Tassoni, F. Polizio, T. Boschi, *J. Chem. Soc., Dalton Trans.* **1995**, 3617-21.
66. I. Harel-Aviv, Z. Gross, *Coord. Chem. Rev.* **2011**, *255*, 717-736.
67. A. L. Ward, W. L. Buckley, W. W. Lukens, J. Arnold, *J. Am. Chem. Soc.* **2013**, *135*, 13965-13971.
68. H. L. Buckley, W. A. Chomitz, B. Koszarna, M. Tasior, D. T. Gryko, P. J. Brothers, J. Arnold, *Chem. Commun.* **2012**, *48*, 10766-10768.
69. R. Paolesse, S. Nardis, M. Venanzi, M. Mastroianni, M. Russo, F. R. Fronczek, M. G. H. Vicente, *Chem Eur J.* **2003**, *9*, 1192
70. M. J. Broadhurst, R. Grigg, G. Shelton, A. W. Johnson, *J. Chem. Soc. D* **1970**, 231-233.
71. M. J. Broadhurst, R. Grigg, G. Shelton, A. W. Johnson, *J. Chem. Soc., Perkin Trans. I* **1972**, *99*, 143-151.
72. Z. Gross, N. Galili, *Angew Chem Int Ed.* **1999**, *38*, 2366.

73. I. Saltsman, I. Goldberg, Z. Gross, *Tetrahedron Lett.* **2003**, *44*, 5669.
74. H. Liu, T. Lai, L. Yeung, C. K. Chang, *Org. Lett.* **2003**, *5*, 617–620.
75. T. H. Ngo, F. Puntoriero, F. Nastasi, K. Robeyns, L. Van Meervelt, S. Campagna, W. Dehaen, W. Maes, *Chem. - Eur. J.* **2010**, *16*, 5691–5705.
76. R. Paolesse, L. Jaquinod, M. O. Senge, K. M. Smith, *J. Org. Chem.* **1997**, *62*, 6193–6198.
77. I. Saltsman, A. Mahammed, I. Goldberg, E. Tkachenko, M. Botoshansky, Z. Gross, *J. Am. Chem. Soc.* **2002**, *124*, 7411–7420.
78. K. Sudhakar, V. Velkannan, L. Giribabu, *Tetrahedron Lett.* **2012**, *53*, 991–993.
79. A. Mahammed, I. Goldberg, Z. Gross, *Org Lett.* **2001**, *3*(22), 3443–3446.
80. A. Mahammed, Z. Gross, *J Porphyrins Phthalocyanines.* **2010**, *14*(10), 911–923.
81. I. Harel-Aviv, Z. Gross, *Chem. Eur. J.* **2009**, *15*, 8382–94.
82. I. Aviv, Z. Gross, *Chem. Commun.* **2007**, 1987.
83. Z. Gross, L. Simkhovich, N. Galili, *Chem. Commun.* **1999**, 599–600.
84. G. Golubkov, J. Bendix, H. B. Gray, A. Mahammed, I. Goldberg, A. J. DiBilio, Z. Gross, *Angew. Chem. Int. Ed. Engl.* **2001**, *40*, 2132–2134.
85. H. Y. Liu, T. S. Lai, L. L. Yeung, C. K. Chang, *Org. Lett.* **2003**, *5*, 617–20.
86. I. Luobeznova, M. Rizman, I. Goldberg, Z. Gross, *Inorg. Chem.* **2006**, *45*, 386–94.
87. A. Mahammed, Z. Gross, *J. Am. Chem. Soc.* **2005**, *127*, 2883.
88. A. Mahammed, Z. Gross, *Angew. Chem.* **2006**, *118*, 6694 –6697.
89. K. J. Barnham, C. L. Masters, A. I. Bush, *Nat. Rev. Drug Discov.* **2004**, *3*, 205–214.
90. J. S. Beckman, *Chem. Res. Toxicol.* **1996**, *9*, 836–44.

91. G. Merenyi, J. Lind, S. Goldstein, G. Czapski, *Chem. Res. Toxicol.* **1998**, *11*, 712-3.
92. R. Bryk, P. Griffin, C. Nathan, *Nature* **2000**, *407*, 211-215.
93. Z. Gershman, I. Goldberg, Z. Gross, *Angew. Chem. Int. Ed. Engl.* **2007**, *46*, 4320-4.
94. A. E. Meier-Callahan, A. J. DiBilio, L. Simkhovich, A. Mahammed, I. Goldberg, H. B. Gray and Z. Gross, *Inorg. Chem.*, **2001**, *40*, 6788.
95. A. Mahammed, H. B. Gray, A. E. Meier-Callahan and Z. Gross, *J. Am. Chem. Soc.*, **2003**, *125*, 1162.
96. Z. Gross, L. Simkhovich and N. Galili, *Chem. Commun.*, **1999**, 599.
97. R. Guillard, F. Jérôme, J. M. Barbe, C. P. Gros, Z. Ou, J. Shao, J. Fischer, R. Weiss, K. M. Kadish, *Inorg. Chem.* **2001**, *40*, 4856-4865.
98. R. Guillard, C. P. Gros, F. Bolze, F. Jérôme, Z. Ou, J. Shao, J. Fischer, R. Weiss, K. M. Kadish, *Inorg. Chem.* **2001**, *40*, 4845-4855.
99. K. M. Kadish, Z. Ou, J. Shao, C. P. Gros, J. M. Barbe, F. Jérôme, F. Bolze, F. Burdet, R. Guillard, *Inorganic Chemistry*. 2002, Vol. 41, No. 15.
100. J. M. Barbe, G. Canard, S. Brandès, F. Jérôme, G. Dubois, R. Guillard, *Dalton Trans.* **2004**, 1208 – 1214.
101. A. Haber, A. Mahammed, B. Fuhrman, N. Volkova, R. Coleman, T. Hayek, M. Aviram, Z. Gross, *Angew. Chem. Int. Ed. Engl.* **2008**, *47*, 7896-900.
102. L. Simkhovich, I. Goldberg, Z. Gross, *Journal of Inorganic Biochemistry*. **2000**, *80*, 235 –238.
103. D. Aviezer, S. Cotton, M. David, A. Segev, N. Khaselev, N. Galili, Z. Gross, A. Yayon, *Cancer Res.* **2000**, *60 (11)*, 2973–2980.

104. A. Mahammed, H. B. Gray, J. J. Weaver, K. Sorasaene, Z. Gross, *Bioconjugate Chem.* **2004**, *15*, 738–746.
105. R. D. Teo, J. Y. Hwang, J. Termini, Z. Gross, H. B. Gray, *Chem. Rev.* **2017**, *117*, 2711–2729.
106. W. M. Campbell, A. K. Burrell, D. L. Officer, K. W. Jolley, *Coord. Chem. Rev.* **2004**, *248*, 1363–1379.
107. Q. Wang, W. M. Campbell, E. E. Bonfantani, K. W. Jolley, D. L. Officer, P. J. Walsh, K. Gordon, R. Humphry-Baker, M. K. Nazeeruddin, M. Gratzel. *J. Phys. Chem. B* **2005**, *109*, 15397–409.
108. Z. Gross and H. B. Gray, *Comments Inorg. Chem.*, **2006**, *27*, 61.
109. D. Walker, S. Chappel, A. Mahammed, J. J. Weaver, B. S. Brunschwig, J. R. Winkler, H. B. Gray, A. Zaban and Z. Gross, *J. Porphyrins Phthalocyanines*, **2006**, *10*, 1259.



## ***CHAPTER 2***

# **Synthesis of urea derivatives via reductive carbon dioxide fixation into contracted porphyrin analogues**

## **2.1 Introduction**

## **2.2 Results and Discussion**

### **2.2.1 Generalization of synthetic procedure**

## **2.3 Spectral Characterization**

### **2.3.1 Mass Spectroscopy**

### **2.3.2 NMR Spectroscopy**

### **2.3.3 IR Spectroscopy**

### **2.3.4 UV-Vis and Emission Spectroscopy**

### **2.3.5 Crystal Structure**

## **2.4 Spin Density Calculations**

## **2.5 Conclusions**

## **2.6 Experimental Section**

### **2.6.1 Materials**

### **2.6.2 Physical measurements**

### **2.6.3 Crystal Structure Determination**

### **2.6.4 Computational Methods**

### **2.6.5 Synthesis**

**2.6.5.1 Synthesis of N<sup>21</sup>,N<sup>22</sup>-carbamide-5,10,15-triphenylcorrole, 1B**

**2.6.5.2 For N<sup>21</sup>,N<sup>22</sup> carbamide-10-(2,4,5-trimethoxyphenyl)5,15-bis-(4-cyanophenyl)corrole, 2B**

**2.6.5.3 For N<sup>21</sup>,N<sup>22</sup>-carbamide-10-(4,7-dimethoxynaphthalen-1-yl)-5,15-bis(4-cyanophenyl)corrole, 3B**

**2.6.5.4 For N<sup>21</sup>,N<sup>22</sup> carbamide-5,10,15-tris(4Benzyloxyphenyl)corrole, 4B**

**2.6.5.5 For N<sup>21</sup>,N<sup>22</sup>-carbamide-5,10,15-tris(4-cyanophenyl)corrole, 5B**

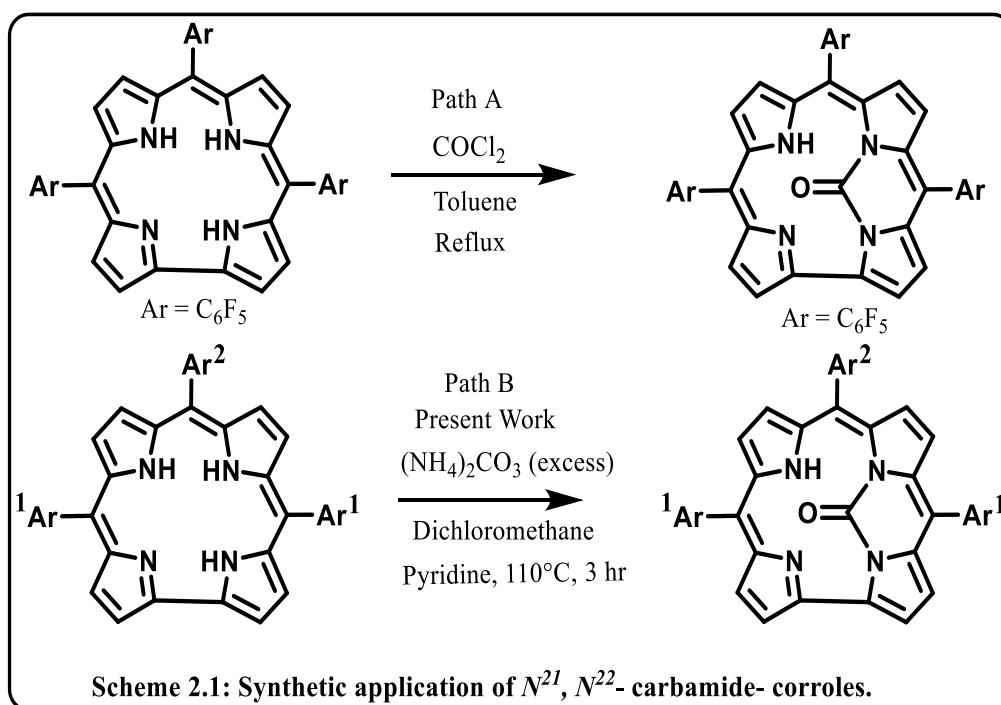
**2.6.5.6 For N<sup>21</sup>,N<sup>22</sup>-carbamide-5,10,15-tris-(2-bromo-5-fluorophenyl)corrole, 6B**

**2.6.5.7 For N<sup>21</sup>,N<sup>22</sup>-carbamide-5,10,15-tris(4-nitrophenyl)corrole, 7B**

## 2.1 Introduction:

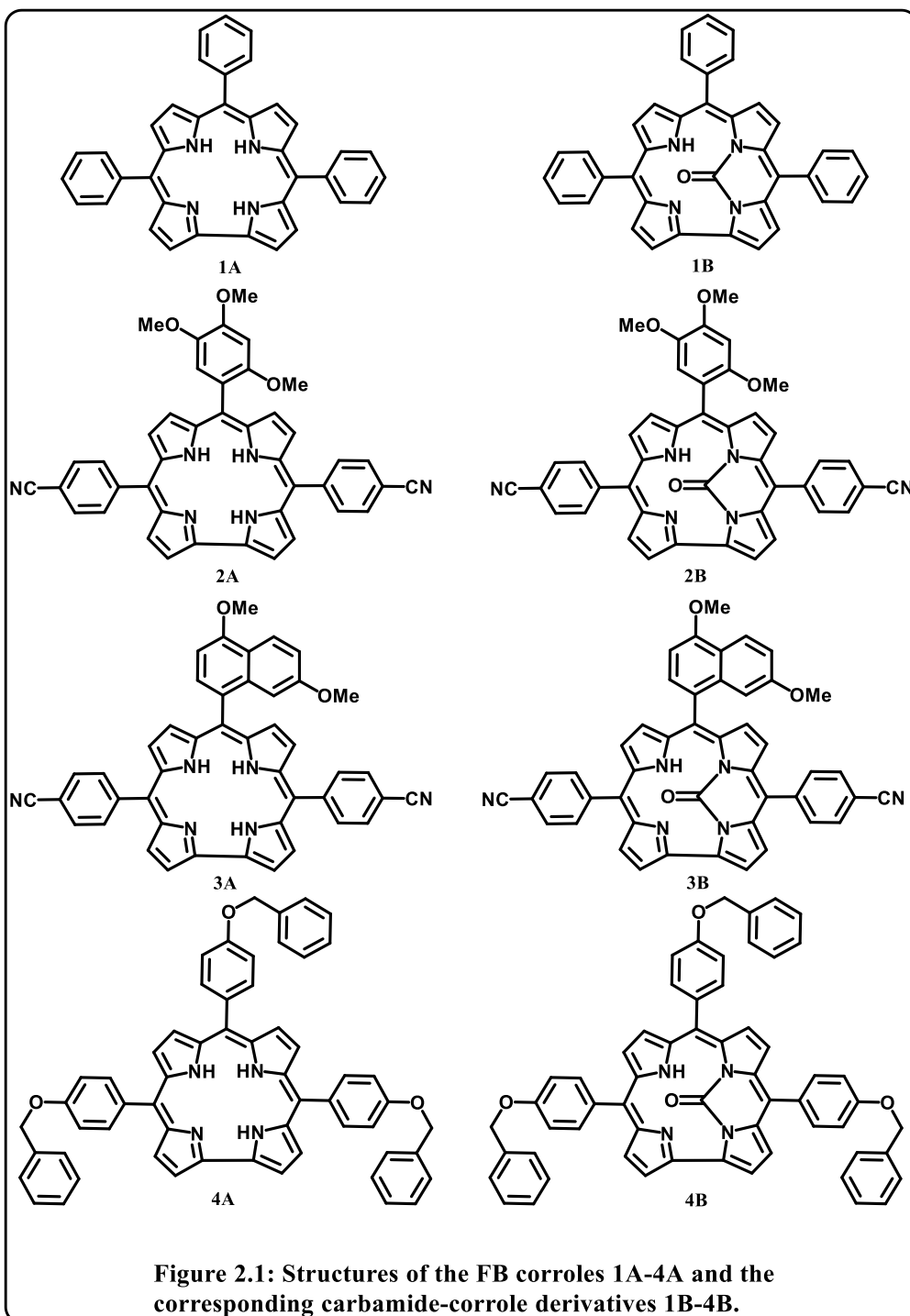
In the earlier chapter, a discussion on some of the important synthesis of differently substituted corrole, different coordination modes of metallocorroles, their application in various fields of science and functionalization of corrole, which includes inner core as well as peripheral functionalization, were outlined in a concise manner. One of the novel synthetic protocol for inner core functionalization to form urea corrole derivative has been discussed in detail in this present chapter. Urea, the wonder molecule, is considered as a bridge between chemistry and biology and is the foundation stone of modern organic chemistry<sup>1-5</sup>. The carbonyl functional group in urea has earned its reputation for inertness, and thus, it has not yet been fully investigated. The urea functional group has been regularly exploited in several areas, including supramolecular chemistry,<sup>6</sup> roles in foldamer structures,<sup>7</sup> in organo-catalysis,<sup>8</sup> as ion transporters,<sup>9</sup> amination reactions,<sup>10</sup> and various rearrangement reactions<sup>11</sup> etc. The various urea derivatives have extensive applications in medicinal chemistry. For example, as anti-atherosclerotic (remove hardening of arteries),<sup>12</sup> antibiotics,<sup>13</sup> hypoglycaemic,<sup>14</sup> antitumour activities,<sup>15</sup> sedatives,<sup>16</sup> anticonvulsants,<sup>17</sup> and as HIV-1 protease inhibitor.<sup>18</sup> In the literature on functionalized ureas, a series of aliphatic,<sup>19</sup> aromatic,<sup>20</sup> alicyclic,<sup>21</sup> and heterocyclic analogues<sup>22</sup> of differently substituted ureas have been synthesized, and their properties have been thoroughly screened for various applications. But surprisingly, there is only a single protocol exist in the literature that deals with the synthesis of  $N^{21}, N^{22}$ -carbamide-corrole derivatives.<sup>23</sup> Among the various porphyrinoids, we have chosen corrole (a contracted porphyrin analogue) here for several reasons, including its extensive applications in many areas.<sup>24-48</sup> N-substituted

corroles were first reported by Johnson and Kay in 1965<sup>49</sup> followed by Gross *et al.* in 1999.<sup>50</sup>  $N^{21}$ ,  $N^{22}$ -carbamide-corrole derivatives were first reported by Gross *et al.* (Path A in Scheme 2.1).<sup>23</sup> They performed the synthesis of  $N^{21}$ ,  $N^{22}$ -carbamide-tris(pentafluorophenyl)-corrole in excellent yields by using phosgene(carbonyl chloride)<sup>23</sup> (Scheme 2.1). However, it is important to keep in mind that the carbonylation agent for this reaction is phosgene. Phosgene is an extremely toxic, poisonous and corrosive gas and needs special technique to handle it. They have further demonstrated the use of a rhodium (I) complex of this chiral carbamide corrole ligand system in asymmetric cyclopropanation reaction.<sup>51</sup> In the following, we present a new synthetic protocol for the facile synthesis of a series of  $N^{21}$ ,  $N^{22}$ -carbamide-corrole derivatives.

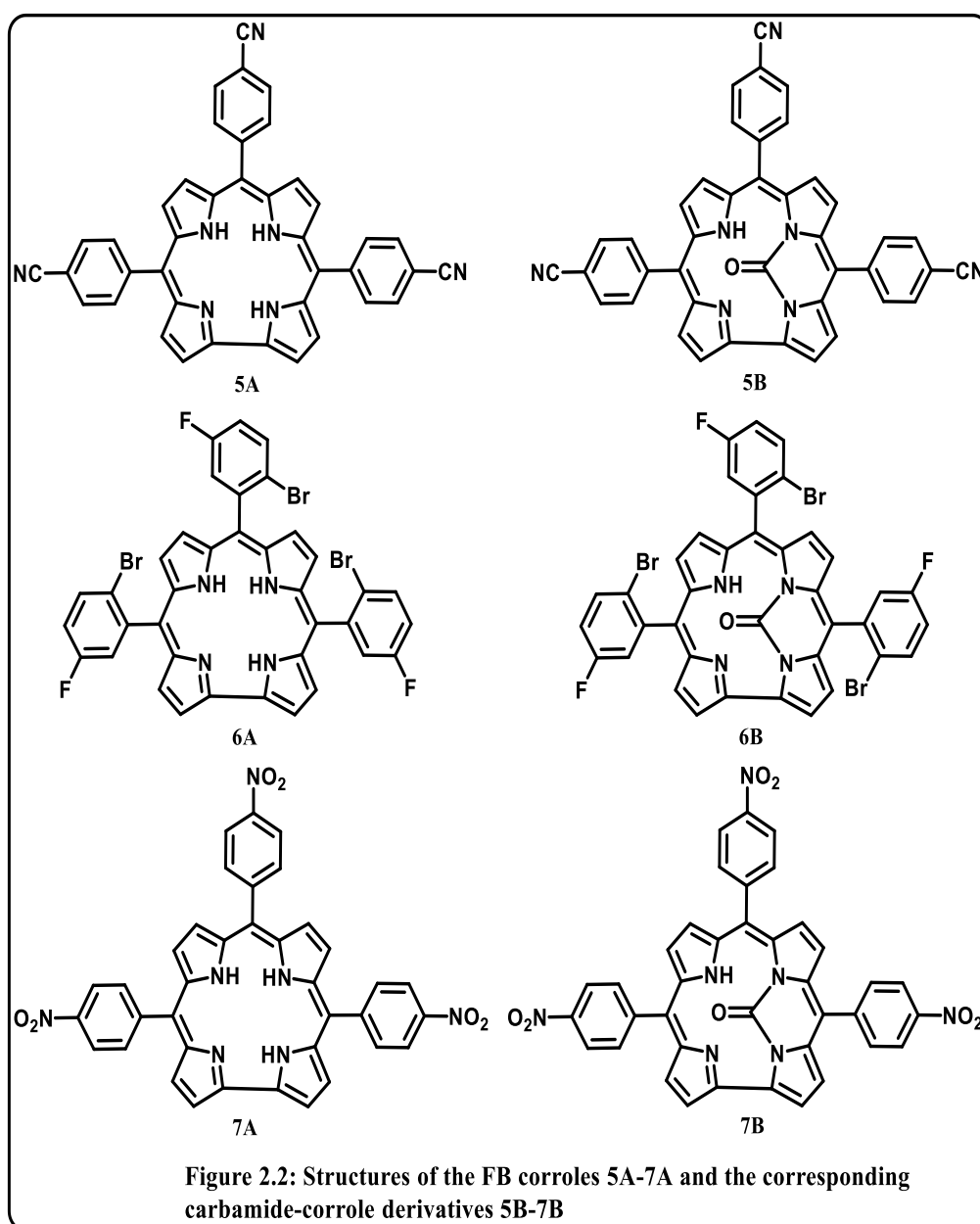


## 2.2 Results and Discussion:

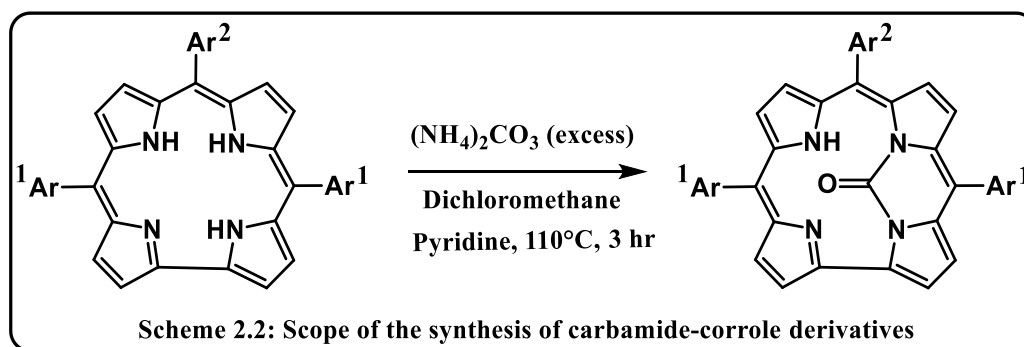
**2.2.1 Generalization of synthetic procedure:** In order to generalize the newly designed reaction protocol, we have explored a series of differently substituted corrole ligand functionalities bearing both electron releasing and electron withdrawing functional groups at the corrole periphery (Figure 2.1 and 2.2).



All of these newly synthesized  $N^{21}$ ,  $N^{22}$ -carbamide-corrole compounds have been thoroughly characterized by various spectroscopic techniques, including single crystal X-ray structural analysis of the representative derivatives (Fig. 2.3- Fig. 2.32). The rich and extensive application of substituted urea derivatives certainly points that the discovery of a new methodology can open up an entirely new avenue with broad applications.



While reacting vanadyl acetylacetonate with FB corroles, surprisingly, we have isolated a new compound ' $N^{21},N^{22}$ -carbamide-corrole' in 1-2% yield. There is a distinct possibility that vanadyl acetylacetonate probably releases a small amount of  $\text{CO}_2$  gas at a higher temperature.<sup>52</sup> On the basis of these observations, we envisioned the role of  $\text{CO}_2$ . Under the optimized reaction conditions, the free base corroles upon treatment with ammonium carbonate at  $110^\circ\text{C}$  in a 3:5 dichloromethane and pyridine mixture and in stirring for 3 hours resulted in the formation of corresponding  $N^{21},N^{22}$ -carbamide-corroles in good yields (Table 2.1). In order to understand the scope and applicability of this newly designed reaction, a variety of different reaction conditions were scrutinized. The solvent effects were investigated with a series of polar solvents such as  $\text{CHCl}_3$ ,  $\text{CH}_3\text{CN}$ ,  $\text{CH}_3\text{OH}$ , and THF. We observed that  $N^{21},N^{22}$ -carbamide-corrole were formed in negligible amount (yields  $< 5\%$ ) in  $\text{CHCl}_3$  solvent only. Thus the reaction is highly solvent specific, e.g., no  $N^{21},N^{22}$ -carbamide-corrole products were observed in other solvents like  $\text{CH}_3\text{CN}$ ,  $\text{CH}_3\text{OH}$ , and THF. In order to understand the mechanism of this reaction, we have screened the effect of pyridine in this reaction. The reaction does not occur at all in the absence of pyridine. While changing the base from pyridine to triethylamine, the reaction also fails.



This methodology was applicable to a large variety of free base corroles, and the resultant  $N^{21}, N^{22}$ -carbamide-corrole are always obtained in considerable yields. The

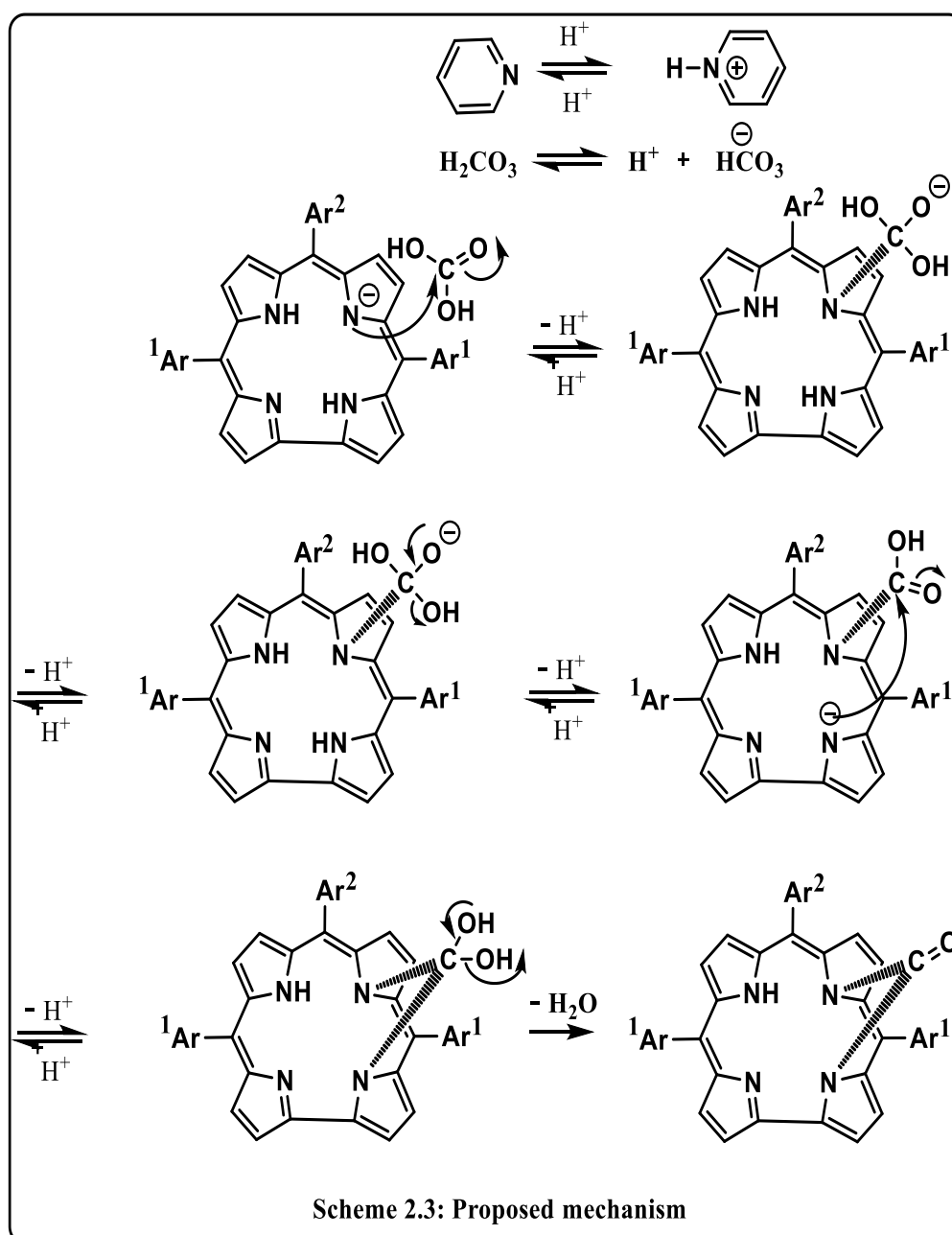
formation of  $N^{21}, N^{22}$ -carbamide-corrole derivatives can be easily monitored by TLC, Microanalysis, UV-vis, FT-IR, and NMR or by ESI-MS techniques (see ESI<sup>†</sup>). In order to understand the substrate specificity of this newly designed reaction, we have tested a wide range of meso-substituted corrole rings (Figure 2.1- Figure 2.2).

To our delight, we have observed that the reaction is equally successful for both the electron releasing and electron withdrawing *meso*-aryl substituents. The reaction tolerated most of the reactive functional groups, including cyanide, nitro, halogen substituents etc. We have used ammonium carbonate salt here in large excess and also heated it to a temperature of  $\sim 110^{\circ}\text{C}$ , thus it induces a facile release of  $\text{CO}_2$  gas. Reactions with various carbonates/bicarbonates, for example,  $\text{NH}_4\text{HCO}_3$  and  $\text{NaHCO}_3$  were also equally efficient. However, purging of  $\text{CO}_2$  gas, instead of using carbonates/bicarbonates salts cannot initiate the desired conversions. Probably the insolubility of  $\text{CO}_2$  gas in the desired solvent system hindered the reaction.

**Table 2.1. Isolated yield of product:**

Compound	Reactant	Product	Yield (%)
1	1A	1B	58
2	2A	2B	62
3	3A	3B	65
4	4A	4B	55
5	5A	5B	70
6	6A	6B	60
7	7A	7B	60

Thus we believe that the  $\text{HCO}_3^-/\text{H}_2\text{CO}_3$  (a soluble version of  $\text{CO}_2$  gas) is responsible for the desired conversions. Pyridine was used here for dual purposes, it can be considered as a solvent (boiling point:  $116^\circ\text{C}$ ) and also as a weak base for the desired reactions to occur. Based on all these observations, we have also proposed a mechanism for this newly designed reaction (scheme 2.3).



## 2.3 Spectral characterization:

### 2.3.2 NMR Spectra:

The  $^1\text{H}$  NMR spectrum of **1B-7B** exhibits sharp peaks in accordance with aromatic protons in the region  $\delta$ ,  $\sim 9.7$ – $7.6$  ppm. It was also observed that the peaks are de-shielded by  $\sim 0.7$  ppm in the carbamide-corrole derivatives (**1B-7B**) corresponding to their FB corrole counterparts (**1A-7A**). The  $^1\text{H}$  and  $^{13}\text{C}$  NMR spectra of the carbamide-corrole derivatives (**1B-7B**) are given below. (Fig. 2.3-Fig. 2.11)

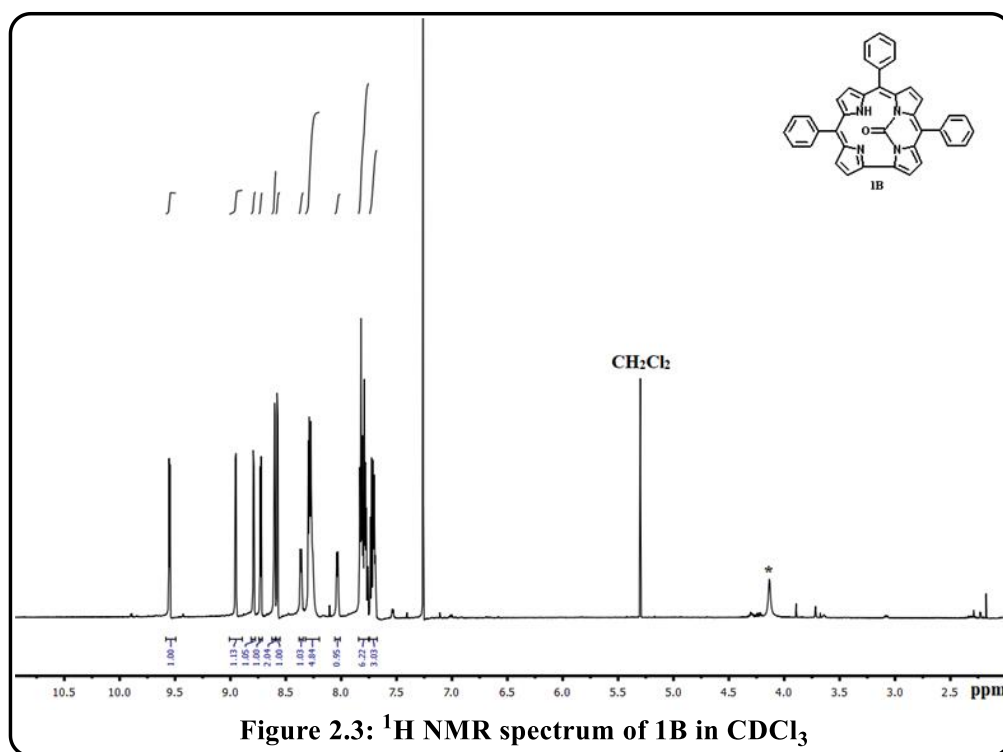
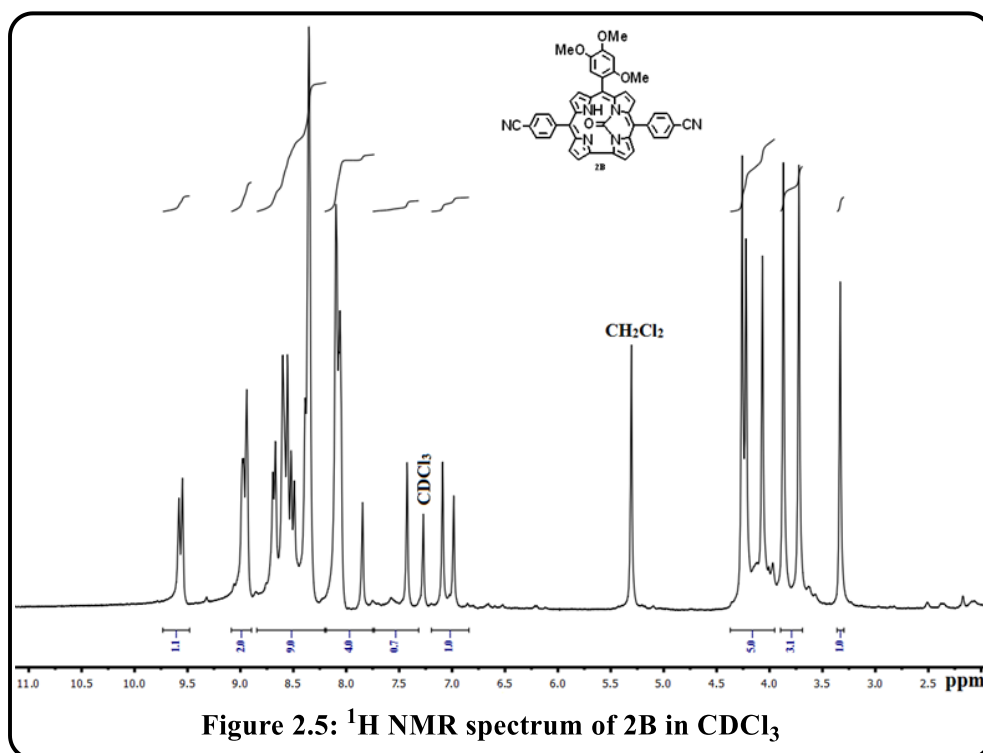
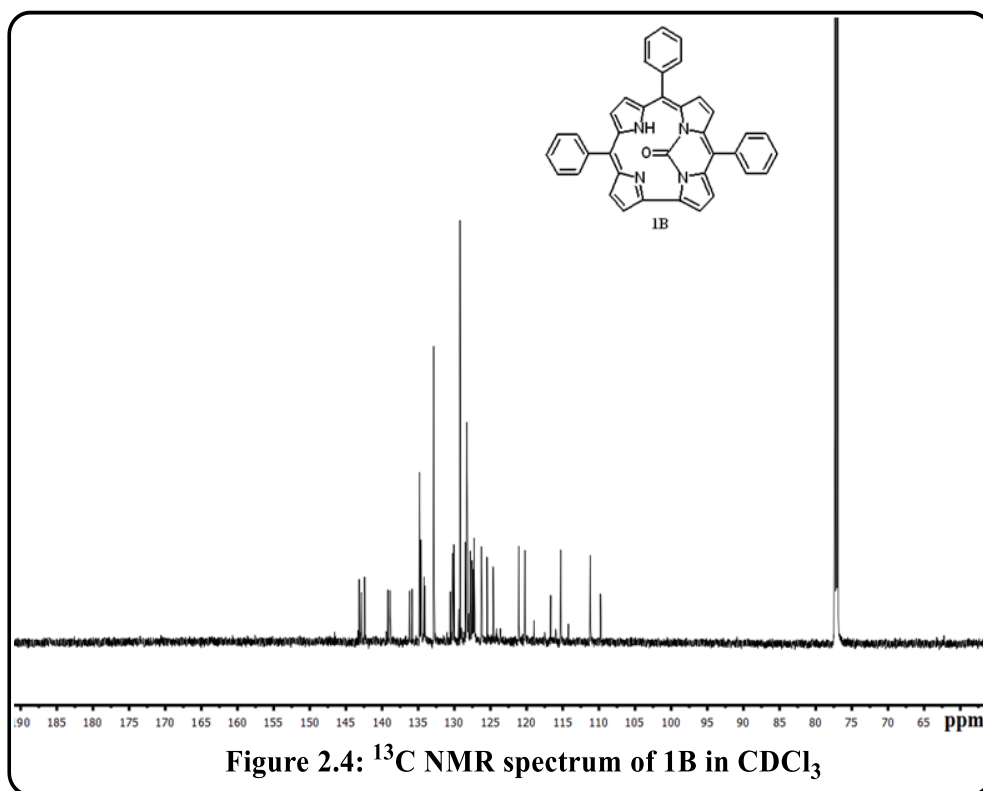


Figure 2.3:  $^1\text{H}$  NMR spectrum of **1B** in  $\text{CDCl}_3$



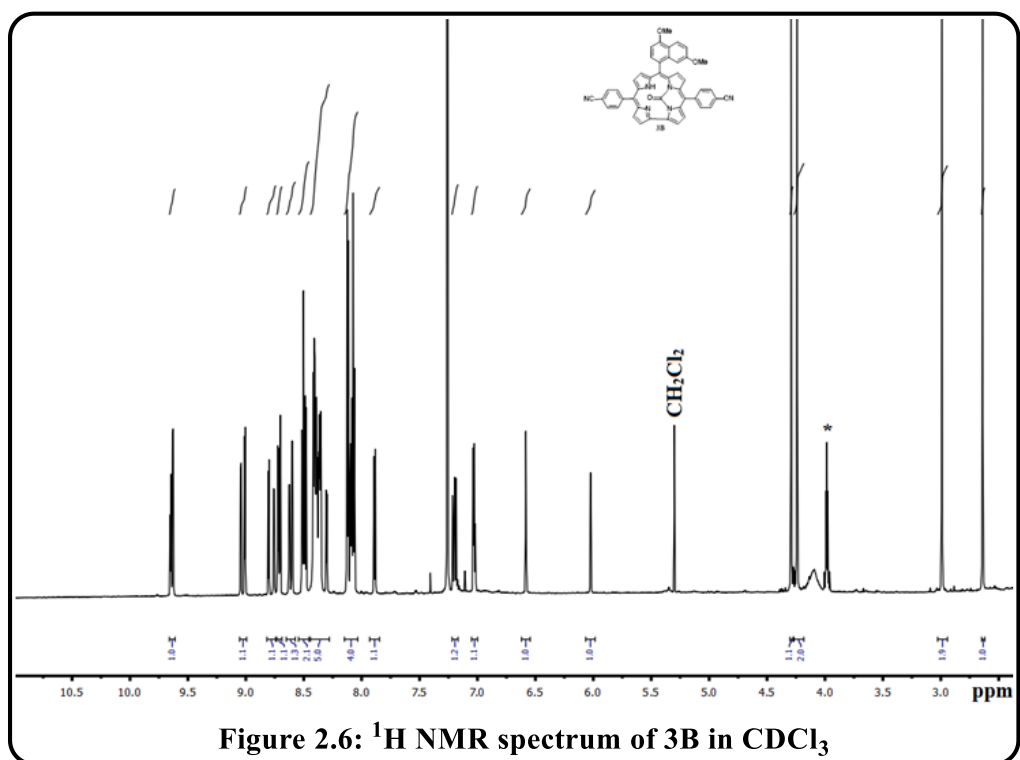


Figure 2.6: <sup>1</sup>H NMR spectrum of 3B in CDCl<sub>3</sub>

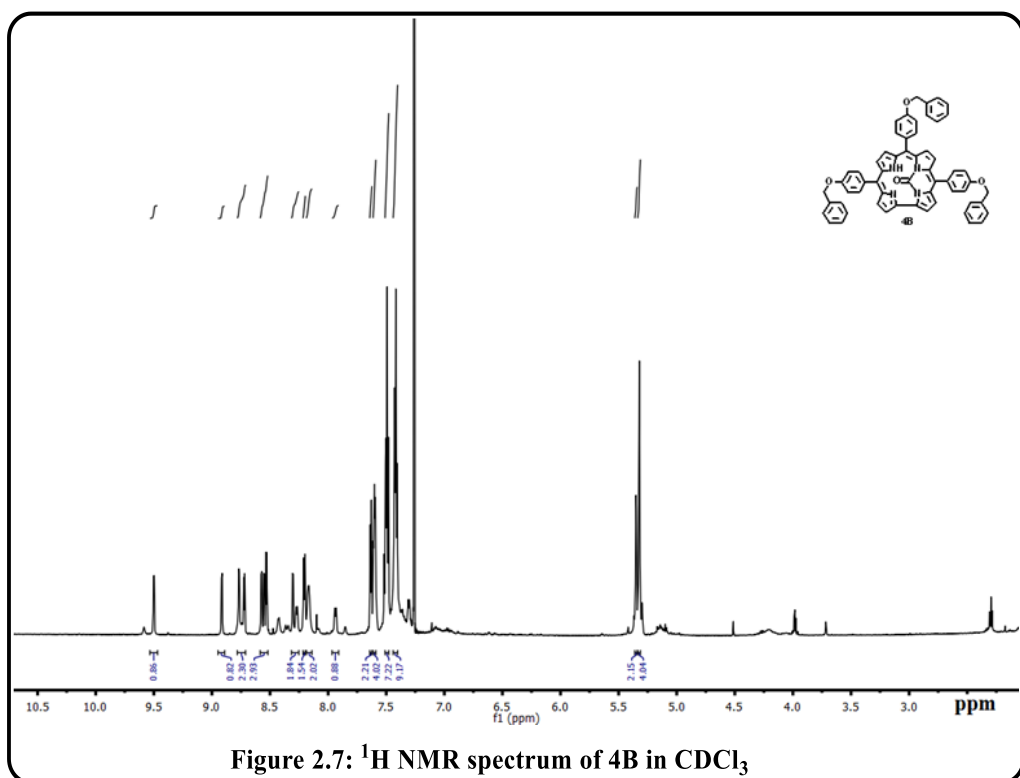
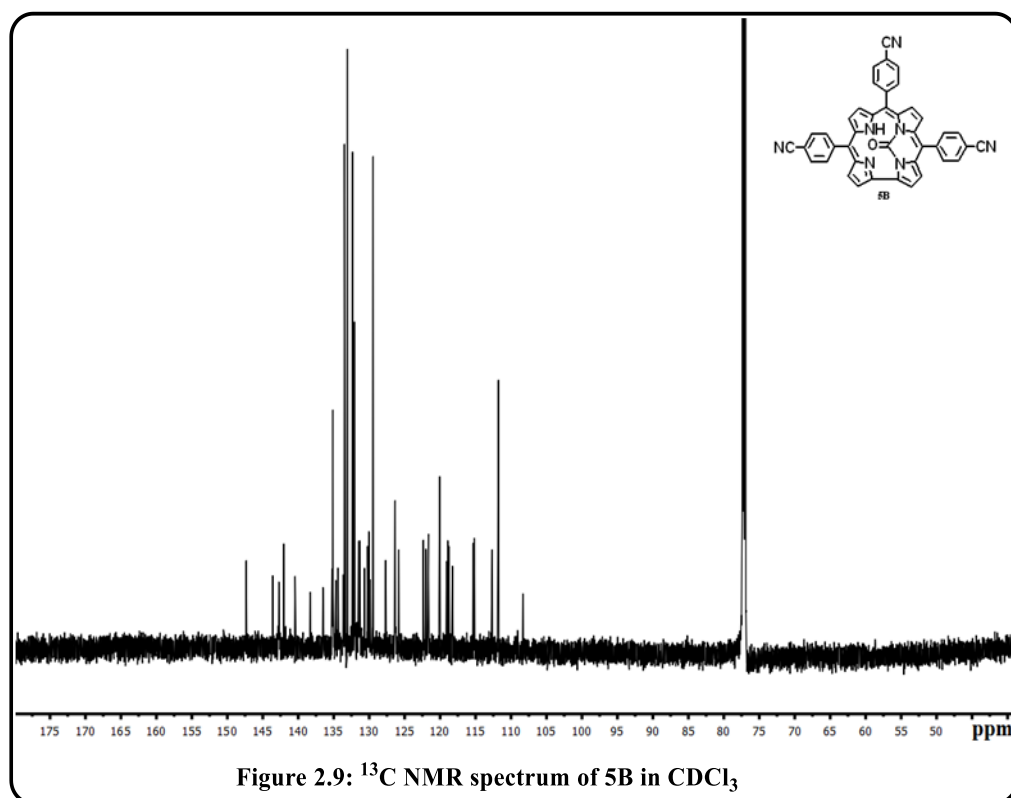
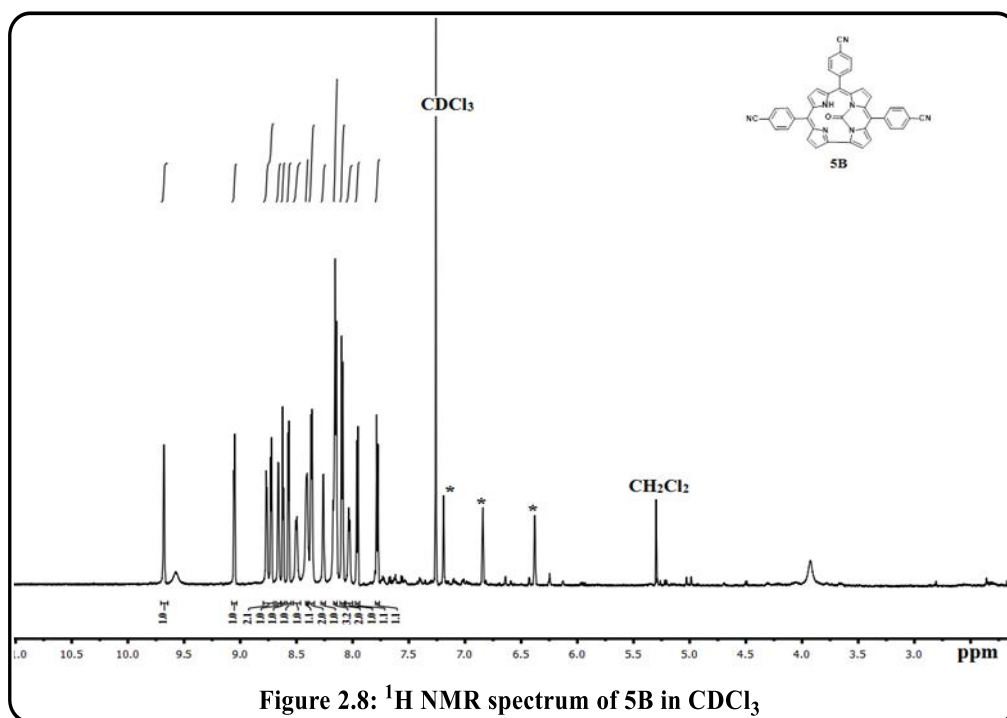
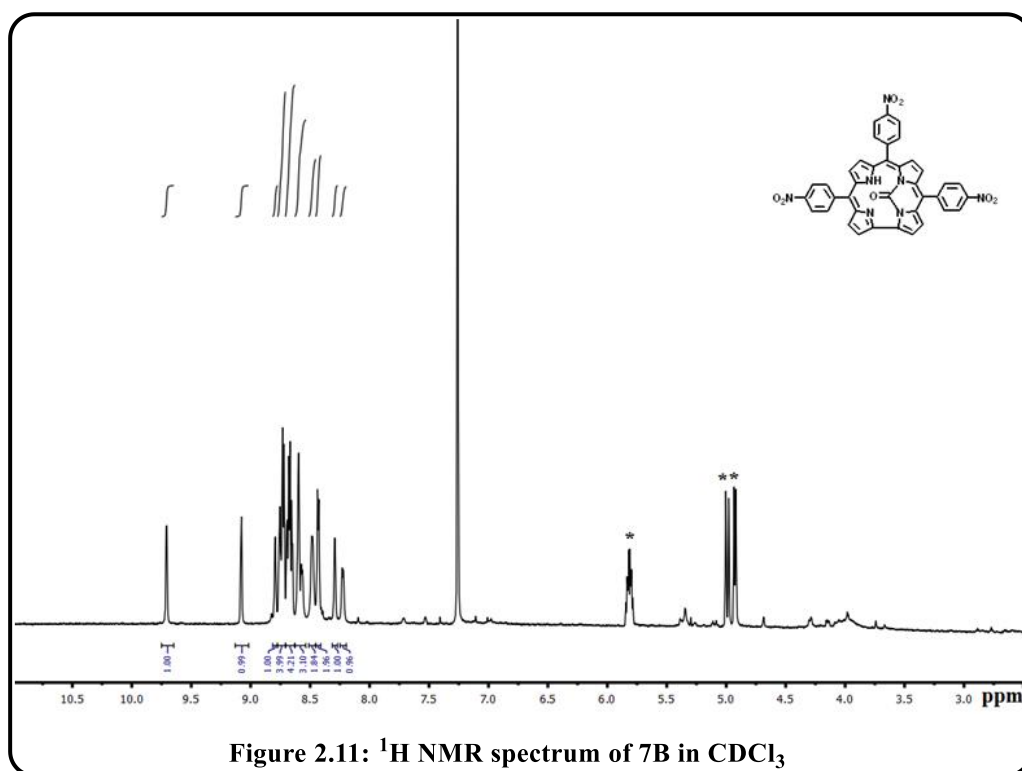
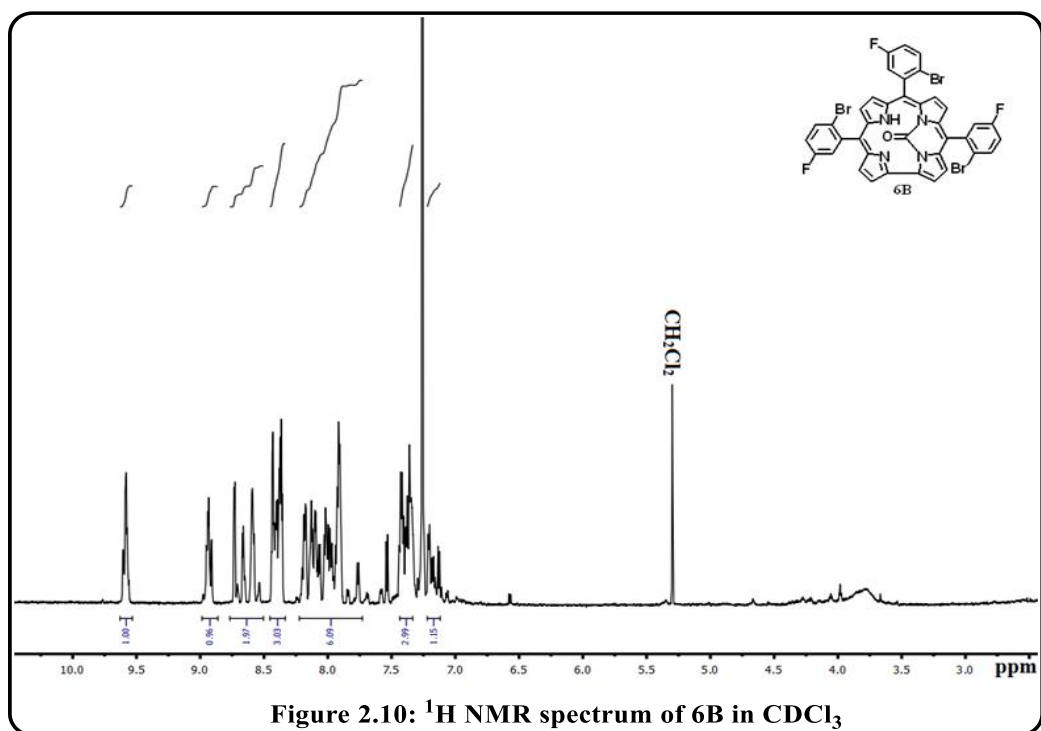


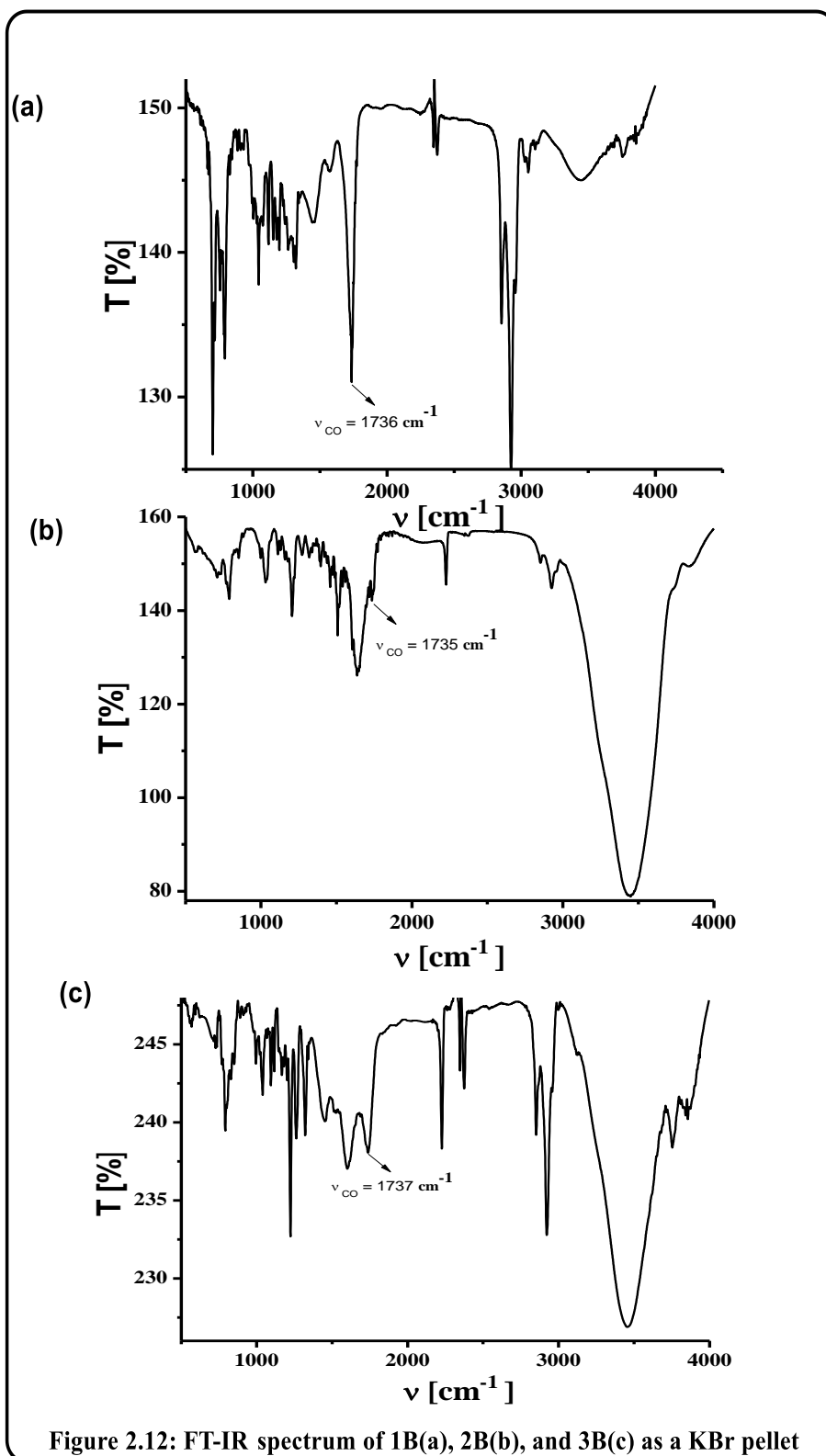
Figure 2.7: <sup>1</sup>H NMR spectrum of 4B in CDCl<sub>3</sub>





### 2.3.3 IR Spectroscopy:

The FTIR spectra of **1B-7B** as KBr pellets showed peaks at 1720-1740  $\text{cm}^{-1}$  due to C=O group stretching ( Fig. 2.12-Fig. 2.14).



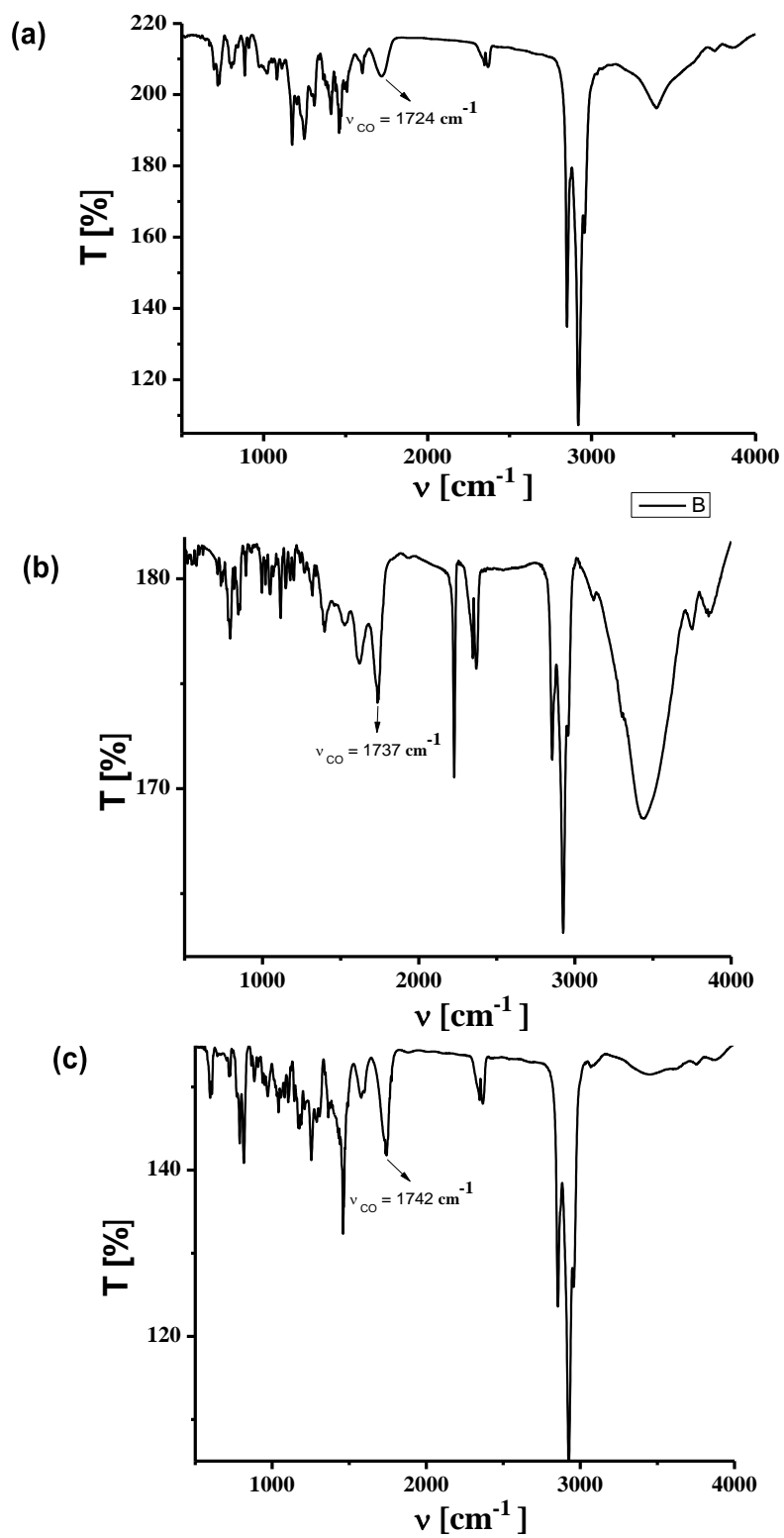
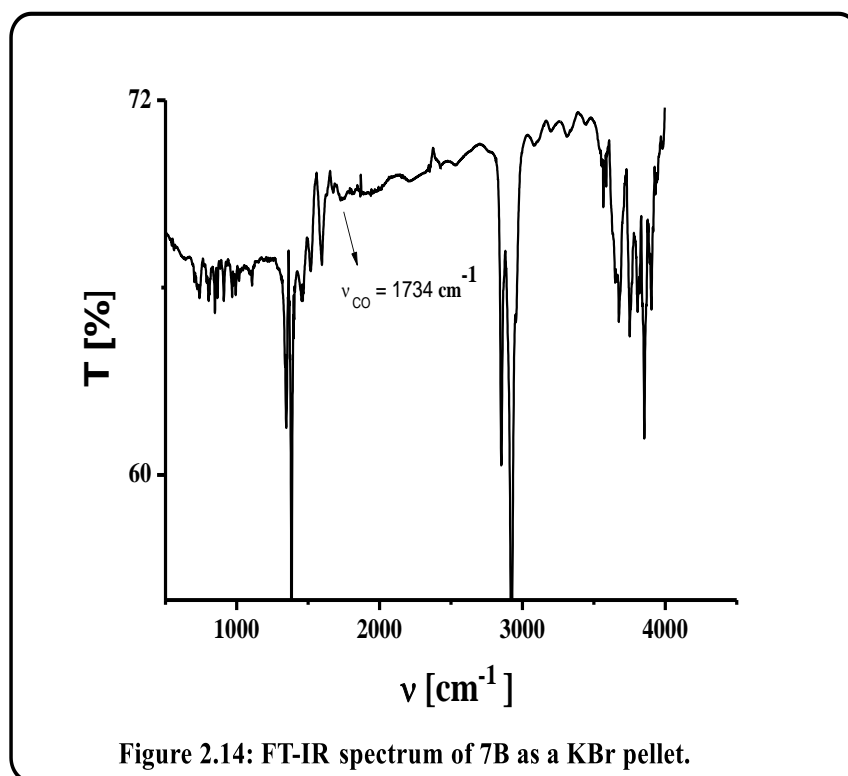


Figure 2.13: FT-IR spectrum of 4B(a), 5B(b) and 6B(c) as a KBr pellet



### 2.3.4 UV-Vis and Emission Spectroscopy:

The absorption and emission spectrum of **1B–7B** in toluene is quite similar in shape across the series but are significantly different to that of the starting corrole derivatives (**1A–7A**) (Table 2.2 and Fig. 2.15-2.20). In contrast to starting corrole derivatives (**1A–7A**), four Q bands were observed in toluene, probably as a result of the carbamide-corrole structure, and the same holds for the blue shift of the Soret and Q bands (Fig. 2.15-2.17).

These molecules emitted differently than the starting corroles and gave a relatively high quantum yield of fluorescence in the solution (Fig. 2.18-2.20). For example, the quantum yield of **3B** in CH<sub>2</sub>Cl<sub>2</sub> is 0.22.

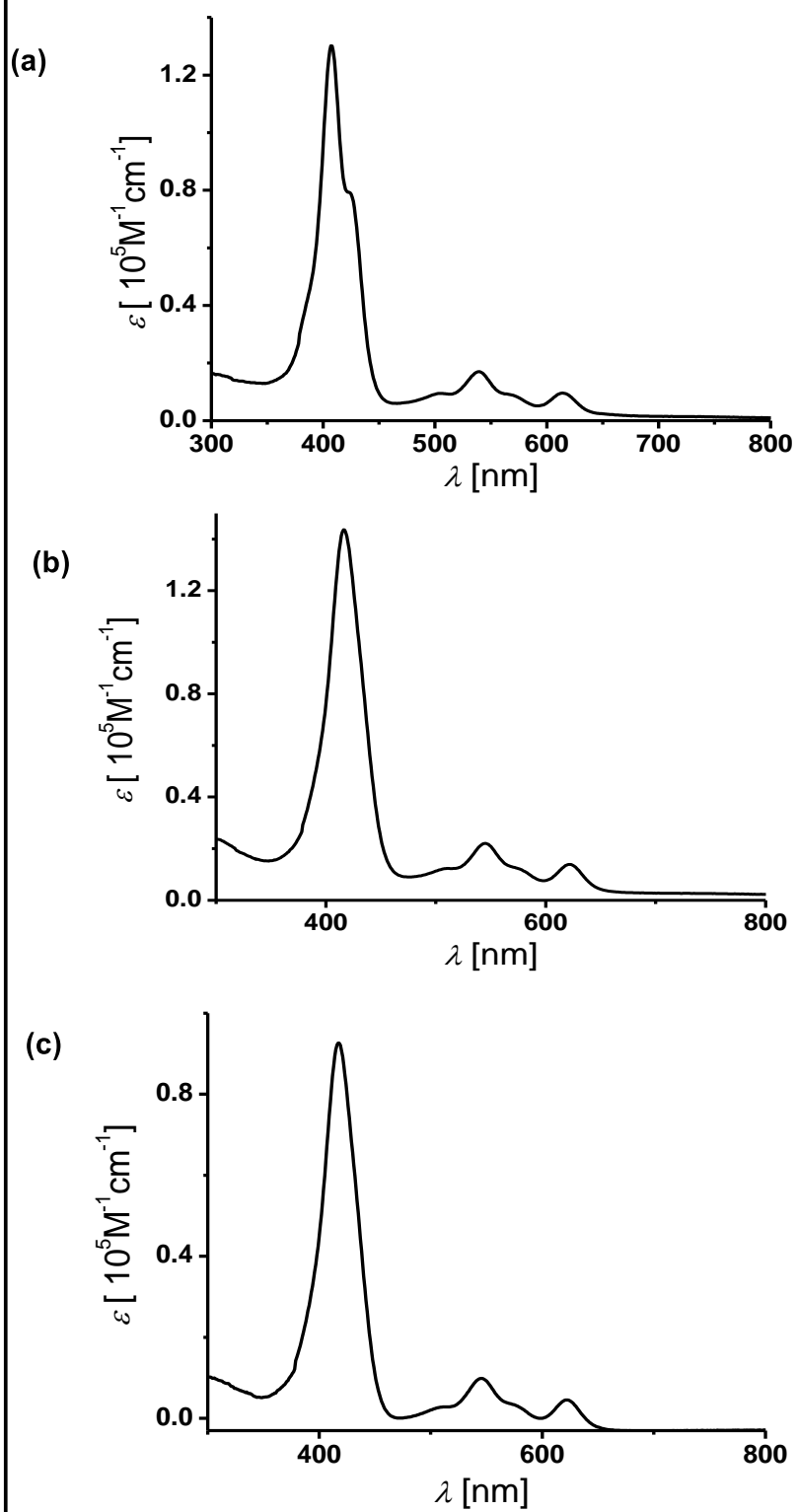


Figure 2.15: Electronic absorption spectrum of 1B(a), 2B(b) and 3B(c) in toluene

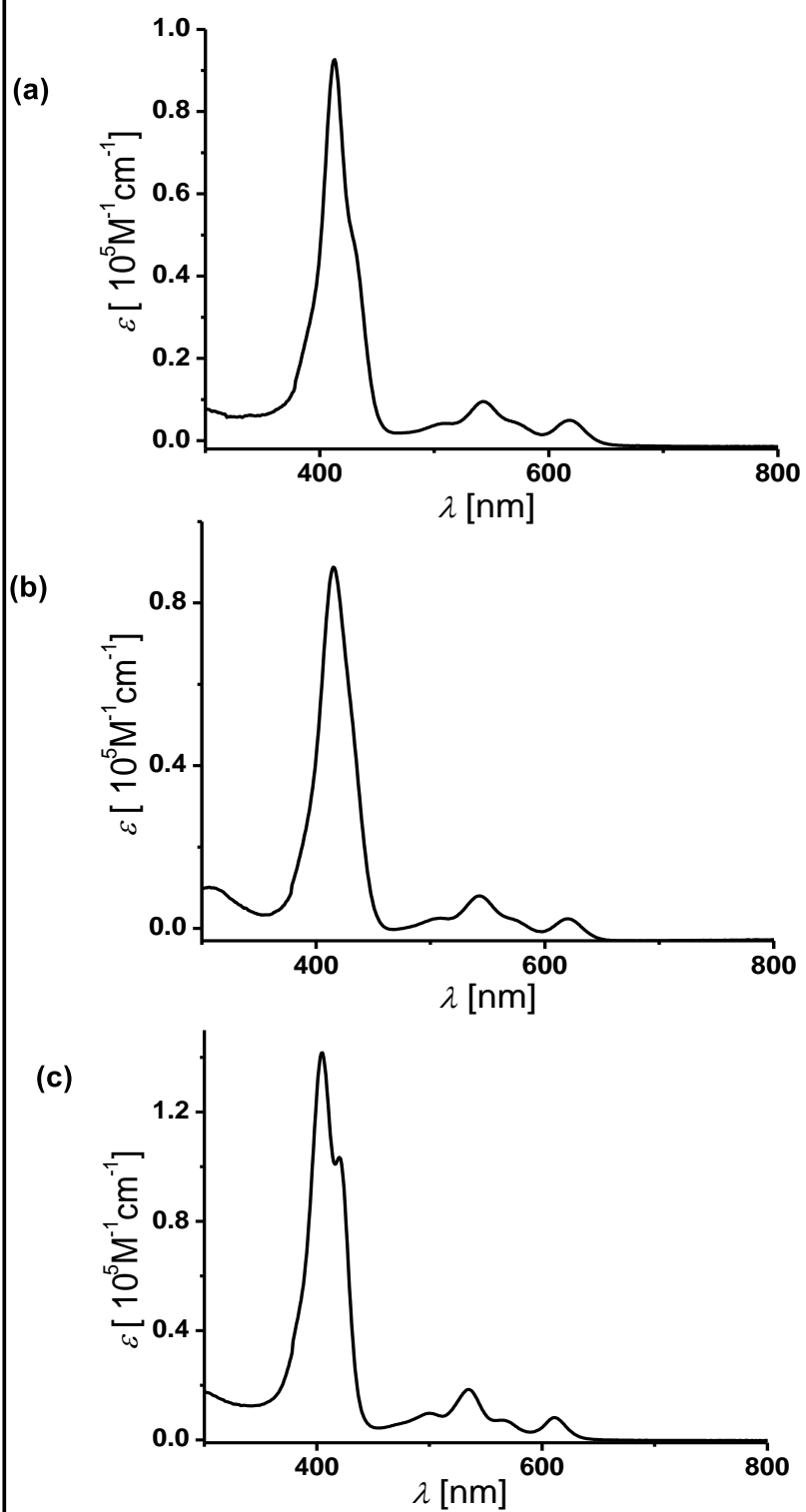
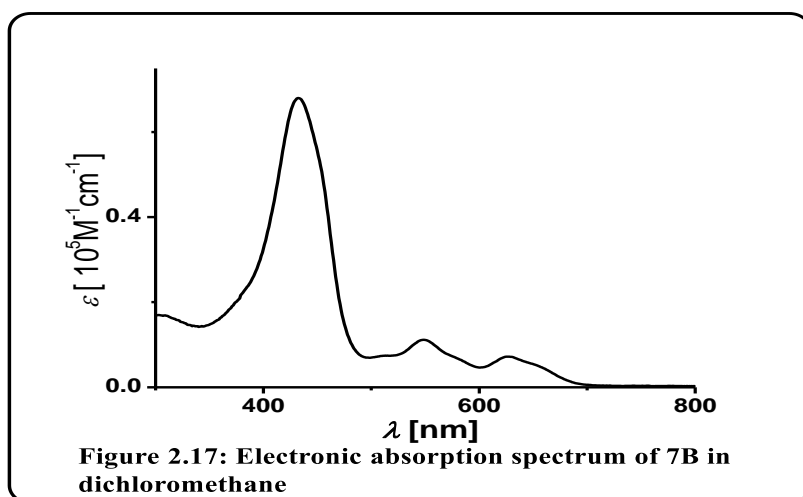
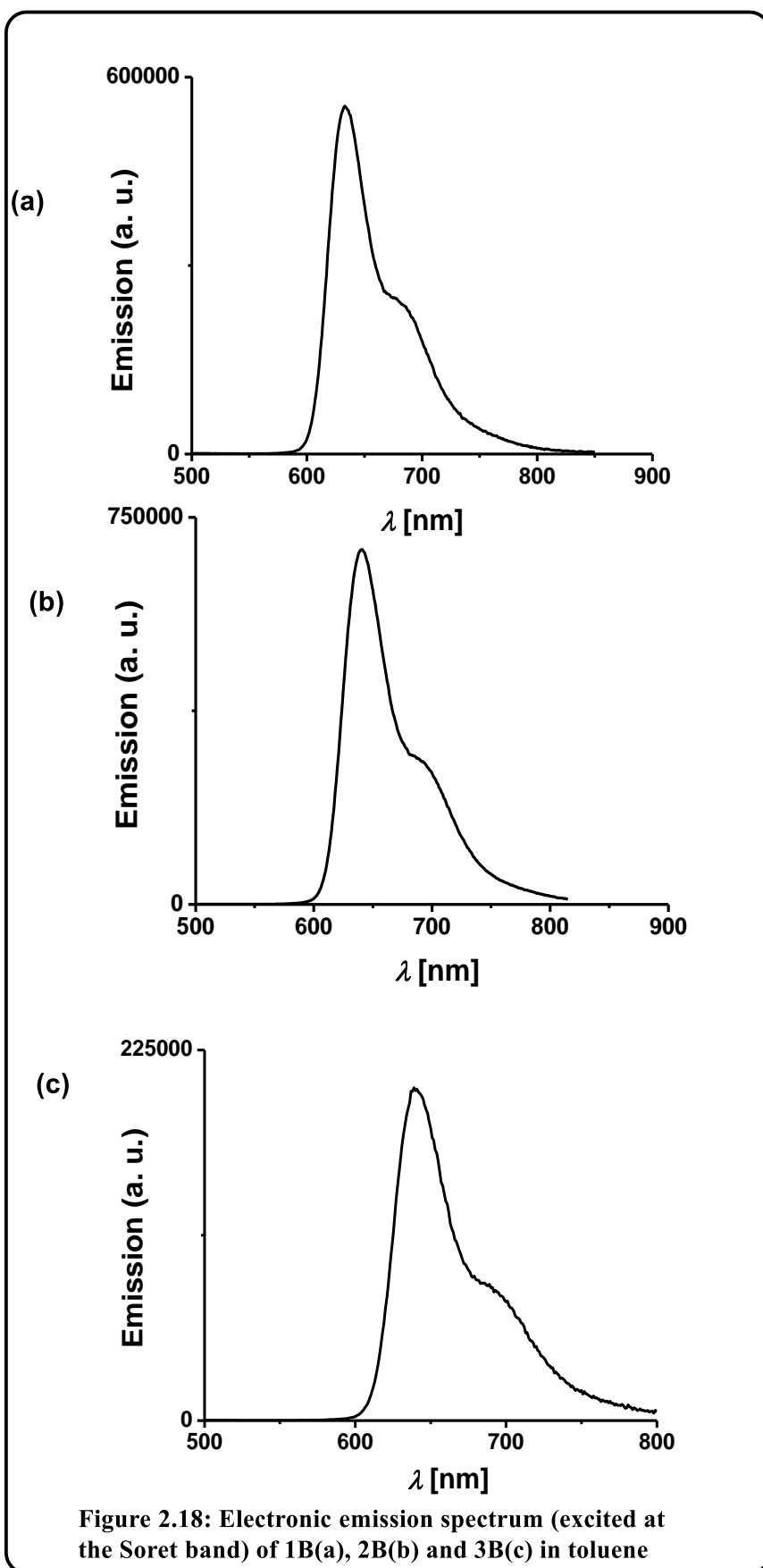


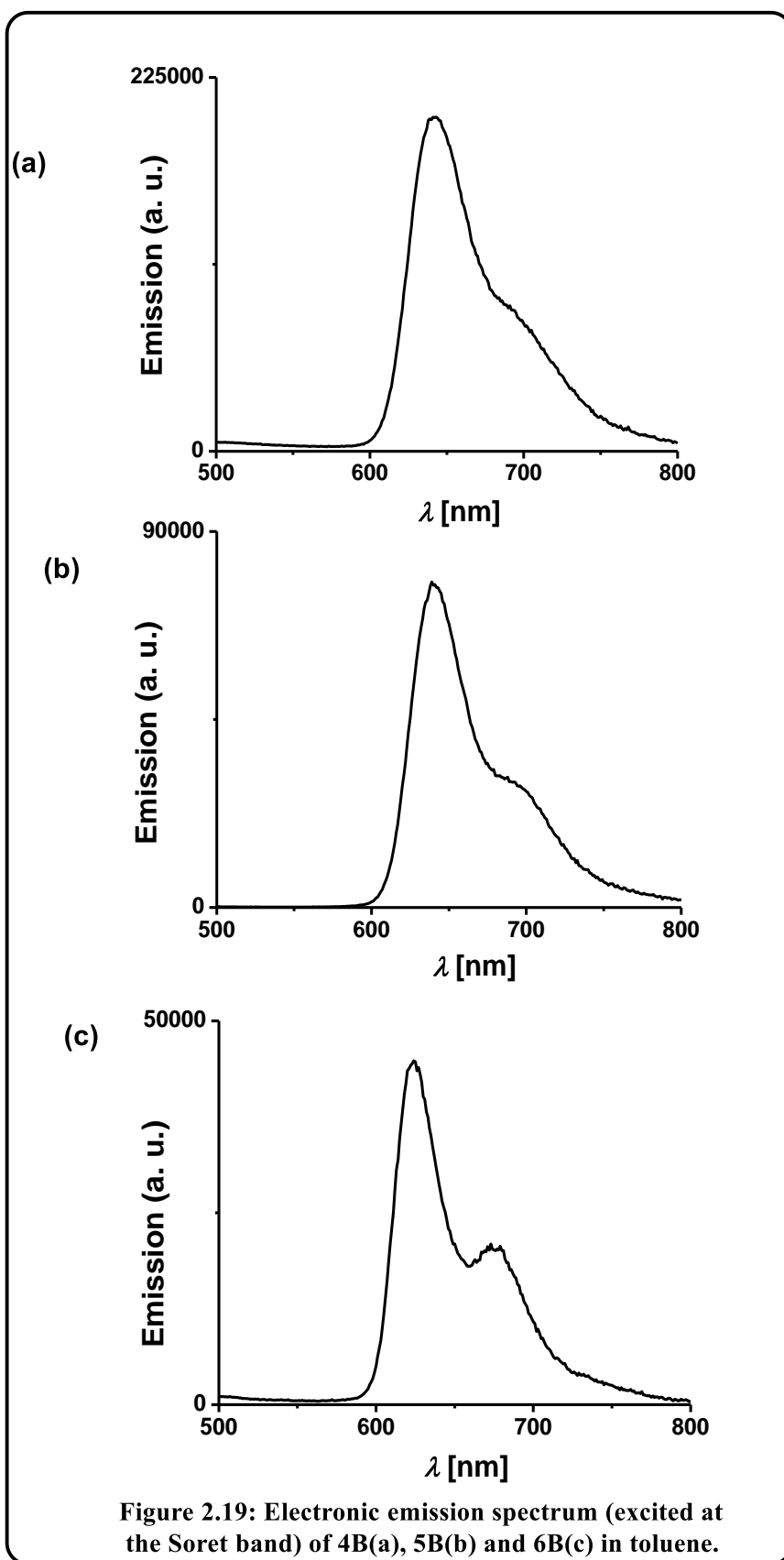
Figure 2.16: Electronic absorption spectrum of 4B(a), 5B(b) and 6B(c) in toluene

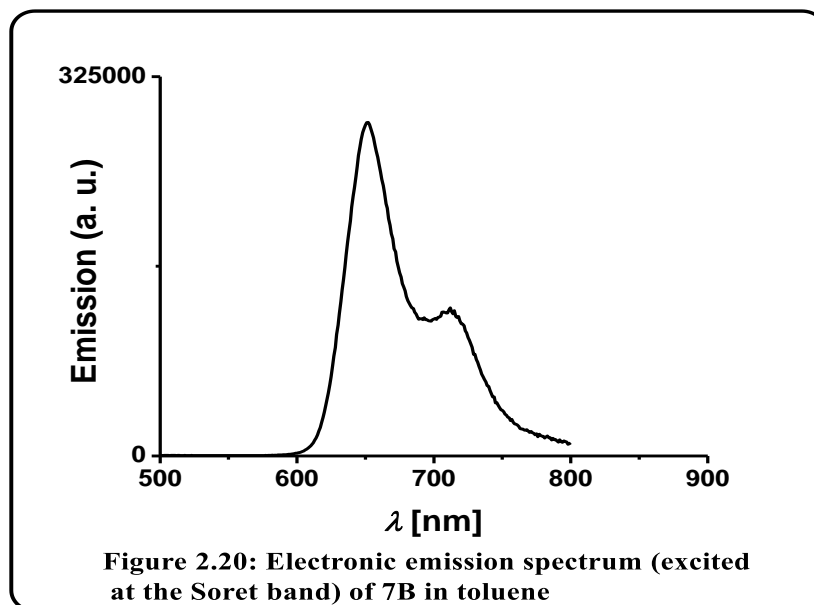


**Table 2.2 UV-Vis. data** <sup>a, b</sup>

Compound ( <sup>a</sup> toluene, <sup>b</sup> DCM)	$\lambda_{\text{max}}$ / nm ( $\epsilon$ / $\text{M}^{-1}\text{cm}^{-1}$ )
1B <sup>a</sup>	407 (131,000), 425sh (80000), 508 (9800), 540 (17500), 566 (9500), 615 (10000)
2B <sup>a</sup>	416 (145,000), 508 (12000), 545 (23000), 576 (12500), 622 (14000)
3B <sup>a</sup>	417 (93,000), 512 (3500), 545 (10500), 576 (3600), 622 (5500)
4B <sup>a</sup>	413 (93,000), 429sh (49,000), 509 (4000), 544 (9000), 571 (4500), 619 (5000)
5B <sup>a</sup>	415 (90,000), 509 (3100), 543 (8500), 572 (2500), 620 (2600)
6B <sup>a</sup>	405 (142,000), 420sh (103,000), 501 (9900), 536 (19000), 564 (7600), 613 (8400)
7B <sup>b</sup>	432 (68,000), 515 (7600), 550 (11000), 578 (7000), 627 (7500)



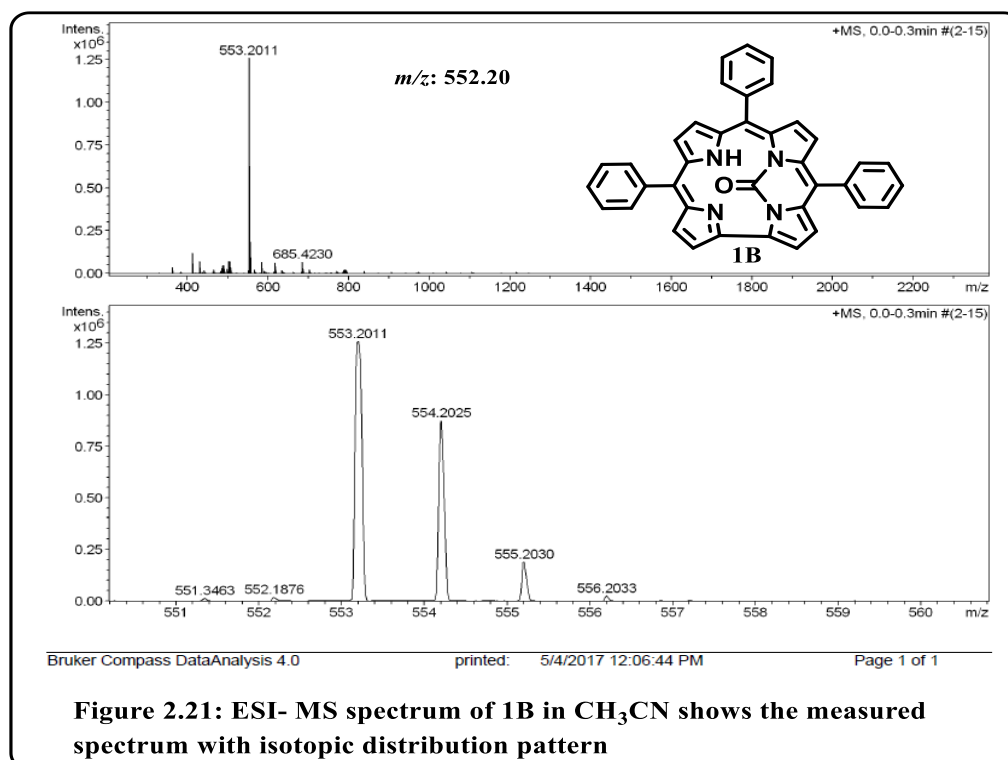


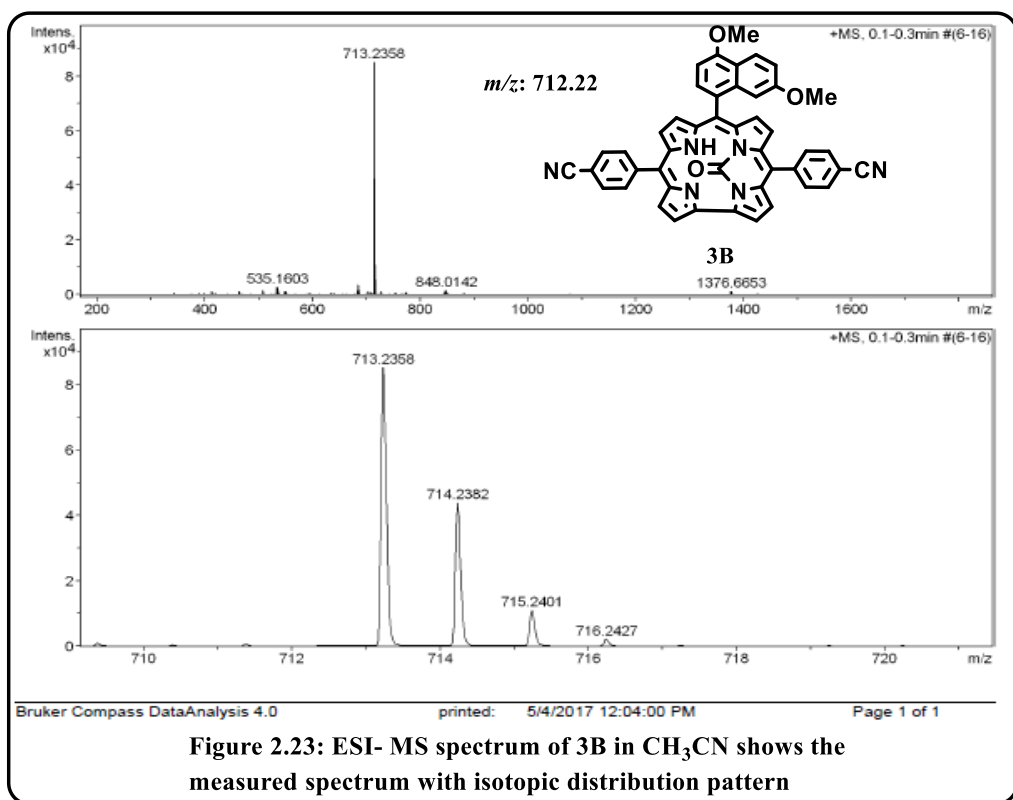
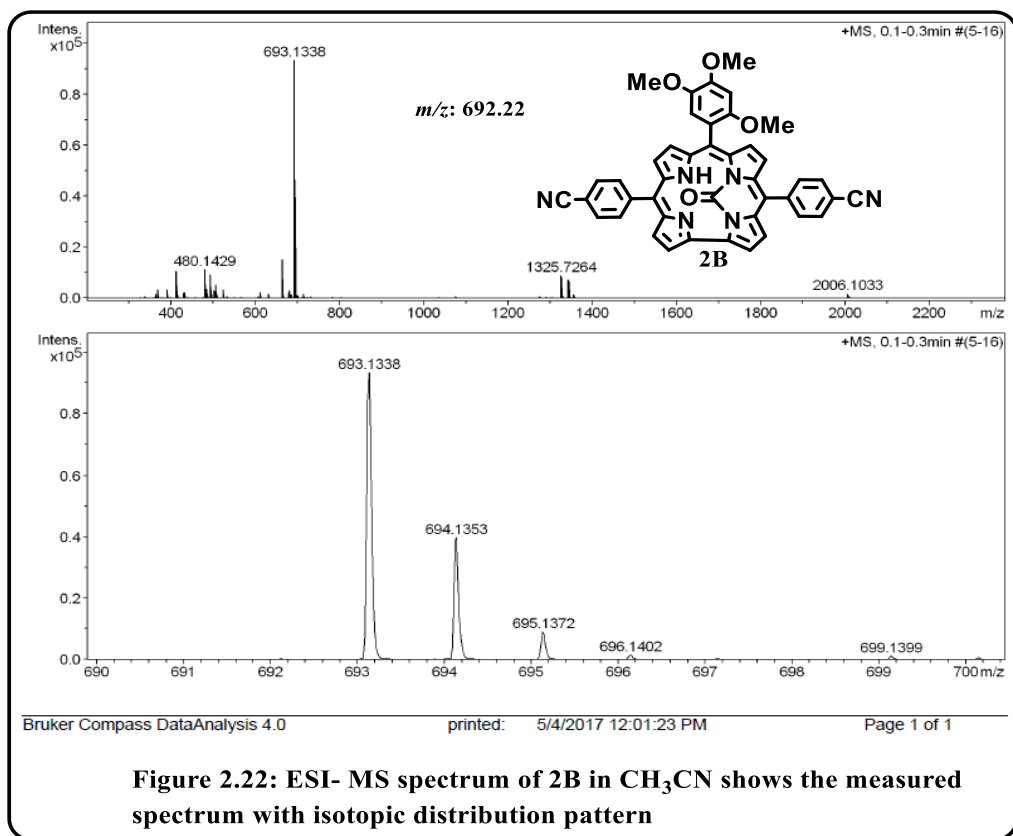


### 2.3.1 Mass Spectroscopy

The electrospray mass spectrum in methanol showed peaks centred at  $m/z = 553.20$  correspond to  $[1\mathbf{B}+\mathbf{H}]^+$  (552.20 calcd for  $\text{C}_{38}\text{H}_{24}\text{N}_4\text{O}$ ) (Fig. 2.21).

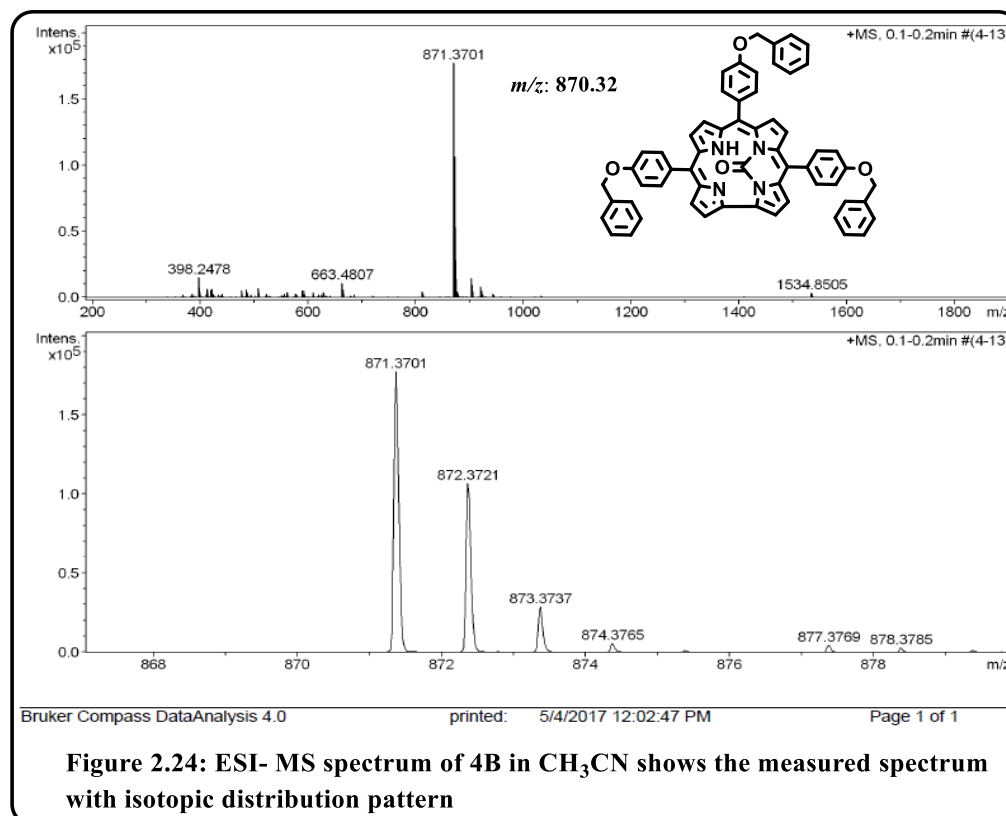
The electrospray mass spectrum in methanol showed peaks centered at  $m/z = 693.23$  correspond to  $[2\mathbf{B}+\mathbf{H}]^+$  (692.22 calcd for  $\text{C}_{46}\text{H}_{28}\text{N}_6\text{O}_3$ ) (Fig. 2.22).





The electrospray mass spectrum in methanol showed peaks centered at  $m/z = 713.23$  correspond to  $[3\mathbf{B}+\mathbf{H}]^+$  (712.22 calcd for  $\text{C}_{46}\text{H}_{28}\text{N}_6\text{O}_3$ ) (Fig. 2.22).

The electrospray mass spectrum in methanol showed peaks centered at  $m/z = 871.37$  correspond to  $[4\mathbf{B}+\mathbf{H}]^+$  (870.32 calcd for  $\text{C}_{59}\text{H}_{42}\text{N}_4\text{O}_4$ ) (Fig. 2.23).



The electrospray mass spectrum in methanol showed peaks centered at  $m/z = 628.58$  correspond to  $[5\mathbf{B}+\mathbf{H}]^+$  (627.18 calcd for  $\text{C}_{41}\text{H}_{21}\text{N}_7\text{O}$ ) (Fig. 2.24).

The electrospray mass spectrum in methanol showed peaks centered at  $m/z = 844.90$  correspond to  $[6\mathbf{B}+\mathbf{H}]^+$  (843.89 calcd for  $\text{C}_{38}\text{H}_{18}\text{Br}_3\text{F}_3\text{N}_4\text{O}$ ) (Fig. 2.25).

The electrospray mass spectrum in methanol showed peaks centred at  $m/z = 688.55$  correspond to  $[7\mathbf{B}+\mathbf{H}]^+$  (687.15 calcd for  $\text{C}_{38}\text{H}_{21}\text{N}_7\text{O}_7$ ) (Fig. 2.26).

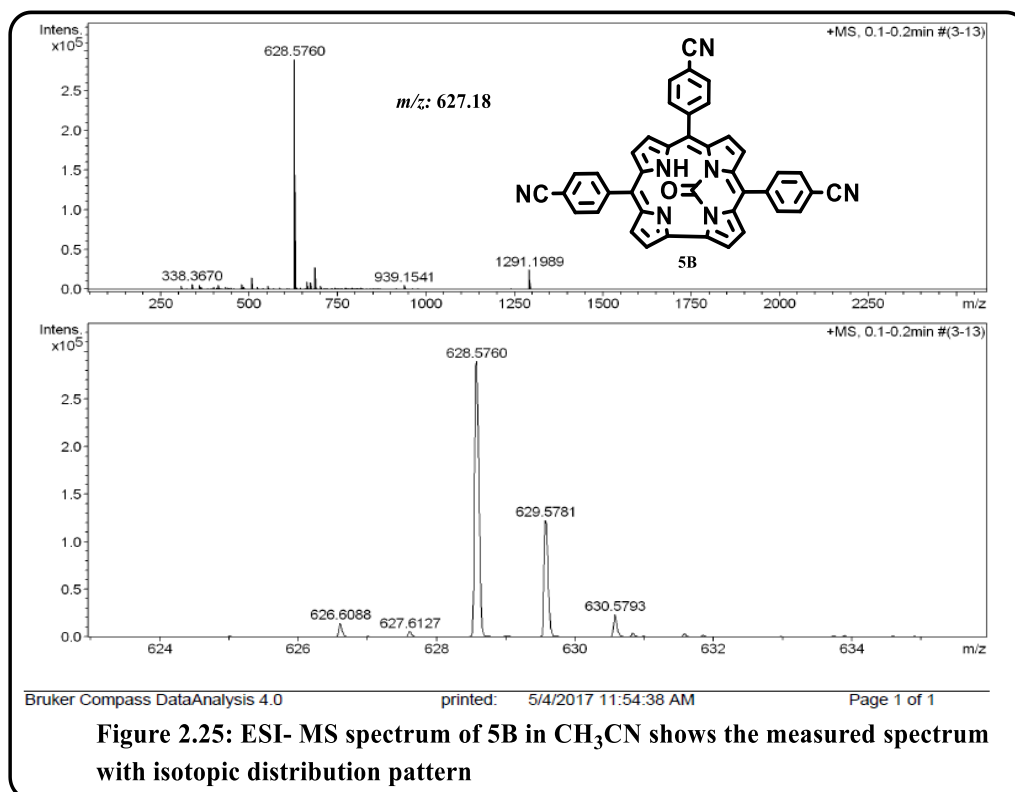


Figure 2.25: ESI- MS spectrum of 5B in CH<sub>3</sub>CN shows the measured spectrum with isotopic distribution pattern

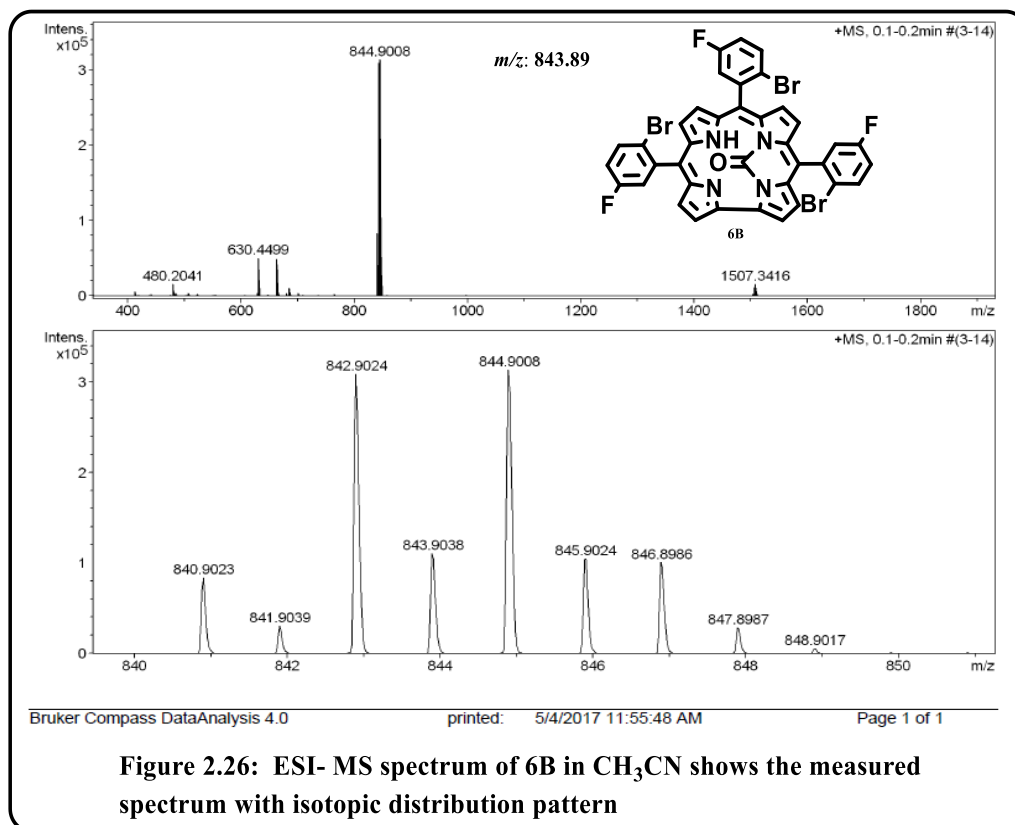
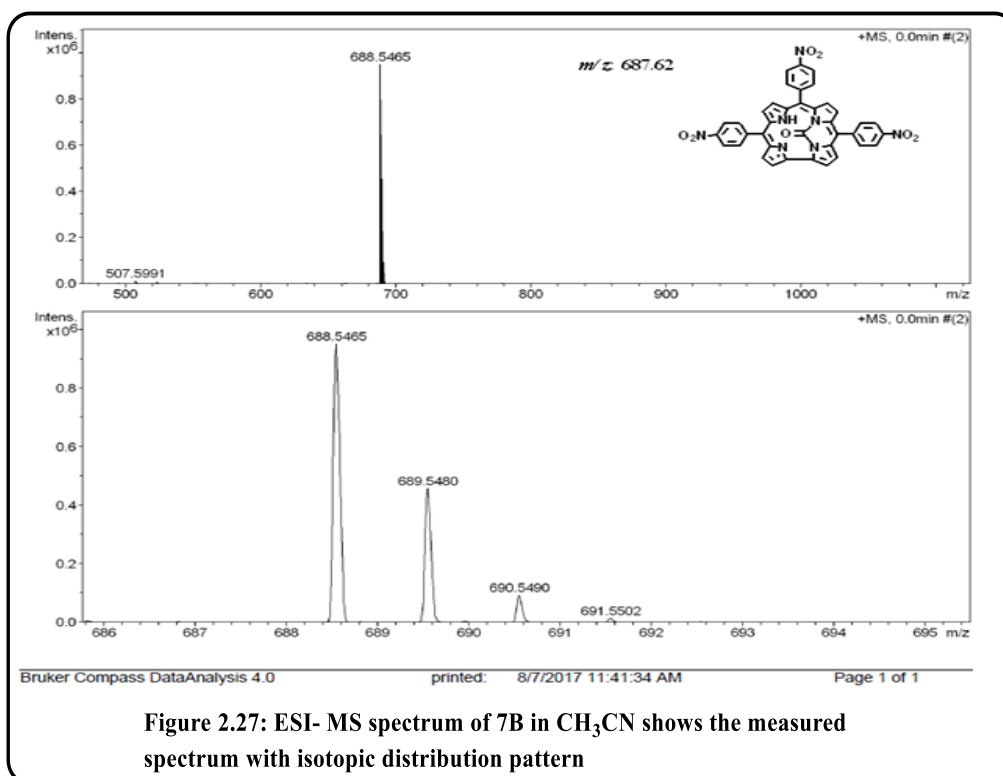
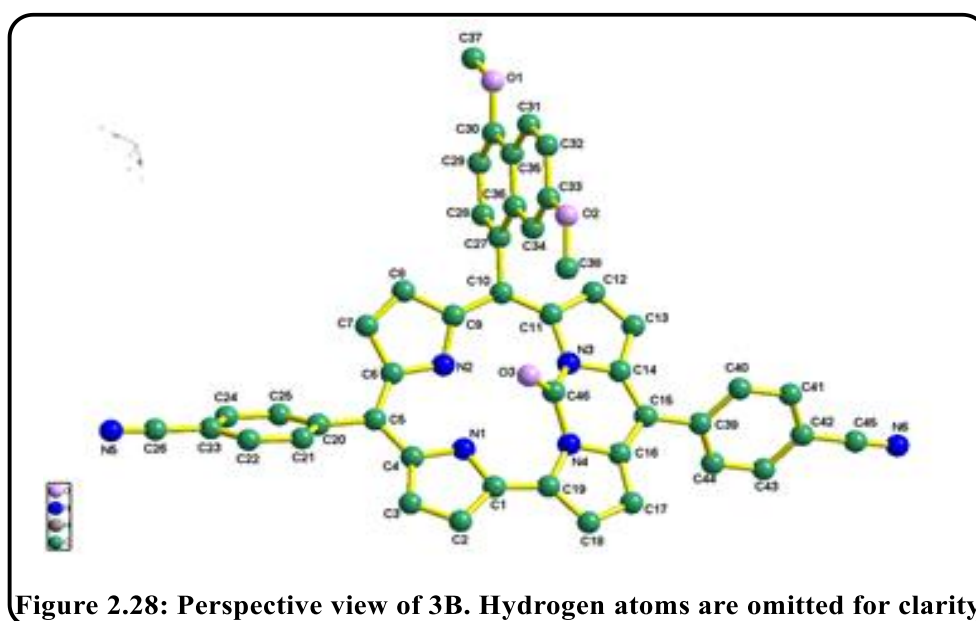


Figure 2.26: ESI- MS spectrum of 6B in CH<sub>3</sub>CN shows the measured spectrum with isotopic distribution pattern

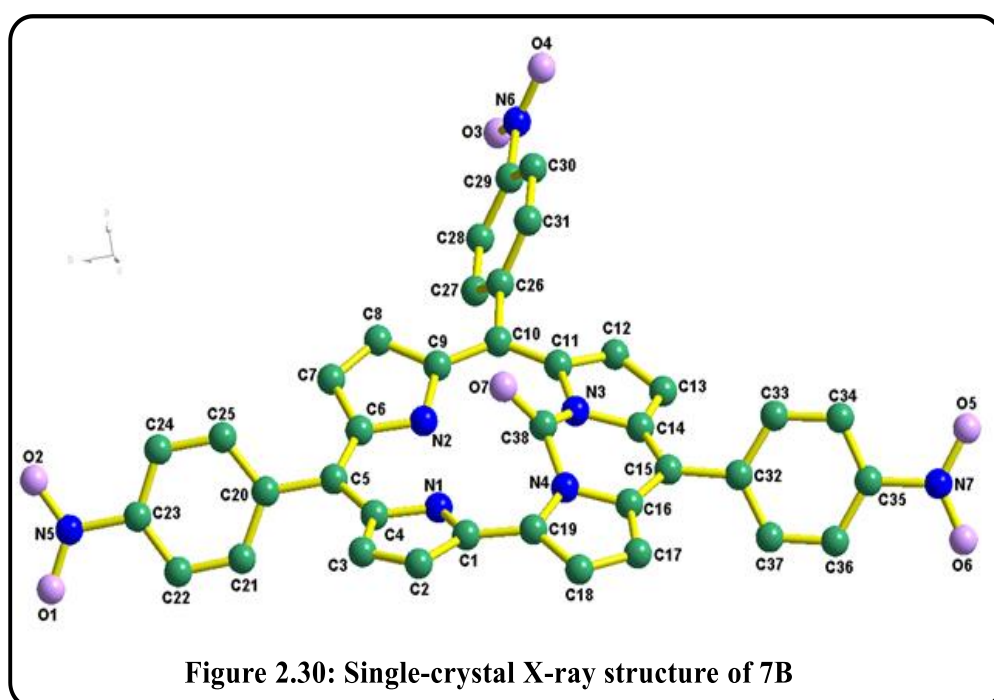
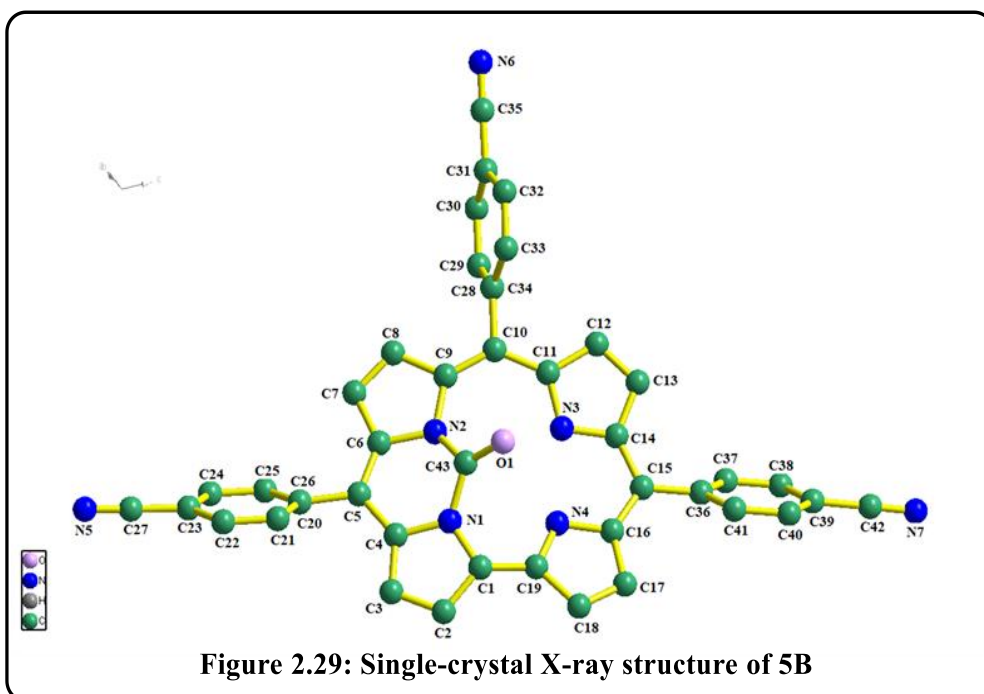


### 2.3.5. Crystal Structure

The crystal structures of **3B**, **5B** and **7B** are shown in Fig. 2.28, Fig. 2.29 and Fig.2.30 respectively. One of the representative structure (**7B**) will be discussed in details.



The crystal system is monoclinic and the unit cell has four **7B** molecules. Important crystallographic parameters for these three derivatives are presented in Table 2.3. Bond distances and angles of **3B**, **5B** and **7B** are in self agreement along the series.



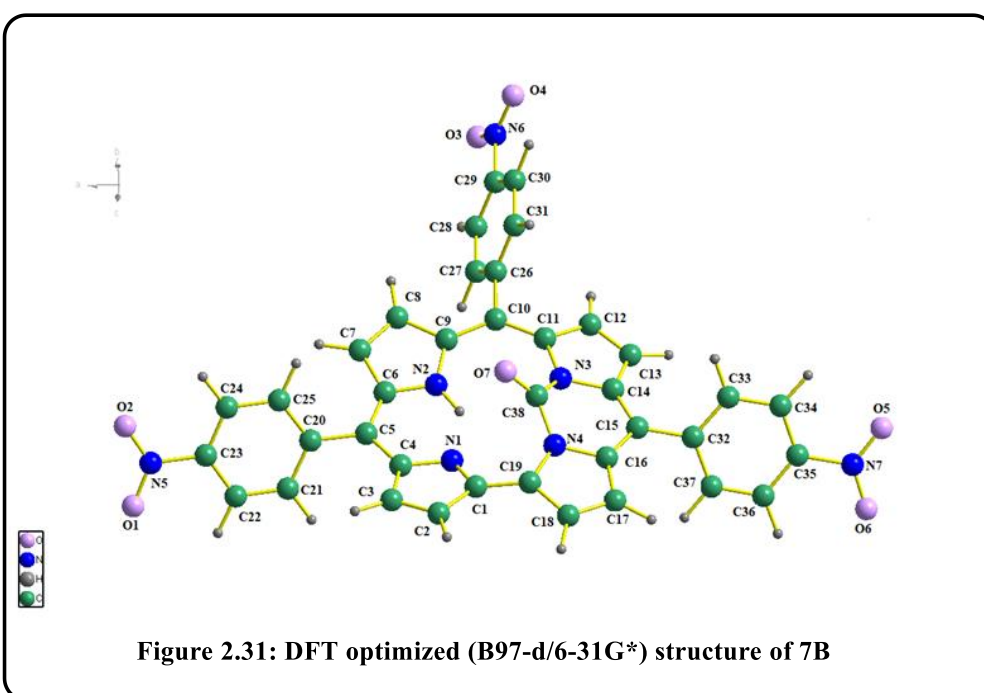
**Table 2.3: Crystallographic Data for 3B, 5B and 7B**

<b>Compound codes</b>	<b>3B</b>	<b>5B</b>	<b>7B</b>
<b>Molecular formula</b>	<b>C<sub>46</sub>H<sub>28</sub>N<sub>6</sub>O<sub>3</sub></b>	<b>C<sub>41</sub>H<sub>21</sub>N<sub>7</sub>O</b>	<b>C<sub>38</sub>H<sub>21</sub>N<sub>7</sub>O<sub>7</sub></b>
<b>F.W.</b>	<b>712.74</b>	<b>627.65</b>	<b>687.62</b>
<b>Radiation</b>	<b>MoK<math>\alpha</math></b>	<b>MoK<math>\alpha</math></b>	<b>Mo K<math>\alpha</math></b>
<b>Crystal symmetry</b>	<b>Triclinic</b>	<b>Triclinic</b>	<b>Monoclinic</b>
<b>Space group</b>	<b>P-1</b>	<b>P-1</b>	<b>P2<sub>1</sub>/c</b>
<b>a(Å)</b>	<b>7.2077 (11)</b>	<b>7.7014 (5)</b>	<b>16.1335 (8)</b>
<b>b(Å)</b>	<b>17.214 (3)</b>	<b>15.7670 (9)</b>	<b>16.7689 (8)</b>
<b>c(Å)</b>	<b>18.628 (3)</b>	<b>17.5273 (10)</b>	<b>13.7048 (6)</b>
<b><math>\alpha</math>(deg)</b>	<b>116.909 (8)</b>	<b>115.061 (4)</b>	<b>90</b>
<b><math>\beta</math>(deg)</b>	<b>91.456 (9)</b>	<b>98.474 (4)</b>	<b>111.276 (2)</b>
<b><math>\gamma</math>(deg)</b>	<b>101.060 (9)</b>	<b>93.397 (4)</b>	<b>90</b>
<b>V(Å<sup>3</sup>)</b>	<b>2006.0 (6)</b>	<b>1889.2 (2)</b>	<b>3455.0 (3)</b>
<b>Z</b>	<b>2</b>	<b>2</b>	<b>4</b>
<b><math>\mu</math> (mm<sup>-1</sup>)</b>	<b>0.08</b>	<b>0.07</b>	<b>0.09</b>
<b>T(K)</b>	<b>296</b>	<b>296</b>	<b>296</b>
<b>D<sub>calcd</sub> (g cm<sup>-3</sup>)</b>	<b>1.180</b>	<b>1.103</b>	<b>1.322</b>
<b>2<math>\theta</math> range (deg)</b>	<b>4.45 to 50.83</b>	<b>4.74 to 51.69</b>	<b>3.64 to 52.18</b>
<b>e data (R<sub>int</sub>)</b>	<b>7371 ( 0.087)</b>	<b>7236 (0.071)</b>	<b>6826 (0.093)</b>
<b>R1 (I&gt;2<math>\sigma</math>(I))</b>	<b>0.070</b>	<b>0.085</b>	<b>0.064</b>
<b>WR2 (all data)</b>	<b>0.176</b>	<b>0.268</b>	<b>0.183</b>

GOF	0.99	0.98	0.96
$\Delta\rho_{\max}, \Delta\rho_{\min} (e \text{ \AA}^{-3})$	0.76, -0.32	0.89, -0.49	0.48, -0.31

## 2.4. Spin Density Calculations:

We performed DFT geometry optimization and frequency calculations at B97-d/6-31G\* level. The DFT calculated bond distances and angles match nicely with those values obtained from XRD (Table 2.4 for **7B**). In **7B** carbon atom of the C=O group deviates from the mean N4 corrole planes by a distance of 0.648 Å (DFT: 0.652 Å) and gives rise to a domed conformation. Pyrrole ring nitrogen atoms deviate from the 19-carbon atom mean corrole plane by distances ranging from 0.229 – (–0.226) Å in **7B**. The dihedral angles between the planes of *meso*-substituted phenyl rings and the 19-atom corrole carbon plane are 49.15–61.18°. The C=O bond distance of **7B** is 1.210 Å (DFT: 1.208 Å). It is worthwhile to mention here that the similar distance in urea is 1.26 Å.



The two C–N (for N (3)–C (38) and N (4)–C (38)) bond distances of **7B** are 1.404 Å (DFT: 1.406 Å) and 1.433 Å (DFT: 1.415 Å) and the N–C–N bond angle is 110.04° (DFT: 110.48°).

**Table 2.4: Selected X-ray and DFT calculated (B97-D/6-31G\*) bond distances (Å) and angles (deg) for 7B.**

Number denotes atoms R= distance A= Angles	7B (X-ray)	7B B97-D/6-31G*
R(1-35)	1.211	1.213
R(2-9)	1.377	1.378
R(2-10)	1.357	1.371
R(3-17)	1.371	1.368
R(3-29)	1.357	1.348
R(4-20)	1.384	1.412
R(4-23)	1.396	1.411
R(4-35)	1.404	1.426
R(5-13)	1.409	1.424
R(5-28)	1.407	1.421
R(5-35)	1.433	1.417
R(6-7)	1.209	1.238
R(6-8)	1.227	1.238
R(6-33)	1.483	1.484
R(9-16)	1.411	1.433

R(9-25)	1.429	1.439
R(10-15)	1.411	1.424
R(10-24)	1.42	1.447
R(11-12)	1.214	1.238
R(11-18)	1.214	1.238
R(11-38)	1.469	1.484
R(13-15)	1.402	1.424
R(13-45)	1.418	1.435
R(14-15)	1.5	1.498
R(14-27)	1.378	1.413
R(14-43)	1.392	1.413
R(16-17)	1.409	1.424
R(16-21)	1.469	1.482
R(17-32)	1.449	1.465
R(19-36)	1.22	1.238
R(19-39)	1.473	1.486
R(19-44)	1.212	1.238
R(20-29)	1.425	1.424
R(20-41)	1.395	1.414
R(21-22)	1.388	1.416
R(21-42)	1.386	1.416
R(22-30)	1.372	1.397

R(23-31)	1.408	1.415
R(23-37)	1.386	1.419
R(24-25)	1.348	1.386
R(26-31)	1.498	1.48
R(26-46)	1.371	1.416
R(26-51)	1.368	1.416
R(27-48)	1.394	1.398
R(28-31)	1.396	1.41
R(28-49)	1.387	1.42
R(29-40)	1.424	1.458
R(30-38)	1.371	1.402
R(32-40)	1.346	1.379
R(33-34)	1.364	1.402
R(33-47)	1.362	1.402
R(34-51)	1.385	1.397
R(37-41)	1.38	1.401
R(38-50)	1.366	1.402
R(39-48)	1.371	1.401
R(39-52)	1.381	1.402
R(42-50)	1.382	1.397
R(43-52)	1.363	1.398
R(45-49)	1.366	1.385

R(46-47)	1.393	1.397
A(1-35-4)	127.6	126.1
A(1-35-5)	122.4	124.3
A(9-2-10)	111.9	112.1
A(2-9-16)	121.9	121.2
A(2-9-25)	105.3	106.1
A(2-10-15)	126.6	126.7
A(2-10-24)	105.2	105.5
A(17-3-29)	108.3	108
A(3-17-16)	119.7	120.3
A(3-17-32)	107.6	108.9
A(3-29-20)	116.7	117.5
A(3-29-40)	109	110.3
A(20-4-23)	109.4	109.7
A(20-4-35)	126.6	127
A(4-20-29)	119.4	119.3
A(4-20-41)	106.3	106.2
A(23-4-35)	121.4	121.2
A(4-23-31)	117.2	118.4
A(4-23-37)	107	106.4
A(4-35-5)	110	109.6
A(13-5-28)	110.4	110

A(13-5-35)	128.6	128
A(5-13-15)	129.9	130.6
A(5-13-45)	104.2	104.7
A(28-5-35)	118.4	119.6
A(5-28-31)	120.3	120.7
A(5-28-49)	106.1	106.6
A(7-6-8)	124.6	125
A(7-6-33)	117.8	117.5
A(8-6-33)	117.6	117.5
A(6-33-34)	119.4	119.1
A(6-33-47)	118.2	119.1
A(16-9-25)	132.5	132.4
A(9-16-17)	119.5	120.3
A(9-16-21)	120.2	120.2
A(9-25-24)	107.8	107.7
A(15-10-24)	128.2	127.9
A(10-15-13)	130.6	130.7
A(10-15-14)	115.6	115.2
A(10-24-25)	109.7	108.4
A(12-11-18)	123.1	125
A(12-11-38)	119	117.5
A(18-11-38)	117.9	117.5

A(11-38-30)	118.9	119.1
A(11-38-50)	118.7	119.1
A(15-13-45)	125.3	124
A(13-15-14)	113.7	114
A(13-45-49)	110	110.3
A(15-14-27)	121.6	120.8
A(15-14-43)	120.3	120.3
A(27-14-43)	118.1	118.9
A(14-27-48)	121.3	120.9
A(14-43-52)	121.7	120.9
A(17-16-21)	120.3	119.3
A(16-17-32)	131.8	129.9
A(16-21-22)	120.3	119.7
A(16-21-42)	121.7	121.7
A(17-32-40)	107.4	106.6
A(36-19-39)	118.7	117.5
A(36-19-44)	124.5	125.1
A(39-19-44)	116.8	117.5
A(19-39-48)	119.8	119
A(19-39-52)	118.4	119.1
A(29-20-41)	132.8	132.6
A(20-29-40)	134.4	132.1

A(20-41-37)	109.2	109.1
A(22-21-42)	118	118.6
A(21-22-30)	121.7	121.1
A(21-42-50)	121	121
A(22-30-38)	118.3	118.8
A(31-23-37)	135.8	135.1
A(23-31-26)	121.9	121.9
A(23-31-28)	118.5	117.2
A(23-37-41)	108.1	108.3
A(31-26-46)	119.2	120.6
A(31-26-51)	122.4	120.8
A(26-31-28)	119.5	120.9
A(46-26-51)	118.3	118.6
A(26-46-47)	121.6	121
A(26-51-34)	121.6	121
A(27-48-39)	118.2	118.7
A(31-28-49)	133.5	132.7
A(28-49-45)	109.4	108.4
A(29-40-32)	107.7	106
A(30-38-50)	122.3	121.8
A(34-33-47)	122.3	121.7
A(33-34-51)	118.3	118.9

A(33-47-46)	117.9	118.8
A(38-50-42)	118.6	118.9
A(48-39-52)	121.8	121.9
A(39-52-43)	118.7	118.7

The theoretical UV and IR spectra are complementing **experimental** data nicely (Fig. 2.32, Table 2.4-2.6 and Fig. 2.31). The experimentally obtained UV–Vis transitions and CO stretching frequencies of the native species **1B-7B**, are in excellent agreement with the computed values (Table 2.5 and 2.6).

**Table 2.5: comparison of experimental and computed UV-Vis transitions of 1B-7B.**

Compound	UV–vis. data	UV–vis. data
	$\lambda_{\max}$ / nm (Experimental)	$\lambda_{\max}$ / nm (Theory)
<b>1B</b>	<b>408, 424</b>	<b>418, 442</b>
<b>2B</b>	<b>413</b>	<b>427</b>
<b>3B</b>	<b>418</b>	<b>438, 470</b>
<b>4B</b>	<b>413, 429</b>	<b>433, 444</b>
<b>5B</b>	<b>416</b>	<b>415, 468</b>
<b>6B</b>	<b>405, 420</b>	<b>420, 434</b>
<b>7B</b>	<b>432</b>	<b>415</b>

For instance, **1B** displays an intense Soret band in the visible spectrum at 408 nm and 424 nm (Table 2.5), and the TD-DFT computed values for these transitions are at 418 nm (HOMO-1 to LUMO+1) and 442 nm (HOMO-1 to LUMO). The experimentally obtained CO stretching frequencies of **1B** occurred at 1736  $\text{cm}^{-1}$  and thus tallied well with the theoretically obtained results (1733  $\text{cm}^{-1}$ ) (Table 2.6).

**Table 2.6:** A comparison of experimental and computed CO stretching frequencies of 1B-7B. A scaling factor of 0.972 is used for the computed vibrational frequencies.

Compound	CO stretching freq.( $\text{cm}^{-1}$ ) (Experimental)	CO stretching freq. ( $\text{cm}^{-1}$ ) (Theory)
<b>1B</b>	1736	1733
<b>2B</b>	1735	1721
<b>3B</b>	1737	1719
<b>4B</b>	1724	1734
<b>5B</b>	1737	1737
<b>6B</b>	1742	1740
<b>7B</b>	1734	1737

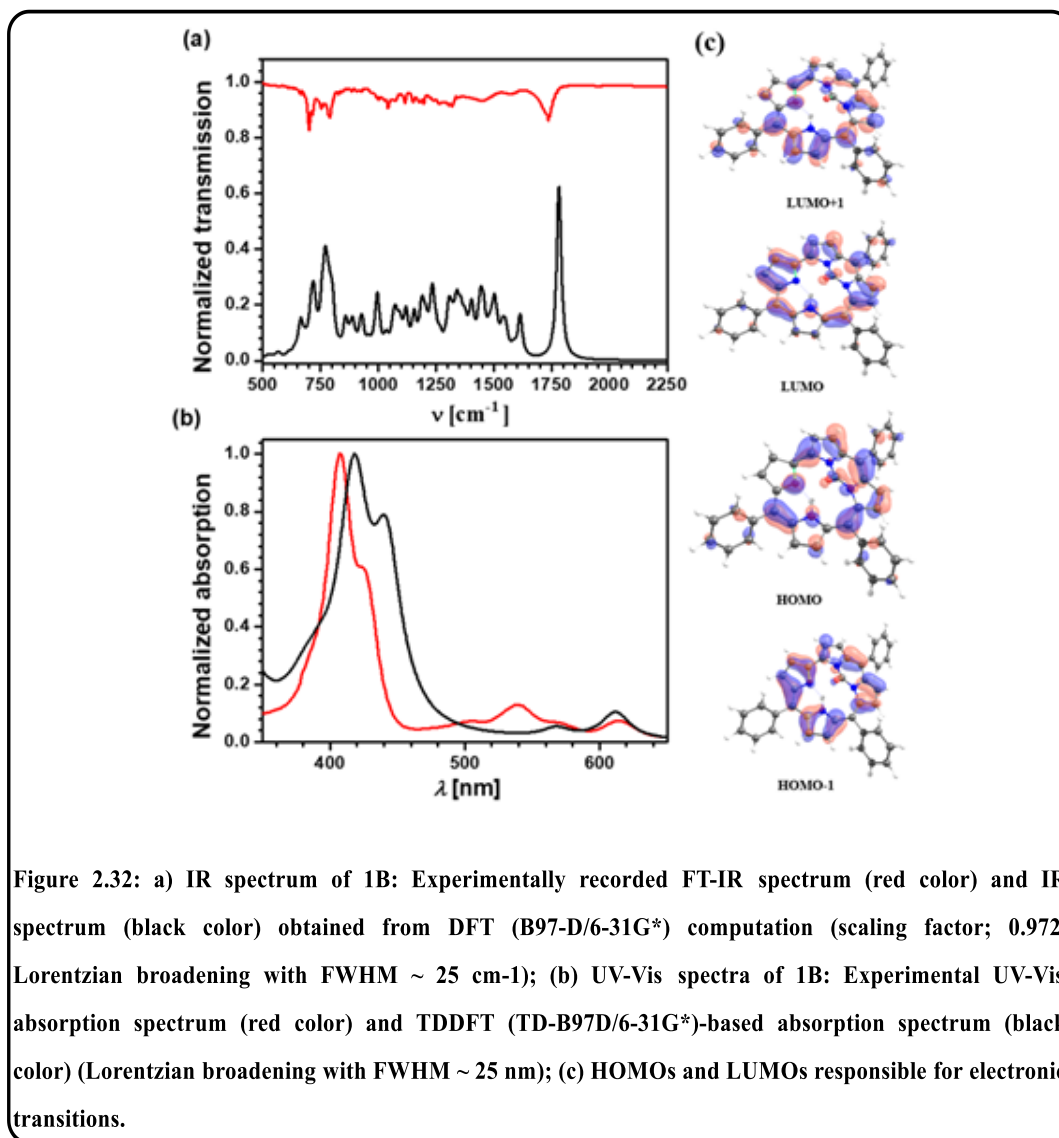


Figure 2.32: a) IR spectrum of 1B: Experimentally recorded FT-IR spectrum (red color) and IR spectrum (black color) obtained from DFT (B97-D/6-31G\*) computation (scaling factor; 0.972, Lorentzian broadening with FWHM  $\sim 25 \text{ cm}^{-1}$ ); (b) UV-Vis spectra of 1B: Experimental UV-Vis absorption spectrum (red color) and TDDFT (TD-B97D/6-31G\*)-based absorption spectrum (black color) (Lorentzian broadening with FWHM  $\sim 25 \text{ nm}$ ); (c) HOMOs and LUMOs responsible for electronic transitions.

## 2.5. Conclusions:

In summary, we have developed an efficient, mild, high-yielding and single-step methodology for the facile synthesis of  $N^{21}, N^{22}$ -carbamide-corrole derivatives without using any toxic chemicals like phosgene, CO, or isocyanate. It has been observed earlier that, the various structural modification of urea moiety resulted the generation of newer varieties of urea-based systems that have shown interesting biological activities. Thus it is logical to consider that these novel carbamide-corrole derivatives and their

possible metal complexes can be utilized in future as potential agents in medicine for detection and in diagnostic purposes.

## **2.6. Experimental Section:**

### **2.6.1. Materials:**

The precursor's pyrrole, *p*-chloranil, and aldehydes were purchased from Aldrich, USA. Ammonium carbonate (minimum 30% ammonia basis) was purchased from Qualigen fine chemicals, India. Other chemicals were of reagent grade. Hexane and CH<sub>2</sub>Cl<sub>2</sub> were distilled from KOH and CaH<sub>2</sub>, respectively. For spectroscopy studies, HPLC grade solvents were used. The synthetic methodologies and complete spectroscopic characterization of **1A-7A** are provided in the previous literatures.<sup>24-48</sup>

### **2.6.2. Physical Measurements:**

UV–Vis spectral studies were performed on a Perkin–Elmer LAMBDA-750 spectrophotometer. Emission spectral studies were performed on a Perkin Elmer, LS 55 spectrophotometer using optical cell of 1 cm path length. The elemental analyses were carried out with a Perkin–Elmer 240C elemental analyzer. FT–IR spectra were recorded on a Perkin–Elmer spectrophotometer with samples prepared as KBr pellets. The NMR measurements were carried out using a Bruker 700 MHz NMR spectrometer. Chemical shifts are expressed in parts per million (ppm) relative to residual chloroform ( $\delta$ = 7.26). Electrospray mass spectra were recorded on a Bruker Micro TOF–QII mass spectrometer.

**2.6.3. Crystal Structure Determination:** Single crystals of **3B**, **5B** and **7B** were grown by slow diffusion of a solution of the **3B**, **5B** and **7B** in dichloromethane into hexane, followed by slow evaporation under atmospheric conditions. The crystal data of **3B**, **5B**

and **7B** were collected on a Bruker Kappa APEX II CCD diffractometer at 293 K. Selected data collection parameters, and other crystallographic results are summarized in Table S1. All data were corrected for Lorentz polarization and absorption effects. The program package SHELXTL<sup>53</sup> was used for structure solution and full matrix least squares refinement on  $F^2$ . Hydrogen atoms were included in the refinement using the riding model. Contributions of H atoms for the water molecules were included but were not fixed. Disordered solvent molecules were taken out using SQUEEZE command in PLATON.<sup>54</sup>

CCDC 1573628-1573630 contain the supplementary crystallographic data for **3B**, **5B** and **7B**. These data can be obtained free of charge via [www.ccdc.cam.ac.uk/data\\_request/cif](http://www.ccdc.cam.ac.uk/data_request/cif).

#### 2.6.4. Computational Methods:

Geometry optimizations of **1B-7B** were carried out using Grimme's functional including dispersion i.e. at B97D/6-31G\*<sup>55</sup> level as implemented in Turbomole<sup>56</sup> software. B97D not only accounts for dispersive attraction but also provides reliable spectroscopic parameters that match with the experimental data (vide infra).<sup>57</sup> Vibrational frequency calculations were also performed at the same level to ensure the optimized structures are the true minima. The vibrational frequencies were scaled by 0.972 to account for the anharmonicity. The TD-DFT calculation was performed at the TD-B97D/6-31G\* level to obtain electronic transitions. Gaussian09<sup>58</sup> software was used for the TD-DFT computation.

#### 2.4.5 Synthesis:

The carbamide-corrole (**1B–7B**) were prepared by following a general procedure. Hence, only one representative case is discussed below.

##### Synthesis of N<sup>21</sup>,N<sup>22</sup>-carbamide–5,10,15–triphenylcorrole, **1B**:

0.050 g (0.095 mmol) of 5,10,15–triphenylcorrole, **1A** was dissolved in 30 mL of dry dichloromethane and subsequently 4.0 g of (NH<sub>4</sub>)<sub>2</sub>CO<sub>3</sub> was added to the reaction mixture in stirring condition. After 5 minutes, 50 mL of pyridine was added and the reaction mixture was refluxed for 3hrs at around 110°C. Then the mixture was evaporated to dryness by rotary evaporation. It was kept for recrystallization in a dichloromethane/hexane mixture for overnight. The residual solvent mixture including the solid mass was dried by rotary evaporation and the reddish colored crude product was purified by using column chromatography through a silica gel (100-200 mesh) bed and by using 55% dichloromethane and 45% hexane as eluent.

##### 2.4.5.1 For N<sup>21</sup>,N<sup>22</sup>-carbamide–5,10,15–triphenylcorrole, **1B**:

Yield: 58% (30 mg). Anal. Calcd (found) for C<sub>38</sub>H<sub>24</sub>N<sub>4</sub>O (**1B**): C, 82.59 (82.68); H, 4.38 (4.31); N, 10.14 (10.25).  $\lambda_{\text{max}}$ /nm ( $\epsilon$ /M<sup>-1</sup>cm<sup>-1</sup>) in toluene: 407 (131000), 425sh (80000), 508 (9800), 540 (17500), 566 (9500), 615 (10000). <sup>1</sup>H NMR (700 MHz, CDCl<sub>3</sub>)  $\delta$  9.55 (d,  $J$  = 4.4 Hz, 1H), 8.95 (d,  $J$  = 4.1 Hz, 1H), 8.79 (d,  $J$  = 4.2 Hz, 1H), 8.73 (d,  $J$  = 5.1 Hz, 1H), 8.60 (dd,  $J$  = 4.4, 2.4 Hz, 2H), 8.58 (d,  $J$  = 5.1 Hz, 1H), 8.36 (d,  $J$  = 7.4 Hz, 1H), 8.32 – 8.22 (m, 5H), 8.03 (d,  $J$  = 7.4 Hz, 1H), 7.86 – 7.75 (m, 6H), 7.75 – 7.68 (m, 3H). (Fig. 2.3). <sup>13</sup>C NMR (176 MHz, CDCl<sub>3</sub>)  $\delta$  143.31, 143.16, 142.85, 142.42, 139.19, 138.88, 136.20, 135.86, 134.82, 134.20, 134.08, 132.87, 132.80, 130.54, 130.26, 129.45, 129.37, 129.21, 128.48, 128.29, 128.18, 127.80, 127.56, 127.38, 127.25,

126.24, 125.49, 124.63, 123.62, 121.08, 120.24, 118.95, 116.67, 115.99, 115.29, 114.22, 111.19, 109.78 (Fig. 2.4). **1B** displayed strong fluorescence at 633 nm and a shoulder at 681 nm in toluene. The electrospray mass spectrum in methanol showed peaks centred at  $m/z = 553.20$  correspond to  $[\mathbf{1B+H}]^+$  (552.20 calcd for  $C_{38}H_{24}N_4O$ ) {Fig. 2.21}.

**2.4.5.2 For  $N^{21}, N^{22}$  –carbamide10–(2,4,5–trimethoxyphenyl) 5,15–bis(4–cyanophenyl)corrole, 2B:**

Yield: 62% (32 mg). Anal. Calcd (found) for  $C_{43}H_{28}N_6O_4$  (**2B**): C, 74.56 (74.67); H, 4.07 (4.15); N, 12.13 (12.22).  $\lambda_{max}/nm$  ( $\epsilon/M^{-1}cm^{-1}$ ) in toluene: 416 (145,000), 508 (12000), 545 (23000), 576 (12500), 622 (14000).  $^1H$  NMR (700 MHz,  $CDCl_3$ )  $\delta$  9.55 (d,  $J = 23.3$  Hz, 1H), 9.05 – 8.88 (m, 2H), 8.67–8.45 (m, 5H), 8.36 (d,  $J = 24.3$  Hz, 4H), 8.07 (d,  $J = 26.9$  Hz, 3H), 7.79 (s, 1H), 7.41 (s, 1H), 7.02 (m, 1H), 4.20– 3.98 (m, 5H), 3.86 (s, 2H), 3.71 (s, 1H), 3.32 (s, 1H) (Figure 2.5). **2B** displayed strong fluorescence at 641 nm and a shoulder at 689 nm in toluene. The electrospray mass spectrum in methanol showed peaks centered at  $m/z = 693.13$  correspond to  $[\mathbf{2B+H}]^+$  (692.22 calcd for  $C_{43}H_{28}N_6O_4$ ) (Figure 2.22).

**2.4.5.3. For  $N^{21}, N^{22}$ –carbamide—10–(4,7–dimethoxynaphthalen-1-yl)-5,15-bis(4–cyanophenyl)corrole, 3B:**

Yield: 65% (34 mg). Anal. Calcd (found) for  $C_{46}H_{28}N_6O_3$  (**3B**): C, 77.52 (77.64); H, 3.96 (3.87); N, 11.79 (11.87).  $\lambda_{max}/nm$  ( $\epsilon/M^{-1}cm^{-1}$ ) in toluene: 417 (93,000), 512 (3500), 545 (10500), 576 (3600), 622 (5500).  $^1H$  NMR (700 MHz,  $CDCl_3$ )  $\delta$  9.64 (dd,  $J = 13.4, 4.5$  Hz, 1H), 9.03 (dd,  $J = 24.1, 4.2$  Hz, 1H), 8.78 (dd,  $J = 32.2, 4.7$  Hz, 1H), 8.71 (dd,  $J = 10.6, 4.7$  Hz, 1H), 8.61 (dd,  $J = 17.4, 4.5$  Hz, 1H), 8.54 – 8.45 (m, 2H), 8.44 – 8.29 (m, 5H), 8.17 – 8.04 (m, 4H), 7.89 (d,  $J = 7.7$  Hz, 1H), 7.23 – 7.18 (m, 1H), 7.06 – 6.97 (m, 1H), 6.58 (d,  $J = 2.5$  Hz, 1H), 6.02 (d,  $J = 2.5$  Hz, 1H), 4.29 (s,

1H), 4.24 (s, 2H), 2.99 (s, 2H), 2.64 (s, 1H) (Figure 2.6). **3B** displayed strong fluorescence at 640 nm and a shoulder at 690 nm in toluene. The electrospray mass spectrum in methanol showed peaks centered at  $m/z = 713.23$  correspond to  $[\mathbf{3B+H}]^+$  (712.22 calcd for  $C_{46}H_{28}N_6O_3$ ) (Figure 2.23).

#### 2.4.5.4 For $N^{21},N^{22}$ -carbamide-5,10,15-tris(4-Benzyloxyphenyl)corrole, **4B**:

Yield: 55% (28 mg). Anal. Calcd (found) for  $C_{59}H_{42}N_4O_4$  (**4B**): C, 81.36 (81.48); H, 4.86 (4.98); N, 6.43 (6.35).  $\lambda_{max}/nm$  ( $\epsilon/M^{-1}cm^{-1}$ ) in toluene: 413 (93,000), 429sh (49,000), 509 (4000), 544 (9000), 571 (4500), 619 (5000).  $^1H$  NMR (700 MHz,  $CDCl_3$ )  $\delta$  9.50 (d,  $J = 4.3$  Hz, 1H), 8.91 (d,  $J = 4.1$  Hz, 1H), 8.77 (d,  $J = 4.1$  Hz, 1H), 8.72 (d,  $J = 5.0$  Hz, 1H), 8.57 (d,  $J = 4.3$  Hz, 1H), 8.55 (d,  $J = 4.3$  Hz, 1H), 8.53 (d,  $J = 5.1$  Hz, 1H), 8.30 (d,  $J = 4.3$  Hz, 1H), 8.27 (d,  $J = 8.1$  Hz, 1H), 8.20 (d,  $J = 8.0$  Hz, 1H), 8.18 – 8.15 (m, 2H), 7.94 (d,  $J = 8.2$  Hz, 1H), 7.63 (d,  $J = 7.5$  Hz, 2H), 7.60 (dd,  $J = 7.5, 4.9$  Hz, 4H), 7.49 (td,  $J = 7.9, 2.1$  Hz, 7H), 7.42 (q,  $J = 7.9, 7.4$  Hz, 9H), 5.35 (bs, 2H), 5.32 (bs, 4H). (Figure 2.7). **4B** displayed strong fluorescence at 642 nm and a shoulder at 692 nm in toluene. The electrospray mass spectrum in methanol showed peaks centered at  $m/z = 871.37$  correspond to  $[\mathbf{4B+H}]^+$  (870.32 calcd for  $C_{59}H_{42}N_4O_4$ ) (Figure 2.24).

#### 2.4.5.5 For $N^{21},N^{22}$ -carbamide-5,10,15-tris(4-cyanophenyl)corrole, **5B**:

Yield: 70% (36 mg). Anal. Calcd (found) for  $C_{41}H_{21}N_7O$  (**5B**): C, 78.46 (78.33); H, 3.37 (3.49); N, 15.62 (15.69).  $\lambda_{max}/nm$  ( $\epsilon/M^{-1}cm^{-1}$ ) in toluene: 415 (90,000), 509 (3100), 543 (8500), 572 (2500), 620 (2600).  $^1H$  NMR (700 MHz,  $CDCl_3$ )  $\delta$  9.68 (d,  $J = 4.4$  Hz, 1H), 9.05 (d,  $J = 4.2$  Hz, 1H), 8.77 (d,  $J = 4.2$  Hz, 1H), 8.73 (d,  $J = 5.1$  Hz, 1H), 8.66 (d,  $J = 4.4$  Hz, 1H), 8.62 (d,  $J = 5.1$  Hz, 1H), 8.57 (d,  $J = 4.4$  Hz, 1H), 8.50 (d,  $J =$

7.8 Hz, 1H), 8.41 (d,  $J = 7.5$  Hz, 1H), 8.37 (d,  $J = 7.6$  Hz, 2H), 8.26 (d,  $J = 4.4$  Hz, 1H), 8.15 (t,  $J = 6.8$  Hz, 3H), 8.09 (d,  $J = 7.8$  Hz, 2H), 8.03 (d,  $J = 7.7$  Hz, 1H), 7.96 (d,  $J = 8.0$  Hz, 1H), 7.78 (d,  $J = 8.1$  Hz, 1H) (Figure 2.8).  $^{13}\text{C}$  NMR (176 MHz,  $\text{CDCl}_3$ )  $\delta$  147.33, 143.60, 142.83, 142.73, 142.07, 140.45, 138.33, 136.51, 135.24, 134.71, 134.39, 133.64, 133.48, 133.06, 132.35, 132.06, 131.49, 130.67, 130.23, 129.86, 129.45, 127.67, 126.40, 126.34, 125.83, 122.37, 122.02, 121.66, 120.06, 119.09, 118.93, 118.75, 118.27, 115.34, 115.20, 112.69, 112.65, 111.85, 111.77, 108.33. (Figure 2.9). **5B** displayed strong fluorescence at 640 nm and a shoulder at 696 nm in toluene. The electrospray mass spectrum in methanol showed peaks centered at  $m/z = 628.58$  correspond to  $[\mathbf{5B}+\mathbf{H}]^+$  (627.18 calcd for  $\text{C}_{41}\text{H}_{21}\text{N}_7\text{O}$ ) (Figure 2.25).

#### 2.4.5.6 For $\text{N}^{21},\text{N}^{22}$ -carbamide-5,10,15-tris(2-bromo-5-fluoro-phenyl)corrole, **6B**:

Yield: 60% (31 mg). Anal. Calcd (found) for  $\text{C}_{38}\text{H}_{18}\text{Br}_3\text{F}_3\text{N}_4\text{O}$  (**6B**): C, 54.12 (54.02); H, 2.15 (2.26); N, 6.64 (6.72).  $\lambda_{\text{max}}/\text{nm}$  ( $\epsilon/\text{M}^{-1}\text{cm}^{-1}$ ) in toluene: 405 (142,000), 420sh (103,000), 501 (9900), 536 (19000), 564 (7600), 613 (8400).  $^1\text{H}$  NMR (700 MHz,  $\text{CDCl}_3$ )  $\delta$  9.58 (tq,  $J = 9.1, 4.3$  Hz, 1H), 8.99 – 8.87 (m, 1H), 8.78 – 8.50 (m, 2H), 8.46 – 8.33 (m, 3H), 8.24 – 7.73 (m, 6H), 7.46 – 7.30 (m, 3H), 7.22 – 7.10 (m, 1H) (Figure 2.10). **6B** displayed strong fluorescence at 624 nm and a shoulder at 676 nm in toluene. The electrospray mass spectrum in methanol showed peaks centered at  $m/z = 844.90$  correspond to  $[\mathbf{6B}+\mathbf{H}]^+$  (843.89 calcd for  $\text{C}_{38}\text{H}_{18}\text{Br}_3\text{F}_3\text{N}_4\text{O}$ ) (Figure 2.26).

#### 2.4.5.7 For $\text{N}^{21},\text{N}^{22}$ -carbamide-5,10,15-tris(4-nitrophenyl)corrole, **7B**:

Yield: 60% (31 mg). Anal. Calcd (found) for  $\text{C}_{38}\text{H}_{21}\text{N}_7\text{O}_7$  (**7B**): C, 66.38 (66.49); H, 3.08 (3.15); N, 14.26 (14.37).  $\lambda_{\text{max}}/\text{nm}$  ( $\epsilon/\text{M}^{-1}\text{cm}^{-1}$ ) in dichloromethane: 432

(68,000), 515 (7600), 550 (11000), 578 (7000), 627 (7500).  $^1\text{H}$  NMR (700 MHz,  $\text{CDCl}_3$ )  $\delta$  9.71 (d,  $J = 3.9$  Hz, 1H), 9.08 (d,  $J = 3.8$  Hz, 1H), 8.79 (s, 1H), 8.74 (dd,  $J = 22.7, 6.5$  Hz, 4H), 8.71 – 8.63 (m, 4H), 8.62-8.53 (m, 3H), 8.49 (s, 2H), 8.43 (d,  $J = 7.8$  Hz, 2H), 8.29 (s, 1H), 8.23 (d,  $J = 7.0$  Hz, 1H) (Figure 2.11). **7B** displayed strong fluorescence at 652 nm and a shoulder at 712 nm in toluene. The electrospray mass spectrum in methanol showed peaks centred at  $m/z = 688.55$  correspond to  $[\mathbf{7B+H}]^+$  (687.15 calcd for  $\text{C}_{38}\text{H}_{21}\text{N}_7\text{O}_7$ ) (Figure 2.27).

## References:

1. N. Volz and J. Clayden, *Angew. Chem. Int. Ed.* **2011**, *50*, 12148-12155.
2. F. Kurzer and P. M. Sanderson, *J. Chem. Educ.* **1956**, *33*, 452.
3. B. J. Bennion and V. Daggett, *Proc. Natl. Acad. Sci. U.S.A.* **2003**, *100*, 5142-5147.
4. T. P. Mommsen and P. J. Walsh, *Science*. **1989**, *243*, 72.
5. M. Boiocchi, L. Del Boca, D. E. Gómez, L. Fabbrizzi, M. Licchelli and E. Monzani, *J. Am. Chem. Soc.* **2004**, *126*, 16507-16514.
6. J. W. Steed, *Chem. Soc. Rev.* **2010**, *39*, 3686-3699.
7. J. J. Mousseau, L. Xing, N. Tang and L. A. Cuccia, *Chem. Eur. J.* **2009**, *15*, 10030-10038.
8. S. H. McCooey and S. J. Connon, *Angew. Chem. Int. Ed.* **2005**, *117*, 6525-6528.
9. Z. Zhang and P. R. Schreiner, *Chem. Soc. Rev.* **2009**, *38*, 1187-1198.
10. R. Zhu, D. Zhang, J. Wu and C. Liu, *Tetrahedron: Asymmetry* **2007**, *18*, 1655-1662.
11. J. Clayden and U. Hennecke, *Org. Lett.* **2008**, *10*, 3567-3570.
12. B. K. Trivedi, A. Holmes, T. L. Stoeber, C. J. Blankley, W. H. Roark, J. A. Picard, M. K. Shaw, A. D. Essenburg, R. L. Stanfield and B. R. Krause, *J. Med. Chem.* **1993**, *36*, 3300-3307.
13. P. P. Seth, R. Ranken, D. E. Robinson, S. A. Osgood, L. M. Risen, E. L. Rodgers, M. T. Migawa, E. A. Jefferson and E. E. Swayze, *Bioorganic Med. Chem. Lett.* **2004**, *14*, 5569-5572.
14. L. J. Lerner, A. Bianchi and A. Borman, *Metab.* **1965**, *14*, 578-582.

15. S. Howard, V. Berdini, J. A. Boulstridge, M. G. Carr, D. M. Cross, J. Curry, L. A. Devine, T. R. Early, L. Fazal and A. L. Gill, *J. Med. Chem.* **2008**, *52*, 379-388.
16. C. Umberger and G. Adams, *Anal. Chem.* **1952**, *24*, 1309-1322.
17. D. Kaufmann, M. Bialer, J. A. Shimshoni, M. Devor and B. Yagen, *J. Med. Chem.* **2009**, *52*, 7236-7248.
18. D. P. Getman, G. A. DeCrescenzo, R. M. Heintz, K. L. Reed, J. J. Talley, M. L. Bryant, M. Clare, K. A. Houseman and J. J. Marr, *J. Med. Chem.* **1993**, *36*, 288-291.
19. W. Schlenk, *Justus Liebigs Ann Chem* **1949**, *565*, 204-240.
20. J. Clayden, M. Pickworth and L. H. Jones, *Chem. Commun.* **2009**, *45*, 547-549.
21. C. Jia, B. Wu, S. Li, Z. Yang, Q. Zhao, J. Liang, Q.-S. Li, X.-J. Yang, *Chem. Commun.* **2010**, *46*, 5376-5378.
22. P. S. Corbin, S. C. Zimmerman, P. A. Thiessen, N. A. Hawryluk, T. J. Murray, *J. Am. Chem. Soc.* **2001**, *123*, 10475-10488
23. I. Saltsman, I. Goldberg, Z. Gross, *Tetrahedron Lett.* **2003**, *44*, 5669-5673.
24. E. Vogel, S. Will, A. S. Tilling, L. Neumann, J. Lex, E. Bill, A. X. Trautwein and K. Wieghardt, *Angew. Chem. Int. Ed.* **1994**, *33*, 731-735.
25. Z. Gross, *J. Biol. Inorg. Chem.* **2001**, *6*, 733-738.
26. R. Paolesse, S. Nardis, M. Stefanelli, F. R. Fronczek and M. G. H. Vicente, *Angew. Chem., Int. Ed.* **2005**, *44*, 3047-3050.
27. R. S. Czernuszewicz, V. Mody, A. Czader, M. Galezowski and D. T. Gryko, *J. Am. Chem. Soc.* **2009**, *131*, 14214-14215.
28. M. Autret, S. Will, E. V. Caemelbecke, J. Lex, J.-P. Gisselbrecht, M. Gross, E. Vogel and K. M. Kadish, *J. Am. Chem. Soc.* **1994**, *116*, 9141-9149.

29. J. H. Palmer, A. C. Durrell, Z. Gross, J. R. Winkler and H. B. Gray, *J. Am. Chem. Soc.* **2010**, *132*, 9230-9231.
30. H.-Y. Liu, Y. Fei, Y.-T. Xie, X.-Y. Li and C. K. Chang, *J. Am. Chem. Soc.* **2009**, *131*, 12890-12891.
31. Brizet, N. Desbois, A. Bonnot, A. Langlois, A. Dubois, J.-M. Barbe, C. P. Gros, C. Goze, F. Denat and P. D. Harvey, *Inorg. Chem.* **2014**, *53*, 3392-3403.
32. S. Kuck, G. Hoffmann, M. Broering, M. Fechtel, M. Funk and R. Wiesendanger, *J. Am. Chem. Soc.* **2008**, *130*, 14072-14073.
33. K. E. Thomas, H. Vazquez-Lima, Y. Fang, Y. Song, K.J. Gajnon, C.M. Beavers, K.M. Kadish, A. Ghosh, *Chem. Eur. J.* **2015**, *21*, 16839-16847.
34. M. Bröring, F. Bregier, E. Cónsul Tejero, C. Hell, M. C. Holthausen, *Angew. Chem. Int. Ed.* **2007**, *46*, 445-448.
35. A. Ghosh, *Chem. Rev.* **2017**, *117*, 3798-3881.
36. R. Orłowski, D. Gryko, D. T. Gryko, *Chem. Rev.*, **2017**, *117*, 3102–3137.
37. Y. Fang, Z. Ou, K. M. Kadish, *Chem. Rev.*, **2017**, *117*, 3377–3419.
38. K. Fujino, Y. Hirata, Y. Kawabe, T. Morimoto, A. Srinivasan, M. Toganoh, Y. Miseki, A. Kudo, H. Furuta, *Angew. Chem. Int. Ed.* **2011**, *50*, 6855– 6859.
39. S. Hiroto, K. Furukawa, H. Shinokubo, A. Osuka, *J. Am. Chem. Soc.* **2006**, *128*, 12380-12381.
40. A. Mahammed, I. Giladi, I. Goldberg, Z. Gross, *Chem. Eur. J.* **2001**, *7*, 4259-4265.
41. S. Hirabayashi, M. Omote, N. Aratani, A. Osuka, *Bull. Chem. Soc. Jpn.* **2012**, *85*, 558-562.
42. B. koszarna, D.T. Gryko, *Chem. Commun.* **2007**, 2994-2996.

43. B. Koszarna and D. T. Gryko, *J. Org. Chem.* **2006**, *71*, 3707-3717.
44. H. L. Buckley, W. A. Chomitz, B. Koszarna, M. Tasior, D. T. Gryko, P. J. Brothers and J. Arnold, *Chem. Commun.*, **2012**, *48*, 10766-10768.
45. W. Sinha, M. G. Sommer, N. Deibel, F. Ehret, M. Bauer, B. Sarkar and S. Kar, *Angew. Chem., Int. Ed.*, **2015**, *54*, 13769-13774.
46. W. Sinha, M. G. Sommer, N. Deibel, F. Ehret, B. Sarkar and S. Kar, *Chem. - Eur. J.* **2014**, *20*, 15920-15932.
47. W. Sinha, M. G. Sommer, L. Hettmanczyk, B. Patra, V. Filippou, B. Sarkar and S. Kar, *Chem. - Eur. J.*, **2017**, *23*, 2396-2404.
48. B. Patra, S. Sobottka, W. Sinha, B. Sarkar, S. Kar, *Chem. - Eur. J.*, **2017**, *23*, 13858-13863.
49. A. Johnson and I. Kay, *J. Am. Chem. Soc.* **1965**, 1620-1629.
50. Z. Gross and N. Galili, *Angew. Chem., Int. Ed.* **1999**, *38*, 2366-2369.
51. I. Saltsman, L. Simkhovich, Y. Balazs, I. Goldberg and Z. Gross, *Inorg. Chim. Acta.* **2004**, *357*, 3038-3046.
52. J. V. Hoene, R. G. Charles and W. M. Hickam, *J. Phys. Chem.* **1958**, *62*, 1098-1101.
53. G. M. Sheldrick, *Acta Crystallogr., Sect. A: Found. Crystallogr.* **2008**, *64*, 112-122.
54. P. Van der Sluis and A. Spek, *Acta Crystallogr., Sect. A: Found. Crystallogr.* **1990**, *46*, 194-201.
55. S. Grimme, *J. Comput. Chem.*, **2006**, *27*, 1787-1799.
56. F. Furche, R. Ahlrichs, C. Hättig, W. Klopper, M. Sierka, and F. Weigend, *WIREs Comput. Mol. Sci.* **2014**, *4*, 91-100.

57. V. R. Mundlapati, S. Gautam, D. K. Sahoo, A. Ghosh and H. S. Biswal, *J. Phys. Chem.Lett.*, **2017**, 8, 4573-4579.
58. M. J. Frisch, G. W. Trucks, H. B. Schlegel, G. E. Scuseria, M. A. Robb, J. R. Cheeseman, G. Scalmani, V. Barone, B. Mennucci, et al. et al. *Gaussian 09, Revision C.01*; Gaussian, Inc.: Wallingford, CT, **2011**.



## **CHAPTER 3**

# **N, N'-bridged corrole: First example of a N<sup>21</sup>, N<sup>22</sup>-methylene-bridged corrole derivative**

### **3.1 Introduction**

### **3.2 Results and Discussion**

#### **3.2.1 Optimization of synthetic route**

### **3.3 Spectral Characterization**

#### **3.3.1 NMR Spectroscopy**

#### **3.3.2 Crystal Structure**

#### **3.3.4 IR Spectra**

#### **3.3.5 Mass Spectrometry**

#### **3.3.6 Electronic absorption spectrum and Emission spectrum**

### **3.4 Conclusions**

### **3.5 Experimental Section**

#### **3.5.1 Materials**

#### **3.5.2 Physical measurements**

#### **3.5.3 Crystal Structure Determination**

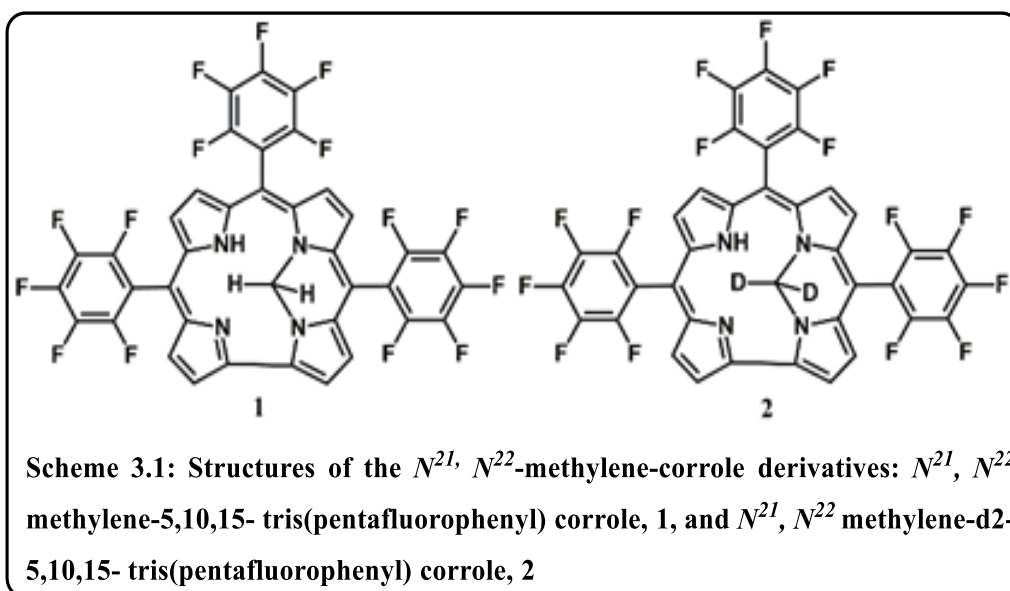
#### **3.5.4 Synthesis**

##### **3.5.4.1 Synthesis of N<sup>21</sup>, N<sup>22</sup>-methylene-5,10,15 tris(pentafluorophenyl) corrole, 1**

### 3.1 Introduction:

In biology, it has been demonstrated that the N-substituted porphyrins can inhibit protohaemferro-lyase strongly.<sup>1</sup> Aida *et al.* has used chiral N-methylated porphyrin free base for the asymmetric catalysis reaction.<sup>2</sup> Mono- N-sustituted or di- N-sustituted porphyrinoids are particularly interesting class of ligands <sup>3-19</sup> considering their fascination to form sitting-atop complexes. Unfortunately, very few research papers describe these unique class of macrocycles.<sup>3-19</sup> Although there are very few examples of distinct metal complexes of mono-alkylated porphyrinoids, the di-alkylated porphyrinoids are even more sacredly reported in the literature.<sup>3-19</sup> Johnson *et al.* has described the synthesis of a N, N' –one carbon bridged porphyrin.<sup>20,21</sup> In addition to that, they have synthesized the PdCl<sub>2</sub>-complex of that porphyrinoid derivative.<sup>20,21</sup> Corrole, a contracted version of porphyrin macrocycle, has one carbon less than porphyrin and possess aromaticity like porphyrin.<sup>22-42</sup> However, contrary to porphyrin (di-anionic in nature), it is tri-anionic in nature and it possess lower symmetry than porphyrin.<sup>22-42</sup> Compared to other tetrapyrrolic macrocycles, the steric crowding in the corrole backbone is reduced on the removal of one proton and thus the formation of monoanionic species is facile in nature.<sup>22-42</sup> It was also observed that the mono N-substituted corrole retains two inner NH moiety, thus it is dianionic in nature and can able to stabilize a series of divalent metals via complexation.<sup>43,44</sup> It is interesting that the first N-sustituted corrole was prepared as early as 1965 by Johnson *et al.*<sup>45</sup> However till date very few N-sustituted corrole are reported in the literature.<sup>46</sup> Compared to mono N-sustituted corroles, N, N' – bridged corrole derivatives are rarely reported in the literature.<sup>47</sup> One such prominent example is the N<sup>21</sup>, N<sup>22</sup>-carbamide-corroles.<sup>47,48</sup> The coordination of this class of ligands has been explored by Gross *et al.*<sup>43,44,46</sup> N-

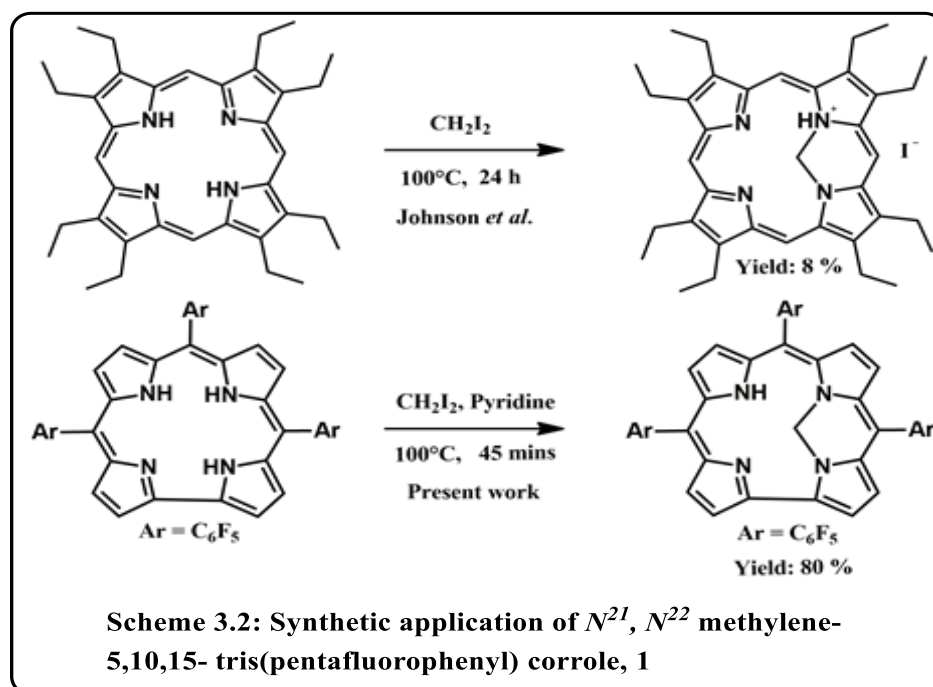
alkylation of *trans*-A<sub>2</sub>B corroles were successfully performed by Dahenet *al.*<sup>49</sup> They have reported the synthesis of two isomeric N-alkylated *trans*-A<sub>2</sub>B corrole derivatives.<sup>[11]</sup> While performing the Vilsmeierformylation on corrole ring, Paolesse *et al.* has observed the formation of a unique N-ethane-bridged corrole (fully substituted).<sup>50</sup> Thus it is evident that the di- N-substituted corroles are hardly reported in the literature. We present herein, the synthesis, structural and spectroscopic characterization of a new N, N' – bridged corrole derivative: *N*<sup>21</sup>,*N*<sup>22</sup>-methylene-5,10,15-tris(pentafluorophenyl)corrole (Scheme 3.1). The choice of the 5,10,15-tris(pentafluorophenyl)corrole backbone to perform the desired conversion is obvious because of its wide application in the synthesis of diverse range of metal complexes and also its stability.<sup>22-42</sup>



### 3.2 Results and Discussion

The newly synthesized *N*<sup>21</sup>, *N*<sup>22</sup>-methylene-corrole derivative, 1, has been thoroughly characterized by different physicochemical techniques, e.g., NMR (<sup>1</sup>H, <sup>19</sup>F, <sup>13</sup>C), ESI Mass, and single crystal X-ray structural analysis (Figures 3.1-3.11) and

Tables 3.1-3.3). Under the optimized reaction conditions, the free base corrole (5,10,15-tris(pentafluorophenyl)corrole, 1A) upon treatment with  $\text{CH}_2\text{I}_2$  in presence of excess pyridine and in stirring for 45 mins at  $100^\circ\text{C}$  resulted the formation of  $N^{21}, N^{22}$ -methylene-corrole complex, **1**, in excellent yield (Scheme 3.2).

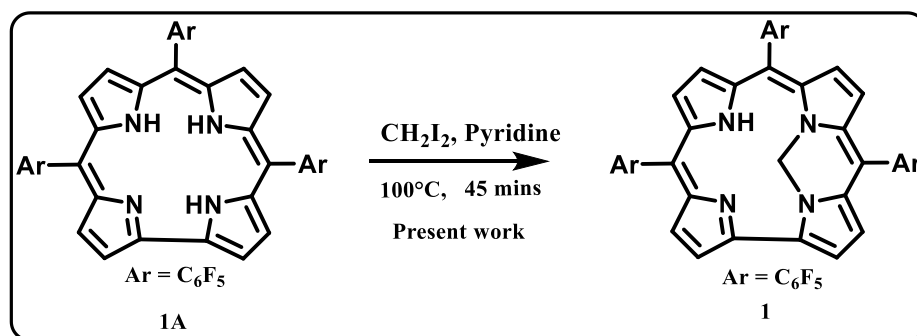


Johnson *et al.* has performed the synthesis of 21, 22-methyleneoctaethylporphyrin via the condensation reaction of 21, 22-octaethylporphyrin and di-iodomethane for the 1<sup>st</sup> time (Scheme 3.2). We have used the same strategy as developed by Johnson *et al.*, however, we have modified it a bit. Instead of neat di-iodomethane, we have used a mixture of di-iodomethane and pyridine.

### 3.2.1 Optimization of synthetic route

Optimization of the  $N^{21}, N^{22}$ -methylene-bridged corrole formation reaction was performed (Table 3.1). Addition of 10 equivalents of  $\text{CH}_2\text{I}_2$  resulted the desired

conversion of the free base corrole to  $N^{21},N^{22}$ -methylene-bridged corrole in optimum yield.



**Table 3.1: Optimization for the formation of  $N^{21}, N^{22}$ -Methylene- Bridged Corrole (1A to 1).**

Equiv. of $\text{CH}_2\text{I}_2$	Yield (%) of <b>1</b>
2	50%
5	70%
10	80%
100	82%
2000	86%

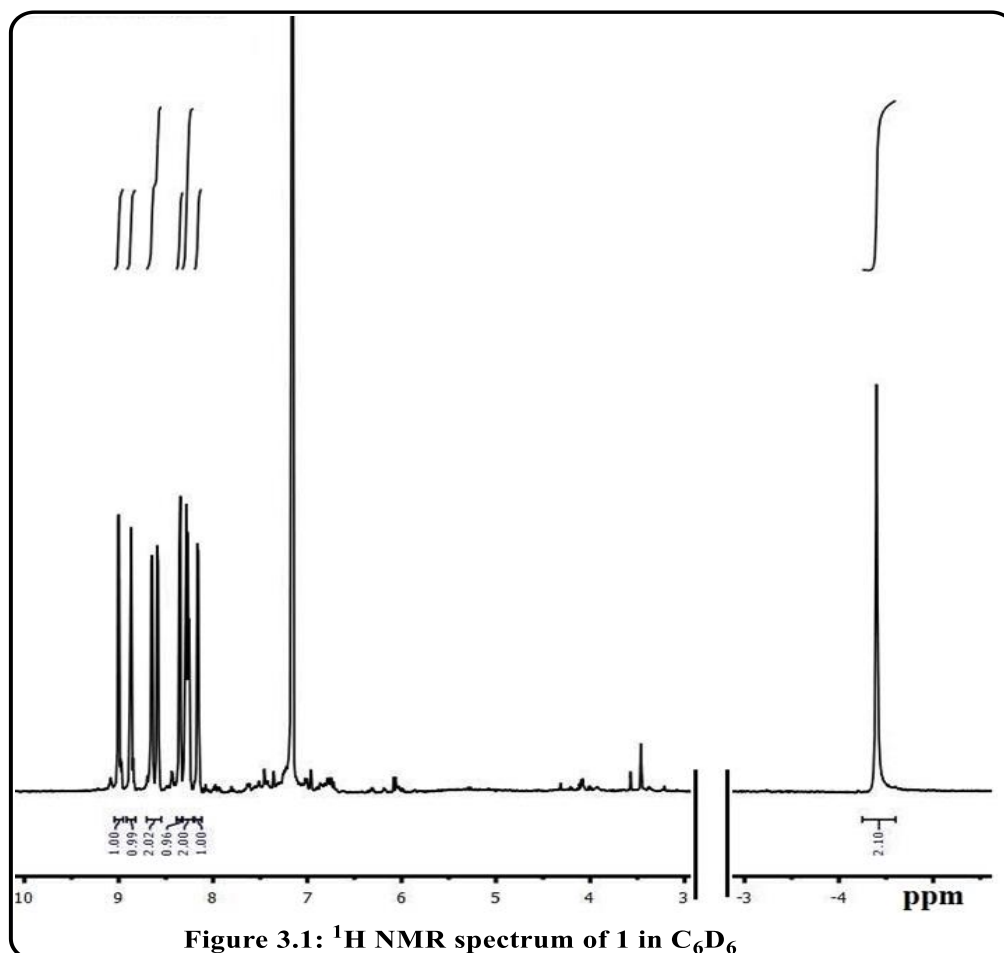
However, in all cases, the reaction has failed to generate the desired product in absence of pyridine. Surprisingly, this slight modification has changed the reaction yield drastically, As compared to the previously reported 8% yield for the synthesis of 21, 22-methyleneoctaethylporphyrin by Johnson *et al.*, we have obtained an overall isolated yield of 80% in the present case. In addition to that, it has also reduced the reaction time and so also the cost of using neat  $\text{CH}_2\text{I}_2$  ( $\text{CH}_2\text{I}_2$  is quite expensive). The role of the pyridine has been thoroughly scrutinized for the reaction as described here. Pyridine is a mild base and is responsible for the deprotonation of the core NH protons of the

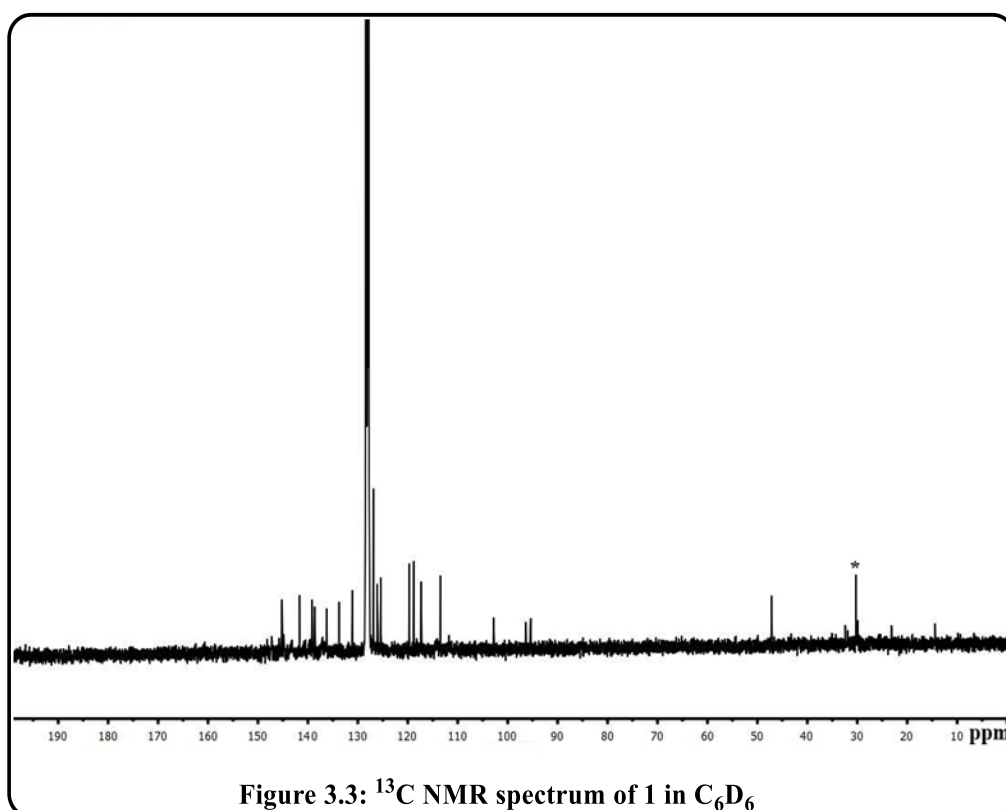
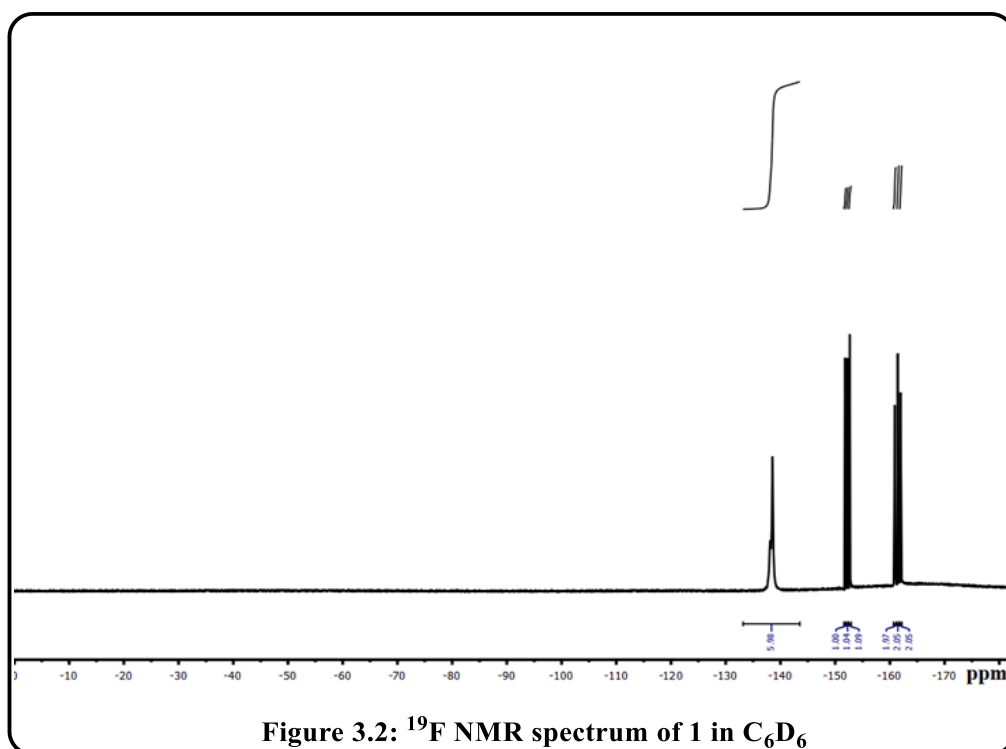
corrole ring. Dipyridinio-methane di-iodide is obtained as a side product due to the reaction of pyridine and  $\text{CH}_2\text{I}_2$ . An authentic sample of dipyridinio-methane di-iodide has been tested on 1A, and as expected, it was found out that it has no role in the methylene group transfer reaction.

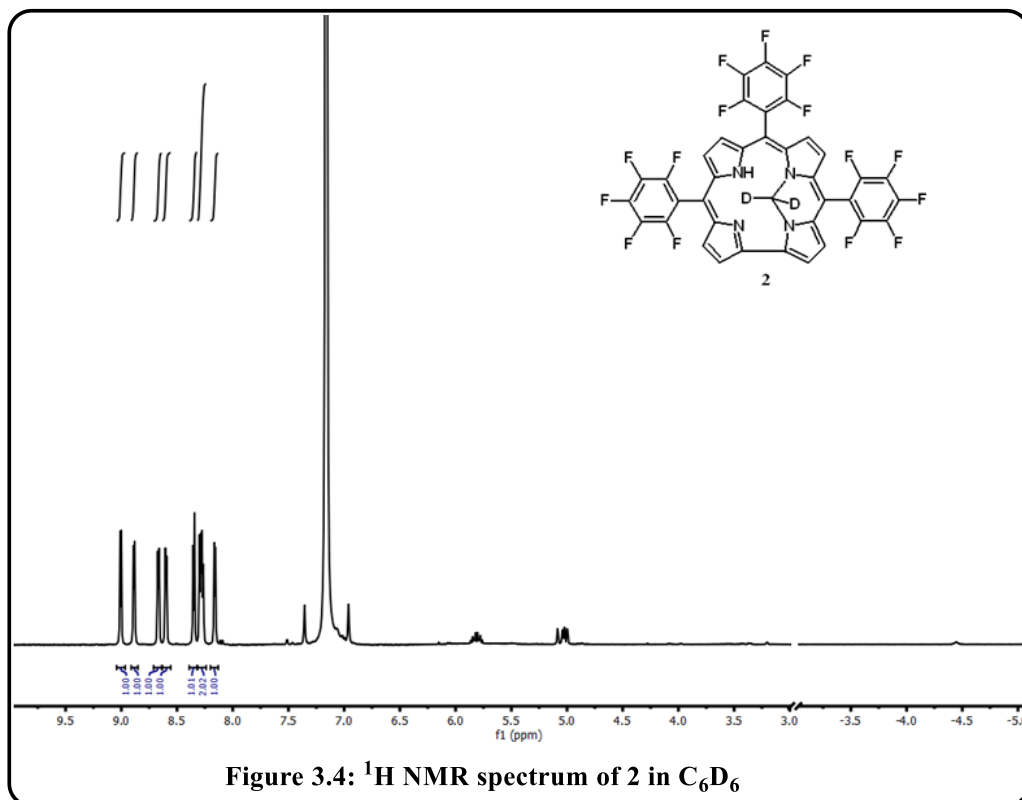
### 3.3 Spectral characterization:

#### 3.3.1 NMR Spectra:

The  $^1\text{H}$ ,  $^{19}\text{F}$  and  $^{13}\text{C}$  NMR spectrum for 1 supports the assigned structure. The aromatic protons exhibit a chemical shift of 9.0-8.16 ppm. Downfield shifts of aromatic protons were observed in 1 when compared to 1A. The methylene protons are most shielded due to diatropic ring current and are observed at -4.40 ppm.





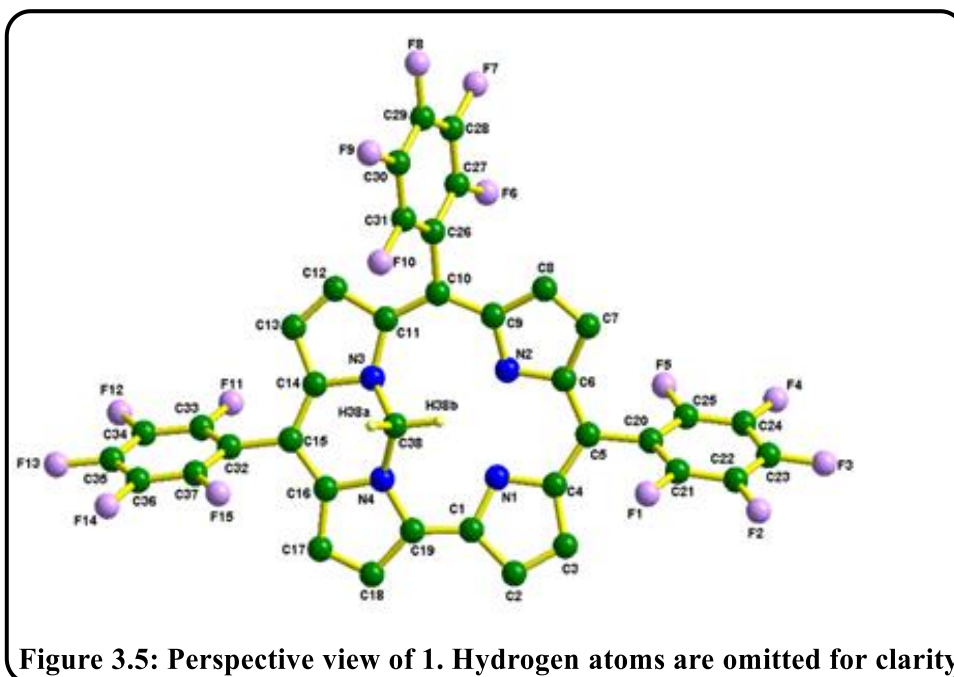


The assignment of the methylene protons are further confirmed by the complete disappearance of methylene signals on deuteration of the methylene protons of 1, which consequently generated the  $N^{21}$ ,  $N^{22}$ -methylene-d2-corrole derivative, 2.

### 3.3.2 Crystal Structure:

The crystal structure of 1 is shown in Figure 3.5. The crystal system is orthorhombic, and the unit cell has three 1 molecules. Important crystallographic parameters for 1 is presented in Table 3.2. In 1, carbon atom of the ‘methylene’ group deviates from the mean  $\text{N}_4$  corrole planes by a distance of  $\sim 0.794 \text{ \AA}$  and gives rise to a domed conformation. Pyrrole ring nitrogen atoms deviate from the mean corrole plane (considering the 19-carbon atom plane as the mean plane) by distances ranging from  $0.303 - (-0.293) \text{ \AA}$  in 1. The dihedral angles between the intersecting planes of pentafluorophenyl rings and the 19-atom corrole carbon plane are between

60.91–66.76°. The N (3)-C (38) and N (4)-C (38) bond distances of **1** are 1.457 Å and 1.459 Å and the N-C-N bond angle is 106.52°.



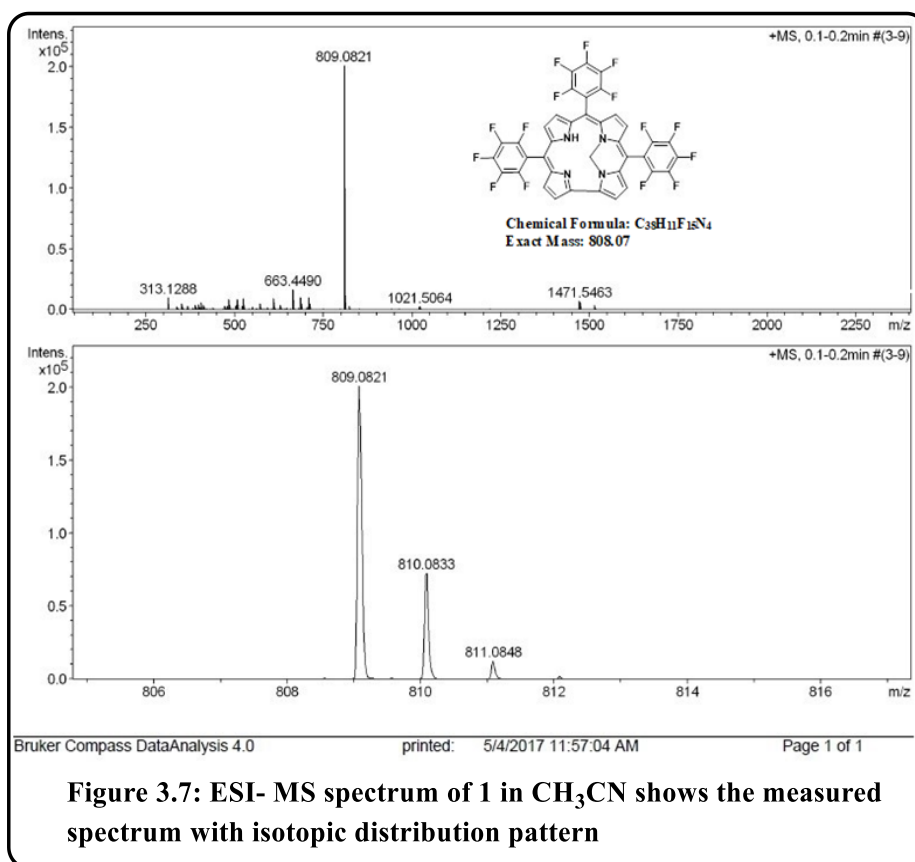
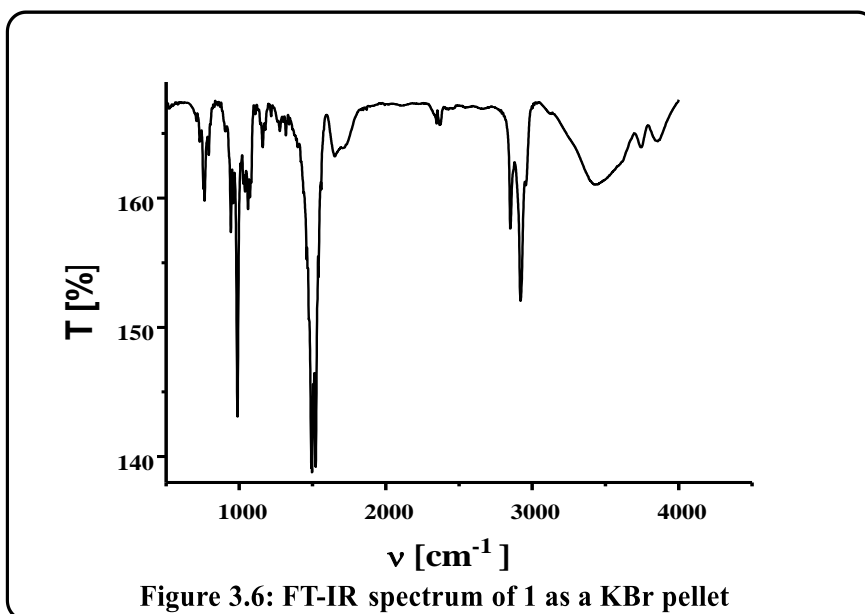
**Table 3.2: Important crystallographic parameters for **1****

<b>Compound code</b>	<b>1</b>
<b>Molecular formula</b>	<b>1.33(C<sub>38</sub>H<sub>11</sub>F<sub>15</sub>N<sub>4</sub>)</b>
<b>F.W</b>	<b>1078.02</b>
<b>Radiation</b>	<b>Cu K<math>\alpha</math></b>
<b>crystal symmetry</b>	<b>Orthorhombic</b>
<b>space group</b>	<b><i>P</i>2<sub>1</sub>2<sub>1</sub>2<sub>1</sub></b>
<b><i>a</i>(Å)</b>	<b>24.6024 (6)</b>
<b><i>b</i>(Å)</b>	<b>18.8820 (4)</b>

<b><i>c</i>(Å)</b>	<b>6.7904 (1)</b>
<b><i>α</i>(deg)</b>	<b>90</b>
<b><i>β</i>(deg)</b>	<b>90</b>
<b><i>γ</i>(deg)</b>	<b>90</b>
<b><i>V</i>(Å<sup>3</sup>)</b>	<b>3154.43 (11)</b>
<b><i>Z</i></b>	<b>3</b>
<b><i>μ</i> (mm<sup>-1</sup>)</b>	<b>1.47</b>
<b><i>T</i>(K)</b>	<b>298</b>
<b><i>D</i><sub>calcd</sub> (g cm<sup>-3</sup>)</b>	<b>1.702</b>
<b>2<i>θ</i> range (deg)</b>	<b>3.59 to 68.22</b>
<b><i>e</i> data (<i>R</i><sub>int</sub>)</b>	<b>5735 (0.095)</b>
<b><i>R</i>1 (<i>I</i> &gt; 2σ(<i>I</i>))</b>	<b>0.068</b>
<b>WR2 (all data)</b>	<b>0.141</b>
<b>GOF</b>	<b>1.04</b>
<b>Δ<i>ρ</i><sub>max</sub>, Δ<i>ρ</i><sub>min</sub> (e Å<sup>-3</sup>)</b>	<b>0.52, −0.65</b>

### 3.3.4 IR Spectra:

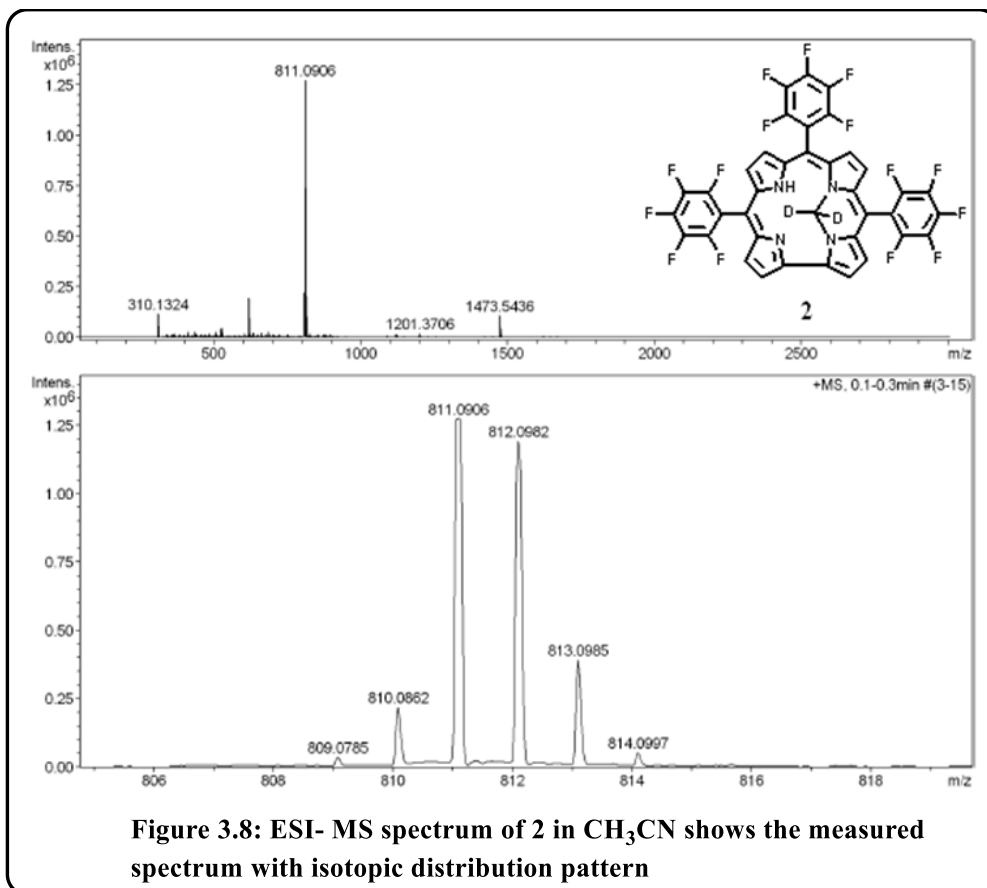
FT-IR spectrum of **compound 1** also indicate the presence of methylene group in its structure (Figure 3.6).



### 3.3.5 Mass Spectroscopy:

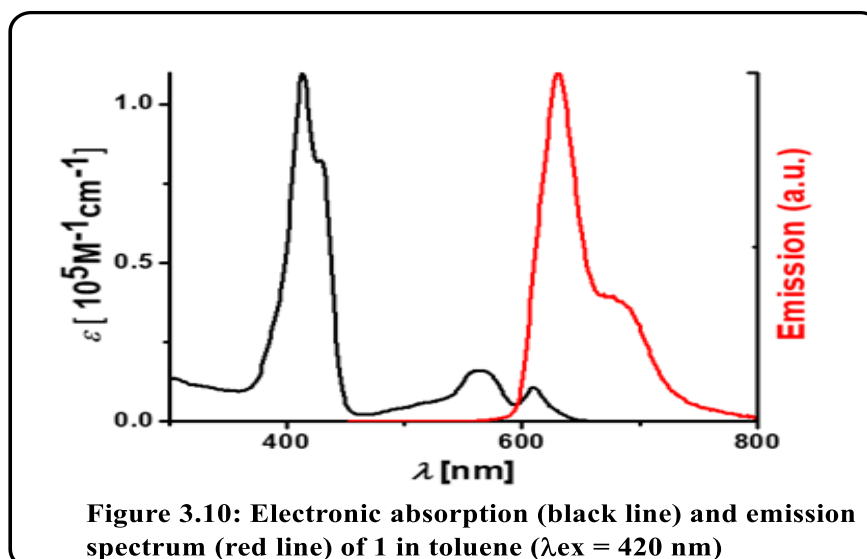
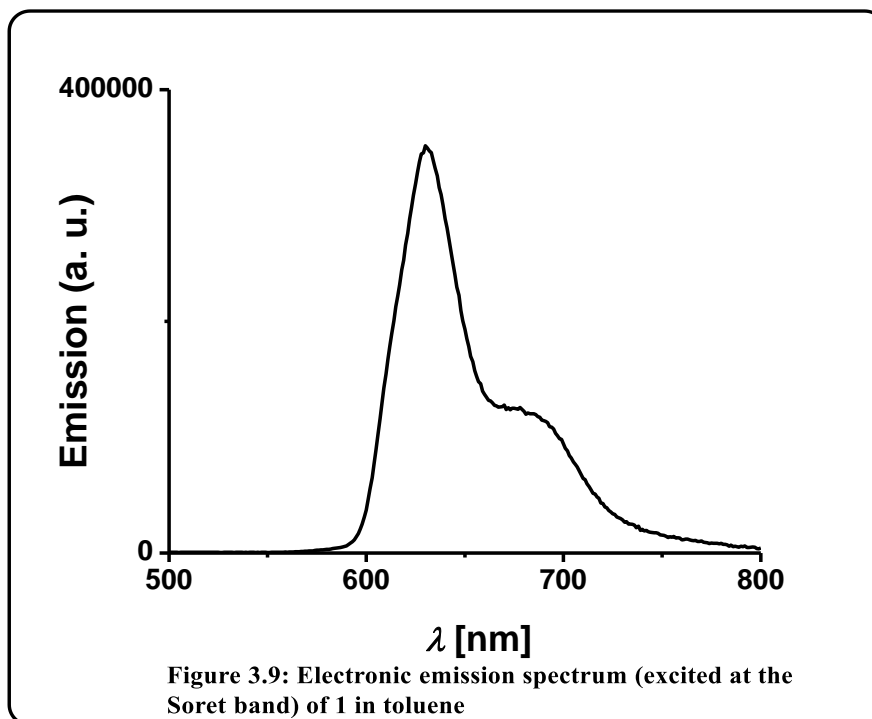
Electrospray mass spectrum in methanol showed peaks centred at  $m/z = 809.08$

correspond to  $[1+H]^+$  (808.07 calcd for  $C_{38}H_{11}F_{15}N_4$ ) {Figure 3.7}. And the mass spectrum for the deuterated compound in methanol showed peaks centred at  $m/z = 811.09$  correspond to  $[2+H]^+$  (810.07 calcd for  $C_{38}H_{11}F_{15}N_4$ ) {Figure 3.8}



### 3.3.6. Electronic absorption spectrum and emission spectrum:

The absorption spectrum of 1 exhibits split Soret bands at 414 and 429 nm and two weaker Q bands at 564 and 610 nm. Compared to the starting free base corrole derivative, 1A, these bands are bit red shifted and interestingly the splitting of the Soret band is clearly manifested in 1 (Figure 3.10).



#### Absorption spectral values of Soret and Q bands of 1 in various solvents:

Various solvents were chosen based on their polarity and their dielectric constants. Interestingly, we have not observed any linear dependency on the shift of  $\lambda_{\text{max}}$  values with solvent polarity (Table 3.3). Marginal or no shifts of  $\lambda_{\text{max}}$  values was observed in

most of the solvents. The free base corrole, **1** emits strongly at 631 nm and a shoulder at 682 nm in toluene (Figure 3.10).

**Table 3.3 Absorption spectral values of Soret and Q bands of **1** in various solvents:**

Solvent	Polarity index <sup>a</sup>	Dielectric constant <sup>a</sup>	UV-vis. data ( $\lambda_{\text{max}}$ / nm)
Hexane	0.1	1.88	406, 423, 554, 608
Toluene	2.4	2.38	414, 429, 564, 610
Chlorobenzene	2.7	5.62	414, 427, 565, 610
Dichloromethane	3.1	8.93	409, 424, 561, 606
Tetrahydrofuran	4.0	7.58	408, 423, 560, 606
Chloroform	4.1	4.81	409, 426, 562, 608
Acetone	5.1	20.7	406, 420, 556, 604
Methanol	5.1	32.70	406, 421, 553, 604
Acetonitrile	5.8	37.5	406, 421, 558, 604

The measured fluorescence quantum yield and lifetime of **1A** at 298 K (in toluene) are: 0.10, 4.4 ns, respectively. The fluorescence quantum yield and lifetime of **1** under the same conditions are: 0.12, 4.3 ns, respectively (Figure 3.11). This study thus confirms that upon N-substitution of corroles, the fluorescence quantum yield and lifetime do not quench.

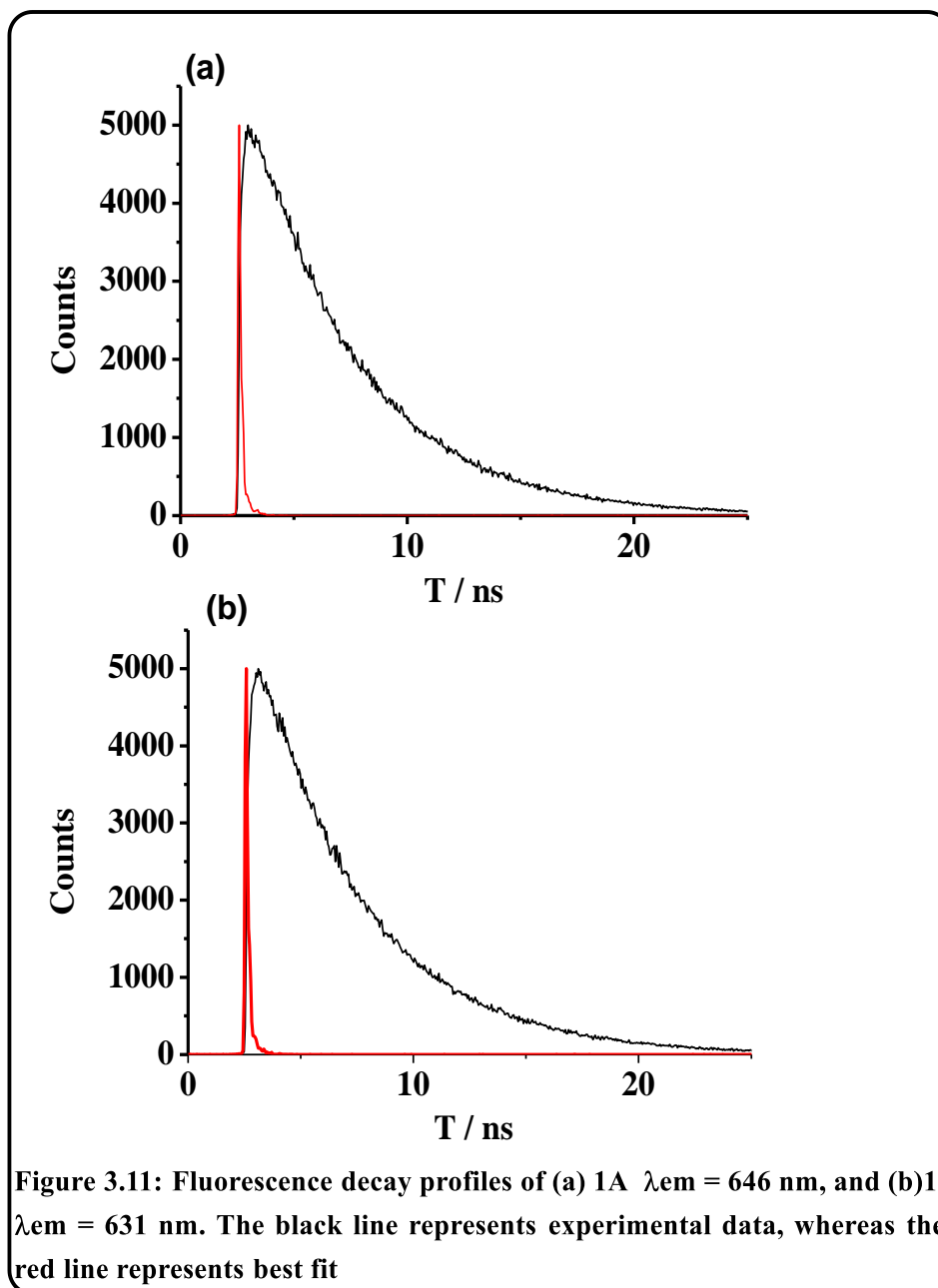


Figure 3.11: Fluorescence decay profiles of (a) 1A  $\lambda_{em} = 646$  nm, and (b) 1,  $\lambda_{em} = 631$  nm. The black line represents experimental data, whereas the red line represents best fit

### 3.4 Conclusions:

In summary, in analogy with the synthesis of N, N'-one carbon bridged porphyrin, as reported by Johnson *et al.*, we have successfully synthesized a similar derivative in corrole macrocycle by using a modified protocol. The newly synthesized  $N^{21}$ ,  $N^{22}$ -methylene-corrole derivative, 1 can resemble nicely with the previously

reported 21, 22-methyleneoctaethylporphyrin. Thus it is obvious that the novel methylene–corrole derivative and its various metal complexes will be of great interest to study further.

### **3.5 Experimental section:**

#### **3.5.1 Materials:**

The precursor's pyrrole, *p*-chloranil, CH<sub>2</sub>I<sub>2</sub>, CD<sub>2</sub>I<sub>2</sub>, and aldehydes were purchased from Aldrich, USA. Other chemicals were of reagent grade. Hexane and CH<sub>2</sub>Cl<sub>2</sub> were distilled from KOH and CaH<sub>2</sub> respectively. For spectroscopy studies, HPLC grade solvents were used. 1A was prepared by following an earlier literature report.<sup>51</sup>

#### **3.5.2 Physical Measurements:**

UV-Vis spectral studies were performed on a Perkin–Elmer LAMBDA-750 spectrophotometer. Emission spectral studies were performed on a Perkin Elmer, LS 55 and a Cary Eclipse fluorescence spectrophotometer using optical cell of 1 cm path length. The fluorescence quantum yields were determined using tetraphenylporphyrin, [TPP] as a reference.<sup>52</sup> Time resolved fluorescence measurements were carried out using a time-correlated single photon counting (TCSPC) spectrometer (Edinburgh, Life Spec II). The elemental analyses were carried out with a Perkin–Elmer 240C elemental analyser. FT–IR spectra were recorded on a Perkin–Elmer spectrophotometer with samples prepared as KBr pellets. The NMR measurements were carried out using Bruker 400 and 700 MHz NMR spectrometer. Chemical shifts are expressed in parts

per million (ppm) relative to residual benzene ( $\delta = 7.16$ ). Electrospray mass spectra were recorded on a Bruker Micro TOF—QII mass spectrometer.

### 3.5.3 Crystal Structure Determination:

Single crystals of **1** were grown by slow diffusion of a solution of the **1** in dichloromethane into hexane, followed by slow evaporation under atmospheric conditions. The crystal data of **1** were collected on a Rigaku Oxford diffractometer at 293 K. Selected data collection parameters and other crystallographic results are summarized in Table S2. All data were corrected for Lorentz polarization and absorption effects. The program package SHELXTL<sup>53</sup> was used for structure solution and full matrix least squares refinement on  $F^2$ . Hydrogen atoms were included in the refinement using the riding model. Contributions of H atoms for the water molecules were included but were not fixed. Disordered solvent molecules were taken out using SQUEEZE command in PLATON.<sup>54</sup> CCDC 1851457 contain the supplementary crystallographic data for **1**. These data can be obtained free of charge via [www.ccdc.cam.ac.uk/data\\_request/cif](http://www.ccdc.cam.ac.uk/data_request/cif).

### 3.5.4 Syntheses:

#### 3.5.4.1 Synthesis of N<sup>21</sup>,N<sup>22</sup>-methylene-5,10,15-tris(pentafluorophenyl)corrole, **1**:

0.10 g (0.013 mmol) of 5,10,15-tris(pentafluorophenyl)corrole, **1A** was dissolved in 18 mL of pyridine and stirred for 5 minutes at inert atmosphere. After that 10  $\mu$ L (0.13 mmol) of CH<sub>2</sub>I<sub>2</sub> was added to it and the reaction mixture was refluxed for 45 mins at around 100°C. The solution turns out to be reddish-green. The residual solvent mixture was dried by rotary evaporation and the reddish colored crude product

was purified by using column chromatography through a silica gel (100-200 mesh) bed and by using 10% dichloromethane and 90% hexane as eluent.

**For N<sup>21</sup>,N<sup>22</sup>-methylene-5,10,15-tris(pentafluorophenyl)corrole:** Yield: 80% (0.008 g). Anal. Calcd (found) for C<sub>38</sub>H<sub>11</sub>F<sub>15</sub>N<sub>4</sub> (1): C, 56.45 (56.61); H, 1.37 (1.46); N, 6.93 (6.83).  $\lambda_{\text{max}}$ /nm ( $\epsilon$ /M<sup>-1</sup>cm<sup>-1</sup>) in toluene: 414 (110,000), 429 (83,000), 564 (16,250), 610 (10800). <sup>1</sup>H NMR (400 MHz, Benzene-*d*<sub>6</sub>)  $\delta$  9.00 (d, *J* = 4.5 Hz, 1H), 8.87 (d, *J* = 4.3 Hz, 1H), 8.65 (d, *J* = 4.5 Hz, 1H), 8.59 (d, *J* = 4.5 Hz, 1H), 8.35 (d, *J* = 5.0 Hz, 1H), 8.27 (dd, *J* = 10.5, 4.8 Hz, 2H), 8.16 (d, *J* = 4.6 Hz, 1H), -4.40 (s, 2H) (Figure 3.1). <sup>19</sup>F NMR (377 MHz, Benzene-*d*<sub>6</sub>)  $\delta$  -138.54 (m, 6F), -151.80 (t, *J* = 21.7 Hz, 1F), -152.21 (t, *J* = 21.8 Hz, 1F), -152.66 (t, *J* = 21.9 Hz, 1F), -160.88 (ddd, *J* = 29.1, 22.9, 7.7 Hz, 2F), -161.29 – -161.60 (m, 2F), -161.77 – -162.21 (m, 2F). (Figure 3.2) <sup>13</sup>C NMR (101 MHz, C<sub>6</sub>D<sub>6</sub>)  $\delta$  145.19, 141.66, 139.17, 138.69, 136.26, 133.75, 131.09, 126.88, 126.10, 125.39, 119.69, 118.85, 117.36, 113.46, 102.78, 96.35, 95.36, 47.14 (Figure 3.3). 1 displayed strong fluorescence at 631 nm and a shoulder at 682 nm in toluene with excited state life time of 4.3 ns (Figure 3.11). The electrospray mass spectrum in methanol showed peaks centred at *m/z* = 809.08 correspond to [1+H]<sup>+</sup> (808.07 calcd for C<sub>38</sub>H<sub>11</sub>F<sub>15</sub>N<sub>4</sub>) {Figure 3.7}.

## References:

1. F. De Matteis, A. H. Gibbs and A. G. Smith, *Biochem. J.* **1980**, *189*, 645-648.
2. A. Ito, K. Konishi and T. Aida, *Tetrahedron Lett.* **1996**, *37*, 2585-2588.
3. H. Callot and T. Tschamber, *J. Am. Chem. Soc.* **1975**, *97*, 6175-6178.
4. Y. Watanabe, T. Aida and S. Inoue, *Macromolecules.* **1990**, *23*, 2612-2617.
5. A. Jackson, *The Porphyrins VI: Structure and Synthesis.* 2012, 341.
6. C. H. Devillers, S. Hebié, D. Lucas, H. l. n. Cattey, S. b. Clément and S. b. Richeter, *J. Org. Chem.* **2014**, *79*, 6424-6434.
7. D. Berezin, N. Zharnikova, V. Andrianov, P. Shatunov and A. Semeikin, *Russ. J. Coord. Chem.* **2002**, *28*, 325-332.
8. M. McLaughlin, *J. Chem. Soc., Perkin Trans. II.* **1974**, 136-140.
9. I. Batinic-Haberle, Z. Rajic, A. Tovmasyan, J. S. Reboucas, X. Ye, K. W. Leong, M. W. Dewhirst, Z. Vujaskovic, L. Benov and I. Spasojevic, *Free Radical Biol. Med.* **2011**, *51*, 1035-1053.
10. J. P. Hill, I. J. Hewitt, C. E. Anson, A. K. Powell, A. L. McCarty, P. A. Karr, M. E. Zandler and F. D'Souza, *J. Org. Chem.* **2004**, *69*, 5861-5869.
11. I. V. Sazanovich, D. B. Berezin, A. van Hoek, A. Y. Panarin, V. L. Bolotin, A. S. Semeykin and V. S. Chirvony, *J. Porphyrins Phthalocyanines.* **2005**, *9*, 59-67.
12. D. E. Goldberg and K. M. Thomas, *J. Am. Chem. Soc.* **1976**, *98*, 913-919.
13. D. K. Lavalley and O. P. Anderson, *J. Am. Chem. Soc.* **1982**, *104*, 4707-4708.
14. W.-P. Chang, W.-C. Lin, J.-H. Chen, S.-S. Wang and J.-Y. Tung, *Dalton Trans.* **2012**, *41*, 13454-13464.

15. Y. W. Chan, M. W. Renner and A. L. Balch, *Organometallics*. 1983, 2, 1888-1889.
16. Y. Takao, T. Takeda, J.-y. Watanabe and J.-i. Setsune, *Organometallics*. **2003**, 22, 233-241.
17. W. Naito, N. Yasuda, T. Morimoto, Y. Shigeta, H. Takaya, I. Hisaki and H. Maeda, *Org. Lett.*, **2016**, 18, 3006-3009.
18. W. McEwen, *J. Am. Chem. Soc.*, **1936**, 58, 1124-1129.
19. A. Jackson, *The Porphyrins VI: Structure and Synthesis*, **2012**, 341.
20. P. Batten, A. L. Hamilton, A. W. Johnson, M. Mahendran, D. Ward and T. J. King, *J. Chem. Soc., Perkin Trans. I.*, **1977**, 1623-1628.
21. A. W. Johnson, D. Ward, P. Batten, A. L. Hamilton, G. Shelton and C. M. Elson, *J. Chem. Soc., Perkin Trans. II.*, **1975**, 2076-2085.
22. V. V. Roznyatovskiy, C.-H. Lee and J. L. Sessler, *Chem. Soc. Rev.* **2013**, 42, 1921-1933.
23. Z. Gross, *J. Biol. Inorg. Chem.* **2001**, 6, 733-738.
24. R. Paolesse, S. Nardis, M. Stefanelli, F. R. Fronczek and M. G. H. Vicente, *Angew. Chem., Int. Ed.* **2005**, 44, 3047-3050.
25. R. S. Czernuszewicz, V. Mody, A. Czader, M. Galezowski and D. T. Gryko, *J. Am. Chem. Soc.* 2009, **131**, 14214-14215.
26. P. J. Brothers, *Chem. Commun.* 2008, 2090-2102.
27. J. H. Palmer, A. C. Durrell, Z. Gross, J. R. Winkler and H. B. Gray, *J. Am. Chem. Soc.* 2010, **132**, 9230-9231.
28. H.-Y. Liu, Y. Fei, Y.-T. Xie, X.-Y. Li and C. K. Chang, *J. Am. Chem. Soc.* 2009, **131**, 12890-12891.

29. B. Brizet, N. Desbois, A. Bonnot, A. Langlois, A. Dubois, J.-M. Barbe, C. P. Gros, C. Goze, F. Denat and P. D. Harvey, *Inorg. Chem.* **2014**, *53*, 3392-3403.
30. S. Kuck, G. Hoffmann, M. Broering, M. Fechtel, M. Funk and R. Wiesendanger, *J. Am. Chem. Soc.* **2008**, *130*, 14072-14073.
31. K. E. Thomas, H. Vazquez-Lima, Y. Fang, Y. Song, K.J. Gajnon, C.M. Beavers, K.M. Kadish and A. Ghosh, *Chem. Eur. J.* **2015**, *21*, 16839-16847.
32. M. Bröring, F. Bregier, E. Cónsul Tejero, C. Hell and M. C. Holthausen, *Angew. Chem. Int. Ed.* **2007**, *46*, 445-448.
33. A. Ghosh, *Chem. Rev.* **2017**, *117*, 3798-3881.
34. R. Orłowski, D. Gryko and D. T. Gryko, *Chem. Rev.* **2017**, *117*, 3102–3137.
35. Y. Fang, Z. Ou and K. M. Kadish, *Chem. Rev.* **2017**, *117*, 3377–3419.
36. K. Fujino, Y. Hirata, Y. Kawabe, T. Morimoto, A. Srinivasan, M. Toganoh, Y. Miseki, A. Kudo and H. Furuta, *Angew. Chem. Int. Ed.* **2011**, *50*, 6855– 6859.
37. W. Sinha, M. G. Sommer, N. Deibel, F. Ehret, B. Sarkar and S. Kar, *Chem. Eur. J.* **2014**, *20*, 15920-15932.
38. W. Sinha, M. G. Sommer, N. Deibel, F. Ehret, M. Bauer, B. Sarkar and S. Kar, *Angew. Chem., Int. Ed.* **2015**, *54*, 13769-13774.
39. W. Sinha, M. G. Sommer, L. Hettmanczyk, B. Patra, V. Filippou, B. Sarkar and S. Kar, *Chem. - Eur. J.* **2017**, *23*, 2396-2404.
40. B. Patra, S. Sobottka, W. Sinha, B. Sarkar, S. Kar, *Chem. - Eur. J.* **2017**, *23*, 13858-13863.
41. A. Garai, S. Sobottka, R. Schepper, W. Sinha, M. Bauer, B. Sarkar and S. Kar, *Chem. - Eur. J.* **2018**, *24*, 12613-12622.

42. B. Patra, S. Sobottka, S. Mondal, B. Sarkar and S. Kar, *Chem. Commun.* **2018**, 54, 9945-9948.
43. Z. Gross and N. Galili, *Angew. Chem., Int. Ed.* **1999**, 38, 2366-2369.
44. L. Simkhovich, P. Iyer, I. Goldberg and Z. Gross, *Chem. - Eur. J.*, **2002**, 8, 2595-2601.
45. A. Johnson and I. Kay, *J. Am. Chem. Soc.* **1965**, 1620-1629.
46. I. Saltsman, L. Simkhovich, Y. Balazs, I. Goldberg and Z. Gross, *Inorg. Chim. Acta.* **2004**, 357, 3038-3046.
47. I. Saltsman, I. Goldberg, Z. Gross, *Tetrahedron Lett.* **2003**, 44, 5669-5673.
48. S. K. Patra, K. Sahu, B. Patra, D. K. Sahoo, S. Mondal, P. Mukherjee, H. S. Biswal, S. Kar, *Green Chem.* **2017**, 19, 5772-5776.
49. T. Rohand, E. Dolusic, T. H. Ngo, W. Maes and W. Dehaen, *Arkivoc.* **2007**, 10, 307-324.
50. R. Paolesse, S. Nardis, M. Venanzi, M. Mastroianni, M. Russo, F. R. Fronczek and M. G. H. Vicente, *Chem. - Eur. J.* **2003**, 9, 1192-1197.
51. Z. Gross, N. Galili and I. Saltsman, *Angew. Chem. Int. Ed.* **1999**, 38, 1427-1429.
52. T. Ding, E. A. Alemán, D. A. Modarelli and C. J. Ziegler, *J. Phys. Chem. A.* **2005**, 109, 7411-7417.
53. G. M. Sheldrick, *Acta Crystallogr., Sect. A: Found. Crystallogr.* **2008**, 64, 112-122.
54. P. Van der Sluis and A. Spek, *Acta Crystallogr., Sect. A: Found. Crystallogr.* **1990**, 46, 194-201.

## CHAPTER 4

# Synthesis, structure, photophysics, and singlet oxygen sensitization by a platinum(II) complex of *meso*-tetra-acenaphthyl porphyrin

### 4.1 Introduction

### 4.2 Results and Discussion

#### 4.2.1 Synthesis and characterization

### 4.3 Spectral Characterization

#### 4.3.1 NMR spectroscopy

#### 4.3.2 Mass spectroscopy:

#### 4.3.3 Crystal structure:

#### 4.3.4 Electrochemistry:

#### 4.3.5 Electronic absorption spectrum and emission spectrum

#### 4.3.6 Emission properties and singlet oxygen sensitization:

### 4.4 Conclusions

### 4.5 Experimental Section

#### 4.5.1 Materials

#### 4.5.2 Physical measurements

#### 4.5.3 Crystal Structure determination

#### 4.5.4 Synthesis

##### 4.5.4.1 Synthesis of [5,10,15,20-tetra(5-acenaphthyl)porphinato] platinum(II),

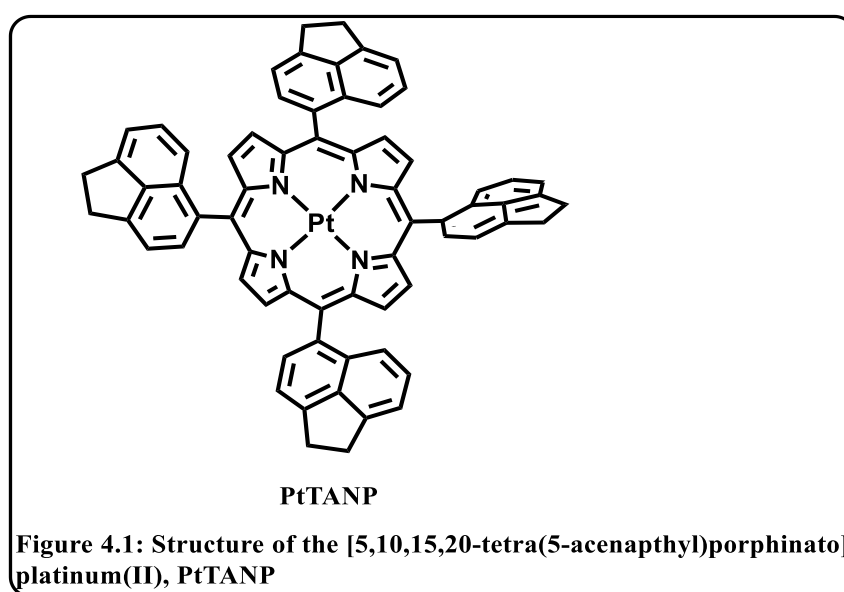
##### PtTANP

#### 4.1 Introduction:

Transition metal complexes have gained a lot of interest, thanks to their peculiar photophysical properties. Upon photoexcitation, transition metal complexes bearing heavy transition metals like ruthenium, iridium, gold, platinum, etc., show a very efficient intersystem crossing (ISC) thanks to the heavy atom effect and produce a triplet excited state.<sup>1-6</sup> This triplet excited state decay back to the ground state by non radiative deactivation or by phosphorescence, with the emission of a photon. The long triplet lifetimes of these complexes (in the order of microseconds) are exploited for various energy transfer/electron transfer reactions. These photoactive transition metal complexes constitute an important class of molecules known as the photosensitizer.<sup>7-12</sup> The energy transfer from these photosensitized molecules to the natural triplet oxygen generates singlet oxygen.<sup>13</sup> Photosensitized singlet oxygen generation is an emerging research area with versatile applications in organic synthesis of fine chemicals,<sup>14</sup> pollution controls,<sup>15</sup> and photodynamic therapy.<sup>16-19</sup> In this regard, Ru(II) polypyridyl complexes,<sup>20</sup> iridium(III),<sup>21-22</sup> gold complexes,<sup>23</sup> and platinum porphyrin complexes<sup>24-28</sup> are well known as the photosensitizer. Platinum porphyrin complexes show intense phosphorescence at room temperature due to high yields of population of the triplet state and high yield of emission quantum yield.<sup>29-32</sup> Platinum porphyrin complexes like platinum octaethylporphyrin (PtOEP), a very strong phosphor, have been used to detect oxygen via phosphorescence quenching phenomena.<sup>33-35</sup> The ideal dye for luminescence O<sub>2</sub> sensing material must be a good triplet emitter with a lifetime suitable for the specific range of oxygen concentration to be detected. Due to those reasons, ruthenium bipyridine complexes and platinum porphyrin complexes are often used as luminescence oxygen sensing materials.<sup>36-38</sup> Although the lifetime of triplet emitters

varies largely from ruthenium-based dyes to platinum-based dyes, it is not so easy to fine-tune their triplet-state lifetime as the various application needs a distinctive triplet-state lifetime of the dye. To achieve that purpose, a suitable design of the ligand system is a prerequisite. Thus there is an intense research interest in newer varieties of dyes having distinctive triplet lifetime. Interestingly, the absorption and emission spectra of platinum(II) porphyrins are very characteristic.<sup>39</sup> These compounds exhibited a large molar absorption coefficient, a large Stokes shift of the emission band, and a high quantum yield of luminescence at room temperature.<sup>40</sup> Due to their intense phosphorescence, platinum(II) porphyrin complexes are well-known photosensitizers and have found applications as phosphorescent markers in immunology,<sup>41</sup> in solar energy conversion and storage,<sup>42</sup> as molecular conductors,<sup>43</sup> and in oxygen sensing devices.<sup>44</sup> Porphyrins having increased conjugation at the  $\beta$  positions, often called  $\pi$ -extended porphyrins, have attracted significant attention as potential candidates for optoelectronic materials.<sup>45</sup> These compounds exhibited phosphorescence in the red-near infrared (NIR) region of the spectrum.<sup>46</sup> However, similar studies with the increased conjugation at the *meso*-phenyl ring have not been covered that much. One possible reason is that the steric interaction between the porphyrin  $\beta$  hydrogen and the *meso*-phenyl ring does not allow appreciable  $\pi$  overlap between them, and thus, there is no significant effect on the electronic structure of the porphyrin.<sup>47</sup> However, it has to be kept in mind that the proper choice of the substituent's (either *meso*- or  $\beta$ -) at the porphyrin periphery can enhance the rigidity of the resulting structure and this might result in an increase of the phosphorescence quantum yield by slowing down non-radiative decay processes of the lowest triplet excited state. It was also reported earlier that steric crowding could enhance the lifetime of the triplet state of porphyrinoids.<sup>47</sup>

Herein, we present the synthesis of a new platinum(II) porphyrin complex: [5,10,15,20-tetra(5-acenaphthyl)porphinato] platinum(II), PtTANP bearing acenaphthyl groups at their *meso*-positions (Figure 4.1). Acenaphthene, an aromatic hydrocarbon obtained from coal tar, is derived via simple modification of naphthalene unit and has found extensive applications in dyes and drugs and is also biocompatible.<sup>48</sup> The compound has been thoroughly characterized by several spectroscopic techniques, including UV-Vis, emission, <sup>1</sup>H and <sup>13</sup>C NMR, ESI-MS data, and single-crystal XRD analysis.

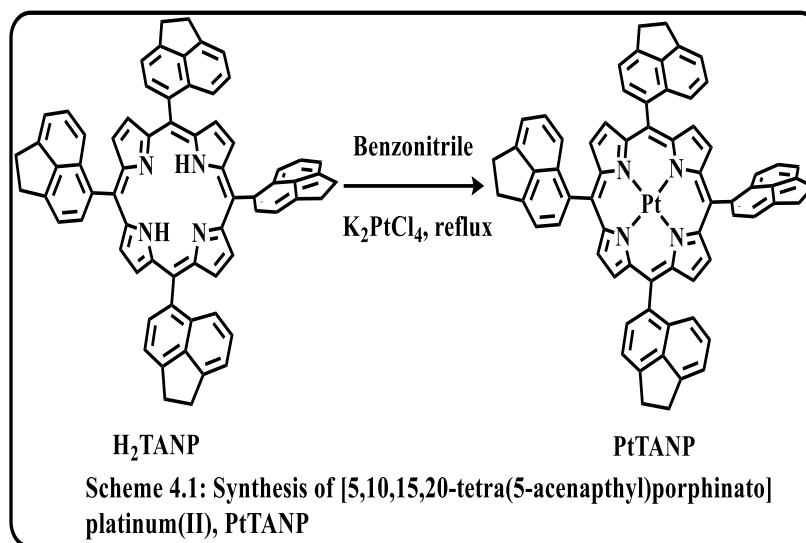


## 4.2 Results and Discussion:

### 4.2.1 Synthesis and characterization:

The reaction of the 5,10,15,20-tetra(5-acenaphthyl) porphyrin, **H<sub>2</sub>TANP** with the platinum precursor complex K<sub>2</sub>PtCl<sub>4</sub> in benzonitrile solution resulted in the formation of the complex, [5,10,15,20-tetra(5-acenaphthyl)porphinato] platinum(II), **PtTANP** (Scheme 4.1). The purity and identity of the platinum (II) complex, **PtTANP** is demonstrated by its satisfactory elemental analyses, ESI-MS data, NMR, UV-Vis, emission, and single-crystal XRD data (Figure 4.2-4.7). The electrospray mass

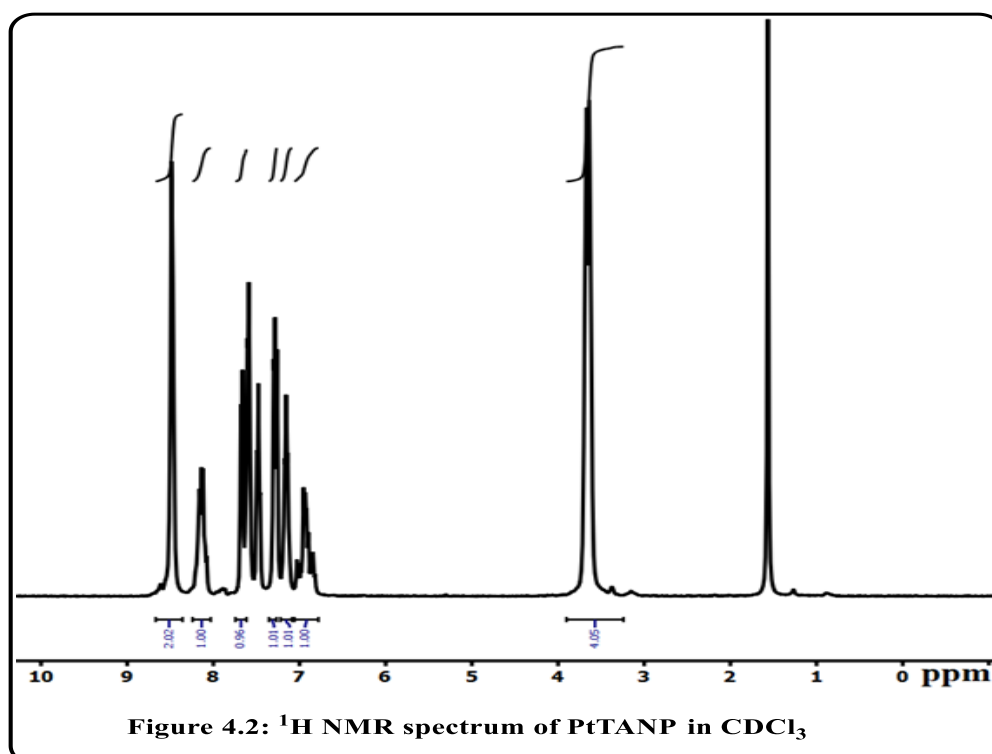
spectrum showed the peaks centered at  $m/z = 1112.3391$  corresponding to  $[\text{PtTANP}+\text{H}]^+$  (calculated molecular mass: 1112.3292) (Figure 4.4) .



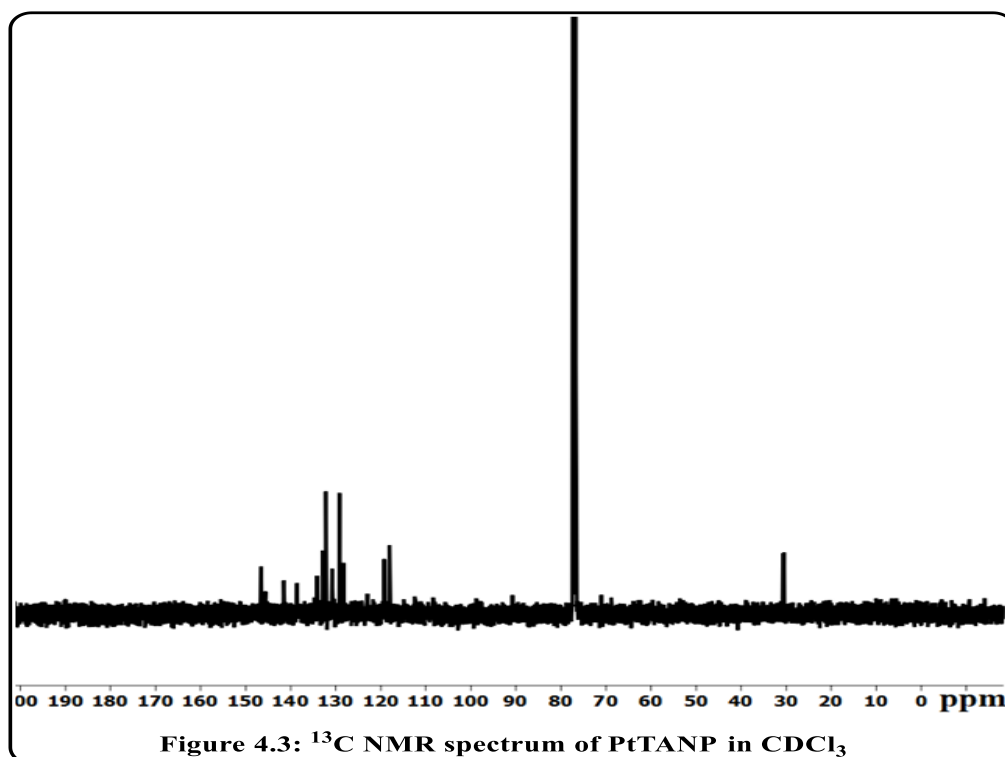
#### 4.3 Spectral Characterization:

##### 3.3.1 NMR Spectroscopy:

The  $^1\text{H}$  NMR and  $^{13}\text{C}$  NMR spectrum of **PtTANP** in  $\text{CDCl}_3$  are shown in Figure (4.2, 4.3). The  $^1\text{H}$  NMR spectrum of **PtTANP** exhibits the expected number of 44 partially

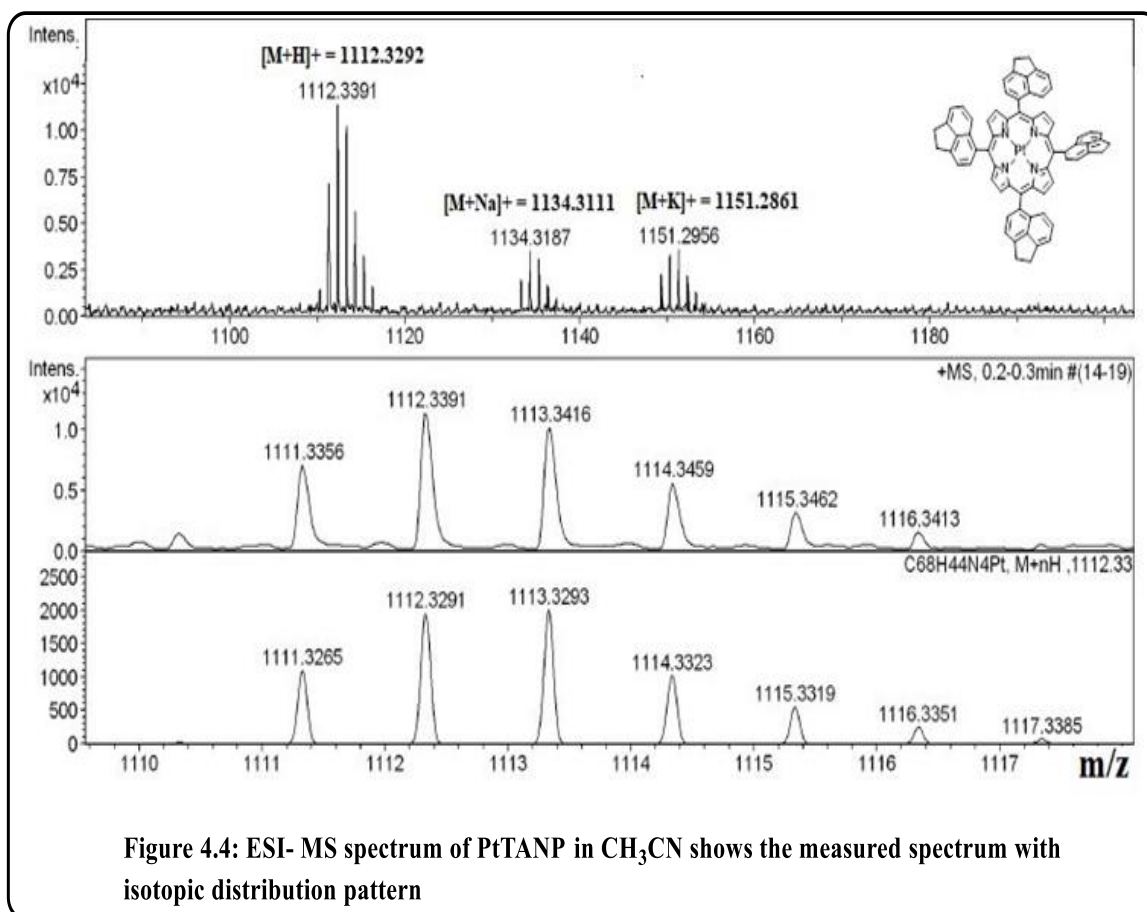


overlapping protons in the region,  $\delta=3.62\text{--}8.50$  ppm (Figure 4.2). The methylene group protons resonate at 3.62-3.70 ppm (m, 16H) in  $\text{CDCl}_3$ . The 28 aromatic protons resonate at 6.81 - 8.50 ppm.



#### 4.3.2 Mass Spectroscopy:

The electrospray mass spectrum showed the peaks centered at  $m/z = 1112.3391$  corresponding to  $[\text{PtTANP}+\text{H}]^+$  (calculated molecular mass: 1112.3292).



### 4.3.3 Crystal Structure:

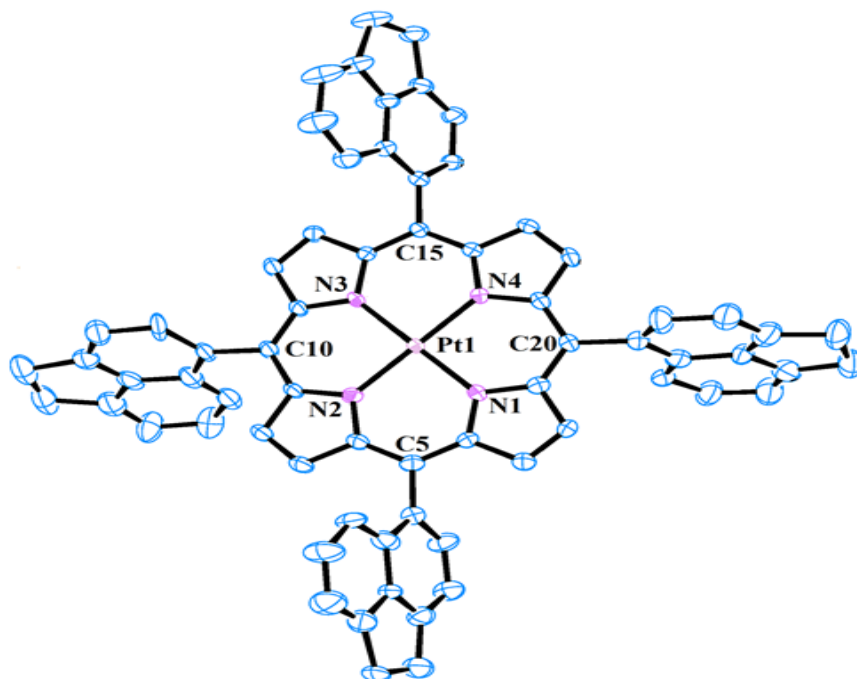
The crystal system of [5,10,15,20-tetra(5-acenaphthyl)porphyrinato] platinum(II), **PtTANP** is triclinic, and the unit cell has two molecules of **PtTANP**. Important crystallographic parameters for **PtTANP** are summarized in Table 4.1. Bond angles and distances of **PtTANP** match nicely with the previously reported other authentic porphyrinatoplatinum(II) derivatives. The deviation of the pyrrolic nitrogen atoms from the mean twenty carbon atom porphyrin plane by distances ranging from 0.008– 0.049 Å in **PtTANP** (Figure 4.5).

The observed deviations in **PtTANP** are in good agreement with that of the previously reported [5,10,15,20-tetra(5-acenaphthyl)porphyrinato] zinc(II) derivative.<sup>49</sup> However, the dihedral angles of the *meso*-substituted acenaphthyl rings and the 20-carbon mean porphyrin plane differs significantly in **PtTANP** in comparison with [5,10,15,20-tetra(5-acenaphthyl)porphyrinato] zinc(II). The corresponding values are of 65.68–75.20° in **PtTANP** and of 81.23–85.32° in [5,10,15,20-tetra(5-acenaphthyl)porphyrinato] zinc(II). While the deviation of the Platinum atom from the mean N4 porphyrin plane is 0.0031 Å, the similar deviation in the case of Zn(II) complex is zero. This can be ascribed to the smaller ionic radius of Zn(II). The geometry around the Pt (II) center is very near to the perfect square planar. The bite angles of N1-Pt-N2, N2-Pt-N3, N3-Pt-N4, and N4-Pt-N1 are 90.24°, 90.13°, 89.76°, and 89.87°, respectively.

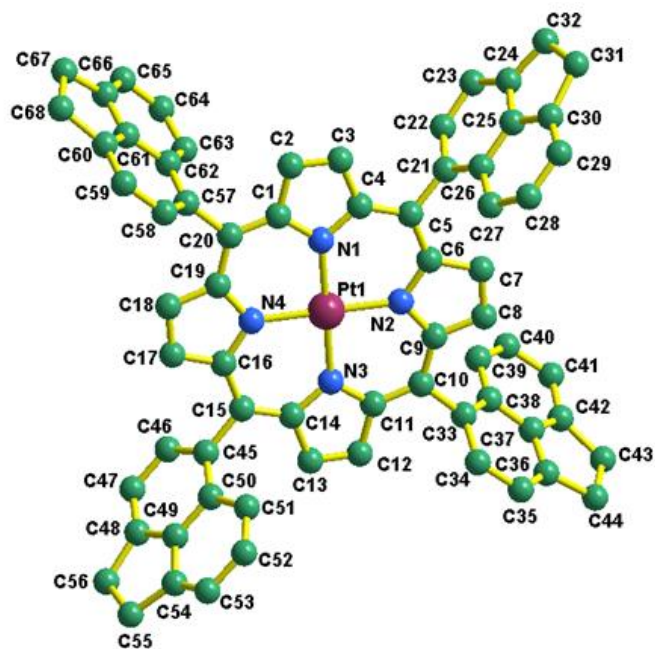
The Pt(II)-N bond distances are in the ranges of 2.005 Å–2.020 Å. These bond distances and angles match reasonably well with the previously reported authentic PtTPP derivatives (TPP=5,10,15,20-tetraphenyl-porphinato).<sup>50</sup> Similar bond distances were reported to be 2.08 Å in PtTPP derivatives.

#### 4.3.4 Electrochemistry

To understand the redox properties of **PtTANP**, the cyclic voltammetric and differential pulse voltammetric measurements were performed. The measurements were performed by using tetraethyl ammonium perchlorate (TEAP, 0.1 M) as a supporting electrolyte (Figure 4.7, Table 4.2) in dichloromethane solution.



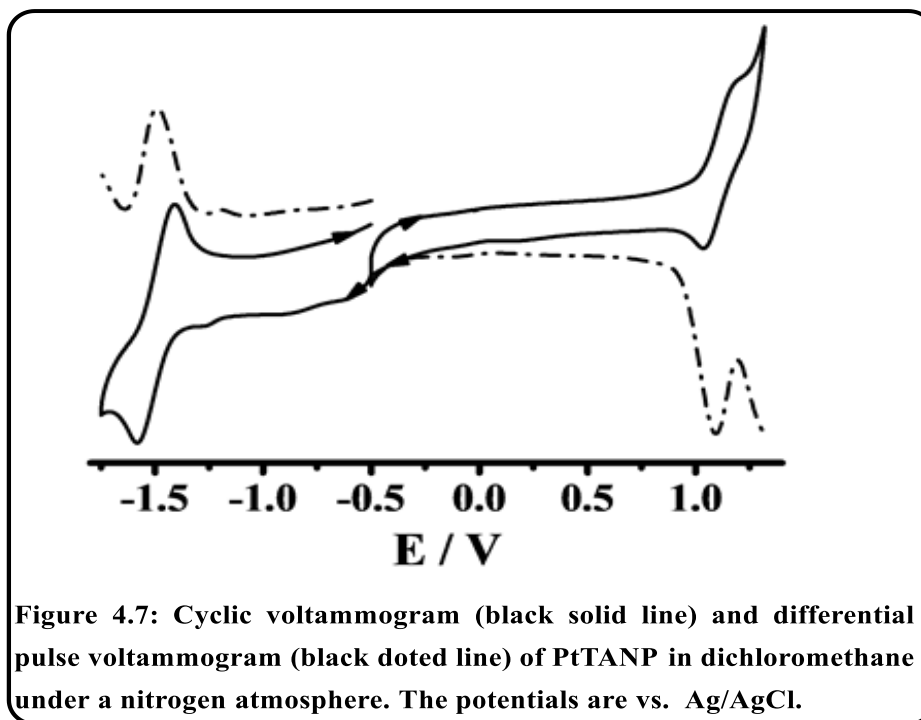
**Figure 4.5 ORTEP diagram of PtTANP. Ellipsoids are drawn at 40% probability**



**Figure 4.6: Single-crystal X-ray structure of PtTANP. Hydrogen atoms are omitted for clarity**

**Table 4.1 Crystallographic data for PtTANP**

<b>Molecular formula</b>	<b>C<sub>68</sub>H<sub>44</sub>N<sub>4</sub>Pt</b>
<b>F.W</b>	<b>1112.16</b>
<b>Radiation</b>	<b>MoK<math>\alpha</math></b>
<b>crystal symmetry</b>	<b>Triclinic</b>
<b>space group</b>	<b>P -1</b>
<b>a(Å)</b>	<b>12.277(5)</b>
<b>b(Å)</b>	<b>16.591(5)</b>
<b>c(Å)</b>	<b>16.668(5)</b>
<b>a(deg)</b>	<b>115.977(5)</b>
<b><math>\beta</math>(deg)</b>	<b>93.922(5)</b>
<b><math>\gamma</math>(deg)</b>	<b>110.766(5)</b>
<b>V(Å<sup>3</sup>)</b>	<b>2750.9(16)</b>
<b>Z</b>	<b>2</b>
<b><math>\mu</math> (mm<sup>-1</sup>)</b>	<b>1.343</b>
<b>T(K)</b>	<b>100(2) K</b>
<b>D<sub>calcd</sub> (g cm<sup>-3</sup>)</b>	<b>1.343</b>
<b>2<math>\theta</math> range (deg)</b>	<b>5.26 to 52.14</b>
<b>e data (R<sub>int</sub>)</b>	<b>10781(0.0605)</b>
<b>R1 (I&gt;2<math>\sigma</math>(I))</b>	<b>0.0539</b>
<b>WR2</b>	<b>0.1406</b>
<b>GOF</b>	<b>1.042</b>



Ag/AgCl reference electrode was used to express the potentials. The **PtTANP** derivative exhibited one reversible oxidation couple at +1.10 V ( $\Delta E_p = 80$  mV). It also showed one reversible reduction couple at -1.47 V ( $\Delta E_p = 80$  mV) versus Ag/AgCl. For a similar platinum porphyrin derivative, PtTPP (TPP= *meso*-**tetraphenylporphyrin**), the 1<sup>st</sup> oxidation couple at 1.15V and the 1<sup>st</sup> reduction couple at -1.35V versus Ag/AgCl in dichloromethane,<sup>51</sup> demonstrating a slight negative shift of the reduction potential of **PtTANP** with respect to PtTPP.

#### 4.3.5 Electronic absorption spectrum and Emission spectrum:

**Table 4.2 UV–Vis and electrochemical data**

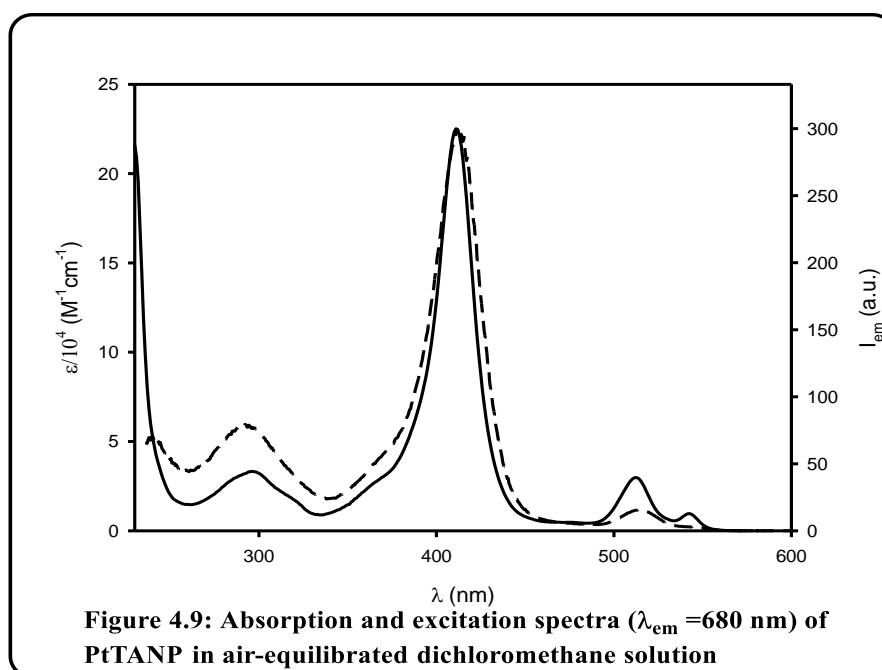
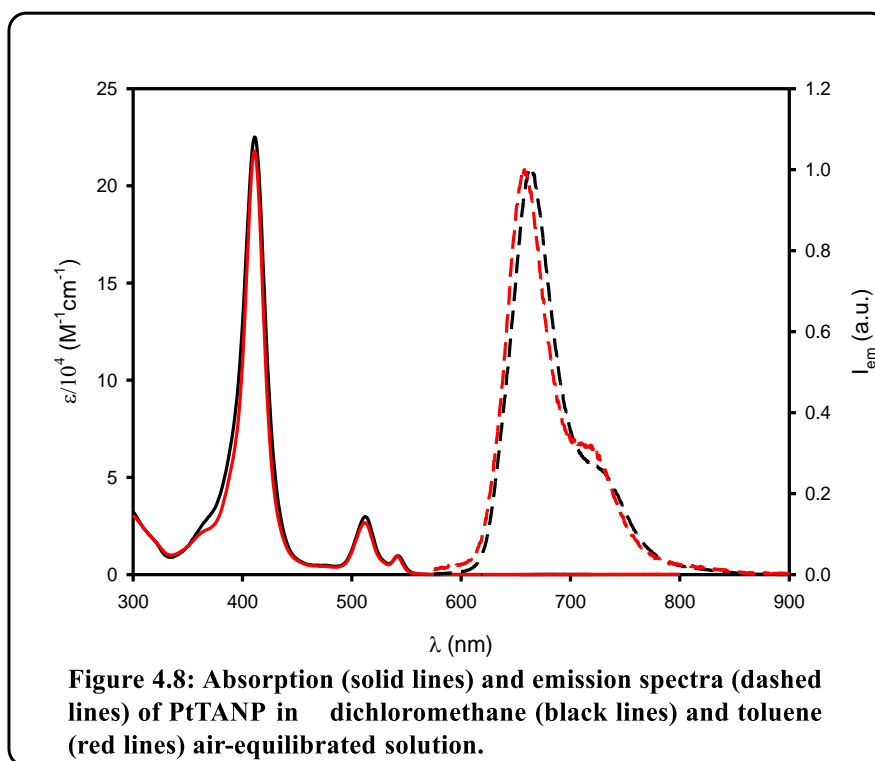
Compound	UV–Vis Data <sup>a</sup> $\lambda_{\text{max}} / \text{nm} (\epsilon / \text{M}^{-1}\text{cm}^{-1})$	Electrochemical data <sup>a, b</sup>	
		Oxidation $E^0, \text{V} (\Delta E_{\text{p}}, \text{mV})$	Reduction $E^0, \text{V} (\Delta E_{\text{p}}, \text{mV})$
PtTANP	410 (224000), 512 (30000), 542 (9000)	1.10(80)	-1.47 (80)

<sup>a</sup>In dichloromethane.

<sup>b</sup>The potentials are *vs.* Ag/AgCl reference electrode.

#### 4.3.6 Photophysical properties and Singlet oxygen sensitization:

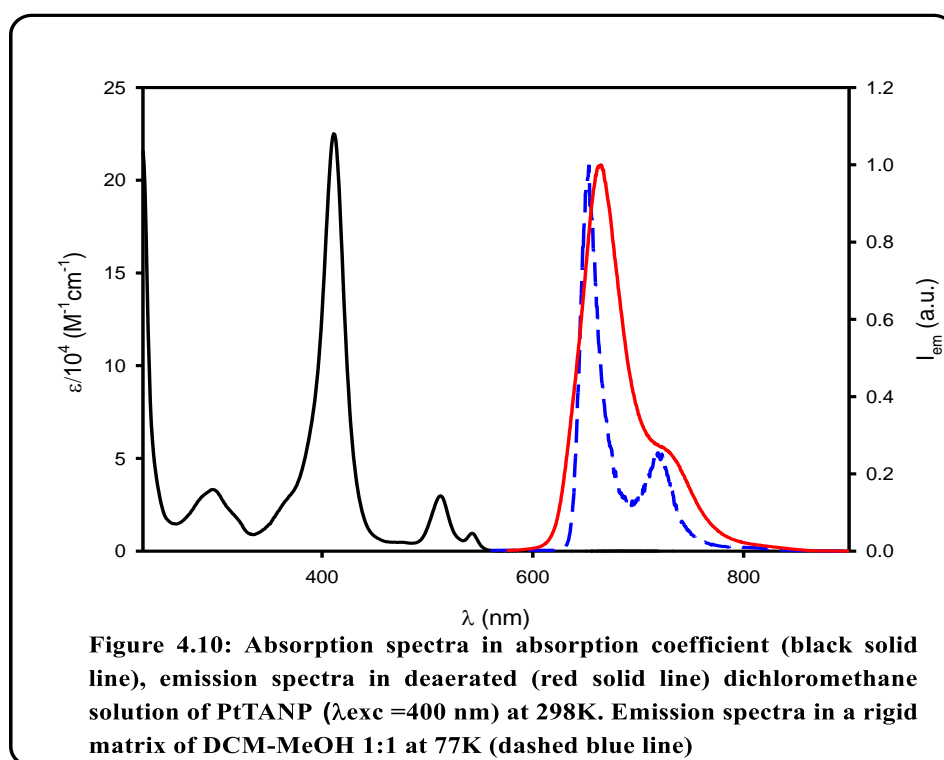
The photophysical characterization of the platinum porphyrin complex, **PtTANP** was carried out in dichloromethane (DCM) or toluene (TOL): no significant difference was observed (Figure 4.9). In the following, the photophysical properties in dichloromethane will be discussed. The absorption spectrum (solid line in Figure 4.10) shows the typical Soret band at 410 nm with an absorption coefficient of  $2.24 \times 10^5 \text{ M}^{-1}\text{cm}^{-1}$  and the typical Q-bands with vibrational structure at 512 nm ( $\epsilon = 3.0 \times 10^4 \text{ M}^{-1}\text{cm}^{-1}$ ) and 542 nm ( $\epsilon = 0.9 \times 10^4 \text{ M}^{-1}\text{cm}^{-1}$ ). The additional band at 290 nm is due to the acenaphthenechromophores (ACN).<sup>52</sup>



In deaerated solution at 298 K, a strong phosphorescence is observed with a maximum at 660 nm (red line in Figure 4.10), emission quantum yield of 35% and

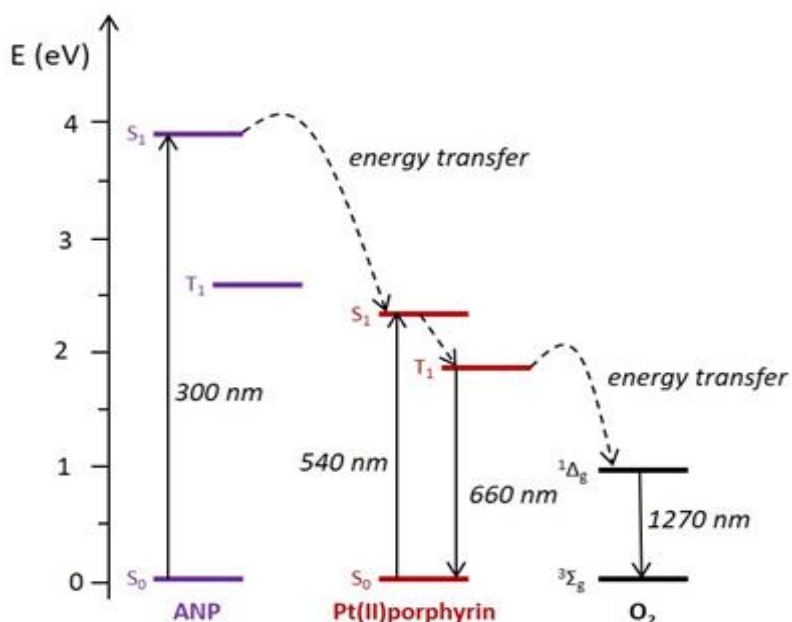
lifetime of 75  $\mu$ s. The excitation spectrum performed at  $\lambda_{em} = 660$  nm well matches the absorption spectrum (Figure 4.9), demonstrating a unitary efficient energy transfer from the acenaphthene chromophores to the Pt(II) porphyrin.

Indeed, upon excitation at 300 nm, where most of the light is absorbed by acenaphthene chromophores, sensitised emission at 660 nm is observed. Therefore, **PtTANP** behaves as a light-harvesting antenna as schematically depicted in (Figure 4.11).



In air-equilibrated solution **PtTANP** exhibits a very weak phosphorescence ( $\Phi_{em} = 0.22\%$ ) with a much shorter lifetime ( $\tau = 910$  ns). The **PtTANP** phosphorescence is strongly quenched by oxygen with a rate constant of  $4.9 \times 10^8 \text{ M}^{-1}\text{s}^{-1}$ . The quenching by oxygen results in singlet oxygen production with a very high quantum yield of 88% (Figure 4.12).<sup>54</sup>

Quantum yield of oxygen production was calculated by comparison between the emission intensity of oxygen (Fig. 4.13) generated by excitation of the standard perinaphthenone and the sample **PtTANP**.



**Figure: 4.11:** Most relevant photophysical processes occurring for **PtTANP**, constituted by a **Pt(II) porphyrin** core (**Pt(II)porphy**) and four acenaphthene chromophores (**ANP**). In air-equilibrated solution energy transfer to **O<sub>2</sub>** quenches the porphyrin phosphorescence at 660 nm. Radiative processes are represented by solid lines and non-radiative processes by dashed lines<sup>53</sup>

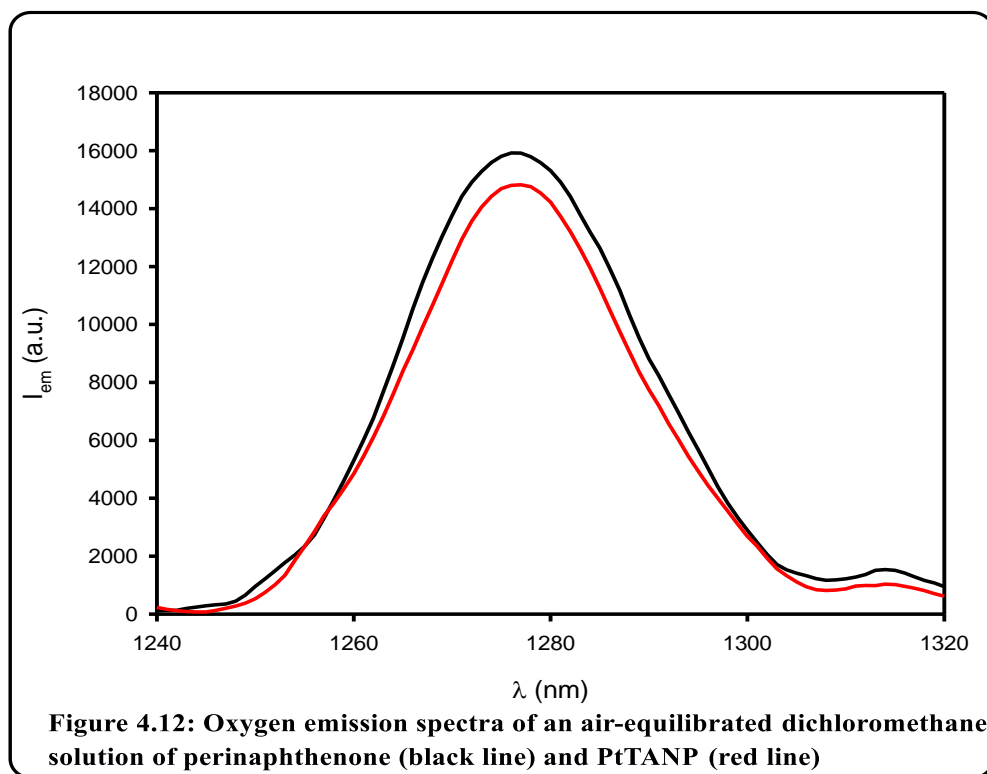
The emission spectrum of **PtTANP** in a rigid matrix of DCM-MeOH 1:1 at 77K shows an intense phosphorescence with a small blue shift, 10 nm compared to the phosphorescence at room temperature in dichloromethane (blue line in Figure 4.11). The emission lifetime is 91  $\mu$ s, a higher value compared to 298 K thanks to the suppression of quenching and non-radiative decay processes at low temperature.

**Table 4.3 Most relevant photophysical data of the PtTANP and the other discussed Pt-porphyrin derivatives:**

Compound	Absorption data				Emission data					Ref.	
	298 K		298 K					77K			
	$\lambda_{\text{max}}$ / nm	$\epsilon/10^4$ M <sup>-1</sup> cm <sup>-1</sup>	$\lambda_{\text{ph}}$ / nm	$\Phi_{\text{ph}}$	$\tau$ / $\mu\text{s}$	$k_{\text{ph}}/10^3$ s <sup>-1</sup>	$k'_{\text{isc}}/10^3$ s <sup>-1</sup>	$\lambda_{\text{ph}}/\text{nm}$	$\tau$ / $\mu\text{s}$		
<b>PtTANP</b>	410, 512, 542	22.4, 3.0, 0.9	663	0.22% (35%) <sup>[g]</sup>	0.91 (75) <sup>[g]</sup>	4.67	0.87	653	91	this work <sup>[h]</sup>	
<b>PtTPP</b> <sup>[a]</sup>	402, 510, 538	22.2, 1.6, 0.4	657	— (4.6%) <sup>[g]</sup>	— (57) <sup>[g]</sup>	0.81	16.7	655	132	54a, 32	
<b>PtTFP</b> <sup>[b]</sup>	409, 512, 540 (sh)	31.6, 2.8, 0.45	679, 741	— (2%) <sup>[g]</sup>	— (22) <sup>[g]</sup>	0.91	44.5	661 730	102	32	
<b>PtTOFP</b> <sup>[c]</sup>	267, 406, 511	—	683, 743	— (11%) <sup>[g]</sup>	— (48) <sup>[g]</sup>	2.29	18.5	669 741	105	54b	
<b>PtOOF</b> <sup>[d]</sup>	267, 406, 511, 541, 599	—	664, 729	— (4.2%) <sup>[g]</sup>	— (54) <sup>[g]</sup>	0.78	17.7	652 722	123	54b	
<b>PtTTEP</b> <sup>[e]</sup>	404 512, 542	27.5, 2.7, 0.8	665, 731	— (5.1%) <sup>[g]</sup>	— (73) <sup>[g]</sup>	0.70	13.0	—	—	55	
<b>PtOEP</b> <sup>[f]</sup>	381, 501, 536	—	644	—	— (50±20) <sup>[g]</sup>	—	—	—	121	55	

<sup>[a]</sup>TPP = 5,10,15,20-tetraphenylporphyrin, <sup>[b]</sup>TFP= 5,10,15,20-meso-tetrakis(fluoren-2-yl)porphyrin, <sup>[c]</sup>TOFP = 5,10,15,20-tetra(4-(2 methoxyfluorenyl)phenyl)porphyrin, <sup>[d]</sup>OOF = 5,10,15,20-octa(3,5-(2 methoxyfluorenyl)phenyl)porphyrin, <sup>[e]</sup>TTEP = 5,10,15,20-tetrakis[2,4,6-triethylphenyl]porphyrin, <sup>[f]</sup>OEP= octaethylporphyrin.

<sup>[g]</sup>Data in parenthesis refer to deaerated solutions. <sup>[h]</sup> in air-equilibrated dichloromethane solution.



We can now compare the photophysical properties of **PtTANP** with that of the parent compound 5,10,15,20-tetraphenylporphyrin Pt(II) complex, **PtTPP** [32, 54-57] (Table 4.3): the energy of the Soret band and Q-bands of **PtTANP** is similar with only a very modest red shift. A similar behavior has been reported previously upon the introduction of fluorenyl units (**PtTFP**)<sup>[32]</sup> and it has been attributed to the so-called in-plane nuclear reorganization. The manifestation of the in-plane nuclear reorganization could be realized while the more conjugated *meso* substituent draws the *meso* carbon away from the porphyrin core. While analysing the crystal data of **PtTPP** and **PtTANP**, we have observed that the distances of *meso*-carbon from the platinum center are ~3.42 Å for **PtTPP**.<sup>[50]</sup> While the similar distances in **PtTANP** are ~3.44 Å. We have

considered the position of  $\text{Pt}^{2+}$  is at the center of the porphyrin core. This observation indicates that as the acenaphthyl is more conjugated than the phenyl ring thus it draws the *meso*-carbon away from the porphyrin core.

Assuming a unitary efficiency of the  $S_1 \rightarrow T_1$  inter system crossing process ( $\eta_{isc}$ ),<sup>[32]</sup> as expected by the presence of a the Pt heavy-atom, we can estimate the radiative ( $k_{ph}$ ) and non-radiative ( $k'_{isc}$ ) decay processes of the phosphorescent  $T_1$  state by the measured values of phosphorescence quantum yield ( $\Phi_{ph}$ ) and lifetime of the  $T_1$  excited state ( $\tau(T_1)$ ) under deaerated conditions, according to the following equations:

$$\Phi_{ph} = \eta_{isc} \frac{k_{ph}}{k_{ph} + k'_{isc}}$$

$$\tau(T_1) = \frac{1}{k_{ph} + k'_{isc}}$$

The corresponding values are reported in Table 4.3

The introduction of the acenaphthyl units brings about an increase in the radiative rate constant ( $k_{ph}$ ) and a decrease of the non-radiative rate constant ( $k'_{isc}$ ), compared to **PtTPP**. Both of these changes contribute to enhance the phosphorescence quantum yield. On the contrary, the previously reported fluorenyl substituent (**PtTFP**) causes an increase of both the radiative and non-radiative rate constants, thus decreasing the overall phosphorescence quantum yield. While comparing the photophysical properties of **PtTANP** with that of the other literature reported platinum porphyrin derivatives (Table 4.3), it is evident that the values of lifetime of the phosphorescent excited state and of the phosphorescence quantum yield in deaerated solutions at 298 K are the highest in the case of **PtTANP**. Furthermore, the phosphorescence quantum yield of **PtTANP** is strongly quenched by dioxygen. Indeed, **PtTANP** shows a very high singlet oxygen quantum yield of 88% in dichloromethane indicating that it is an

excellent photosensitizer for the production of singlet oxygen and potential application in the field of photodynamic therapy as well as oxygen sensors.<sup>58-60</sup>

#### 4.4 Conclusions:

In conclusion, we have synthesized a new platinum(II) porphyrin complex, [5,10,15,20-tetra(5-acenaphthyl)porphinato] platinum(II), **PtTANP** bearing acenaphthyl group at the *meso* position of the porphyrin ring. This complex has been thoroughly characterized via various spectroscopic techniques, including single-crystal XRD analysis. It was observed that the Pt(II) center in **PtTANP** is very near to the perfect square planar geometry. The Pt(II)-N bond distances are in the ranges of 2.005 Å–2.020 Å. The **PtTANP** derivative exhibited one reversible oxidative couple at +1.10 V and a reversible reductive couple at -1.47 V versus Ag/AgCl. In deaerated solution, a strong red phosphorescence is observed with emission quantum yield as high as 35% and emission lifetime of 75  $\mu$ s. **PtTANP** works as a light-harvesting antenna: upon UV excitation of acenaphthene chromophores energy transfer to the Pt(II) porphyrin core takes place with unitary efficiency and results in the photosensitized phosphorescence. It was also demonstrated that the **PtTANP** molecule is an excellent photosensitizer having singlet oxygen production quantum yield of 88% in dichloromethane. A close comparison of **PtTANP** with that of the previously reported platinum porphyrin derivatives demonstrates its superiority. The lifetime of the phosphorescent excited state of **PtTANP** in deaerated solutions at 298 K is longer and its phosphorescence quantum yield is also significantly higher than the other reported platinum porphyrin

derivatives. These results indicate that the **PtTANP** molecule will have potential applications in the field of photodynamic therapy as well as oxygen sensors.

## 4.5 Experimental Section:

**4.5.1 Materials:** The precursor's pyrrole, benzonitrile, DDQ (2,3-Dichloro-5,6-dicyano-1,4-benzoquinone), 5-acenaphthene carboxaldehyde,  $K_2PtCl_4$  (Potassium tetrachloroplatinate(II)), and TEAP (Tetraethyl ammonium perchlorate) were purchased from Aldrich, USA. Other chemicals were of reagent grade. Hexane and dichloromethane were distilled from KOH and  $CaH_2$ , respectively. For spectroscopy and electrochemical studies, HPLC grade solvents were used. **H<sub>2</sub>TANP** was prepared by following an earlier literature report.<sup>61</sup>

## 4.5.2 Physical Measurements:

Luminescence measurements at 77 K were performed in dichloromethane/methanol (1:1 v/v). UV-vis absorption spectra were recorded with a PerkinElmer 140 spectrophotometer using quartz cells with path length of 1.0 cm. Emission spectra were obtained with either a Perkin Elmer LS55 spectrofluorometer, equipped with a Hamamatsu R928 phototube, or an Edinburgh FLS920 spectrofluorometer equipped with a Ge-detector for emission in the NIR spectral region. Correction of the emission spectra for detector sensitivity in the 550-1000 nm spectral region was performed by a calibrated lamp.<sup>53</sup> Excitation spectra in the visible range were acquired with the fluorimeter Perkin-Elmer LS55. Emission quantum yields were measured following the method of Demas and Crosby<sup>62</sup> (standards used:  $[Ru(bpy)_3]^{2+}$  in air-equilibrated aqueous solution  $\Phi = 0.0405$ ).<sup>63</sup> Quantum yield of oxygen production is calculated by comparison between the oxygen phosphorescence generated by the

sample and by a standard (standard used: 1H-Phenalen-1-one in toluene,  $\Phi_A = 0.95$ ).<sup>64</sup> Photophysical characterization in the absence of oxygen was carried out on samples of dye solutions after degassing them by freeze–pump–thaw cycling ( $P = 10^{-9}$  Bar; liquid nitrogen as cooling medium) in a custom-made quartz cuvette. Emission intensity decay measurements in the range 10  $\mu$ s to 1 s were performed on a homemade time-resolved phosphorimeter. Lifetimes shorter than 10  $\mu$ s were measured by the above-mentioned Edinburgh FLS920 spectrofluorimeter equipped with a TCC900 card for data acquisition in time-correlated single-photon counting experiments (0.5 ns time resolution) with 405 nm laser. The estimated experimental errors are: 2 nm on the absorption and emission band maximum, 5% on the molar absorption coefficient and luminescence lifetime, and 10% on the luminescence and photoisomerization quantum yields. The elemental analyses were carried out with a Perkin–Elmer 240C elemental analyzer. FT–IR spectra were recorded on a Perkin–Elmer spectrophotometer with samples prepared as KBr pellets. The NMR measurements were carried out using a Bruker AVANCE 400 NMR spectrometer. Tetramethylsilane (TMS) was the internal standard. Electrospray mass spectra were recorded on a Bruker Micro TOF–QII mass spectrometer. Cyclic voltammetry measurements were carried out using a CH Instruments model **CHI1120A** electrochemistry system. A glassy–carbon working electrode, a platinum wire as an auxiliary electrode, and a saturated calomel reference electrode (SCE) were used in a three–electrode configuration. Tetraethyl ammonium perchlorate (TEAP) was the supporting electrolyte (0.1M), and the concentration of the solution was  $10^{-3}$ M with respect to the complex. The oxidation and reduction processes at the positive and negative sides of the Ag–AgCl reference electrode were measured by using a glassy–carbon working electrode. The half-wave potential  $E_{298}^0$  was set equal to

$0.5(E_{pa} + E_{pc})$ , where  $E_{pa}$  and  $E_{pc}$  are anodic and cathodic cyclic voltammetric peak potentials, respectively. The scan rate used was  $100 \text{ mV s}^{-1}$ .

**4.5.3 Crystal Structure Determination:** Single crystals of [5,10,15,20-tetra(5-acenaphthyl)porphinato] platinum(II), **PtTANP** were grown by slow diffusion of a solution of the metal complexes in diethyl ether into dichloromethane, followed by slow evaporation under atmospheric conditions. The crystal data of **PtTANP** was collected on a Bruker Kappa APEX II CCD diffractometer at 293 K. Selected data collection parameters and other crystallographic results are summarized in Table S1. All data were corrected for Lorentz polarization and absorption effects. The program package SHELXTL<sup>65</sup> was used for structure solution and full matrix least-squares refinement on  $F^2$ . Hydrogen atoms were included in the refinement using the riding model. Contributions of H atoms for the water molecules were included but were not fixed. Disordered solvent molecules were taken out using SQUEEZE command in PLATON.<sup>66</sup> CCDC- 2075384 contains the supplementary crystallographic data for **PtTANP**. These data can be obtained free of charge via [www.ccdc.cam.ac.uk/data\\_request/cif](http://www.ccdc.cam.ac.uk/data_request/cif).

#### 4.5.4 Synthesis:

**4.5.4.1 Synthesis of [5,10,15,20-tetra(5-acenaphthyl)porphinato] platinum(II), PtTANP:** **PtTANP** was prepared by slight modifications of an earlier reported protocols.<sup>67</sup> In a 100ml R.B. flask, 40 ml of benzonitrile was taken in a dry, degassed atmosphere.  $\text{K}_2\text{PtCl}_4$  (167 mg, 0.4 mmol) was added to this benzonitrile (40ml) solvent, and the mixture was heated with stirring under an  $\text{N}_2$  atmosphere at  $100^\circ\text{C}$ . After 15 minutes, the solution turned out to be yellow. Then the 5,10,15,20-tetra(5-acenaphthyl)

porphyrin, **H<sub>2</sub>TANP** (50 mg, 0.05 mmol) was added, and the resulting mixture was heated with stirring at reflux temperature for 48 hr. The mixture was cooled to room temperature, and the benzonitrile was removed by using rotary evaporation. Then the dried mass was subjected to column chromatography (Silica gel, dichloromethane/hexane eluent). The purest fractions were combined and dried by using rotary evaporation and crystallized as orange plates.

**For [5,10,15,20-tetra(5-acenaphthyl)porphinato] platinum(II), PtTANP:** Yield 38 mg (62 %); Anal. Calcd (found) for C<sub>68</sub>H<sub>44</sub>N<sub>4</sub>Pt (**PtTANP**): C, 73.43 (73.51); H, 3.99 (3.84); N, 5.04 (5.17). UV-Vis (dichloromethane):  $\lambda_{\text{max}}$ /nm ( $\epsilon/\text{M}^{-1}\text{cm}^{-1}$ ): 410 (224000), 512 (30000), 542 (9000). <sup>1</sup>H NMR (400 MHz, chloroform-*d*)  $\delta$  3.62-3.70 (m, 16 H), 6.81 - 7.02 (m, 4 H), 7.12 - 7.20 (m, 4 H), 7.29 - 7.30 (d, *J*=6.9 Hz, 4 H), 7.66 - 7.68 (d, *J*=7.6 Hz, 4 H), 8.08 - 8.18 (m, 4 H), 8.46 - 8.50 (m, 8 H) (Figure S1). <sup>13</sup>C NMR (101 MHz, CDCl<sub>3</sub>)  $\delta$  151.25, 146.68, 145.72, 141.64, 138.72, 134.80, 134.26, 132.92, 132.32, 131.80, 130.88, 129.26, 128.38, 123.04, 121.86, 119.36, 118.16, 114.99, 112.60, 30.83, 30.57 (Figure S2). The electrospray mass spectrum in acetonitrile (Figure S3) showed the peaks centered at  $m/z = 1112.3391$  corresponding to [**PtTANP**+H]<sup>+</sup> (calculated molecular mass: 1112.3292). **PtTANP** displayed strong phosphorescence at 663 nm and 725 nm (Table 1).

**Electronic supplementary information (ESI<sup>†</sup>) available:** Synthesis and characterization of **PtTANP**. <sup>1</sup>H NMR, <sup>13</sup>C NMR, ESI-MS spectrum and crystallographic data of **PtTANP**. CCDC 2075384 contains the supplementary crystallographic data for **PtTANP**. These data can be obtained free of charge via [www.ccdc.cam.ac.uk/data\\_request/cif](http://www.ccdc.cam.ac.uk/data_request/cif).

## References:

1. Y. You and W. Nam, *Chem. Soc. Rev.* **2012**, *41*, 7061-7084.
2. J. Zhao, W. Wu, J. Sun and S. Guo, *Chem. Soc. Rev.* **2013**, *42*, 5323-5351.
3. K. Kalyanasundaram and M. Grätzel, *Coord. Chem. Rev.* **1998**, *177*, 347-414.
4. P. S. Wagenknecht and P. C. Ford, *Coord. Chem. Rev.* **2011**, *255*, 591-616.
5. V. Balzani, P. Ceroni, A. Juris, M. Venturi, S. Campagna, F. Puntoriero and S. Serroni, *Coord. Chem. Rev.* **2001**, *219*, 545-572.
6. V. Balzani, G. Bergamini, F. Marchioni and P. Ceroni, *Coord. Chem. Rev.*, **2006**, *250*, 1254-1266.
7. O. S. Wenger, *Coord. Chem. Rev.* **2009**, *253*, 1439-1457.
8. N. A. Ludin, A. A.-A. Mahmoud, A. B. Mohamad, A. A. H. Kadhum, K. Sopian and N. S. A. Karim, *Renew. Sustain. Energy Rev.* **2014**, *31*, 386-396.
9. A. Carella, F. Borbone and R. Centore, *Front. Chem.* **2018**, *6*, 481.
10. M. Parasram and V. Gevorgyan, *Chem. Soc. Rev.* **2017**, *46*, 6227-6240.
11. D. M. Guldi, M. Maggini, E. Menna, G. Scorrano, P. Ceroni, M. Marcaccio, F. Paolucci and S. Roffia, *Chem. Eur. J.* **2001**, *7*, 1597-1605.
12. V. Balzani, G. Bergamini and P. Ceroni, *Rendiconti Lincei.* **2017**, *28*, 125-142.
13. M. C. DeRosa and R. J. Crutchley, *Coord. Chem. Rev.* **2002**, *233*, 351-371.
14. N. Adarsh, R.R. Avirah and D. Ramaiah, *Org. Lett.* **2010**, *12*, 5720-5723.
15. S. Mostafa and F.L. Rosario-Ortiz, *Environ. Sci. Technol.* **2013**, *47*, 8179-8186.
16. Y. Qin, L. J. Chen, F. Dong, S.T. Jiang, G.Q. Yin, X. Li, Y. Tian and H.B. Yang, *J. Am. Chem. Soc.* **2019**, *141*, 8943-8950.

17. A. Galstyan, Y. K. Maurya, H. Zhylitskaya, Y.J. Bae, Y.L. Wu, M.R. Wasielewski, T. Lis, U. Dobrindt and M. Stępień, *Chem. Eur. J.* **2020**, *26*, 8262-8266.
18. P. Pushpanandan, D.H. Won, S. Mori, Y. Yasutake, S. Fukatsu, M. Ishida and H. Furuta, *Chem. Asian J.* *14*, 1729-1736.
19. S. Callaghan and M.O. Senge, *Photochem. Photobiol. Sci.* **2018**, *17*, 1490-1514.
20. F. Heinemann, J. Karges and G. Gasser, *Acc. Chem. Res.* **2017**, *50*, 2727-2736.
21. H. Huang, S. Banerjee and P.J. Sadler, *ChemBioChem.* **2018**, *19*, 1574-1589.
22. W. Sinha, L. Ravotto, P. Ceroni and S. Kar, *Dalton Trans.* **2015**, *44*, 17767-17773.
23. L. Huang, M. Rudolph, F. Rominger and A. S. K. Hashmi, *Angew. Chem. Int. Ed.* **2016**, *55*, 4808-4813.
24. M. Yang, J. Deng, D. Guo, J. Zhang, L. Yang and F. Wu, *Org. Biomol. Chem.* **2019**, *17*, 5367-5374.
25. G.K. Couto, B.S. Pacheco, V.M. Borba, J.C.R. Junior, T.L. Oliveira, N.V. Segatto, F.K. Seixas, T.V. Acunha, B.A. Iglesias and T. Collares, *J. Photochem. Photobiol. B*, **2020**, *202*, 111725.
26. P. Lang, J. Habermehl, S.I. Troyanov, S. Rau and M. Schwalbe, *Chem. Eur. J.* **2018**, *24*, 3225-3233.
27. H.C. Chen, D.G. Hetterscheid, R.M. Williams, J.I. van der Vlugt, J.N. Reek and A.M. Brouwer, *Energy Environ. Sci.* **2015**, *8*, 975-982.
28. C. Lottner, K.C. Bart, G. Bernhardt and H. Brunner, *J. Med. Chem.* **2002**, *45*, 2064-2078.

29. R.C. Kwong, S. Sibley, T. Dubovoy, M. Baldo, S.R. Forrest and M.E. Thompson, *Chem. Mater.* **1999**, *11*, 3709-3713.
30. J. R. Sommer, A.H. Shelton, A. Parthasarathy, I. Ghiviriga, J.R. Reynolds and K.S. Schanze, *Chem. Mater.* **2011**, *23*, 5296-5304.
31. I. Toubia, C. Nguyen, S. Diring, L.M. Ali, L. Larue, R. Aoun, C. Frochot, M. Gary-Bobo, M. Kobeissi and F. Odobel, *Inorg. Chem.* **2019**, *58*, 12395-12406.
32. S. Drouet, C.O. Paul-Roth, V. Fattori, M. Cocchi and J.G. Williams, *New J. Chem.* **2011**, *35*, 438-444.
33. A.-K. Bansal, W. Holzer, A. Penzkofer and T. Tsuboi, *Chem. Phys.* **2006**, *330*, 118-129.
34. O. S. Finikova, A. Y. Lebedev, A. Aprelev, T. Troxler, F. Gao, C. Garnacho, S. Muro, R. M. Hochstrasser and S. A. Vinogradov, *ChemPhysChem.* **2008**, *9*, 1673-1679.
35. T. V. Esipova, H. c. J. Rivera-Jacquez, B. Weber, A. m. E. Masunov and S. A. Vinogradov, *J. Am. Chem. Soc.* **2016**, *138*, 15648-15662.
36. J. N. Demas, B. A. DeGraff and P. B. Coleman, *Anal. Chem.* **1999**, *71*, 793A-800A.
37. S. Ji, W. Wu, W. Wu, P. Song, K. Han, Z. Wang, S. Liu, H. Guo and J. Zhao, *J. Mater. Chem.* **2010**, *20*, 1953-1963.
38. W.W.S. Lee, K.Y. Wong and X.M. Li, *Anal. Chem.* **1993**, *65*, 255-258.
39. S.W. Lai, Y.J. Hou, C.M. H.L. Che, K.Y. Wong, C.K. Chang and N. Zhu, *Inorg. Chem.* **2004**, *43*, 3724-3732.
40. V.D. Rumyantseva, N.P. Ivanovskaya, L.I. Konovalenko, S.V. Tsukanov, A.F. Mironov and N.S. Osin, *Russ. J. Bioorganic Chem.* **2008**, *34*, 239-244.

41. R.R. de Haas, R.P. van Gijlswijk, E.B. van der Tol, H.J. Zijlmans, T. Bakker–Schut, J. Bonnet, N.P. Verwoerd and H.J. Tanke, *J. Histochem. Cytochem.* **1997**, *45*, 1279-1292.
42. J. Kalinowski, W. Stampor, J. Szmytkowski, M. Cocchi, D. Virgili, V. Fattori and P. Di Marco, *J. Chem. Phys.* **2005**, *122*, 154710.
43. A.N. Filippin, J.R. Sanchez-Valencia, J. Idígoras, M. Macias-Montero, M. Alcaire, F.J. Aparicio, J.P. Espinos, C. Lopez-Santos, F. Frutos, A. Barranco and J.A. Anta, *Advanced Materials Interfaces.* **2017**, *4*, 1601233.
44. Y. Amao, K. Asai, T. Miyashita and I. Okura, *Polym. Adv. Technol.* **2000**, *11*, 705-709.
45. M.M. Alam, F. Bolze, C. Daniel, L. Flamigni, C. Gourlaouen, V. Heitz, S. Jenni, J. Schmitt, A. Sour and B. Ventura, *Phys. Chem. Chem. Phys.* **2016**, *18*, 21954-21965.
46. K.R. Graham, Y. Yang, J.R. Sommer, A.H. Shelton, K.S. Schanze, J. Xue and J.R. Reynolds, *Chem. Mater.* **2011**, *23*, 5305-5312.
47. The Porphyrin Handbook, ed. K. M. Kadish, K. M. Smith and R. Guilard, Academic Press, San Diego, **2000**.
48. C. Jellimann, M. Mathé-Allainmat, J. Andrieux, S. Kloubert, J.A. Boutin, J.P. Nicolas, C. Bennejean, P. Delagrangé and M. Langlois, *J. Med. Chem.* **2000**, *43*, 4051-4062.
49. A. Garai, M. Kumar, W. Sinha, S. Chatterjee, C.S. Purohit, T. Som and S. Kar, *RSC Adv.* **2014**, *4*, 64119-64127.
50. A.C. Hazell, *Acta Crystallogr. Sec.C: Crystal Structure Communications.* **1984**, *40*, 751-753.

51. P. Chen, O.S. Finikova, Z. Ou, S.A. Vinogradov and K.M. Kadish, *Inorg. Chem.* **2012**, *51*, 6200-6210.
52. E. L. Elliott, A. Orita, D. Hasegawa, P. Gantzel, J. Otera and J. S. Siegel, *Org. Biomol. Chem.* **2005**, *3*, 581-583.
53. M. Montalti, A. Credi, L. Prodi, T. M. Gandolfi, *Handbook of Photochemistry*, 3rd ed., Taylor & Francis, Boca Raton, **2006**.
54. C.M. Che, Y.J. Hou, M.C. Chan, J. Guo, Y. Liu and Y. Wang, *J. Mater. Chem.* **2003**, *13*, 1362-1366.
55. W. Wu, W. Wu, S. Ji, H. Guo, X. Wang and J. Zhao, *Dyes Pigm.* **2011**, *89*, 199-211.
56. C.O. Paul-Roth, S. Drouet, A. Merhi, J.G. Williams, L.F. Gildea, C. Pearson, M.C. Petty, *Tetrahedron* **2013**, *69*, 9625-9632.
57. A.G. Moiseev, E.A. Margulies, J.A. Schneider, F. Bélanger-Gariépy, D.F. Perepichka, *Dalton Trans.* **2014**, *43*, 2676-2683.
58. S. Mathai, T.A. Smith, K.P. Ghiggino, *Photochem. Photobiol. Sci.* **2007**, *6*, 995-1002.
59. N. Molupe, B. Babu, E. Prinsloo, A.Y. Kaassis, K. Edkins, J. Mack, T. Nyokong, *J Porphyr Phthalocyanines*. **2019**, *23*, 1486-1494.
60. XD Wang, OS. Wolfbeis, *Chem. Soc. Rev.* **2014**, *43*, 3666-761.
61. Z. I. Zhilina, S. V. Vodzinskii and S. A. Andronati, *Ukr. Khim. Zh. (Russ. Ed.)*, **1990**, *56*, 1084-1088.
62. G. A. Crosby, J. N. Demas, *J. Phys. Chem.* **1971**, *75*, 991-1024.
63. K. Suzuki, A. Kobayashi, S. Kaneko, K. Takehira, T. Yoshihara, H. Ishida, Y. Shiina, S. Oishi, S. Tobita, *Phys. Chem. Chem. Phys.* **2009**, *11*, 9850-9860.

- 64. F. Prat, C. Martí, S. Nonell, X. Zhang, C. S. Foote, R. G. Moreno, J. L. Bourdelande, J. Font, *Phys. Chem. Chem. Phys.* **2001**, *3*, 1638-1643.
- 65. G. M. Sheldrick, *Acta Crystallogr., Sect. A: Found. Crystallogr.* **2008**, *64*, 112-122.
- 66. d. S. P. Van, A. L. Spek, *Acta Crystallogr., Sect. A: Found. Crystallogr.* **1990**, *A46*, 194-201.
- 67. L. M. Mink, M. L. Neitzel, L. M. Bellomy, R. E. Falvo, R. K. Boggess, B. T. Trainum, P. Yeaman, *Polyhedron* **1997**, *16*, 2809.

## ***SUMMARY OF THE THESIS***

Corrole, one of the most promising contracted porphyrinoids having one less meso carbon atom than porphyrin and shares a similar basic skeleton to corrin bearing direct pyrrole-pyrrole linkage, but in terms of aromaticity, it is parallel to porphyrin ring having  $18\pi$  electrons aromatic system. Absence of one methine bridge makes a contracted coordination cavity. Besides inner core contains three ionizable pyrrolic hydrogens. These two factors make its chemistry too much interesting, especially the stabilization of higher oxidation states of metal ions. Nowadays, corrole and metallocorroles have diverse applications over multidisciplinary field such as catalysis, sensor, solar cell, medicinal field, and so on. In this thesis, I have discussed the continuous development of facile synthetic protocols of corroles, different coordination modes of metallocorroles, corroles, and metallocorroles based applications and lastly functionalization of corroles. Of them, Mono-N –substituted and di- N-substituted corroles are rarely reported and investigated in the literature. This thesis mainly highlights such inner core modification of corroles. Here we have developed an efficient, high yielding, single step and relatively greener methodology for facile synthesis of  $N^{21}$ ,  $N^{22}$  –carbamide corroles derivative. Further complete characterizations of these carbamide corroles derivative and generalization of the newly designed synthetic protocol have done. In the next part, the First report of the methylene bridge of 5,10,15-tris(pentafluorophenyl)corrole has also outlined. The superiority of this protocol over previously reported N, N'-one carbon bridged porphyrin by Johnson et al. is also discussed here. Optimization of the invented methodology and comprehensive characterization of new macrocycle has been done by different physicochemical techniques. In addition, the synthesis of a new

platinum(II) porphyrin and its characterization is reviewed. In order to understand the redox property of this PtTANP cyclic voltammetric and differential pulse voltammetric measurements were performed. We have exposed that **PtTANP** behaves as a light-harvesting antenna due to the presence of acenaphthene chromophores in the Pt (II) porphyrin. In a deaerated solution at 298 K, a strong phosphorescence is observed with the maximum at 660 nm, emission quantum yield of 35% and a lifetime of 75  $\mu$ s but a very weak phosphorescence ( $\Phi_{\text{em}} = 0.22\%$ ) with a much shorter lifetime ( $\tau = 910$  ns) is observed in air-equilibrated solution. The quenching by oxygen results in singlet oxygen production with a very high quantum yield of 88%, indicating its potential applications in the field of photodynamic therapy as well as oxygen sensors.

